# Dynamics of High Energy Environment: Processes at the Turkish Strait System (DEEP)
-
# Yüksek Enerji Çevre Dinamiği: Türk Boğazlar Sistemi'nde Süreçler (TURBO)

**TÜBİTAK**

**Program Kodu:** 1001

**Proje No:** 111Y308


Proje Yürütücüsü:
**Prof. Dr. Emin ÖZSOY**

Araştırmacılar:
Prof. Dr. Süleyman TUĞRUL
Dr. Roberta DELFANTI
Dr. Gianmaria SANNINO

Bursiyer:
Adil SÖZER



AĞUSTOS 2015
ERDEMLİ, MERSİN

**Scientific and Technical Team**

We thank the following personnel taking part in the collaborative work under the Project:

*Modeling Development:*
Adil Sözer – Bosphorus and TSS Modeling
Gianmaria Sannino – TSS modeling
Özgür Gürses – TSS modeling

*R/V BİLİM cruise June-July 2013:*
Emin Özsoy – physical oceanography experiment
Süleyman Tuğrul – chemical oceanography experiment
Özgür Gürses – physical oceanography measurements
Mayotte Patron – physical oceanography measurements
(summer practice student INSTA France)
Ersin Tutsak – chemical oceanography measurements
Mehmet Kaptan – chemical oceanography measurements
Devrim Tezcan – coordination with the R/V Pelagia team
Şehmuz Başduvar – chemical oceanography measurements
Esabil Kakaç – chemical oceanography measurements
Metehan Çetin – electronics operation
Mehmet T. Eliuz – systems operation
Mertkan Tüer – acoustic systems operation
+ captains and seamen of R/V BİLİM

## Abstract

The Turkish Straits System (TSS) controls the exchange between the Black Sea and the Mediterranean Sea. A sound understanding of the circulation and transport mechanisms of this complex system depends on a series of experimental investigations and modelling development that have been carried out. We focus on the characterization of the exchange through the TSS, the influence on the adjacent seas and in particular, the ventilation of the Black Sea by the effluent of Mediterranean water exiting the TSS. Experimental investigations highlighted the fine-scale details of the exchange and the intrusions and mixing of water masses between adjacent basins. High resolution modeling of the TSS is undertaken to assess its transport and mixing properties.

**Keywords:** Water and material exchange, transport, mixing, ventilation, water masses, Bosphorus and Dardanelles Straits, Marmara Sea, Black Sea.

--

## Özet

Türk Boğazlar Sistemi (TBS) Karadeniz ve Akdeniz arasındaki alışverişi kontrol eder. Bu karmaşık sistemin dolaşım ve taşınım mekanizmalarının anlaşılması, burada gerçekleştirilen deneysel incelemelere ve model gelişimine bağlıdır. Çalışmamız, TBS aracılığıyla gerçekleşen denizler arası madde iletişiminin, çevre denizlerde gerçekleşen etkilerin ve Karadeniz ventilasyonunun karakterizasyonu üzerine odaklanmaktadır. Deneysel araştırmalar komşu havzalar arası su kütlelerinin alışverişine ve karışımlarına ilişkin ince ölçekli ayrıntıları vurgulamaktadır. TBS'nin yüksek çözünürlüklü bir modelli taşınım ve karışım özelliklerinin değerlendirilmesi için gerçekleştirilmiştir.

**Anahtar Kelimeler:** Su ve madde değişimi, taşınım, karışım, ventilasyon, su kütleleri, İstanbul ve Çanakkale Boğazları, Marmara Denizi, Karadeniz.

# 1. INTRODUCTION AND LITERATURE REVIEW

## 1.1 Geography

The Turkish Straits System (TSS, Fig. 1) forms the transition zone between the two major basins of the Mediterranean and the Black Seas.

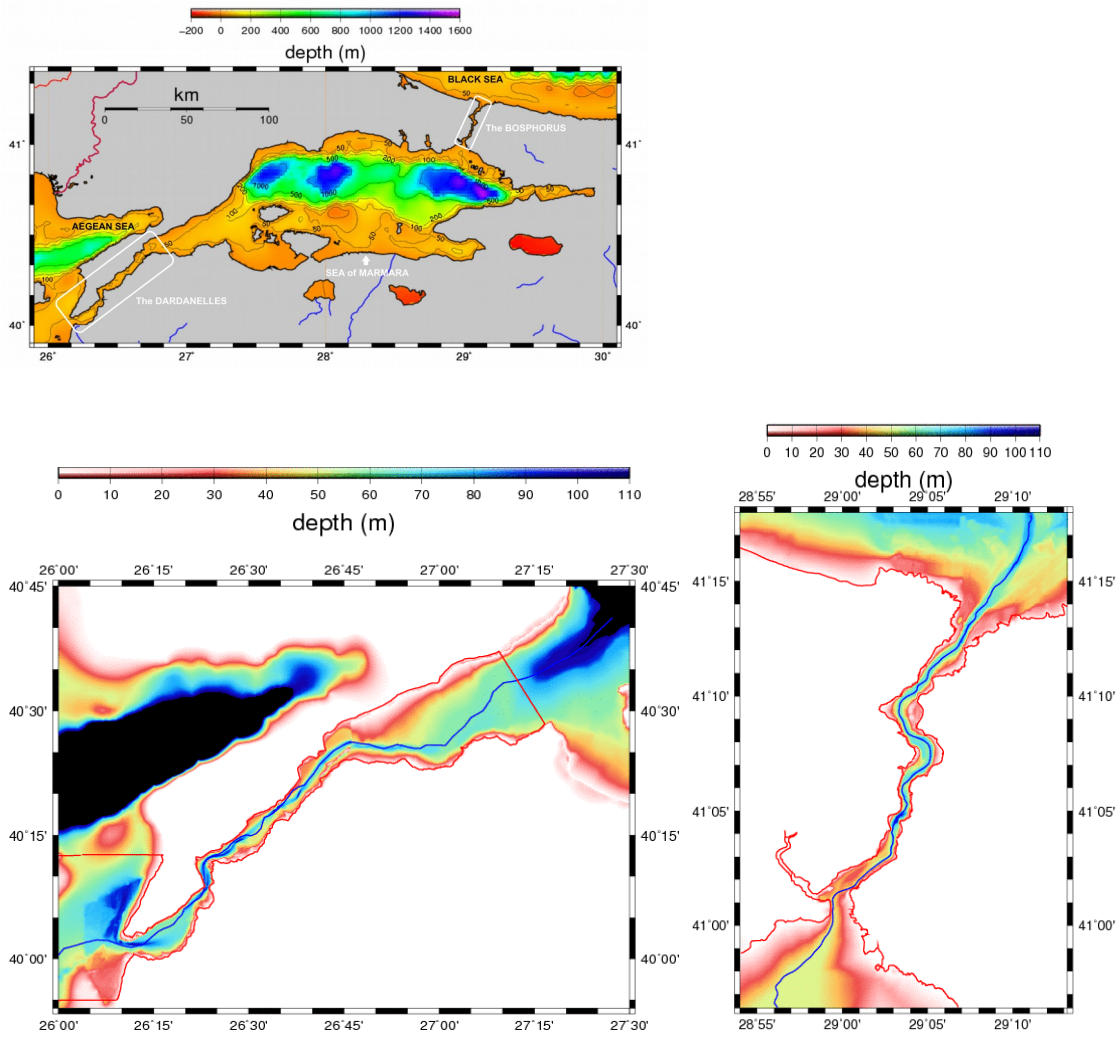


*Figure 1: Location and bottom topography maps for the (a) Turkish Straits System (TSS) including the (b) Dardanelles and (c) Bosphorus Straits. The blue line denotes the thalweg along the strait channels.*

The TSS consists of the Sea of Marmara (surface area 11,500 $km^2$) connecting to the Aegean and Black Seas respectively through the Dardanelles (length 75 km, min. width 1.3 km) and Bosphorus (length 35 km, min. width 0.7 km) Straits. The Marmara Sea has three elongated depressions (max. depth ~1350 m) interconnected by sills (depth ~600 m) and adjoining continental shelves.

The TSS is also a meeting point of marine waters and continents where significant contrasts occur in climate, therefore being a region that is sensitive to climatic changes (Özsoy, 1999; Yavuz et al., 2003; Gündüz and Özsoy, 2006; Lionello et al., 2006; Hero, 2007). In this complex system the two straits controlling the exchange are the most limiting elements, with the Bosphotus Strait playing a key role dominating the system with very specific natural control mechanisms.

A short review of role of the TSS in the interactions of the Mediterranean and Black Seas has been given in Schroeder et al. (2012). Even though the size of the domain is much smaller than the neighboring seas, the TSS is a theater of the world ocean where intense nonlinear and turbulent interactions are encountered under conditions of strong stratification, setting the fundamental behaviour patterns of the system. Processes such as hydraulic controls and hydraulic jumps, down-slope gravity flows, internal waves, turbulent entrainment, double diffusive instabilities and convection, non-hydrostatic flow, basin oscillations, continental shelf and deep-sea interactions, flow separation and recirculation, set the stage in this unique high energy environment.

### 1.2 Past measurement campaigns

Consistent observational data sets covering the TSS have been collected with the R/V BILIM of the IMS-METU during 1985-2001 and sporadically in many other scientific cruises since then. Detailed mapping of the Bosphorus currents and hydrography was undertaken in 1998-1999 for the TURBO administration, when detailed ADCP and CTD measurements were extended to small bays and bends using a small diving boat, Atmaca II. Recent measurements have been acquired from automated coastal meteorology, sea level and ADCP stations (http://moma.ims.metu.edu.tr) operated under a coastal network (Özsoy et al., 2009). Further detailed measurements were obtained

during the recent SESAME European project in a collaborative sampling program of the Mediterranean and Black Seas.

### 1.3 TSS Exchange

Changes in properties through the TSS are exemplified in Fig. 2a,b, based on data collected in May 2007. The interface separating the Black Sea and Mediterranean Sea waters dips down strongly in the two straits, relative to its relatively constant depth of about 25m in the Sea of Marmara. The Cold Intermediate Water (CIW) of the Black Sea with a core temperature of less than 8°C invades the Bosphorus and continues as a submerged tongue transiting across the TSS, while some of the cold water surfaces south of the Bosphorus (Fig. 2a). The cold-water above the pycnocline is largely maintained by local winter cooling re-stratified by surface warming. Aegean water of 14°C temperature entering from the Dardanelles Strait is colder and denser than the 15°C water at the same level in the Marmara Sea interior and sinks down as a gravity current, as shown by earlier observations (Beşiktepe et al., 1993, 1994) and modeling (Hüsrevoğlu, 1999). The upper layer salinity in Fig 2b increases steadily from the Black Sea to the Aegean, with the highest rate in the southern part of the Bosphorus, and western part of the Dardanelles due to hydraulic adjustments (see later). As a result of wind mixing, the upper layer in the Marmara Sea has rather uniform properties, although becoming re-stratified in the spring months (Fig. 2a).

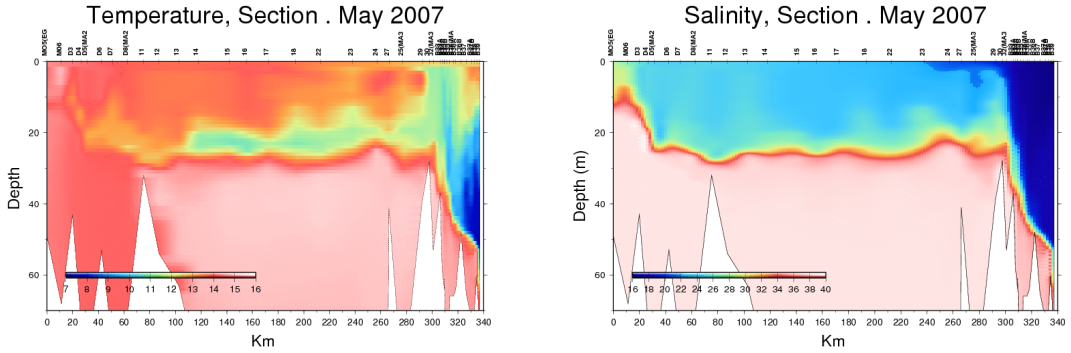


*Figure 2. Transects of (a) temperature and (b) salinity across the TSS in May 2007, along the main axis extending from the Aegean Sea to the Black Sea (covering the*

*Dardanelles at 0-100 km, Marmara Sea at 100-300 km and the Bosphorus at 300-340 km ranges on the distance scale).*

There is a strong contrast in the annual net water budget Q = E – P – R (evaporation – precipitation – river inflow) across the TSS, resulting from the different water regimes in the Mediterranean (Q > 0) and the Black Sea (Q < 0). In the Black Sea, the total freshwater input (P=300 $km^3$/yr and R=350 $km^3$/yr) is twice as large as the loss term (E=350 $km^3$/yr). Making use of an assumption of steady state mass balance, and multi-year averages of salinity measurements at the junctions of the straits, Ünlüata et al. (1990) have computed the annual average fluxes through the TSS from a two-layer idealization of a box model, updated later with an seasonal version provided by Tuğrul et al. (2002) and Beşiktepe (2003). An updated description is provided here based on the review given in Schroeder et al. (2012).

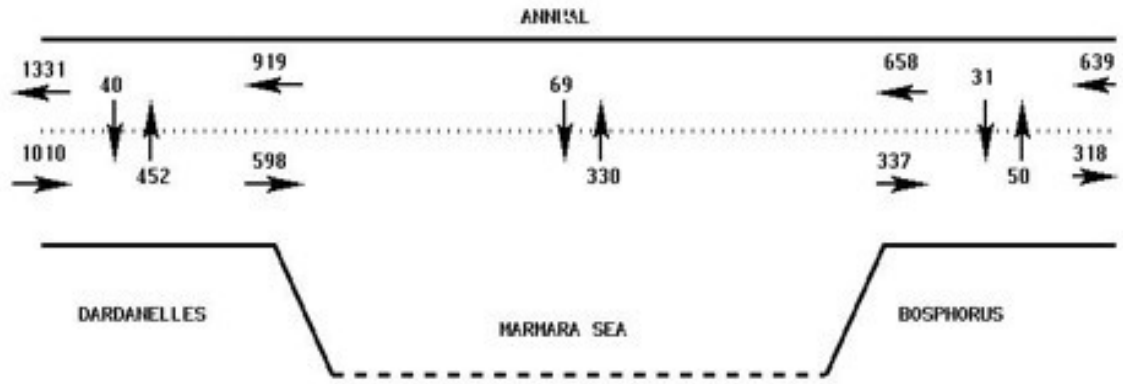


*Figure 3. Steady-state annual mean fluxes ($km^3$/yr) through the TSS and between its individual compartments (after Tuğrul et al. 2002).*

The annual two-layer volume fluxes of the TSS are shown in Fig. 3. The exchange through the TSS increases in the spring-early summer, and weakens markedly in autumn (within a margin of about □40% of the annual mean) in response to the freshwater input to the Black Sea (Tuğrul et al., 2002).

The input into the Marmara Sea by the upper layer flow of the Bosphorus is estimated as 657 $km^3$/yr and the outflow into the Black Sea in the lower layer is estimated as 318 $km^3$/yr (Fig. 3) based on the measurements during the years 1985-1995 (Tuğrul et al.

2002), amounting to 263 mm/yr and 127 mm/yr respectively, if divided by the area of the Mediterranean Sea (2.5 x $10^{-6}$ $km^2$).

The input into the Aegean Sea by the upper layer flow of the Dardanelles was found to be 1331 $km^3$/yr and the outflow into the Marmara Sea in the lower layer was 1010 $km^3$/yr in the same period (Tuğrul et al. 2012), amounting to 532 mm/yr and 404 mm/yr respectively, if divided by the area of the Mediterranean Sea (2.5 x $10^{-6}$ $km^2$), and the net flux into the Mediterranean Sea therefore amounting to 132 mm/yr, about 10% of the net annual loss of water from the entire Mediterranean Basin.

Bosphorus fluxes computed from ADCP data (Özsoy et al., 1996, 1998) show the same seasonal behaviour as reviewed above, but reveal maxima of about $Q_{upper}$ = 1600 $km^3$/yr and $Q_{lower}$ = 630 $km^3$/yr for the upper and lower layers respectively, including blocked cases, indicating instantaneous fluxes 2-3 times larger than the annual mean. Despite large scatter in data due to sampling, overall average values of $Q_{upper}$ = 540 $km^3$/yr and $Q_{lower}$ = 115 $km^3$/yr were computed, the latter value possibly being underestimated as a result of data loss near the bottom. Oğuz et al. (1990) concluded that the upper or lower layer flow would be blocked when the net flux exceeds -580 $km^3$/yr or 800 $km^3$/yr, in respective directions, the latter estimate being consistent with the results of a two-layer model.

The input into the Aegean Sea by the upper layer flow of the Dardanelles was 1170 $km^3$/yr and the outflow into the Marmara Sea in the lower layer was 980 $km^3$/yr in the years 2008-2009 (Jarosz et al. 2012), amounting to 468 mm/yr and 392 mm/yr respectively, if divided by the area of the Mediterranean Sea (2.5 x $10^{-6}$ $km^2$), and the net flux therefore amounting to 76 mm/yr.

Indirect estimates of the net transport via Bosphorus based on long-term water fluxes and sea-level variations in the Black Sea (Stanev and Peneva, 2002) indicate seasonal anomalies with variations of the order of □75% of the mean, that is considerably larger than the □40 % estimated by Tuğrul et al. (2002) from the seasonal based mass budget. These differences arise from data uncertainties as well as differences in the averaging (monthly versus seasonal) applied to the data. However, both methods yield the same general pattern of seasonal variability.

The measurements of the 2008-2009 campaign with moored instruments indicated much larger ranges of the layer fluxes, deviating by several times the mean values Jarosz et al., 2012). However statistical values such as standard deviation are not given, just because of that, i.e. they would be meaningless when there is such great variability. For the same reason, and because statistical evaluations are not made, it is not possible to estimate mean and variances of heat and salt fluxes.

### 1.4 Bosphorus and Dardanelles Straits

The first scientific study of the Bosphorus Strait by Marsili (1681) in the 17$^{th}$ century established the counter-current of Mediterranean water below the surface flow of Black Sea water (Defant, 1961; Soffientino and Pilson, 2005; Pinardi, 2009), although this fact was first revealed to Marsili by local fishermen, also referred to in the sixth century note of Procopius of Ceasarea (Gill, 1982; Deacon, 1982; and Neumann, 1993) and by Gylii (1561) based on *Anaplous Bosporou* by Byzantios (Gungerich, 1958) as early as 5$^{th}$ century AD, but still until recently debated. Early exploration up to the early 20$^{th}$ century (Makarov, 1885; Shpindler, 1896; Nielsen, 1912; Möller; 1928) established further understanding of the TSS.

Tidal oscillations are exceptionally small, on the order of ~10 cm in the TSS, especially east of the Nara Pass of Dardanelles. Basin oscillations with periods of 2-5 h have been observed in sea level records (Alpar and Yüce, 1998). Coupled Helmholtz mode oscillations of the Black Sea and the TSS (e.g. Ducet et al., 2002) with 14.7 d and 1.9 d periods and a two-layer exchange adjustment time scale of 42 d have been estimated (Özsoy et al., 1998). Current-meters and both ship-mounted and bottom mounted ADCP measurements in the Bosphorus (Pektaş, 1953; De Filippi et al., 1986; Gregg and Özsoy, 1999; Çetin, 1999; IMS-METU, 1999; Özsoy et al., 1998, 2009, 1999; Gregg and Özsoy, 2002; Yüksel et al., 2003; Güler et al, 2006; SHOD, 2009; Jarosz et al., 2011a,b) and Dardanelles (Jarosz et al., 2012) have revealed many different time-scales of oscillations in the TSS, ranging from inertial, semi-diurnal, diurnal to several days periods influenced by the adjacent basins (Yüce, 1993; IMS-METU, 1999).

A sill standing at 60m depth on the canyon cutting across the Black Sea shelf and a contraction in the southern Bosphorus (Latif et al., 1990) are the expected locations of two hydraulic controls, establishing the unique maximal exchange regime of Farmer and

Armi (1986), while a single contraction at the Nara pass subjects the Dardanelles Strait to submaximal hydraulic control (Latif et al., 1990; Ünlüata et al., 1990). The exchange flows in both straits have many small-scale features linked to turbulence, interfacial instabilities, hydraulic transitions and downstream “jumps” revealed by high-resolution measurements (Özsoy et al., 2001; Gregg and Özsoy, 2002).

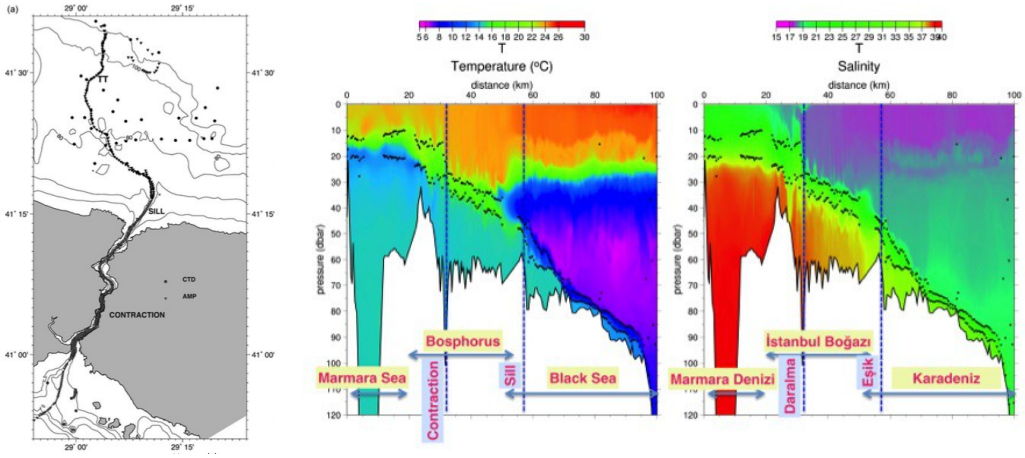


***Figure 4.*** *Locations of the dense profiling network (a) and the continuous distribution of temperature (b) and (c) salinity along the Bosphorus, from Marmara Sea to the Black Sea obtained from 178 profiles. Black dots separate the upper, interfacial and lower layers estimated from salinity profiles (Özsoy et al., 2001).*

The narrow Bosphorus and Dardanelles Straits are frictionally dominated shallow regions with complex topography, where sills and constrictions lead to hydraulically controlled flow. Mixing and entrainment processes in the Bosphorus Strait modify Mediterranean and Black Sea waters during their short but intense encounter in the Strait as shown by the high-resolution temperature and salinity sections through the Bosphorus in Fig. 4 (Özsoy et al., 2001). Hydraulic controls at a sill near the Black Sea exit and a contraction inside the Bosphorus Strait constitute a unique example of the maximal exchange regime, as foreseen by the cardinal work of Farmer and Armi (1986). In contrast, sub-maximal exchange, with hydraulic control at a contraction occurs at the Dardanelles Strait. Short-term, transient responses to meteorological events are frequent, leading to blocked flows in the Bosphorus. The fine scale channel topography plays a major role in the dynamics and determines to which extent the water masses are modified in transit through the system.

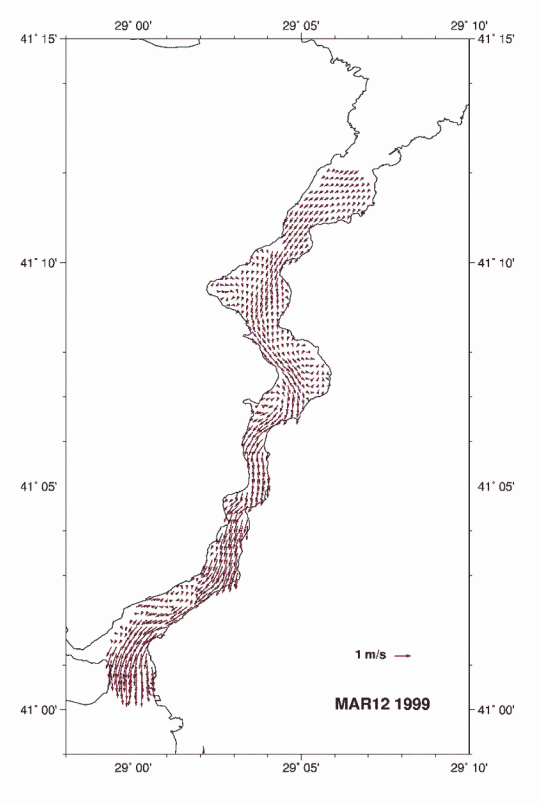
29° 00'
29° 05'
29° 10'
41° 15'
41° 10'
41° 05'
41° 00'
1 m/s
MAR12 1999

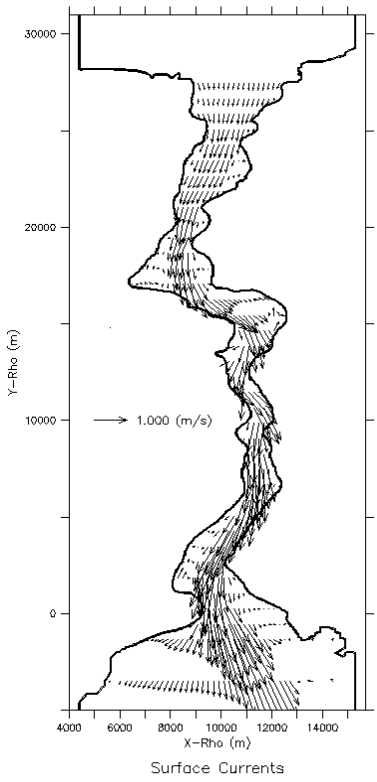
30000
20000
10000
0
Y-Rho (m)
1.000 (m/s)
4000
6000
8000
10000
12000
14000
X-Rho (m)
Surface Currents

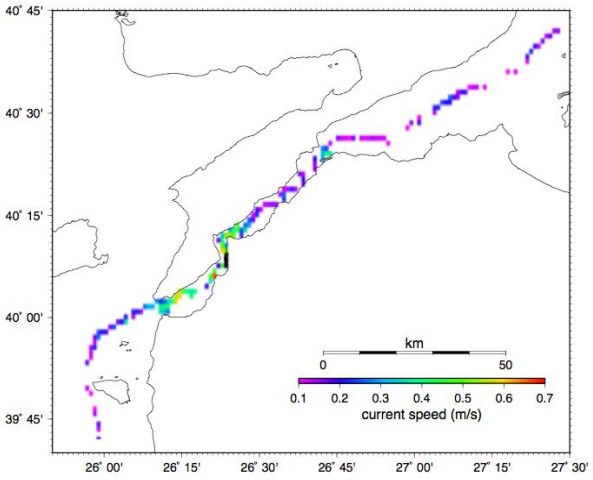
40° 45'
40° 30'
40° 15'
40° 00'
39° 45'
km
0
50
0.1
0.2
0.3
0.4
0.5
0.6
0.7
current speed (m/s)
26° 00'
26° 15'
26° 30'
26° 45'
27° 00'
27° 15'
27° 30'

*Figure 5. Surface currents based on (a) ADCP measurements on March 12, 1999 (interpolated to grid) and (b) obtained from the ROMS model (section 4.1) in the Bosphorus and (c) ADCP current magnitude on March 22, 1999 in the Dardanelles (IMS-METU, 1999).*

The meandering surface currents often exceed 1 m/s past the contraction in the southern Bosphorus (Fig 5a,b) and reach 2-3 m/s at the southern exit. Similarly, surface currents of about 1 m/s occur past the narrows (Nara Pass) of the Dardanelles Strait (Fig. 5c). Such features are evident in current-meter and ship-mounted ADCP measurements (Fig 5a, IMS-METU, 1999; Özsoy et al., 2002), but also in model simulations (Fig. 5b). The last one of these recirculation cells at Beşiktaş, described by Marsili (1681) and Möller (1928), was recognized earlier in *Anaplous Bosporou* of Byzantios ($5^{th}$ century AD) and recorded by Gyllii (1561), who attributed it to the interception of the flow by the protruding Sarayburnu (Byzantion Pt.). The eddy diverted schools of Pelamydes (palamut, bonito) into the Keras (Golden Horn) estuary, caught to benefit the fish trade from ancient until recent times (Bursa, 2010; Tekin, 2010).

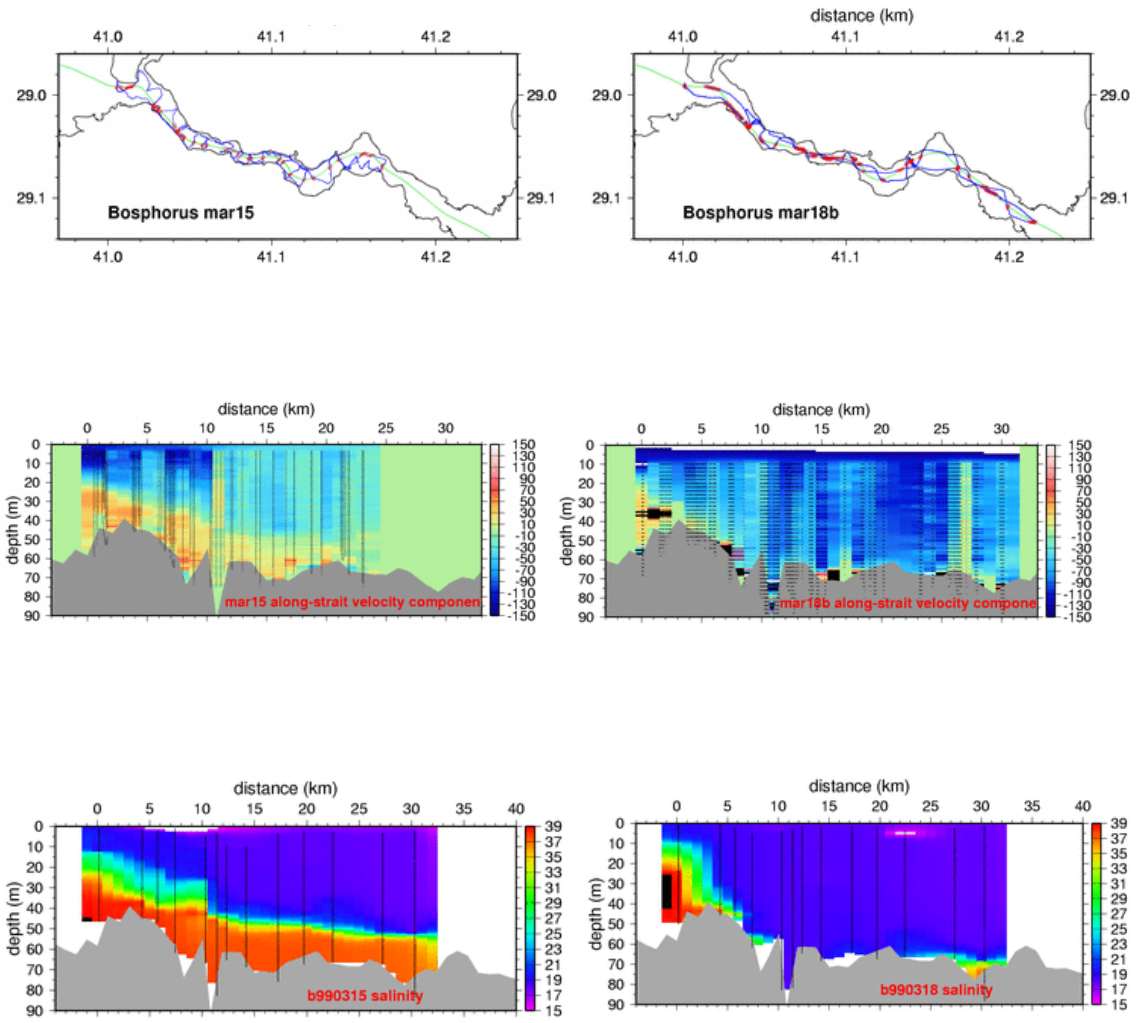


*Figure 6. ADCP current and CTD measurements along the Bosphorus on March 15 (left) and March 18 (right), 1999, top: ship route (blue), the thalweg (green) and ADCP stations mapped (red), middle: ADCP current velocity aligned along the thalweg (cm/s), bottom: salinity at CTD stations projected along the thalweg.*

Short-term blocking of the flows in either layer is a well-known phenomenon in the Bosphorus (Ünlüata et al., 1990; Latif et al., 1991; Özsoy et al., 1995, 1996, 1998, 2001; Özsoy and Ünlüata, 1997, 1998; Jarosz et al., 2011a,b) in response to transient events in the adjacent basins. Oğuz et al. (1990) contended that a sea-level difference of more than 50 cm and less than 10 cm would be needed, respectively for the upper or the lower layers to be blocked, although barometric pressure, winds and net water fluxes of adjacent basins are indicated as dynamical forces creating blocking conditions (Özsoy et al, 1998, Gregg and Özsoy, 1999).

The lower layer is occasionally blocked in spring and summer, with increased Black Sea influx, mostly under the effect of northerly winds. Chosen as examples from the many similar sets of measurements, the March 15, 1999 the ADCP current and salinity vertical sections in Fig. 6 (left) indicate exchange flows across the Bosphorus, with currents of about 0.5 m/s in either layer, the upper layer currents increasing to about 1.5 m/s past the contraction region, where the halocline also becomes thicker. The lower layer was completely blocked on March 18 (Fig. 6, right) after northerly winds, creating southerly currents of 1 m/s almost completely flushing out the Mediterranean water, replaced by Black Sea water. Upper layer blocking events ('Orkoz') coincide with the reversal of the net flow in response to southerly winds ('Lodos') in the fall and winter (Gunnerson and Özturgut, 1974; Ünlüata et al., 1990; Latif et al., 1991), often causing a three-layer situation with the Marmara waters backed up into the strait.

Time series of the bottom-mounted ADCP currents at Baltalimanı, sea level, wind velocity and barometric pressure at stations in adjacent seas (see Fig. 1b) are presented in Fig. 7 for selected monthly periods, to illustrate typical variations in the Bosphorus currents as a function of environmental conditions. During the initial part of the record in Fig. 5a, rather steady currents of 0.5-1.0 m/s are observed in the upper 30m under calm weather conditions. The sudden drop of barometric pressure (30 mb in about 30 h) of an atmospheric disturbance creates temporary reversals in flow direction and subsequent oscillations. The oscillatory and mixing effects created by this particular storm have been likened to a 'meteorological bomb' (Book et al., 2014), based on an extensive set of measurements by Jarosz et al. (2011). Interestingly, the sea level rises in the Marmara Sea and falls in the Black Sea in response to the southwesterly winds of the storm, resulting in a negative sea-level difference of about 40 cm with the Marmara Sea being higher than the Black Sea, as opposed to the positive difference of about 10-50 cm earlier. Sustained northerly winds in January 2010 (Fig. 7b), following an initial period of reversals in the first days, result in the sea level difference building up to about 1m, with currents of up to 2 m/s covering the entire depth, leading to blocking of the lower layer currents.

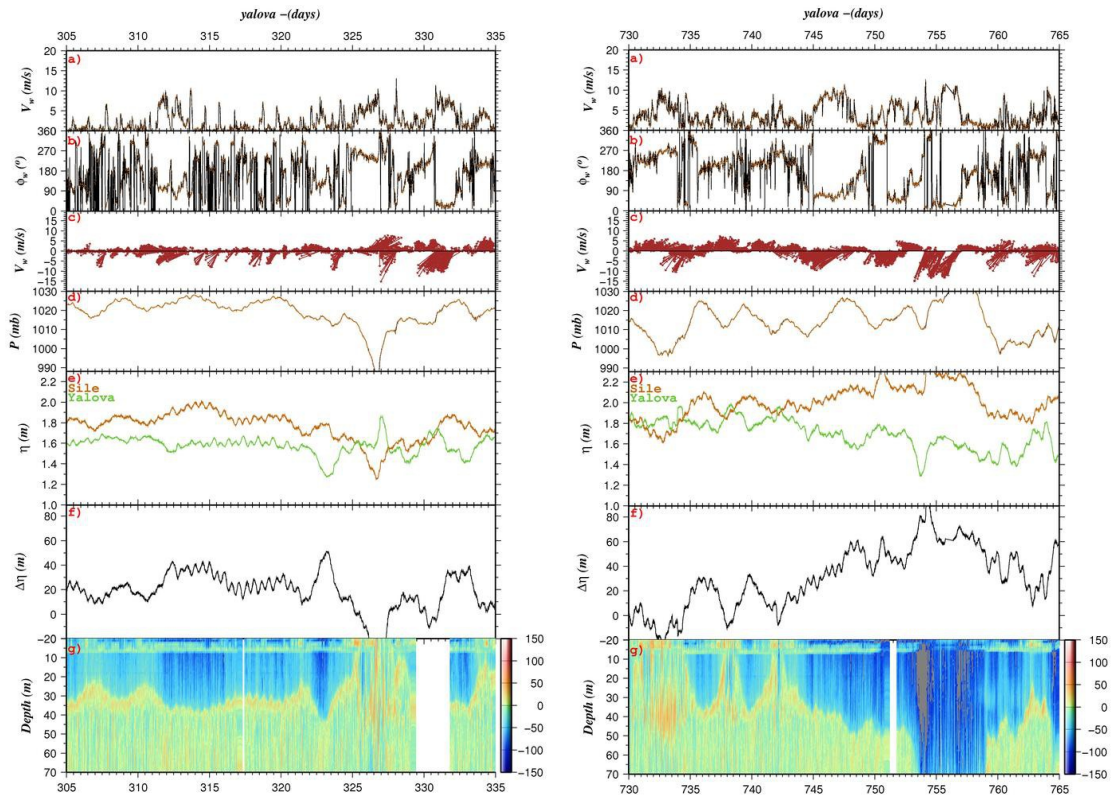


*Figure 7. Monthly time series of wind, pressure, sea-level and ADCP currents in (a) November 2008 and (b) January 2010. In each panel, the wind speed and direction (measured from east), wind vector and barometric pressure at the Yalova station, inverse barometer corrected sea level at Şile (red) and Yalova (green) stations and their differences, the magnitude and sense of ADCP currents in the north-south direction (north is positive) at Baltalimanı are shown from top to bottom (Tutsak, 2013).*

Somewhat similar behavior is expected at the Dardanelles Strait. Under typical conditions represented by 21 May 1987 (Fig. 8, left), the halocline is located at 25 m depth east of the Nara Pass and remains about the same in the rest of the Marmara Sea, but rises sharply at the narrows so that it remains at a depth of about 5-10 m upon exit to the Aegean Sea. The cold intermediate water (Marmara CIW) of about 8°C sneaks in from the east, but terminates past Nara Pass where it encounters intensive mixing.

During the exceptional cold winter of 17 February 1993 (Fig. 8, right), temperatures of less than 4°C are observed, when the upper layer depth increased to 40 m in the eastern part the Marmara Sea in response to wind stirring, decreasing to about 20 m after the Nara Pass where the temperature is increased to about 8°C by mixing with the warmer waters below. The lower layer water entering from the Aegean entrance with a temperature of 12°C terminates at the plunge point at the exit of the strait where it sinks to the depths of the Marmara Sea. While the lower layer salinity is about 38.5 in both dates illustrated above, the upper layer salinity is about 24 near the surface on 21 May 1987, while it increases up to 28 at entry to the Dardanelles and to about 32 at exit into the Aegean Sea on 17 February 1993, as a result of mixing processes.

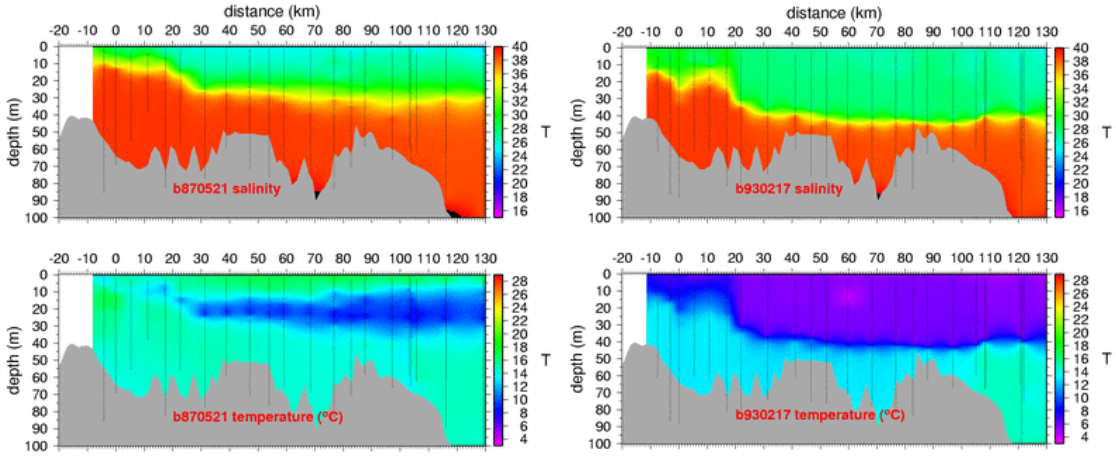


*Figure 8. Salinity (top) and temperature (bottom) on the dates 21 May 1987 (left) and 17 February 1993 (right) in the Dardanelles Strait based on CTD measurements.*

### 1.5 Marmara Sea deep basins and tracers

While the exchange at the Bosphorus Strait drives the surface circulation of the Marmara Sea, the exchange at the Dardanelles Strait determines the fate of its lower layer waters lying below a shallow upper layer of only about 25 m depth. The dense water of Aegean origin flows through a deep channel of about 75m depth along the Dardanelles Strait. The dense water flows along the wide southern shelf in summer and when its density is higher in winter it sinks as a gravity flow to the westernmost deep basin and fills the lower layer of the Marmara Sea (Beşiktepe et al., 1993, 1994; Hüsrevoğlu, 1999;

Staschuk and Hutter, 2001). The inflow of Mediterranean water efficiently ventilated in the Aegean Sea is the only source of oxygen for the lower layer waters of the Marmara Sea because the surface supply of oxygen is intercepted by a very sharp halocline separating the upper layer from the lower (Beşiktepe et al., 1993, 1994).

In the Marmara Sea, the property variations in the lower layer are indeed very small, with typical mean values of about 14.2-14.5 and 38.5 in temperature and salinity respectively, despite some small changes due to long-term instrument and climate drifts. A temperature maximum of 14.5-15°C is often observed at depths of 50-70m, surviving after the summer-autumn influx of the Dardanelles inflow below the halocline. Further below, the temperature monotonically decreases to 14.2-14.3°C at mid-depth. The salinity on the other hand reaches a minimum at about 200m and is either uniform or increases slightly till the bottom (Beşiktepe et al., 1994).

The relatively small but significant changes in the lower layer of the Marmara Sea reflect deep-water renewal processes in the Marmara Sea (Beşiktepe et al., 1993, 1994, 2000). The dense water entering via Dardanelles entrains water and sinks to the depth of equilibrium with the interior. Depending on the initial density contrast Dardanelles and the weak interior density stratification of the interior, the renewal process has inter-annual dependence. A reduced gravity model has shown the influx to reach the bottom of the western basin in winter, later to overflow into the central basin in a time frame of few months. In summer, with a smaller density contrast, the flow is found to first proceed preferentially along the shallow depths of the southern shelf, eventually overflowing into the interior (Hüsrevoğlu, 1999).

CFC-11 below the halocline in Marmara Sea shows two maxima, one up to 300m and the other below 700m depth, confirming the seasonal divergence of the Dardanelles inflow either penetrating deep or staying at intermediate depth in the Marmara Sea (Beşiktepe, 1994). Isotope tracers Oxygen-18, deuterium and tritium (Rank et al., 1998; Özsoy et al., 2002) and Cs-137 (Delfanti et al., 2013) demonstrate interactions between the adjacent basins, making coupled system models (e.g. Maderich, 1998) relevant.

A comprehensive set of data collected during 1990-2001 enables estimation of the nutrient fluxes in Turkish Straits System, based on the annual water fluxes of Ünlüata et al. (1990), later revised on a seasonal basis by Tuğrul et al. (2002). Nutrient exchange

fluxes in the straits vary markedly with season, due to changes in both the concentrations and volume fluxes (Polat, 1995; Polat and Tuğrul, 1995; Polat et al., 1998). During its transit through the Marmara Sea, the dissolved oxygen content of the Mediterranean water decreases to suboxic levels of 30-50 μM, with concomitant increases in nitrate and reactive phosphate by aerobic oxidation of POM snowing down from the productive upper layer. On the other hand, oxygen supply to the suboxic lower layer of the Marmara Sea is limited by the strong density stratification and depends solely on the inputs from the Dardanelles Strait, just sufficient to prevent anoxia from developing in the deep basins as a result of the oxygen consumption.

The mean residence times based on annual volume fluxes have been estimated to be a few months for the upper layer and about 6-7 yr for the lower layer of the Marmara Sea (Beşiktepe et al., 1994), which according to CFC tracer measurements (Lee et al., 2002) has much higher range of 12-32 yr for the 100-450m depth range of their measurements in the eastern basin, estimated from a box model. Based on the same model, oxygen utilization rates of 6–18 μmol $kg^{-1}$ $yr^{-1}$ have been calculated at the particular time of the measurements only in the Straits exits and the eastern deep basin waters adjourning longer (Lee et al., 2002). A simple calculation using an oxygen concentration of 250 μM for the Dardanelles inflow with discharge of 560 $km^3$/yr, 30-50 μM for the average Marmara lower layer volume of about 3.5 x $10^3$ $km^3$, the apparent oxygen utilization rate is found to be about 35 μmol $kg^{-1}$ $yr^{-1}$, which is greater than the above estimate. However, both estimates are subject to a lot of variation accounting for model assumptions, accuracy and seasonal variations of fluxes (e.g. Tuğrul et al., 2002).

Increased winter activity is evident in the upper layer flux of nutrients through the Dardanelles Strait, although the seasonal concentration values are about 20% smaller than the Bosphorus due to consumption in the Marmara Sea, although the net transport is of equal size due to larger water fluxes in the Dardanelles. The salty Mediterranean water enters from the Aegean Sea with very low nitrate and phosphate concentration for most of the year. The lower layer water is then enriched by about 15 to 40-fold (nitrate: 8-12 μM; phosphate: 0.7-1.2 μM) during its residence in the Marmara Sea, finally reaching the Black Sea at similar levels. Because the contribution of particulate nutrients to TN and TP pool in the Marmara lower layer is very small (Polat, 1995, Polat and Tuğrul, 1995; Polat et al., 1998), dissolved inorganic nutrients are dominant in the total N, P export to the Black Sea by the Bosphorus underflow.

Long-term nutrient data obtained in the Bosphorus Strait during 1987-2001, as well as other unpublished data in the 2000-2010 period indicate increased lower layer pools of nitrate and phosphate in the TSS, while the decreased N/P ratio at the same time frame suggests increased denitrification in suboxic waters of the lower layer. Since nitrate and phosphate are excessively utilized by eutrophication in the Marmara upper layer, nutrient discharges to the Aegean Sea occur mostly in dissolved and particulate organic forms (Polat et al., 1998).

### 1.6 Transport effects on Ecosystems and Climate

Material transport between the Mediterranean and the Black Sea takes place in both directions within both the lower and upper layer flows of the TSS and greatly affects the Marmara Sea and the neighboring basins of the Mediterranean and the Black Seas.

A unique opportunity to visualize the detailed strauctures of the surface flows through the TSS and in the adjacent basins is offered by space photographs, notably during the recent International Space Station observations by astronauts. Examples are provided in Fig.s 9-11. In Fig. 9 the Bosphorus surface flows are shown, with the southward flow issuing into the Marmara Sea in the form of a jet. This jet flow then spreads into the Marmara Sea as shown in Fig. 10. The remarkable picture in Figure 11 shows flows of material originating from the Black Sea coast (near the planned new site of the 3$^{rd}$ airport of İstanbul) entering the Bosphorus and reaching the Marmara Sea in the form of a surface jet, which then curls towards the cape of İnceburun.

Figure 9. The Bosphorus and the surface flow of Black Sea water as seen by astronaut Chris Hadfield aboard the International Space Station, 7 July 2013. https://twitter.com/Cmdr_Hadfield/status/350012636345270272/photo/

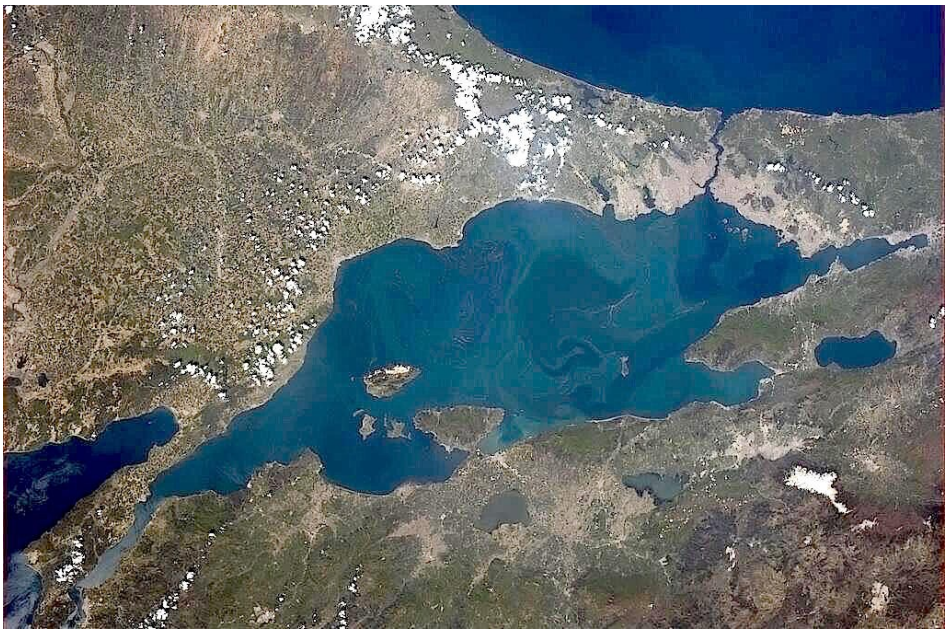

Figure 10. Marmara Sea as seen by astronaut Chris Hadfield aboard the International Space Station, 30 April 2013.
https://twitter.com/Cmdr_Hadfield/status/329139344411619328/photo/1

*Figure 11. The Bosphorus and the eastern part of the TSS as seen by astronaut Samantha Cristoforetti* aboard the International Space Station*, 9 June 2015. https://twitter.com/astrosamantha/status/608197918395400192*

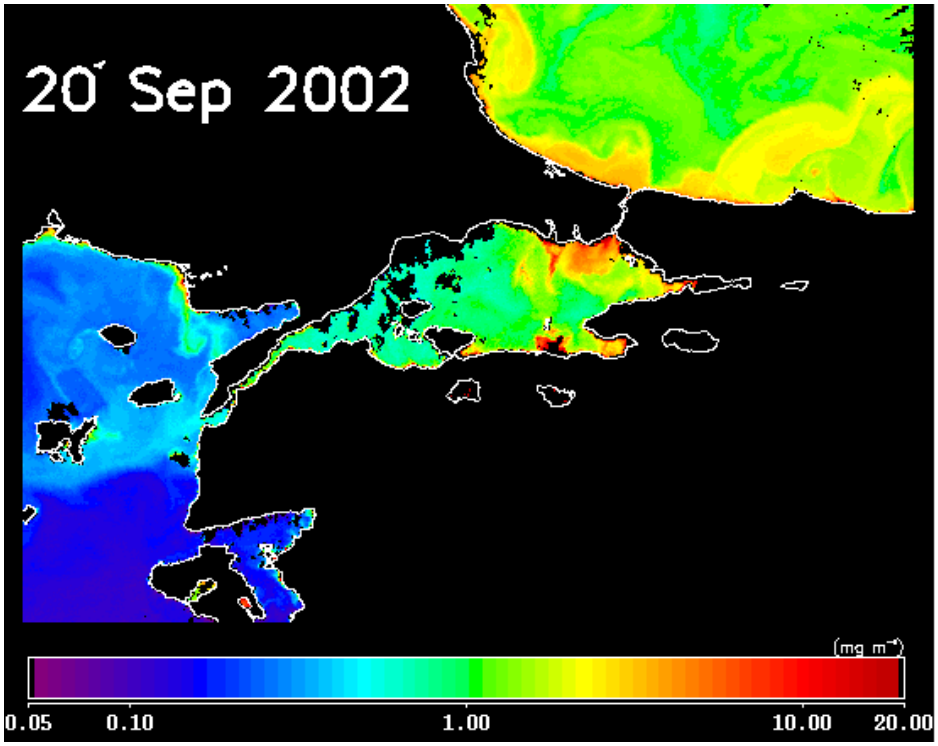


*Figure 12. Satellite images showing the interaction of the Turkish Straits System with the neighboring seas: (a) chlorophyll distribution on September 20, 2002, (b) MODIS aqua*

*image showing an ongoing Emiliana huxleyi bloom on June 23, 2003 (http://disc.sci.gsfc.nasa.gov/oceancolor/additional/science-focus/ocean-color/marmara.shtml).*

Significant mixing occurs inside the Straits and further by surface buoyant jets upon exit to the wider sea regions from the two Straits. The surface plumes carrying relatively fresh water and chemical / biological signatures from their sources affect material cycling in the target basins not only through transport, but also as a result of efficient turbulent mixing and entrainment in the exit regions. Interfacial mixing at the straits and jet mixing near their exit regions yield the highest horizontal rates of change in properties within the TSS (Fig. 12) and largely determine the cycling of matter and biological productivity of the confined waters of the Marmara Sea; a fact emphasized earlier by Ünlüata et al. (1990) and Beşiktepe et al. (1994),

The nutrient transport across the TSS (Polat and Tuğrul, 1995; Tuğrul et al., 2003; Tuğrul and Beşiktepe, 2007) fuels the interactions between ecosystems of the neighboring seas. Surface chlorophyll variations across the TSS are exemplified in Fig. 12a, where the transport and local variations from the Black Sea to the Aegean, via jets created at the exits of the Bosporus and Dardanelles are indicated. In Fig. 12b, a phytoplankton bloom in the Marmara Sea (Coccolith Emiliana huxleyi, well known for its turquoise blue colour) follows after a similar bloom occuring earlier in May. The observed event is part of the Marmara local primary production process and the dark color of the current flowing in from the Bosporus exit is the Black Sea water. Finally the bloom formed in the Sea of Marmara reaches the Aegean Sea with a jet flow exiting the Dardanelles Strait.

Significant changes have occurred in our lifetime in the ecological status of the TSS, and mainly after the 1960's industrialization and population expansion. The eutrophic Marmara Sea waters fed by Black Sea nutrients (Polat and Tuğrul, 2005), as well as the efficient jet induced local recycling makes this small basin a region of high productivity often far exceeding the Black Sea (Fig.13), with increasing occurrences of mucus and harmful algae blooms (Fig. 14, 15). The plans for what is often inappropriately called as 'development' pose increasing risks of ecosystem crises and failures in the TSS, with implied effects on adjacent basins, as many signs of deterioration are already easily discernible.

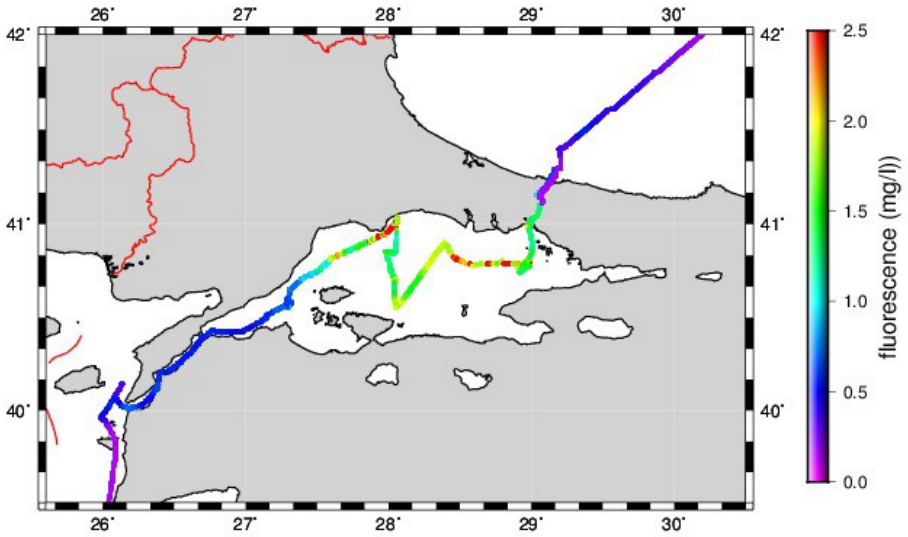


*Figure 13. Chlorophyll concentration on the course of R/V BİLİM during April 2008.*

Migration of live fish between the two seas and local production invites intense fishing activity, and the pressures of the highly populated and industrialiized coastal environment implies that the marine life is adversely affected by excessive pollution, especially in the breeding period of fish.

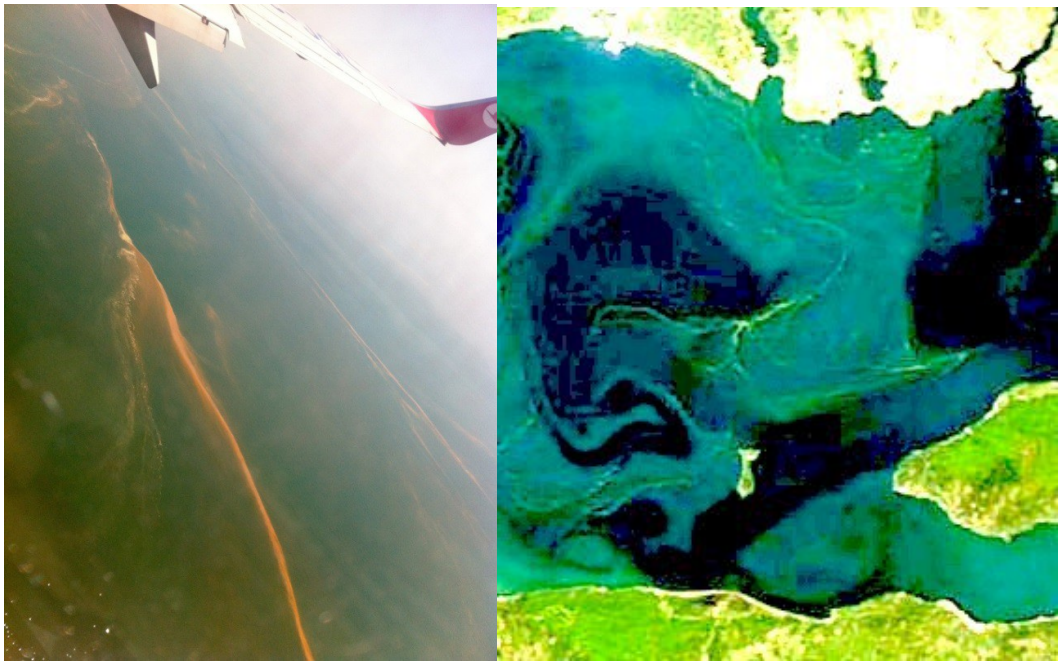

*Figure 14. Harmful algal blooms observed (a) near Tekirdağ; Milliyet, 24 April 2013 (b) from a flight over the Marmara Sea on 28 April 2013 (Photo: Dr. Bettina Fach, IMS-*

*METU), (c) MODIS ocean colour image on 25 April 2013, (all in the same period as observed by Chris Hadfield in Fig. 10) showing the Bosphorus jet (black) surrounded by coccolith (green) and harmful plankton (orange) blooms.*

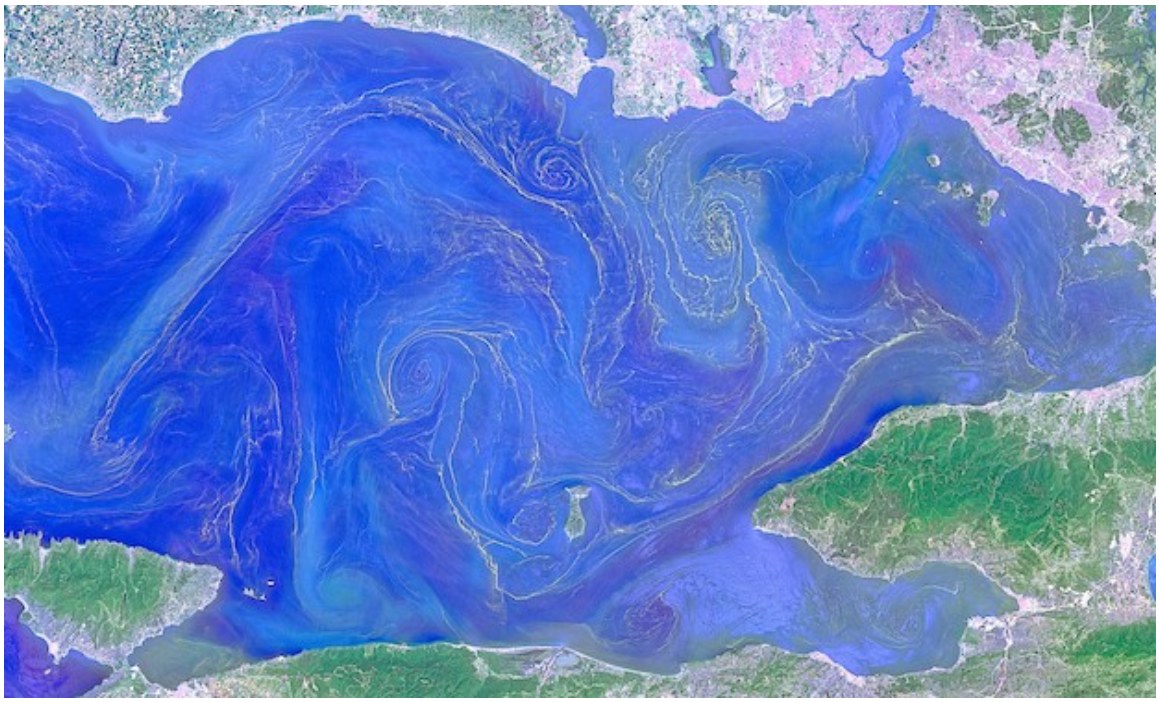

*Figure 15. (a) Image from NASA Earth Observatory, Spiral eddies, jets and dinoflagel-*

*late blooms (red tide) in the Marmara Sea, 17/05/2015 http://earthobservatory.nasa.gov/IOTD/view.php?id=85947&eocn=image&eoci=related_image, accessed June 2015), (b) local aerial picture of the coastal area of the Marmara Sea south of İstanbul, showing the same bloom published in the daily journal Milliyet on 20/05/2015 (http://www.milliyet.com.tr/marmara-iste-boyle-oluyor-gundem-2061522/).*

The hydrological regime, circulation, ecosystem and tectonics, all display extremes in the region. The great transformations of the system between fresh water lake and sea basin are well known (Yanko-Hombach et al., 2006), with projected impacts on human societies (Ryan et al, 1997; Runnels and Özdoğan, 2001; Turney and Brown, 2007). Climatic changes with rather short cycles of about 150-300 year periods are recorded in the bottom sediments of the Black Sea (Hay and Honjo, 1989). Large-scale climate patterns such as the NAO, NCP and Indian Monsoons have great regional importance (Gündüz and Özsoy, 2004; Lionello et al., 2006), with impacts on ecosystems (Oğuz, 2003). Yet it is not known what kind of risks are posed on the region by the present trend of global warming, combined with extreme weather, floods, earthquakes, especially as İstanbul, already a monster of a city, heads for further expansion, determined to destroy its remaining vital resources.

## 1.7 Influence of the TSS exchange on the Black Sea

The influence of the dense water outflows from the Bosphorus Strait onto the Black Sea continental shelf have been examined by Latif et al. (1991), Di Iorio, and the Yüce (1999), Gregg et al. (1999) and Özsoy et al. (2001). The main features of this flow past the northern sill of the Bosphorus and through the canyon cutting through the continental shelf have been well reproduced (Figure 16) in the reduced gravity flow model of Özsoy et al. (2001) and also have been compared with measurements. The flow loses much of its energy through a hydraulic jump immediately past the sill at 60 m depth. The warm saline Mediterranean water is rapidly diluted by intense mixing in the exit region and spreads as a thin layer on the the continental shelf where it is cooled and diluted by being inluenced by the Cold Intermediate Water (CIW) of the Black Sea, finally reaching the shelf edge partially overflowing the various capillary channels. The flow is acceler-

ated by the sudden deepening at the shelf edge, introducing rapid entrainment of Black Sea water into the gravity flow sinking along the continental slope.

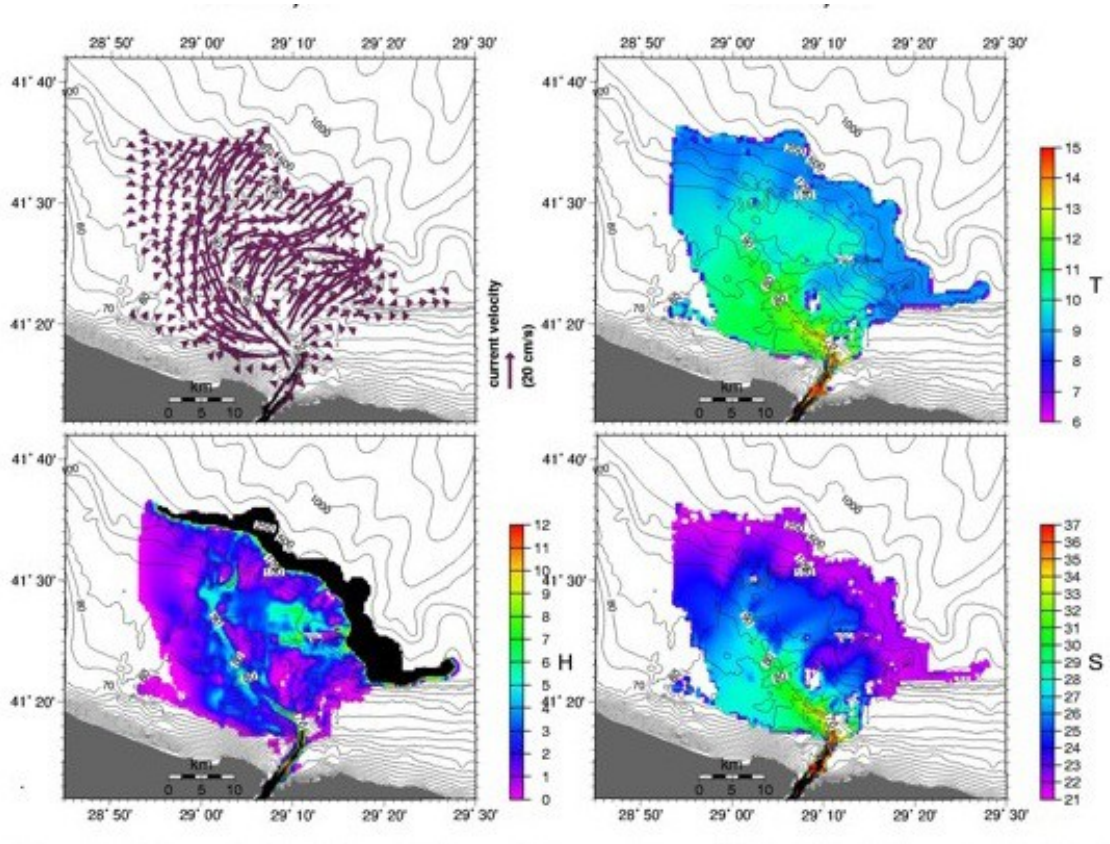


*Figure 16. Features of the dense water outflow at the northern exit of the Bosphorus and the Black Sea continental shelf obtained from a model of the gravity flow by Özsoy et al., 2001: (a) discharge rate, (b) layer thickness (c) temperature, (d) salinity.*

The introduction of the 'Mediterranean effluent' into the Black Sea in the form of a dense water outflow first spreading on the continental shelf and then intruding into the deeper layers along the continental slope has important inluences on the circulation and mixing of the Black Sea. In addition to physical influences, this process has important environmental consequences since the introduction of large volumes of an external water mass into this closed sea carries with it material properties and the sediment and contaminant signatures it has acquired though its history past the TSS and along the shelf. The dense water cascading from the continental shelf sinks to intermediate depths below the pycnocline into the anoxic layer of the Black Sea and is moved eastward by the cyclonic circulation of the Black Sea, its intrusions and horizontal spreading at depth creating convection and intrusive mingling of the different water masses. The physical and hydrochemical impacts of the intruding waters can be traced throughout the southwestern Black Sea up to a depth of 500m (Özsoy et al., 1993, 2001; Özsoy and Beşiktepe, 1995).

The gravity flow of dense water with newly acquired temperature and salinity characteristcs contrasts with the ambient waters, forming a lateral sources of heat and salt along the continental slope, at depths of 100-200m in particular. This brings the Black Sea waters under the influence of double diffusive convective instabiliies that partially serve for the maintenance of the Black Sea stratification (Figure 17a, b) and the thermohaline circulation (Özsoy et al., 1993, 1994, 1996; Özsoy and Beşiktepe, 1995; Özsoy and Ünlüatq, 1997, 1998). The sinking of anomalous dense waters modified on the continental shelf to intermediate depths below the halocline influences the Black Sea waters up to depths of 500 m, carrying with them the oxygen, sediment, contaminants and radioactive elements originating from the upper ocean (Buesseler et al., 1991, Özsoy et al., 1993). Based on the latest measurements in 2007-2008, Delfanti et al. (2013) found rapid deepening of $^{137}Cs$ isotopes (Figure 17c) used as a tracer of the Chernobyl event, leading to significant transport across the Black Sea halocline by entrainment into the cascading effluent along the adjacent Black Sea shelf and continental slope (Özsoy et al., 2001, Stanev et al., 2001). This mechanism implies a 'strait pump' that carries material (carbon, nutrients, tracers and dissolved oxygen) across the halocline from the surface to deep waters in the Black Sea, thus modifying its internal structure as suggested by Özsoy et al. (1993), Özsoy and Ünlüata (1997, 1998)

and Tuğrul et al. (2013). Oxygen, deuterium and tritium isotope measurements have shown that trace substances including those of of atmospheric origin could not penetrate to depths greater than 500m despite being introduced below the halocline by the Bosphorus intrusions. The same measurements have alo been used to determine fluxes through the TSS (Rank et al., 1998; Özsoy et al., 2002).

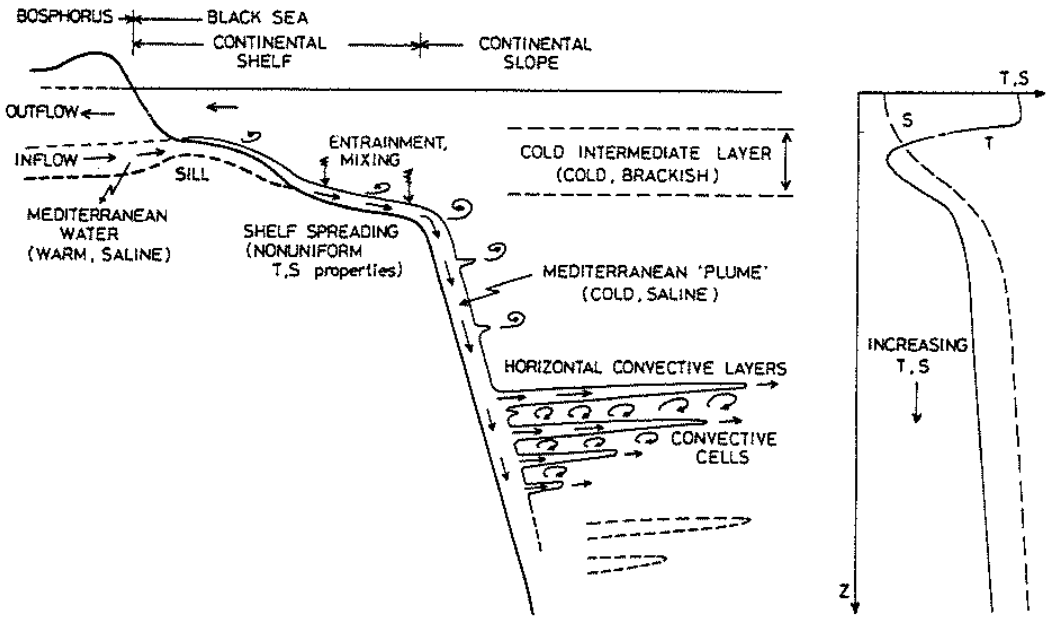
BOSPHORUS
BLACK SEA
CONTINENTAL SHELF
CONTINENTAL SLOPE
OUTFLOW
INFLOW
SILL
ENTRAINMENT, MIXING
COLD INTERMEDIATE LAYER (COLD, BRACKISH)
MEDITERRANEAN WATER (WARM, SALINE)
SHELF SPREADING (NONUNIFORM T,S properties)
MEDITERRANEAN 'PLUME' (COLD, SALINE)
HORIZONTAL CONVECTIVE LAYERS
CONVECTIVE CELLS
T,S
S
T
INCREASING T,S
Z

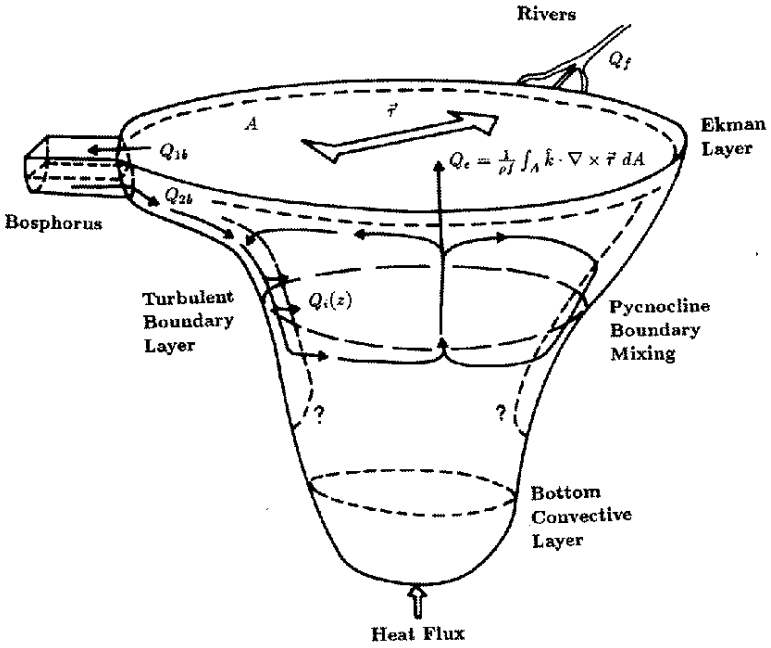
Rivers
$Q_f$
$A$
$\vec{\tau}$
$Q_e = \frac{1}{\rho f}\int_A \hat{k}\cdot\nabla\times\vec{\tau}\,dA$
Ekman Layer
$Q_{1b}$
$Q_{2b}$
Bosphorus
Turbulent Boundary Layer
$Q_t(z)$
Pycnocline Boundary Mixing
?
?
Bottom Convective Layer
Heat Flux

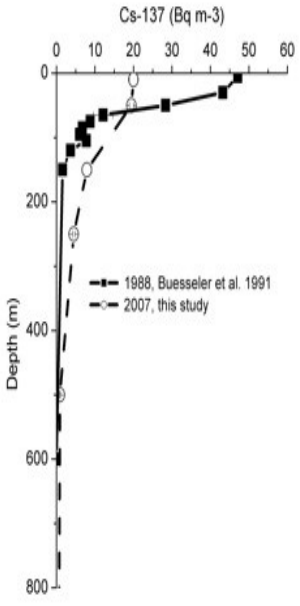
Cs-137 (Bq m-3)
0
10
20
30
40
50
60
0
200
400
600
800
Depth (m)
1988, Buesseler et al. 1991
2007, this study

*Figure 17. The effects of Bosphorus dense water outflow to the Black Sea. (a) intrusions along the continental slope created by the double-diffusive convective motions (b) the thermohaline circulation induced by the intrusions penetrating into the Black Sea (Özsoy et al., 1993), (c) the changes in the Black Sea $^{137}$Cs profiles observed between 1991 and 2007 (Delfanti et al., 2011).*

In experiments conducted during the relatively quiescent summer conditions, Gregg and Özsoy (1999) found very low levels of turbulence, which implied that internal mixing by internal wave breaking or tidal mixing mechanisms were not sufficiently energetic in the Black Sea, as a consequence of a very low tidal amplitude. The intrusive effects of the waters originating from the Bosphorus, in addition to whatever influence that the surface winds impart on the upper layers of the basin waters therefore turns out to be the most effective two mechanisms creating mixing in the Black Sea.

The Black Sea has an active surface circulation (Sur et al, 1994, Özsoy and Ünlüata 1997, 1998). This circulation transports the relatively brackish water originated from the large rivers Danube, Dnieper, Dniester in the north attached to the coast along the shallow western continental shelf, while interacting with the rim-current (Fig. 18). The mixing of nutrients originating from the rivers, and oxygen, chlorophyll, pollutants, sediment, and other materials transported by the currents and their mixing and entrainment into the Bosphorus induced density currents by further dispersion determine Black Sea chemical structure, mixing and biological production mechanisms.

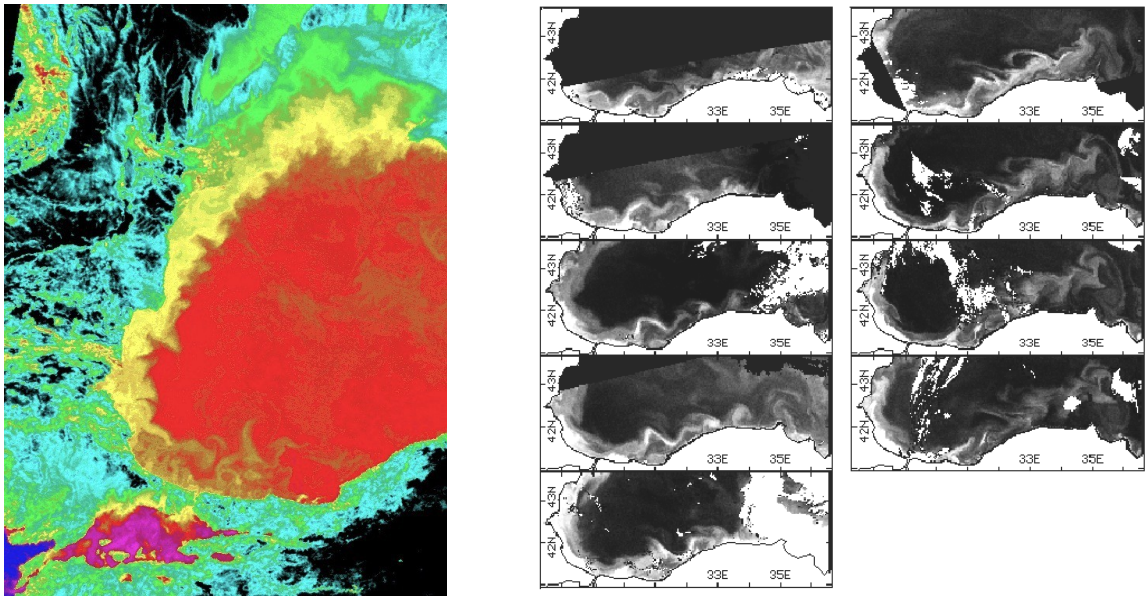


Figure 18. Examples of Black Sea property distributions in relation to its circulation, based on data from NOAA satellites: (a) February 28, 1980 surface temperature (Özsoy and Ünlüata, 1998), (b) changes in surface temperature in response to evolving coastal currents during a period of about 15 days (Sur et al., 1994).

Review of historical data from the western Black Sea (Sorokin, 2002) and the river Danube (Cociasu et al., 2008) indicates increased nitrate and phosphate (DIP) inputs to the NW Black Sea after the 1970's. The riverine inputs to the Black Sea (with high N/P ratios) reached maximum levels in the late 1980's, followed by a gradual decrease since the mid 1990's (Ludwig et al., 2009). These changes similarly influenced contributions to the upper layer TN, TP pools of the western Black Sea and the exports by the Bosphorus (Polat and Tuğrul, 1995; Sorokin, 2002); thereby enhancing the eutrophication in the Marmara Sea (Polat et al., 1998), increasing the nutrient stocks and creating suboxic conditions in the lower layer much different from the "pristine" state of

the sea, consequently leading to the enhanced nutrient and reduced oxygen contents exported by the Bosporus underflow back to the Black Sea.

Being a closed basin receiving large amounts of freshwater from major rivers, the Black Sea exhibits a strong density stratification and has quite unique hydrological and biochemical properties. Anoxic deep waters underlie a relatively small upper layer where oxic conditons exist. Below 100 m depth, hydrogen sulfide replaces oxygen and a suboxic transition region separates the two regions. Vertical distributions of nutrients, oxygen and redox-sensitive metal concentrations extending from the surface to slightly below the transition region have shown significant changes since the rapid industrialization period, especially after the 1970s (Tuğrul et al., 2011). Although the starting depth of the sulfated waters have not changed since the 1970s, the suboxic zone has greatly expanded near the center of the basin, the depths of the nitrate maximum and phosphate minimum, the starting depth of Mn (II) and the depth of the particle Mn maximum have decreased. A major cause underlying these changes is percieved to be the changes in nutrient contents of the major rivers such as the Danube. As a result, the nitrate inventory of the Black Sea has increased by 2-4 times as compared to the pre-1970 concentrations, while the silicate inventory in the upper waters has decreased significantly and the phosphate inventory has remained almost the same. As a result, the N / P ratio which used to have a very low value in the surface waters has, while the Si / N ratio formerly with higher values has decreased.

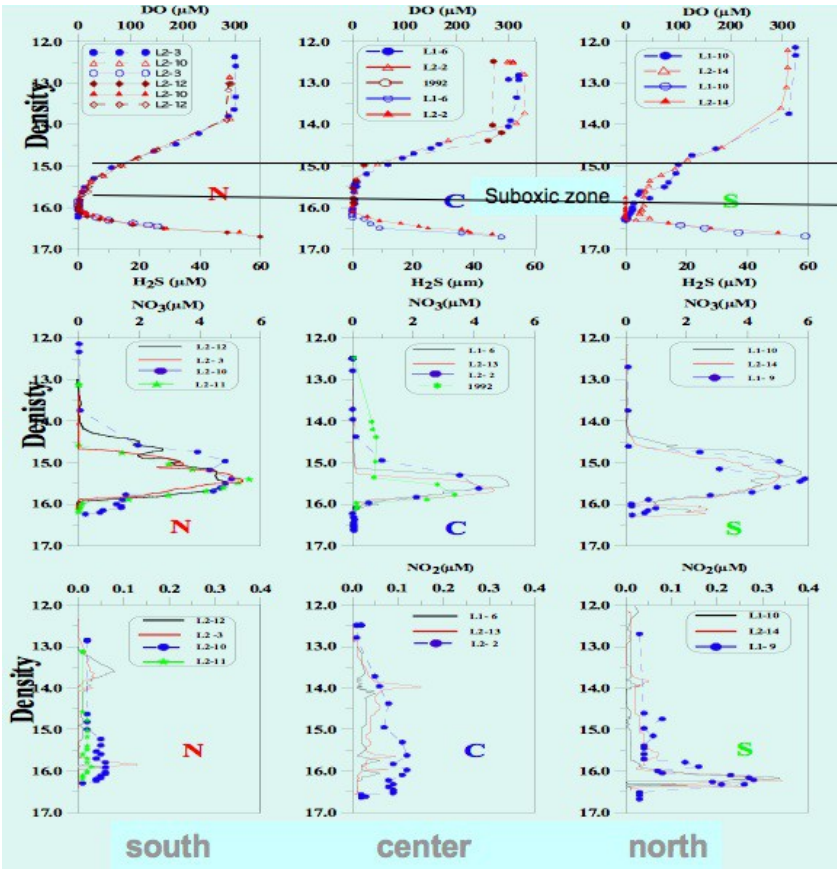


*Figure 18. Chemical profiles in the southern, middle and northern Black Sea regions (Tuğrul et al., 2011).*

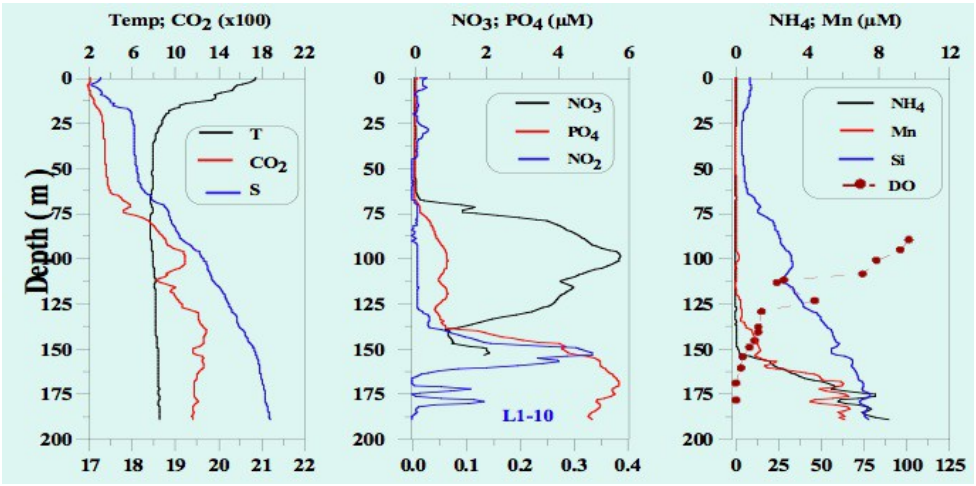


*Figure 19. Chemical profiles in the southwestern Black Sea near Istanbul Strait (Tuğrul et al., 2011).*

Spatial variations have occurred in characteristics of nutrients and the suboxic zone in response to these changes (Fig. 19). Especially in the southwest region of the Black Sea coast, the distribution of materials is greatly affected by the sinking of water entering form the Bosphorus Strait (Fig. 20). In this region, the oxygenated water penetrating below the halocline into the anoxic zone is immediately reduced, but the sulphide layer is pushed deeper, often indicated by a secondary oxygen peak, and also evident in Mn (II), nitrate and ammonia profiles, inducing short-term variations. Similar effects in other trace materials have been demonstrated by Özsoy et al. (1993).

### 1.8 Modeling of the TSS exchange

Constructing a model of the entire TSS uniformly representing the rich diversity of observed hydrodynamic processes in this small domain of complex geometry has been a most demanding undertaking. This is why only simplified models have been attempted in the past. The strong topographic control, non-linear hydrodynamics, strong stratified turbulence, hydraulic controls, separated flows, multi-scale interactions, turbulent mixing and entrainment processes make modeling of the TSS, a ***grand challenge*** in oceanography and a formidable problem far beyond reach of most of the present day ocean models.

The immense computational power requirements for addressing the coupling between the straits and the three adjacent basins in the past has only been addressed by a series of simplified models of the individual elements of the system. Two-layer, one-dimensional or two-dimensional models solving either horizontally or vertically integrated hydrodynamic equations have been developed for the Bosphorus (Oğuz et al., 1990; Ilıcak et al., 2009) and Dardanelles (Oğuz and Sur; 1989; Staschuk and Hutter, 2001) Straits. Three-dimensional models solving the full set of primitive equations have also been developed for the Bosphorus Strait (Sözer and Özsoy, 2002; Oğuz, 2005) and Dardanelles (Kanarska and Maderich, 2008) Straits. Some observed features, including the blocking and hydraulic transitions of the flow (Latif et al., 1991), sharp changes of the free surface at the contraction (Gregg and Özsoy, 1999, 2002), and the separation of the zero-velocity line with the pycnocline (Tolmazin, 1985; Gregg and Özsoy) (1999) have

been demonstrated by some of the above models, which however are far from being fully representative of the coupled dynamics of the TSS in an integrated way.

## 2. METHODOLOGY

### 2.1 TSS and Black Sea Shelf Experiment

In the experimental part of the project a detailed oceanographic survey of the Turkish Straits System (TSS) and the Black Sea continental shelf / slope has been designed and executed. The experiment has been designed to sample along the whole TSS region including the deepest locations along the main thalweg and at various cross-sections in the Sea of Marmara, in the Bosphorus and Dardanelles Straits, and also along and across the various canyons and offshore of them on the Black Sea continental shelf / slope. The objective for the TSS experiment was to capture the post-spring re-stratified conditions in the system, while the objective for the Black Sea experiment was to capture the existing conditions on the shelf and slope regions while following the fate of the Mediterranean effluent as it flows through the shelf and canyons to reach the basin with an eye on the transport characteristics.

Observation data on physical and chemical variables in the region have been collected on board the R/V BİLİM during 18 June – 06 July 2013. The stations occupied by R/V BİLİM and the bathymetry are shown in Fig.s 20-22.

The equipment used on board the R/V BİLİM included the following:

SBE 911 Plus and SBE 16 CTD systems
(standard CTD sensors, DO, fluorometer, transmissometer)
Rosette sampler with 12 bottles
5lt Nansen sampler bottles
30lt Nansen sampler bottles
Ocean Surveyor ADCP
Turner Designs fluorometer and pumps
Simrad scientific echosounder
Autoanalyzer set
Winkler titration system
Ph-meter
Vacuum pumps and filtering systems
Hydrographic winches
Computers and printers

Temperature, salinity profiling at stations has been carried out with the SBE 911 Plus CTD system, while continuous velocity profiling has been carried out with the vessel mounted RD Instruments Ocean Surveyor 150Khz ADCP system. Continuous chlorophyll sampling was done with the Turner fluorometer sampling temperature and chlorophyll from a pumped water system. Water samples obtained with a Hydro Products rosette sampler were then used for laboratory analysis of chemical parameters: nutrients, DO, H2S, suspended matter. Chemical measurements in the point designated in this station network by applying international standard methods (Grasshoff et al., 1983). Furthermore, seawater samples were obtained from intermediate depths and analysed for particulates whereever fine particulate matter of slow deposition rates was observed.

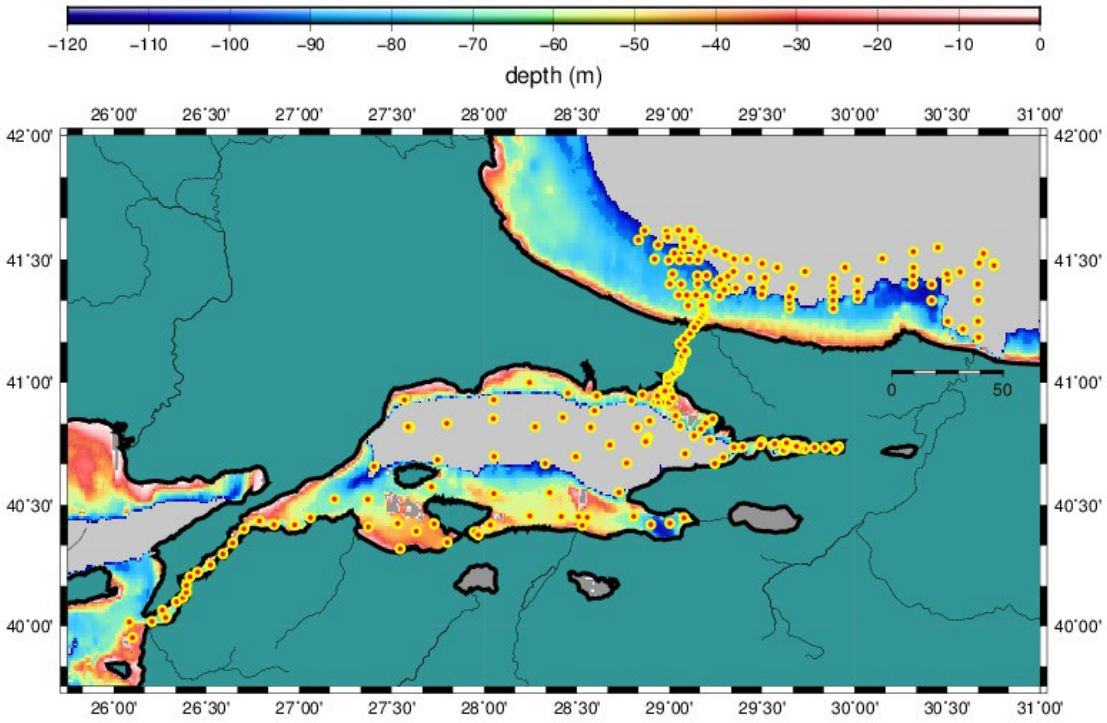


*Figure 20. Oceanographic stations occupied by R / V BİLİM during the 18 June - 6 July 2013 Turkish Straits System (TSS) and the Black Sea continental shelf / slope experiment. Bathymetry is shown only for the shelf areas (0-120m depth range).*

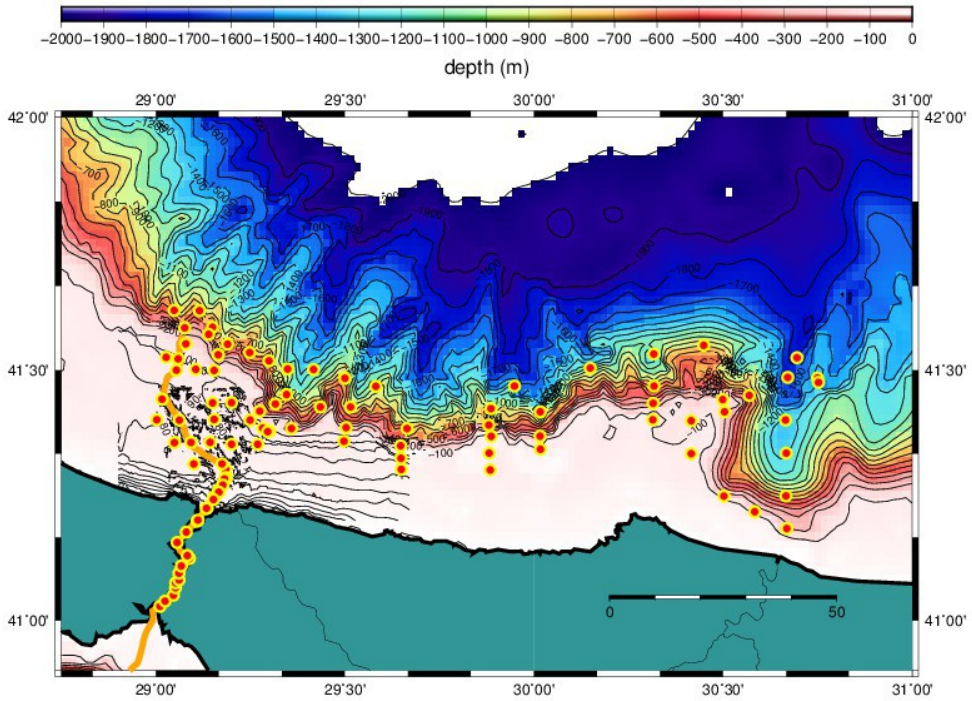


*Fig 21. R/V BİLİM stations in the Black Sea continental shelf / slope region visted during the 28 June - 6 July 2013.*

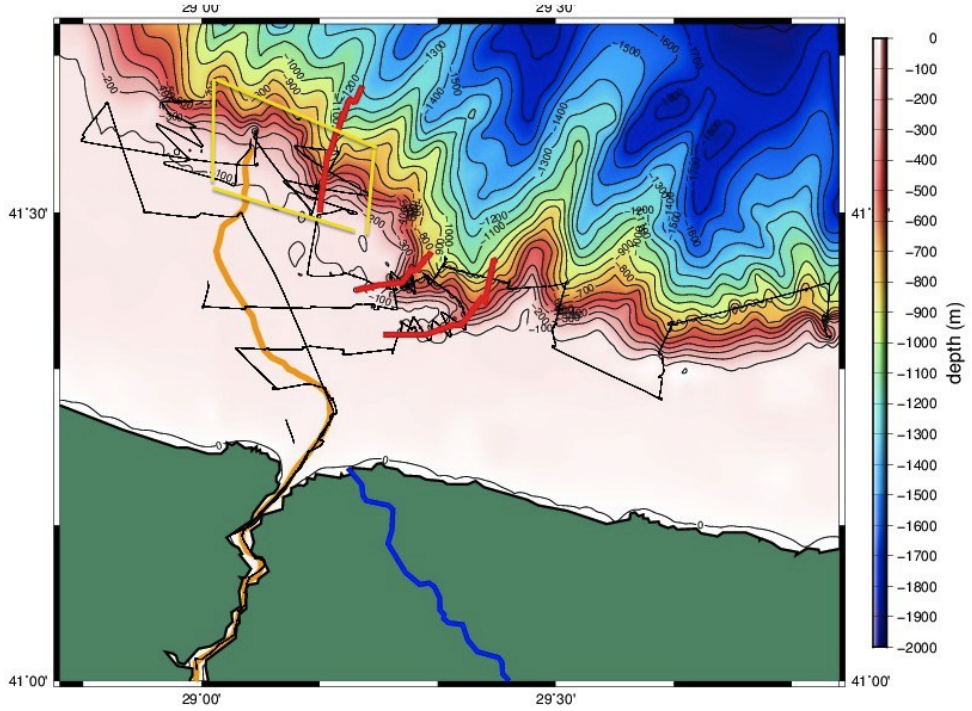


*Fig 22. R/V BİLİM bathymetry sections and main outflow canyon section in the Black Sea continental shelf / slope region.*

The research vessel R/V BİLİM finished work in the Dardanelles Strait during 18-19 June 2013 and moved to collect data in the Marmara Sea during 19-23 June, with data obtained in the Bosphorus Strait on 23 June, having obtained data in a total of 73 stations within the TSS during this part of the cruise.

The cruise in the southwestern Black Sea was started on 28 June, after a break due to stormy weather. However a further break was enforced by bad weather on 29 June, and the study was continued after 2 July, ending up on 6 July, when data were collected at a total of 164 stations covering the Black Sea continental shelf and continental slope region adjacent to the Bosphorus, including the sill region at the exit of the Bosphorus and the various canyons on the shelf / slope region.

In addition to the R/V BİLİM, through the collaboration and coordination developed before the cruise, a second ship R/V PELAGIA collected seawater oceanographic data as well as echosounding and sampling data on bottom features of the various canyons and bottom features in the exit region of the Bosphorus outflow. The cooperation for the joint expedition of the two ships R/V BİLİM and R/V PELAGIA was developed between University of Leeds and the IMS-METU. Communication that has been continued with Prof. Jeff Peakall ve Prof. Dan Parsons and a visit to England by Prof. Emin Özsoy culminated in a joint cruise plan using both ships during the planned period. In addition, the University of Leeds scientists have visited the IMS_METU during 30 to 31 January 2014 for the first archiving and joint evaluation of the data.

### 2.2 Model Development

#### 2.2.1 Data sources used for modeling

Consistent observational data sets covering the TSS have been collected with the R/V BILIM of the IMS-METU during 1985-2001 and sporadically in many other scientific cruises since then. Detailed mapping of the Bosphorus currents and hydrography was undertaken in 1998-1999 for the TURBO administration, when detailed ADCP and CTD measurements were extended to small bays and bends using a small diving boat, Atmaca II. Recent measurements have been acquired from automated coastal meteorology, sea level and ADCP stations (http://moma.ims.metu.edu.tr) operated under

a coastal network (Özsoy et al., 2009). Further detailed measurements were obtained during the recent SESAME European project in an unprecedented collaborative sampling of the Mediterranean and Black Seas. The data obtained during the present Project in June – July 2013 has been used to initialize fine resolution models used in the Project.

The high-resolution (20 m gridded) bathymetric data used for Bosphorus and Dardanelles hydrodynamics models have been kindly made available by our late colleague Erkan Gökaşan (Gökaşan 2005, 2007) with the permission of the Turkish Navy, Navigation, Hydrography and Oceanography Office.

### 2.2.2 ROMS Model for the Bosphorus Strait

Model development for the Bosphorus Strait has initially been started outside the Project, as a PhD thesis by Adil Sözer, who has continued his work towards completion during the Project.

The modeling of the Bosphorus Strait hydrodynamics is based on the ROMS, a well-documented and tested community model (Hedström, 1997; Haidvogel et al., 2000; Shchepetkin and McWilliams, 2005) allowing selectable options of higher-order advection and turbulence closure schemes, with compatible boundary conditions. There are two different versions of the model used for the Bosphorus: (i) an idealized geometry version only used for the analysis of model sensitivity, (ii) a realistic geometry version with full topography to study the response of the Bosphorus Strait. Extensive work accomplished on the sensitivity tests and dynamical behavior of the model is described in the PhD thesis (Sözer, 2013).

The idealized geometry of the Bosphorus Strait (Fig. 23) is a straight channel ~34 km in length, 70m in depth and 1300 m in width, with a contraction of 700 m width located at one-third of its length and a sill of 500 m length and 57 m depth at the crest located near the lower density end of the strait. The model domain is a 55x512x35 rectilinear grid of $\Delta x = \Delta y$ = 100 m with variable vertical spacing of $\Delta z$ = 1.42 - 2.0 m in generalized s-coordinates. The model is integrated with a baroclinic time-step of $\Delta t_i$ = 3.5 s, while the external or barotropic time-step $\Delta t_e$ is usually set to a value 20 times smaller. For

reduced computational cost and simplicity, only salinity effects on density are considered in the idealized geometry case, and the model is initialized with a lock-exchange configuration of uniform salinity values 38 and 19 respectively in the southern and northern halves of the strait. Constant horizontal and vertical diffusivity values of $\mathbf{K_h}$ = 15 m/s$^2$ and $\mathbf{K_V}$ = $10^{-4}$ m/s$^2$ are respectively used for momentum and tracers. The no-slip boundary conditions at the sidewalls and quadratic bottom friction (RDRG2 = 0.005) are employed. The recursive MPDATA advection scheme is used to minimize over/under shooting often resulting in the presence of sharp gradients. Radiation boundary conditions are specified for 3d variables at the open boundaries, while the north-south barotropic velocity and the gradient boundary conditions for the other 2d variables are specified at the two ends of the strait.

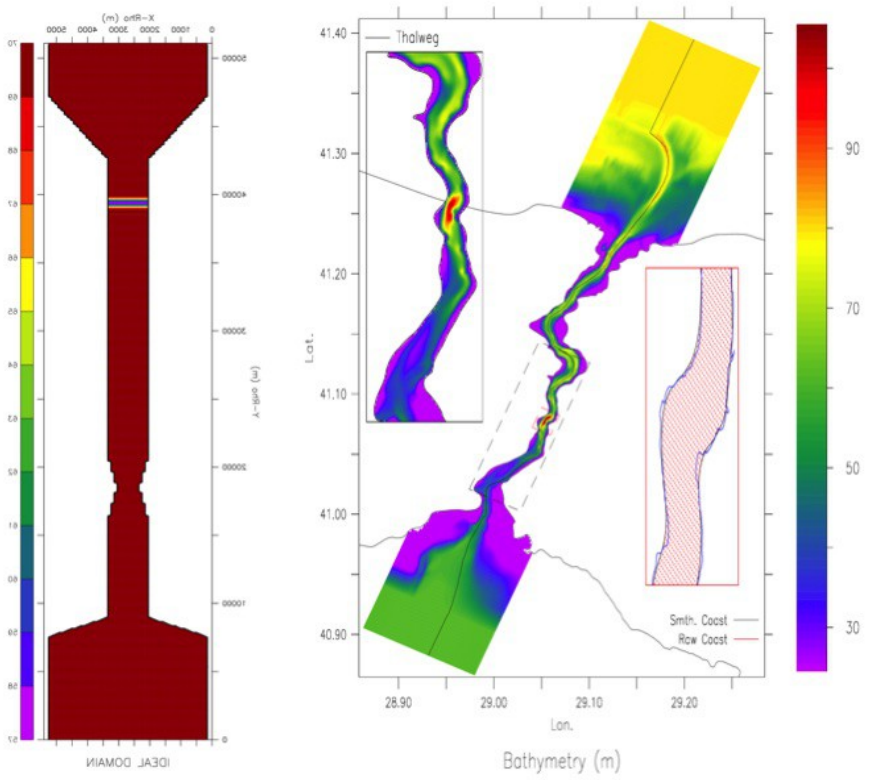


*Figure 23. ROMS model configuration: (a) Layout of the domain for the idealized Bosphorus model, (b) topography of the realistic Bosphorus model domain and the layout of the model grid-points in the contraction zone.*

For the model configured with the realistic geometry of the Bosphorus (Fig. 23b), high resolution bathymetric data of Gökaşan (2005) have been first resampled and interpolated to a variable resolution rectilinear grid of 163x716 nodes with $\Delta\mathbf{x}$ = 50 - 200 m, $\Delta\mathbf{y}$ = 50 - 325 m and 35 s-levels with vertical spacing of 0.7 - 2.85 m, then subjected to scale-selective smoothing, setting also the minimum depth to 25 m. The model domain includes rectangular boxes at the two ends of the strait representing the topographic features in the neighboring seas, joined through gentle slopes at the junctions. The Generic Length-Scale (GLS) turbulence scheme with the k-epsilon formulation was used, yielding realistic features with interfacial layer thickness comparable with observations. Radiation conditions were used for the 2d and 3d flow variables at the north and south open boundaries, while the 2d velocity prescribed at the southern boundary imposed the net volume flux through the strait. The MPDATA advection scheme to handle sharp gradients of tracers, the third-order upstream horizontal advection of 3D momentum and the fourth-order centered vertical advection of momentum were found to be the essential ROMS options to be used to advantage. The volume-conservation switch VOLCONS is activated at the open boundaries. The use of the non-linear equation of state was also essential because of the wide range of properties of the water masses being mixed. Lateral diffusivity and viscosity are parameterized by the Smagorinsky formulation on constant geopotential surfaces. No-slip boundary conditions are assumed at the side-walls and a quadratic bottom friction coefficient (RDRG2=0.005) is implemented at the bottom, while all surface fluxes are set to zero.

The model domain chosen extends over the entire TSS, including also part of the northeast Aegean Sea at south, and the Black Sea at north of the domain. A non-uniform curvilinear orthogonal grid, tilted and stretched at the Bosphorus and Dardanelles Straits to better follow the main axis of the real straits, covers the domain at variable resolution: from less than 50 m in the two Straits up to about 1 Km in the Marmara Sea. To adequately resolve the complex hydraulic dynamics of the TSS, the model grid is made by 100 inhomogeneous distributed vertical z-levels. The thickness exponentially ranges from 1.2 m at the surface to 80 m at the bottom with most of the levels concentrated in the first 100 m. The very high horizontal resolution adopted in MITgcm, together with the

partial cell formulation result in a very detailed description of the bathymetry (Fig. 24).

### 2.2 The MITgcm Model for the Turkish Straits

In this study the Massachusetts Institute of Technology general circulation model (MITgcm, http://mitgcm.org) is used to study this extreme environment with full details of its contrasting properties.

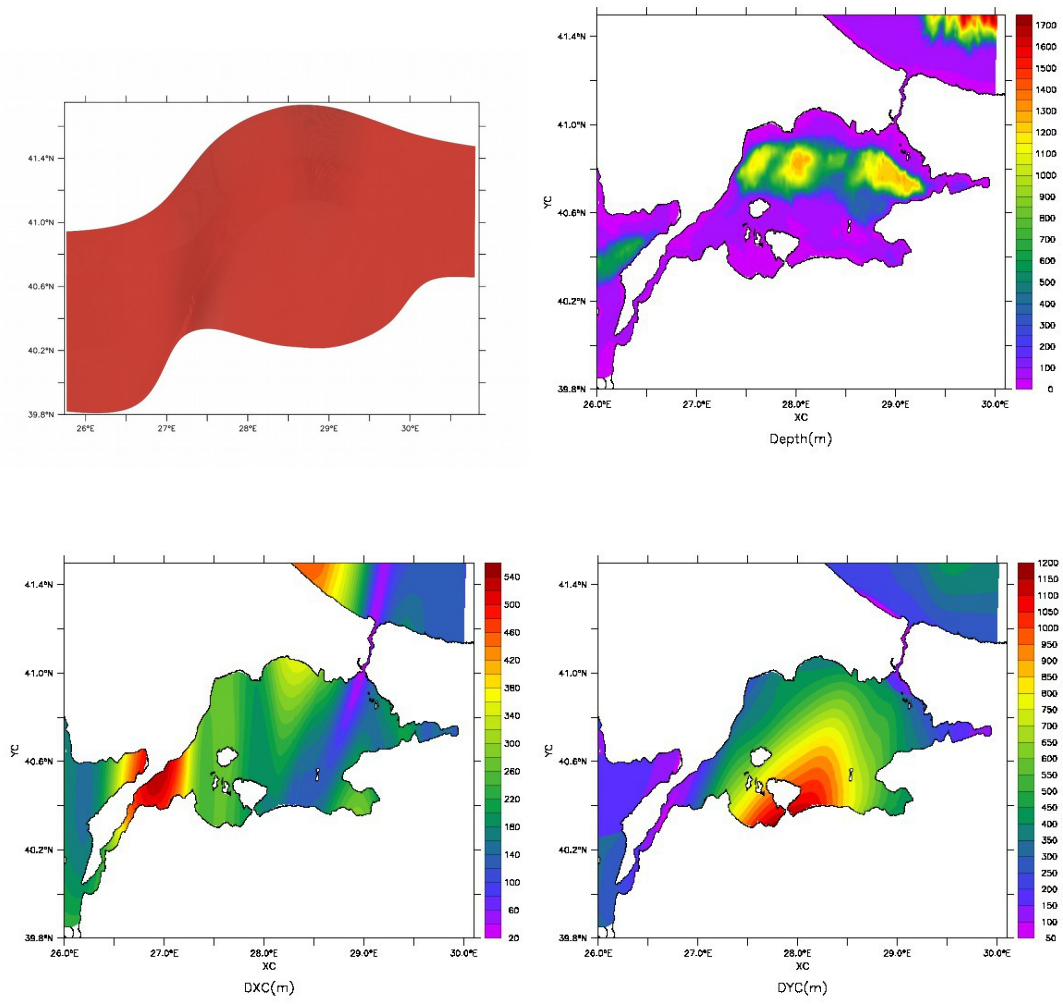


*Figure 24. (a) Model domain in curvilinear coordinates, (b) model topography (depth in m), and the variation of model spatial discretization steps (step size in m) in (c) lengthwise and (d) transverse directions.*

The model domain chosen extends over the entire TSS, including also parts of the north-east Aegean Sea and the Black Sea at its two ends. A non-uniform curvilinear orthogonal grid (1728 × 648 grid points) covers the domain at variable resolution: from less than 50 m in the two Straits up to about 1 km in the Marmara Sea.

The model is initialized with three different water masses filling the western part of the domain, the Marmara Sea and the eastern side of the domain respectively, with vertical profiles selected from CTD casts obtained during the cruise of the R/V BILIM of the Institute of Marine Sciences in June-July 2013. With the initial condition specified as lock-exchanges at the two straits, the model is left free to adjust to the expected two-way exchange. The capability of MITgcm to represent the two-layer exchange dynamics both in the straits and in the Marmara Sea is examined. The non-uniform grid and the vertical resolution implemented have demonstrated to be suitable to capture the fine scales within the two Straits and also to well represent mesoscale in the Marmara Sea. The response of the currents and density structure over the water column to different net flow is also examined through the setup of experiment with varying net barotropic volume fluxes.

No-slip conditions were imposed at the bottom and lateral solid boundaries. The selected tracer advection scheme is a third-order direct space-time flux limited scheme due to Hundsdorfer et al. [1995]. Following the numerical experiments conducted by Sannino et al. [2014] to investigate the 3-D evolution of LAIWs in the Strait of Gibraltar, the turbulent closure parametrization for vertical viscosity and diffusivity proposed by Pacanowski and Philander [1981] was used. Horizontal diffusivity coefficient is $\kappa h=1\cdot10^{-2}$ $m^2s^{-1}$, whereas variable horizontal viscosity follows the parameterization of Leith [1968].

The simulations carried out in MOTUS have been performed on the IBM Power 775 (called Boreasz) installed at the Maciej Cytowski, ICM, University of Warsaw.The theoretical performance of Boreasz are about 8 flops/core x 3.83 Ghz x 32 cores/node x 80 nodes = 78.43 Teraflops. Thanks to the very good performances of Boreasz we succeed in performing all the scheduled simulations. The system was easy to use thanks to the prompt assistance and support given by the technicians that manage Boreasz. The storage was quickly increased during the project under our specific requests. Moreover the file transfer resulted to be very fast and efficient. In conclusion,

from our point of view, Boreasz is a system optimally suited for high-resolution ocean modelling studies.

## 3. RESULTS

### 3.1 Experimental results – June 2013 R/V BİLİM cruise

The CTD data obtained at a total of 238 stations occupied during the 18 June – 06 July 2013 cruise of the R/V BİLİM, at the TSS and the adjoining Black Sea continental shelf / slope area are listed in Table 1 of Appendix 1. The data have been analyzed to review the exchange through the TSS and the dense water outflow from the Bosphorus into the Black Sea.

#### 3.1.1 Hydrography of the TSS

Starting from outside the Dardanelles Strait in the Aegean Sea, we see in Fig. 25 the profiles of temperature, salinity, oxygen and chlorophyll at station #2 (see station identifiers in Table 1, Appendix 1 hereafter for full reference) that the station is well stratified in its properties. The warm upper layer is influenced by the low salinity water of Black Sea water exiting the Dardanelles Strait in the upper 10m, where also the chlorophyll peaks up. Oxygen is generally low and uniform throughout the water column.

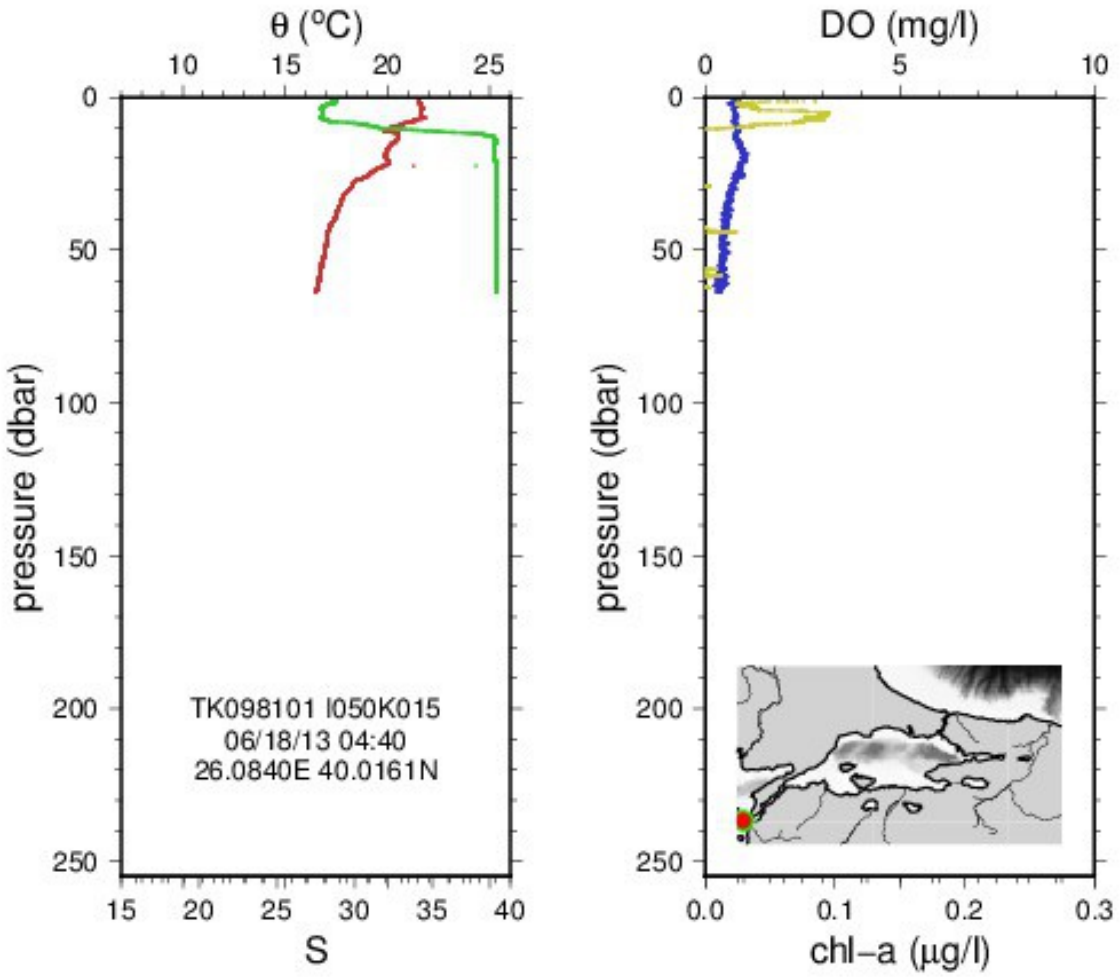


*Figure 25. Profiles of (a) temperature (°C, red) and salinity (green), (b) dissolved oxygen (mg/l, blue) and chlorophyll (µg/l, dark yellow) at station #2 in the Aegean Sea. (station position shown in the inset map, for full list of stations refer to Table 1, Appendix 1).*

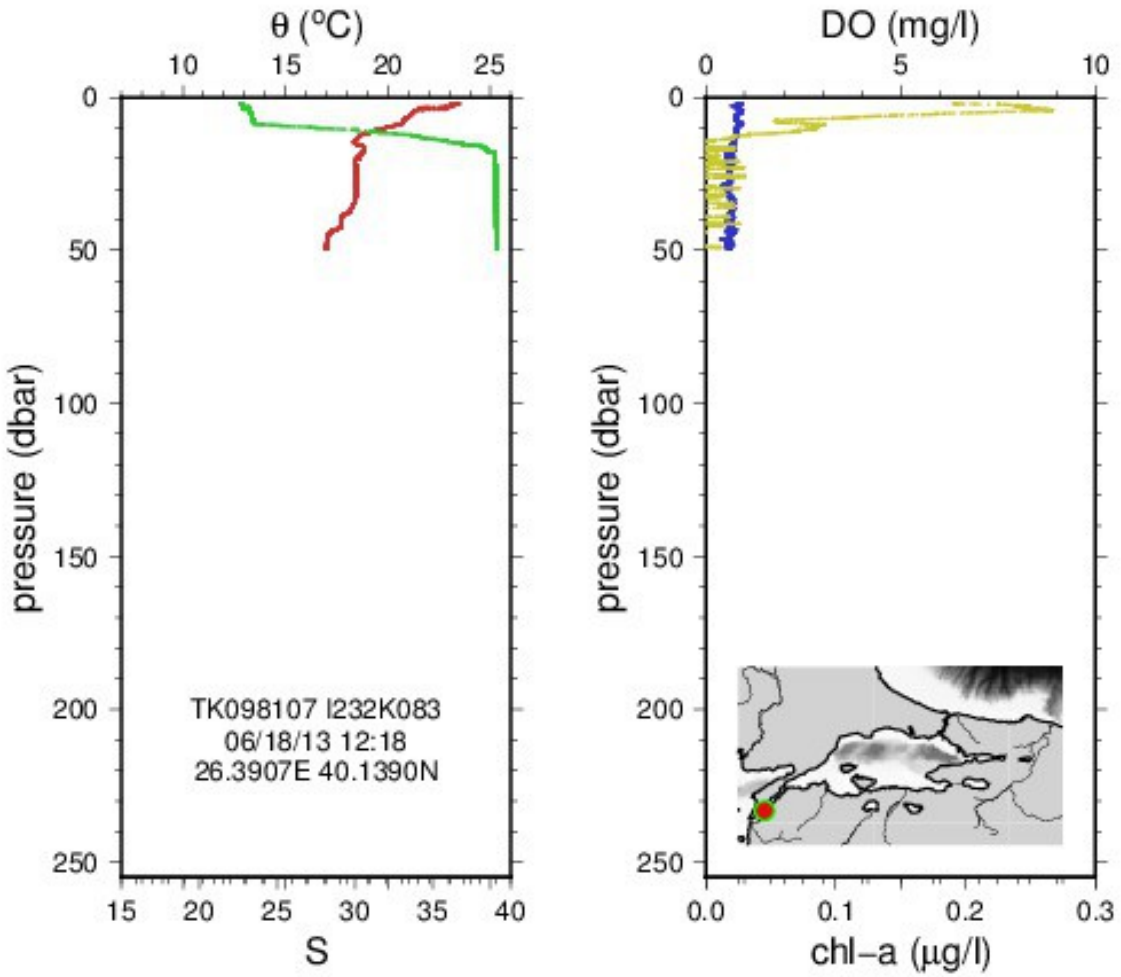


*Figure 26. Profiles of (a) temperature (°C, red) and salinity (green), (b) dissolved oxygen (mg/l, blue) and chlorophyll (µg/l, dark yellow) at station #8 west of the Nara Pass in the Dardanelles Strait.*

Station #7 in Fig. 26, located immediately West of the narrows at Nara Pass in the Dardanelles Strait, essentially shows similar features, with an upper layer of warm, low salinity water above 10m and an interfacial layer of sharp salinity gradient at 10-15m. At station #11 immediately east of the Nara Pass, Fig. 27, the profile is significantly different: now the interface is much sharper and deeper at 25m. The warm surface layer continues to dominate but a trace of cold water right at the interface is observed. This cold water is a remnant of the Cold Intermediate Water that we will see in the Marmara Sea as well as the Black Sea, that penetrates till the Nara Pass but vanishes in the west because of efficient mixing by a hydraulic jump past the narrows. The fact that the

interface depth changes abruptly at the narrows shows hydraulic control working at the Nara Pass, the narrowest section of the Dardanelles.

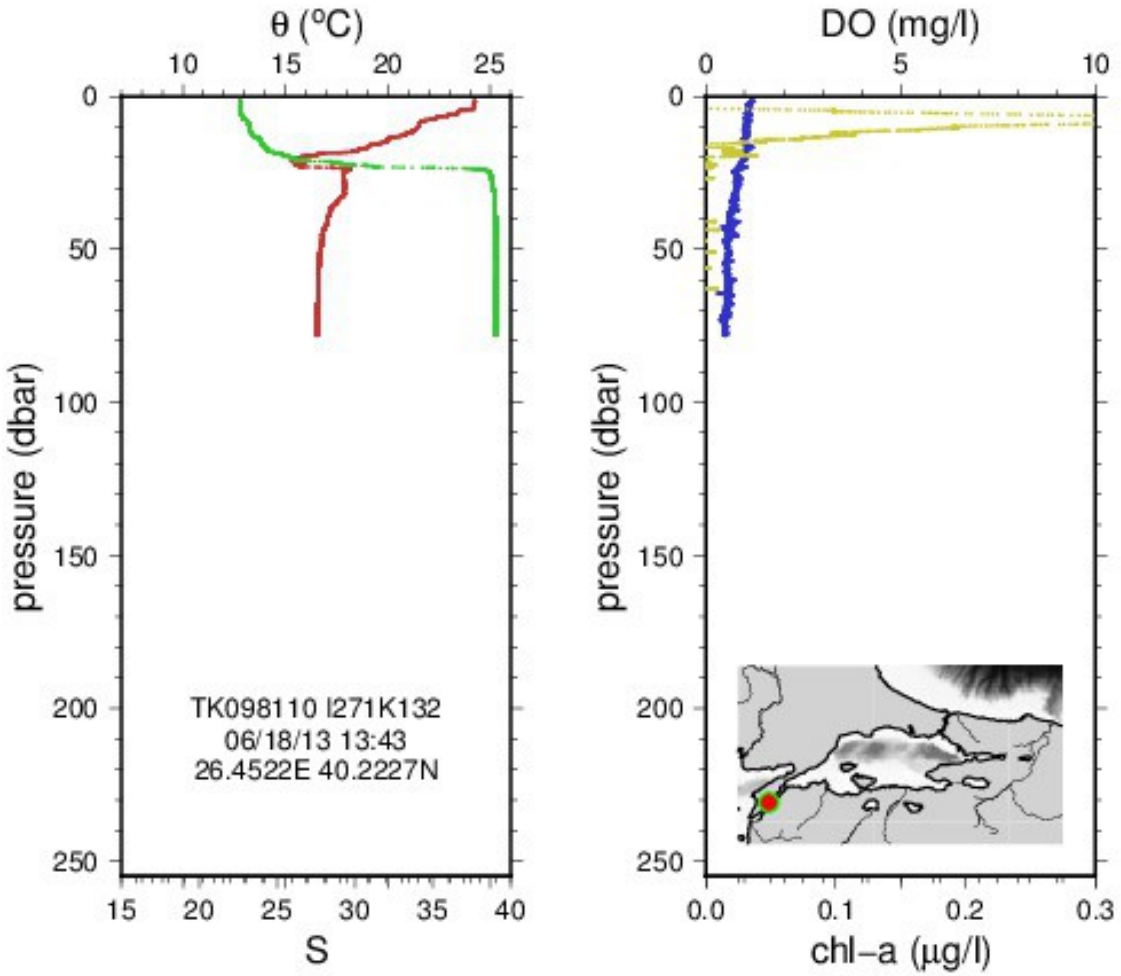


*Figure 27. Profiles of (a) temperature (°C, red) and salinity (green), (b) dissolved oxygen (mg/l, blue) and chlorophyll (µg/l, dark yellow) at station #11 east of the Nara Pass in the Dardanelles Strait.*

The sectional displays of temperature, salinity and density along the Dardanelles Strait in Fig. 28 show that the upperlayer flow of water proceeds with uniform depth of about 25m into the Strait, until it undergoes a rapid change of depth at the Nara Pass, where also the mixing created after the hydraulic transition results in a very thin and stratified upper layer. The vein of cold water feding in from the Marmara Sea immediately above the interface ends up past the Nara Pass by turbulent mixing. Warm water with temperature of about 18°C and high salinity of about 38.5 below the halocline is observed to enter the Marmara Sea from the Dardanelles Strait.

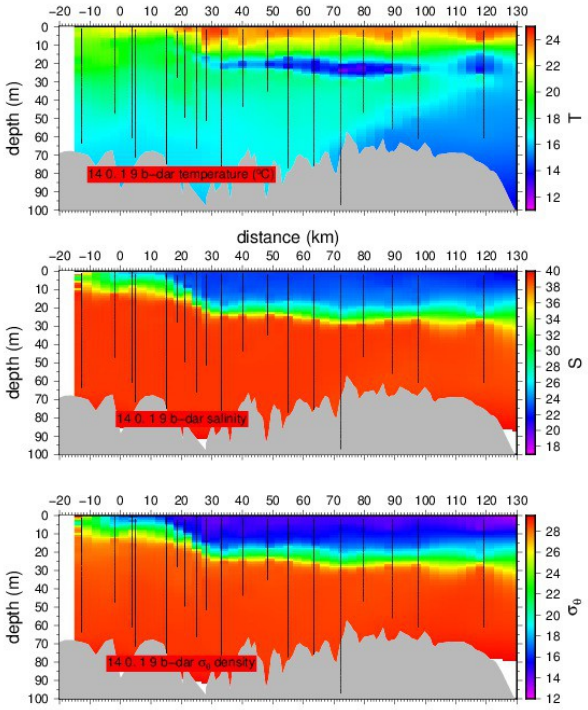


*Fig 28. Sections of (a) temperature (°C), salinity and ve (c) $\sigma_\Theta$ density across the Dardanelles Strait.*

In the entire section extending along the TSS in Fig. 29, the complete Picture is better observed. Brackish waters of salinity about 18 enter the Bosphorus from the Black Sea. The Black Sae waters have a temperature of about 24°C in the upper mixed layer of 25m depth, below which is the Cold Intermediate Layer (CIL), with a minimum temperature of slightly more than 7°C at its core. This water mass sits above the outflowing dense water from the Bosphorus, traces of which can be seen at the bottom. Then comes the rapid variations in the Bosphorus Strait which will be described next. In the Marmara Sea past the Bosphorus, surface layers of alternating warm and cold waters are seen subject to the circulation. Then below is a cold layer, just above the halocline at 25m depth, which is the Cold Intermediate Layer partly formed in the Marmara Sea and partly a memory of CIL leaked in at earlier times from the Black Sea. The minimum temperature of this thin cold layer of the Marmara Sea is about 12°C, which only penetrates the Dardanelles Strait until Nara Pass as reviewed above. The warm water entering the Marmara Sea below the halocline at Dardanelles Strait can be easily recognized in Fig. 29. This water trapped immediately below the pycnocline thins

out in the Marmara Sea because of buoyant spreading just below the light upper layer.

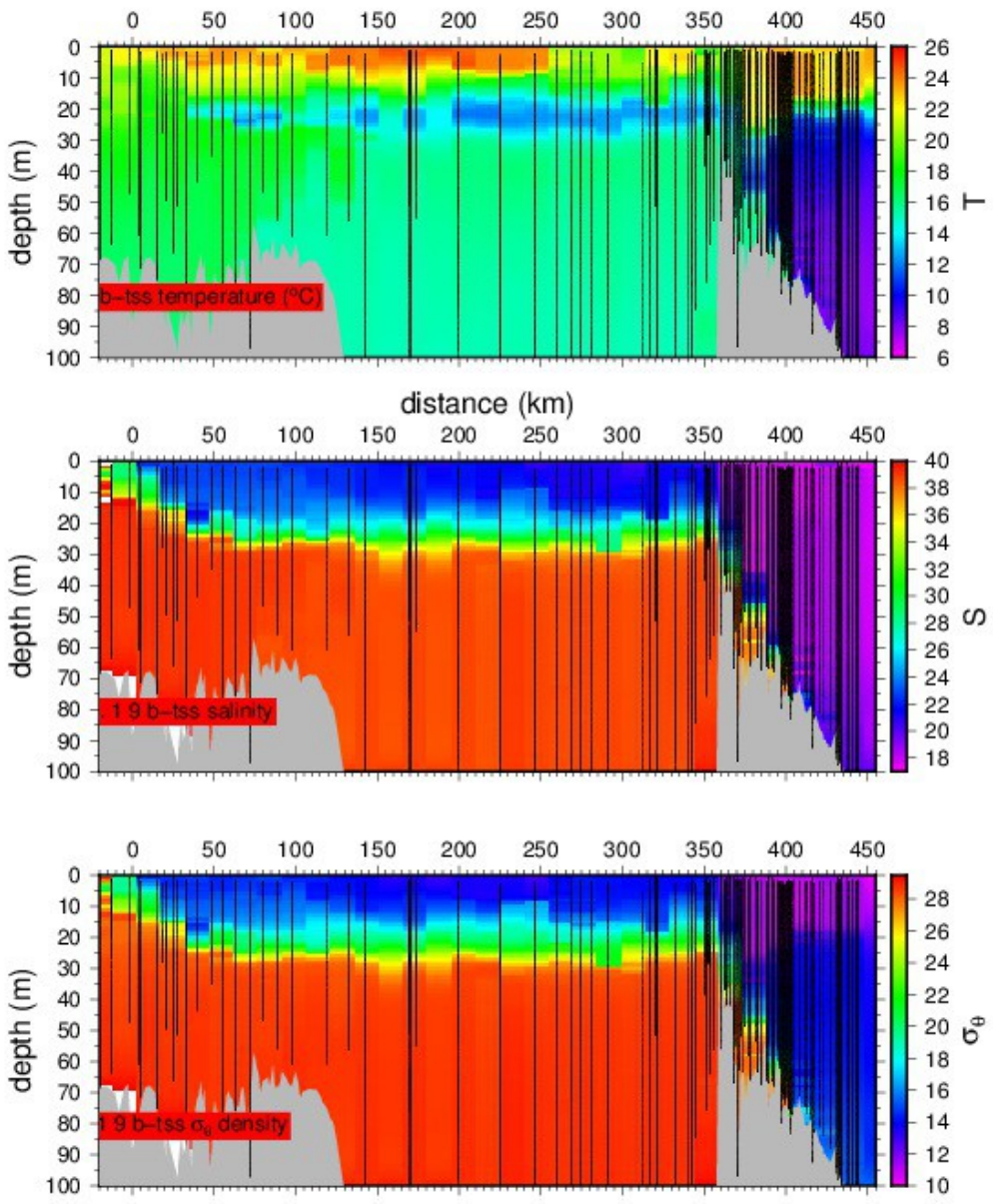


*Figure 29. Sections of (a) temperature (°C), salinity and ve (c) $\sigma_\Theta$ density across the TSS.*

The features of vertical profiles in the Marmara Sea proper are shown in Fig.s 30 and 31. In the western deep basin of the Marmara Sea in Fig. 30, the upper layer temperature stratification with the cold water core lies above a thick interface with great salinity variation. Below the pycnocline a warm layer reaching a maximum temperature of 16°C implies the feeding of this layer by warm waters from the Dardanelles Strait. At

deeper depths the temperature joins in with the rather uniform temperatures of deep Marmara basin at a temperature of 14.5°C and a salinity of 38.5, which are accepted as rather fixed values of Mediterranean water in the Marmara Sea. Dissolved oxygen is abundant in the upper layer, but drops to low levels below the pycnocline, which however correspond to the levels supplied by the Dardanelles Strait. Further decrease of oxygen occurs below 150m depth. Chlorophyll production only occurs at the upper layer, as the lower layer is limited in oxygen and also does not receive much sunlight.

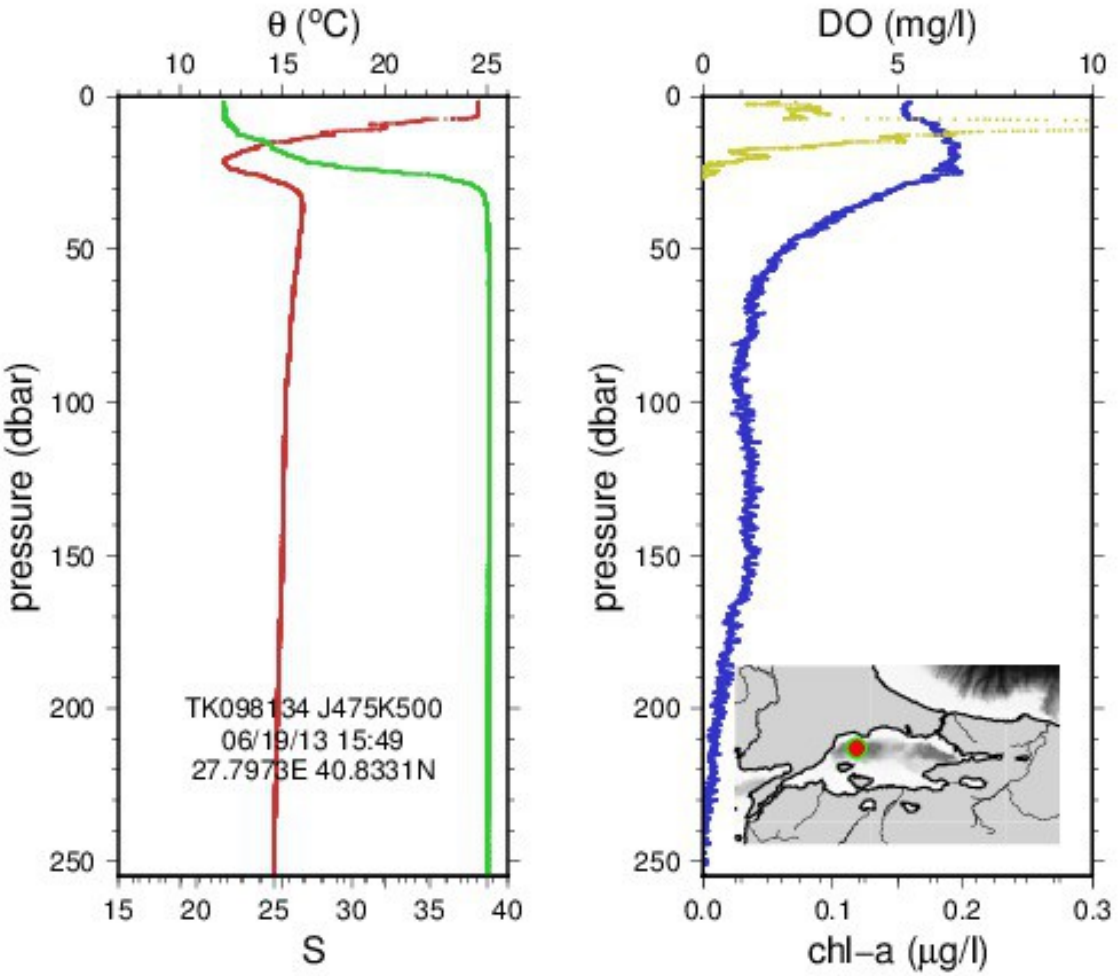


*Figure 30. Profiles of (a) temperature (°C, red) and salinity (green), (b) dissolved oxygen (mg/l, blue) and chlorophyll (µg/l, dark yellow) at station #35 in the western basin of the Marmara Sea.*

In Fig. 31 displaying profiles in the eastern Marmara Sea deep basin, the physical properties are similar, but the oxygen levels below the pycnocline are now much smaller, due to the remoteness of this basin from the Dardanelles source of oxygen.

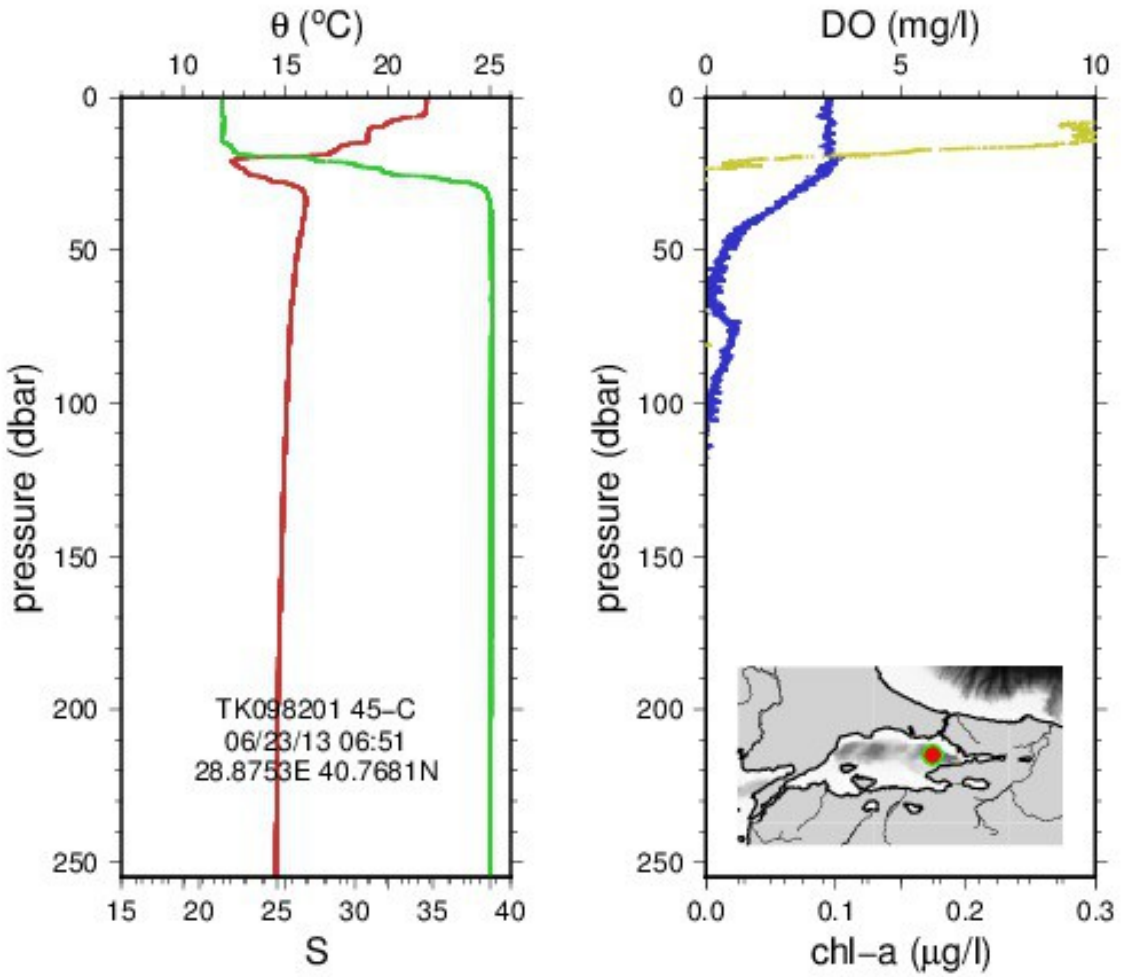


*Figure 31. Profiles of (a) temperature (°C, red) and salinity (green), (b) dissolved oxygen (mg/l, blue) and chlorophyll (µg/l, dark yellow) at station #102 in the eastern basin of the Marmara Sea.*

The sections along the Bosphorus are shown in Fig. 32. The upper mixed layer has temperature and depth variations within itself as the Black Sea water flows to the Bosphorus. Below this layer the CIL with a 7°C temperature minimum wedges into the Bosphorus, and further below is the warmer Mediterranean water flowing towards the Black Sea. The salinity of the lower layer of Mediterranean water is decreased by entrainment as it moves towards the North. The presence of rapid depth variations of the inteface near the Bebek-Kandilli contraction section (also the deepest point in the strait) and also at the northern sill are evidences fort he presence of haydraulic controls at these locations, followed by mixing zones in either case.

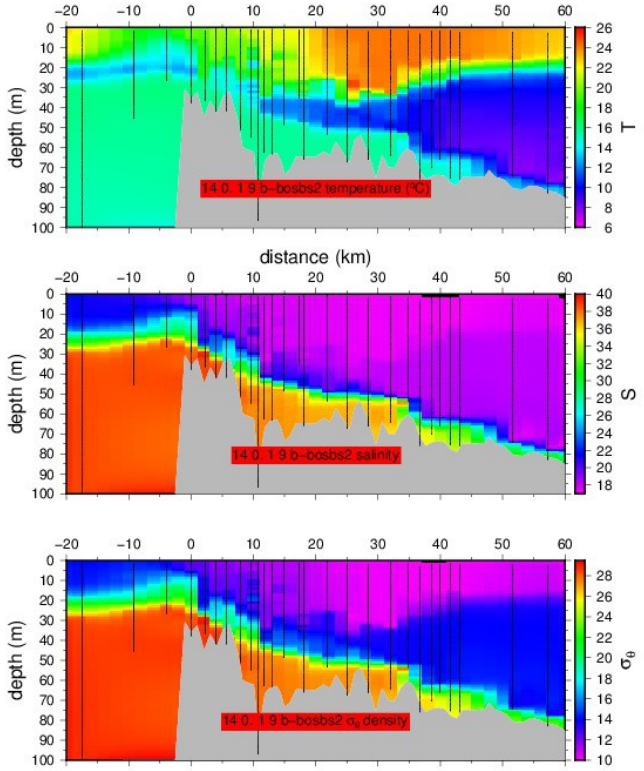


*Fig 32. Sections of (a) temperature (°C), salinity and ve (c) $\sigma_\Theta$ density across the Bosphorus Strait.*

Examples of CTD profiles in the Bosphorus are given in Fig.s 33 and 34. In Fig33a, in the southern exit region the thin and stratified upper layer is only 25m thick and includes the tongue of CIL penetrating to the Marmara Sea; in Fig. 33b, at the narrowest and deepest section of the contraction the layers are separated by a sharp salinity gradient and a thich interface extending between 30-45m. In Fig. 34a, just north of the northern exit of the Bosphorus and over the sill, the interface deepens to 50m, with the lower layer of Mediterranean water only 10m thick above the sill at 60m. The upper mixed layer has a sharp contrast with the CILof 20m thickness from 30-50m below. Then in Fig. 34b, past the sill and inside the canyon leading northwest along the shelf, the lower layer trapped inside the canyon is much deeper from 60 to 75m, and is thoroughly mixed in the hydraulic jump region. The CIL is thicker, from 30-60m.

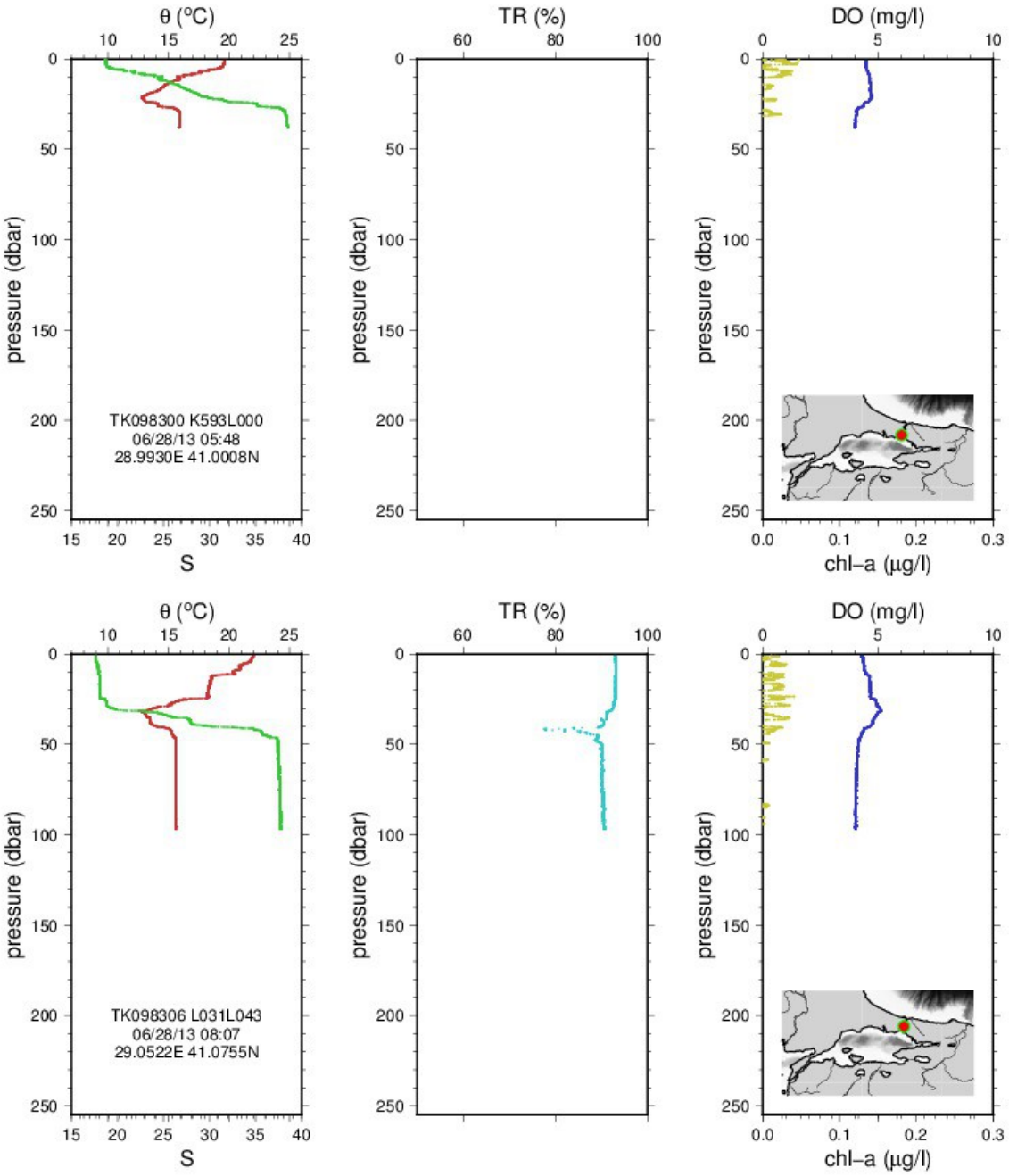


*Figure 33. Profiles of (a) temperature (°C, red) and salinity (green), (b) light transmission (%, light green) (c) dissolved oxygen (mg/l, blue) and chlorophyll (µg/l, dark yellow) (from left to right), at stations #120 (upper) and #126 (lower) in the Bosphorus.*

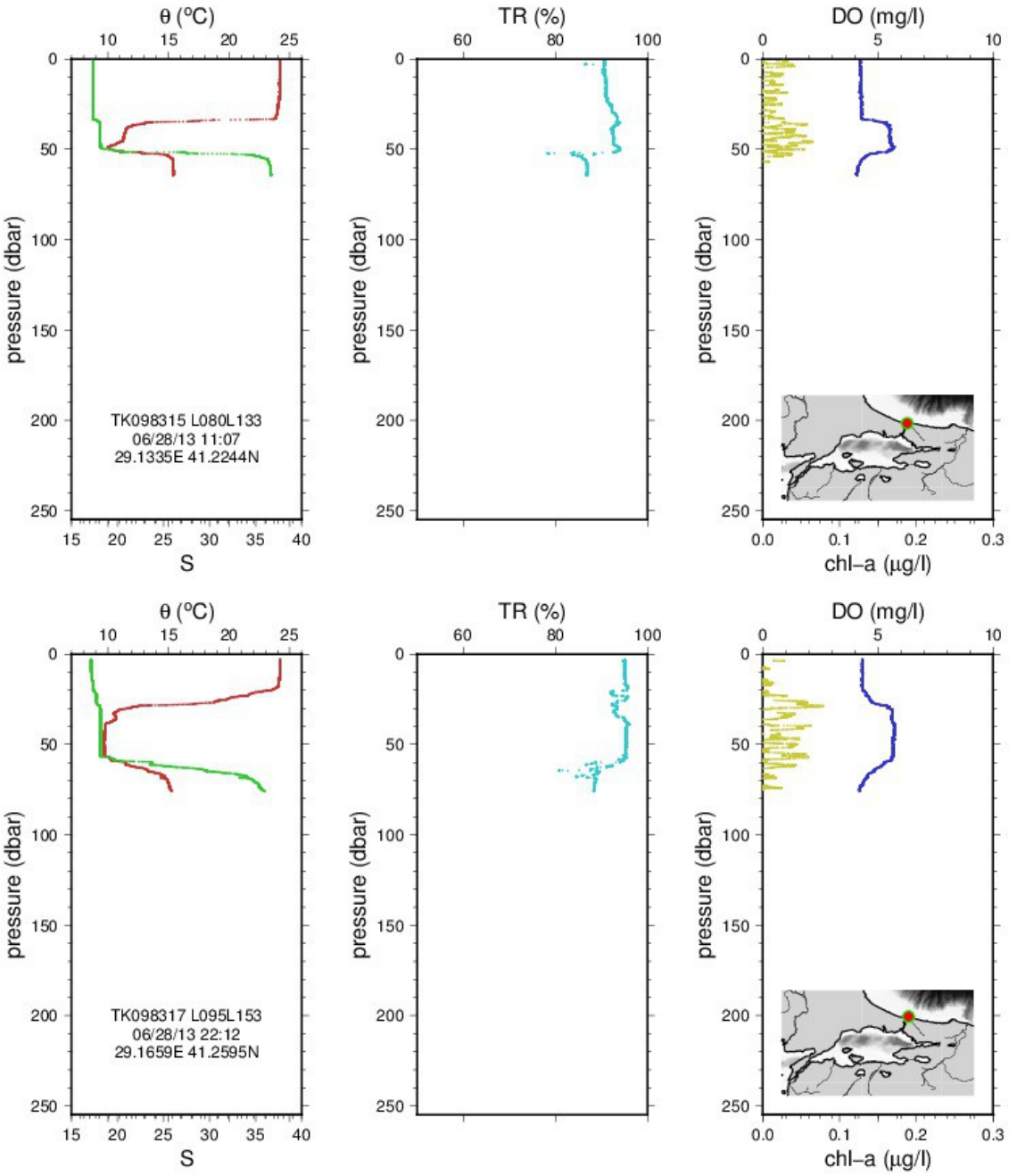


*Figure 34. Profiles of (a) temperature (°C, red) and salinity (green), (b) light transmission (%, light green) (c) dissolved oxygen (mg/l, blue) and chlorophyll (µg/l, dark yellow) (from left to right), at stations #135 (upper) and #137 (lower) north of Bosphorus.*

### 3.1.2 Hydrography of the southwestern Black Sea continental shelf / slope area

To determine the fate of the dense water outflow from the Bosphorus into the Black Sea, we analyze the temperature, salinity sigma-theta density, oxygen, chlorophyll and light transmission profiles in the southwetern Black Sea continentale shelf and slope region in Fig.s 35-39, along selected transects.

Temperature is influenced from the interactions of the atmosphere and ocean and other sources of heat and energy conversions; therefore it is not a conservative property. Salinity is a conservative property but of course it is dependent on sources of fresh and salt water and the evaporation process at the sea surface. Density is a dynamic variable that relates to motion and static stability, which is combined function of temperature and salinity. Light transmission is related to particulates in water of both inorganic and organic form, which is a good indicator of fine sediment transport and dispersal in the sea.

Unfortunately, CTD oxygen sensor is an instrument that lacks quantitative accuracy because of its nonlinear calibration. The oxygen sensor yield only qualitative measurements relative to a mean level they are calibrated, and therefore not very functional in areas such as the TSS and the Black Sea where very different water masses and even hypoxic and anoxic conditions exist. The chlorophyll measurements are based on fluorometry and indicate the general level of phytoplankton concentration in the sea.

In fig. 35 the west to east transect starting at the shelf region influenced by the Bosphorus outflow plume and continues along the shelf edge adjacent to the many canyons along the shelf, the largest of which are the Bosphorus and Sakarya Canyons.
The canyons on this transect often reach depths of 200-500 m and extend inshore from the shelf edge delienated by the 100 m depth contour. The temperature near the surface is influenced by the summer mixed layer structure. Deeper, at depths of 60-80m, the CIL with a minimum temperature of 7°C appears as discontinuous patches along the shelf edge, which shows the influence of the canyons on the 3-D intermediate circulation and mixing along the shelf edge. The halocline and therefore the pycnocline appears to be at depths of around 100m, being the lower bound for CIL. In the west of the section (station KK3) in the canyon at the shelf bottom, a vein of dense water originating from the Bosphorus and running across the shelf is detected. Chlorophyll is maximum at depths

of 20-40 m due to light limitation at the surface, while layers of increased oxygen and particulates are observed at the same depths.

At deeper depths of 120-200 m along the shelf edge in the eastern part, a particulate layer of minimum light transmission levels is seen to intermittently extend into the various canyons.

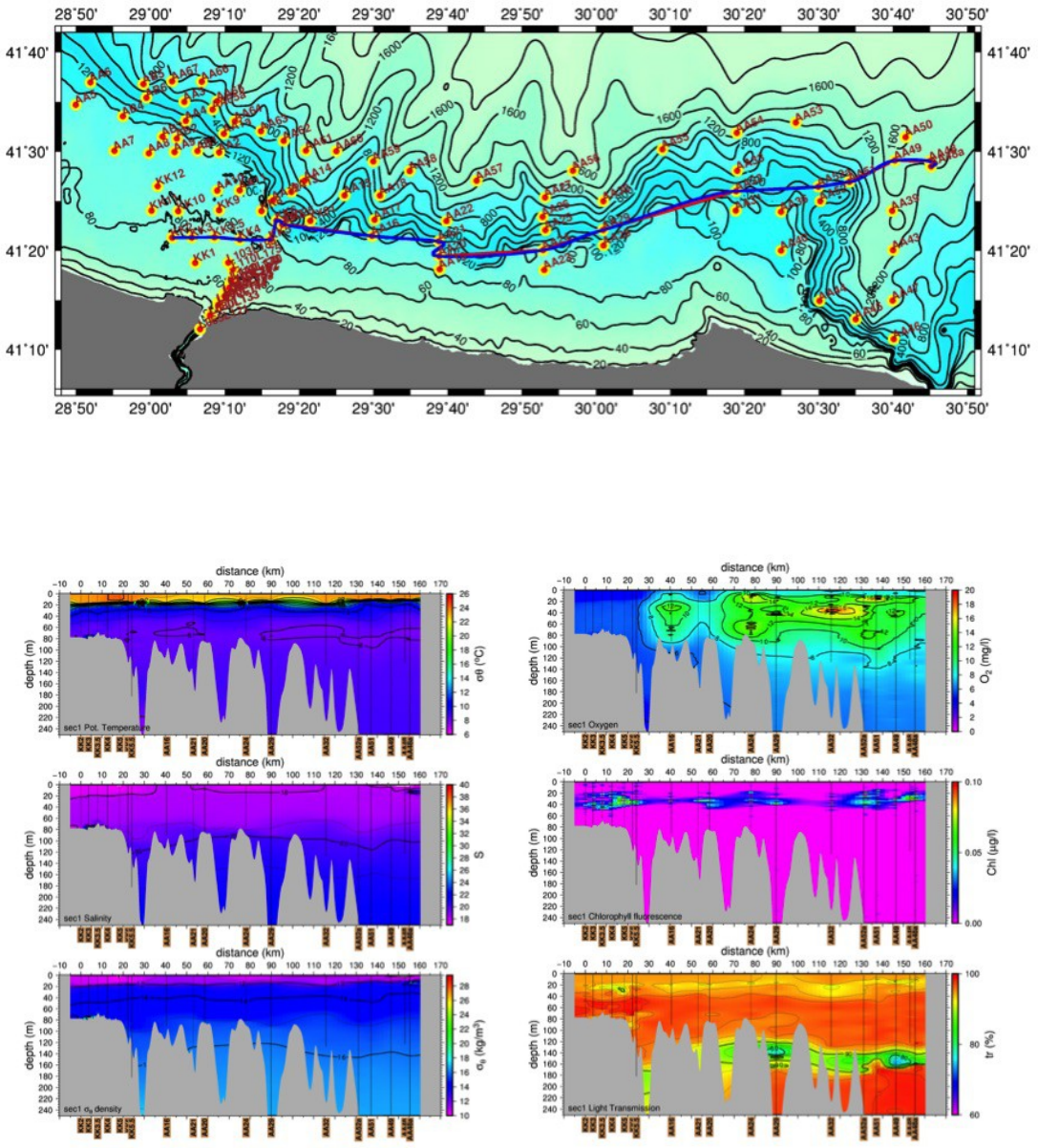


*Fig 35. (a) Station map for the Black Sea continental shelf / slope region and the west-east transect near mouths of canyons along the shelf edge, with sections of (b)*

*temperature (°C), salinity and ve $\sigma_\Theta$ density (top to bottom) and (c) dissolved oksygen (mg/l), chllorophyll (µg/l) and light transmission (%) (top to bottom) along the transect.*

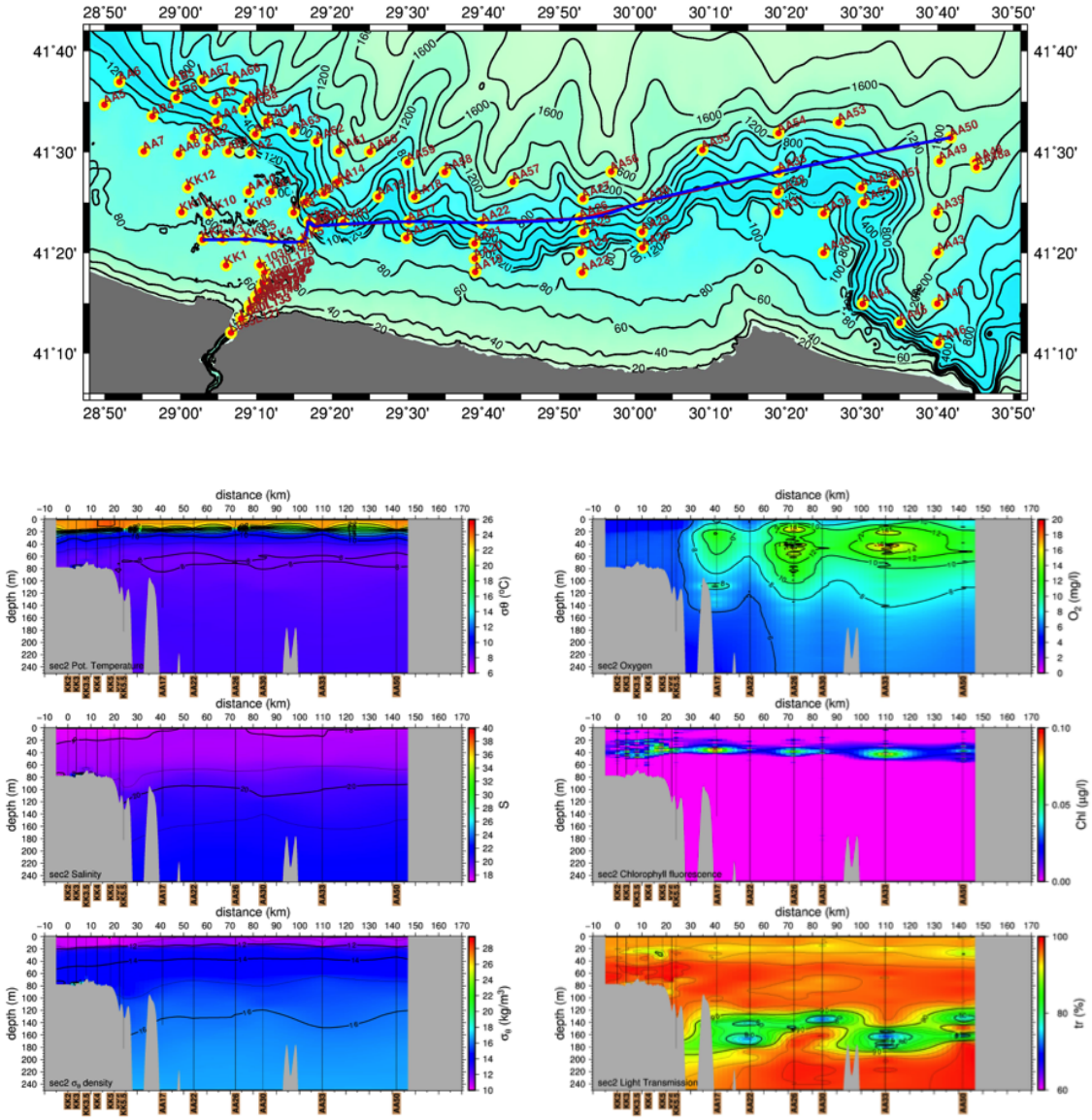


*Fig 36. (a) Station map for the Black Sea continental shelf / slope region and the west-east transect along the shelf and slope, with sections of (b) temperature (°C), salinity and ve $\sigma_\Theta$ density (top to bottom) and (c) dissolved oksygen (mg/l), chllorophyll (µg/l) and light transmission (%) (top to bottom) along the transect.*

In a transect located further offshore, in Fig. 36, the CIL layer and the particulate layers that were earlier observed to be discontinuous because of the influence of canyons are

now observed to be continuous. The particulate maximum (light transmission minimum) at depths of 120-180m is connected throughout the section but still indicates the

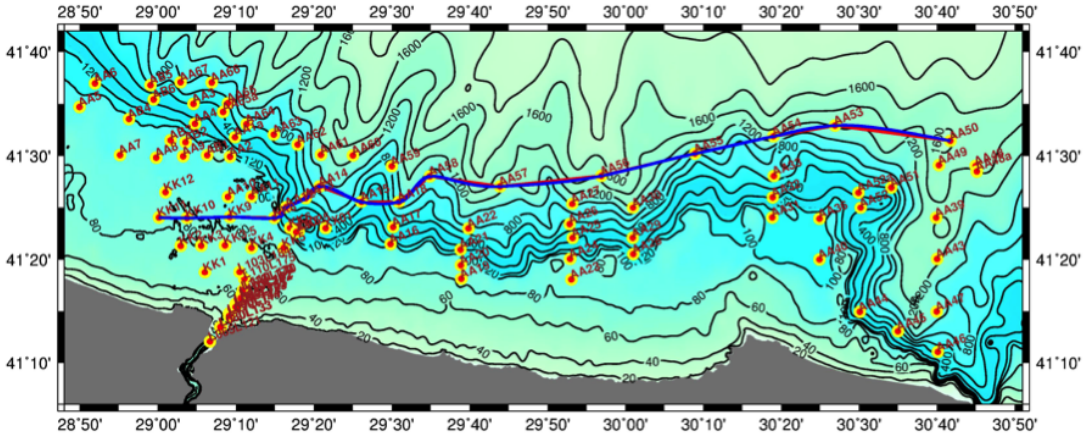


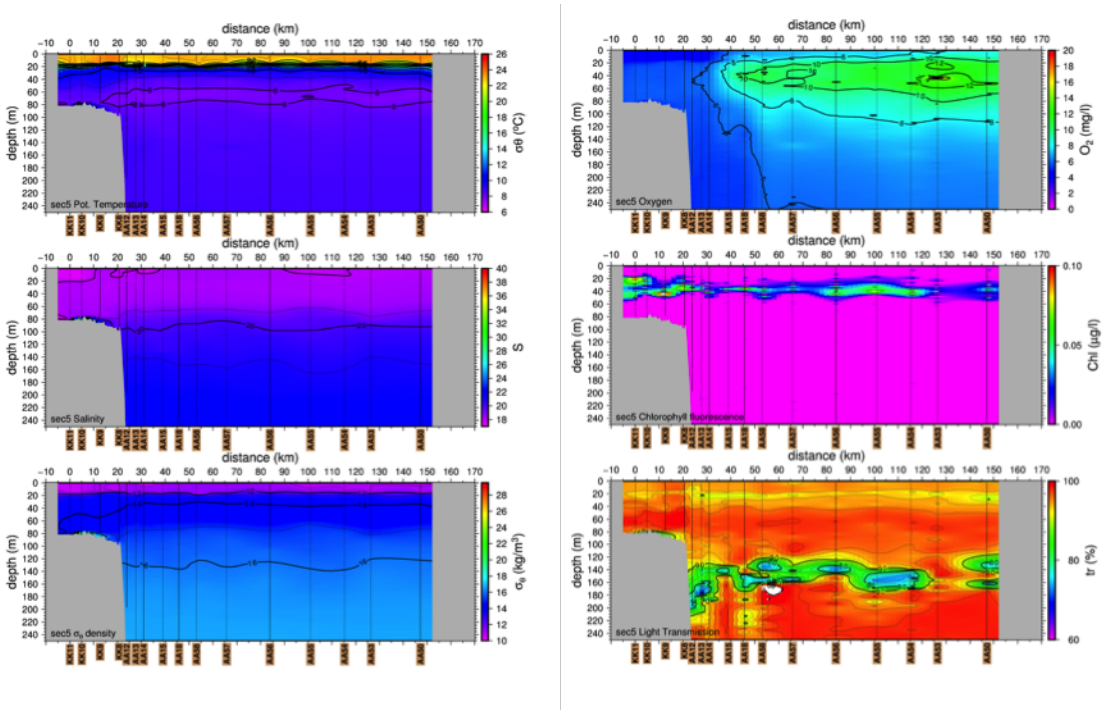


*Fig 37. (a) Station map for the Black Sea continental shelf / slope region and the west-east transect along the shelf and slope, with sections of (b) temperature (°C), salinity*

*and ve $\sigma_\Theta$ density (top to bottom) and (c) dissolved oxygen (mg/l), chllorophyll (µg/l) and light transmission (%) (top to bottom) along the transect.*

The further offshore section in Fig. 37 displays more uniform properties in all variables including the particulate maximum at depths of 120-220m. At the Bosphorus Canyon, a larger indentation at the continental slope (stations AA12-AA14) and its neigboring area (station AA18) the particle maximum penetrates deeper to cover depths of 120-250 m, suggesting a richer source that may be associated with a gravity flow linked to the Bosphorus and the shelf region. In fact, the anomaly of the dense water source on the shallow canyon leading up from the Bosphorus is seen on the shallower section (station KK10) to the left of the transect in terms of temperature, salinity and particulate maxima at the shelf bottom. The information available suggests a link between the shelf particulates carried by the dense water outflow over the shelf carried to the shelf edge by the shallow canyon and the particulate suspensions injected at the larger Bosphorus Canyon, although a direct link can not be established by the network of observations.

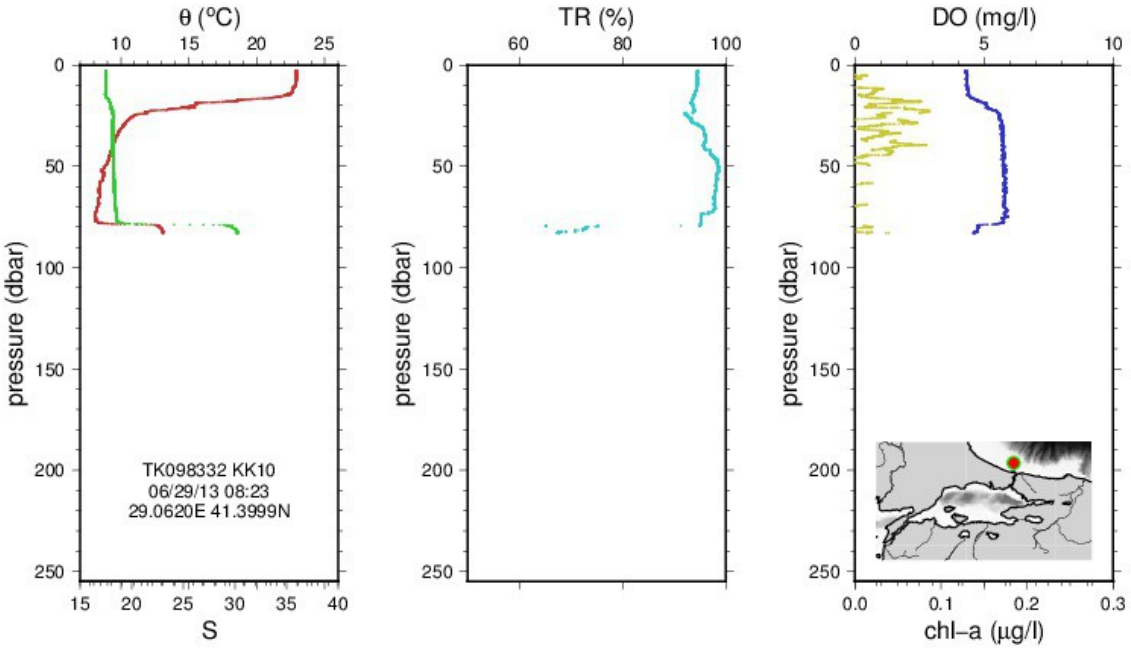


*Figure 38. Profiles of (a) temperature (°C, red) and salinity (green), (b) light transmission (%, light green) (c) dissolved oxygen (mg/l, blue) and chlorophyll (µg/l, dark yellow) (from left to right), at station #152 (KK10).*

The profiles at stations KK10, AA12, AA13 and AA14 are shown in Fig.s 38-41. In Fig. 38, station KK10 inside the shallow shelf canyon, a temperature and salinity anomaly associated with a particulate anomaly is observed at the bottom of the profile, corresponding to the dense water outflow channeled by the canyon on the shelf.

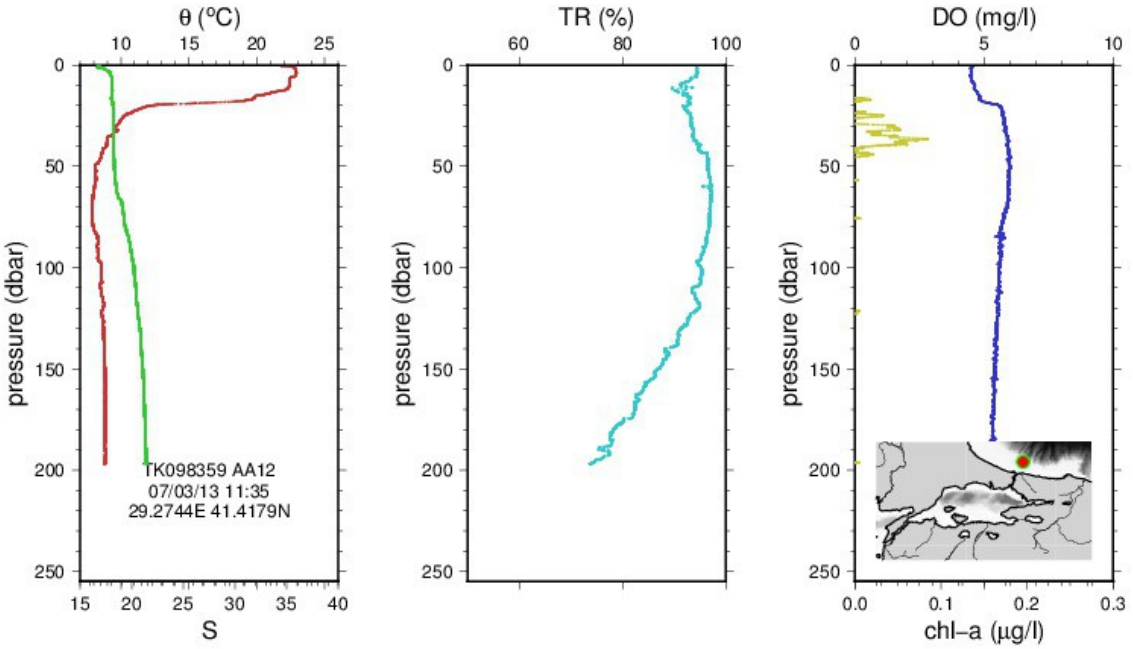


*Figure 39. Profiles of (a) temperature (°C, red) and salinity (green), (b) light transmission (%, light green) (c) dissolved oxygen (mg/l, blue) and chlorophyll (µg/l, dark yellow) (from left to right), at station #179 (AA12).*

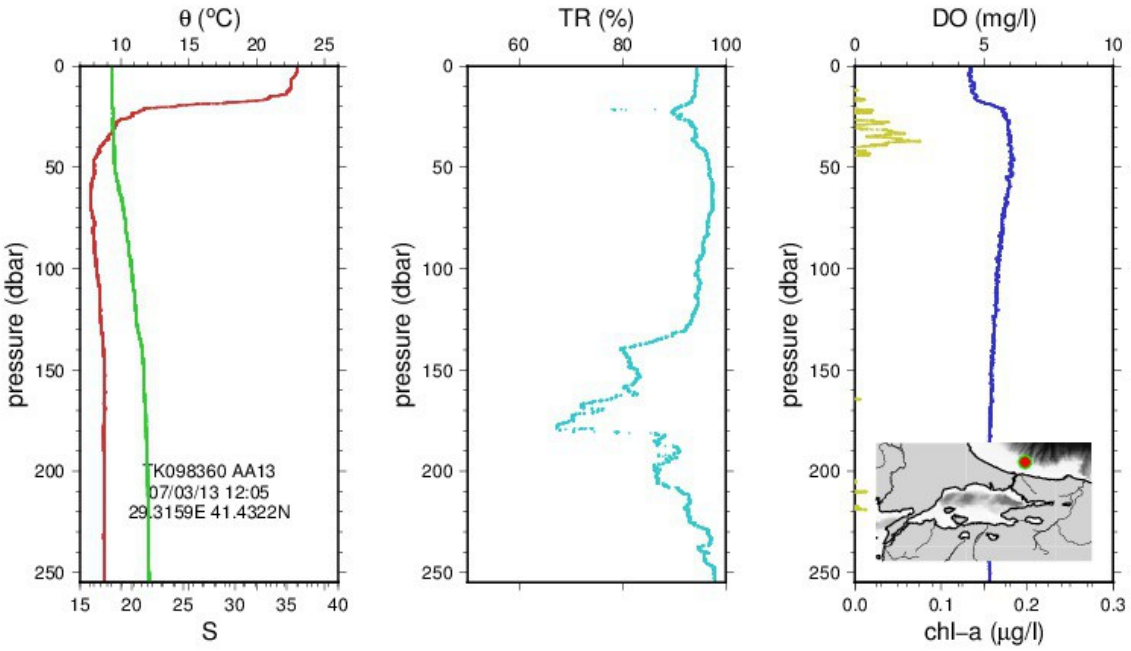


*Figure 40. Profiles of (a) temperature (°C, red) and salinity (green), (b) light transmission (%, light green) (c) dissolved oxygen (mg/l, blue) and chlorophyll (µg/l, dark yellow) (from left to right), at station #180 (AA13).*

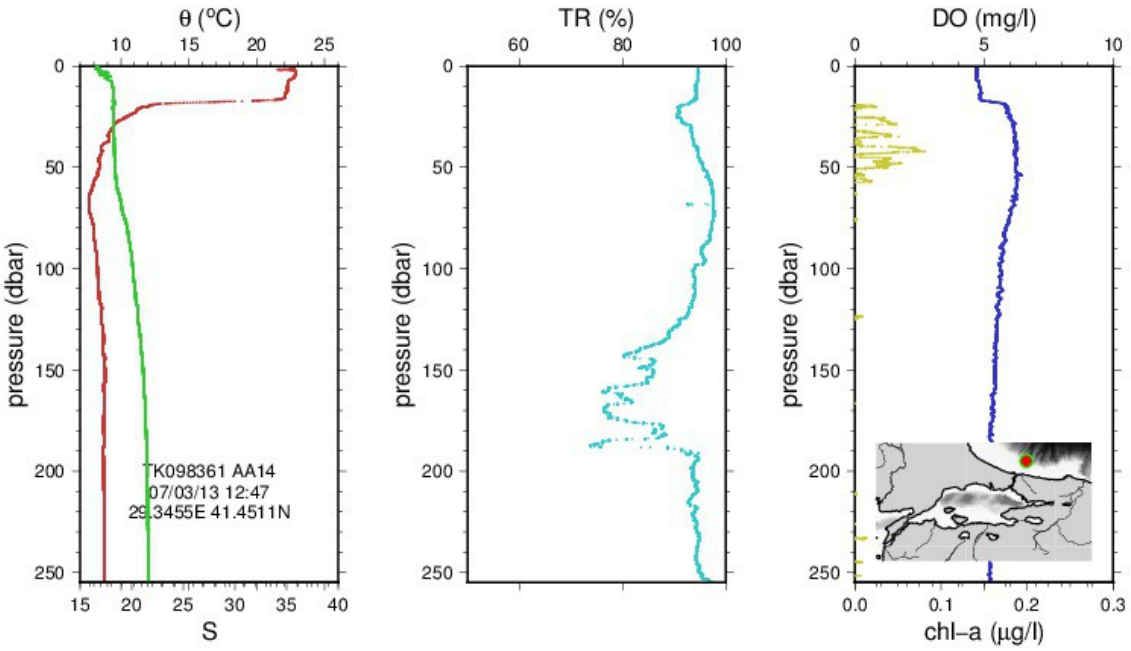

*Figure 41. Profiles of (a) temperature (°C, red) and salinity (green), (b) light transmission (%, light green) (c) dissolved oxygen (mg/l, blue) and chlorophyll (µg/l, dark yellow) (from left to right), at station #181 (AA14).*

The full load of particulates at depths of 120-250m occupy the larger scale gorge of the Bosphorus Canyon on the continental slope as shown in Fig.s 39-41. Fine scale anomalies in the temperature and salinity profiles at these depths are evident when these features are viewed on enlarged scale. We remind however that the oxygen profiles are only qualitative and should not be trusted at all below intermediate depths as these waters in fact contain hydrogen sulfide rather than oxygen, beyond the sensitivity range of the sensor.

At the deepest section along the continental slope that is furthest from the coast in Fig. 42, the CIL and chlorophyl are continuous across the domain. The deep particulate maximum (light transmission minimum) is however is discontinous between the east and west of the section, being greater in the east at depths 120-160 m. No sign of an intruding mass is seen in the shallower western slopes except a few isolated patches (stations AB6 and AA62, at 180-250 m), although here the slope is closer to the shelf edge termination of the shallow shelf canyon carrying the Bosphorus vein. The fact that the particulate layer is observed continuously along the slope in Fig.s 35-37, the deeper part starting off from the Bosphorus Canyon, and not observed at the western slope section but rather east of the Canyon in Fig. 42, suggest that the particulate layer is injected at the Bosphorus Canyon and thereafter carried along the slope.

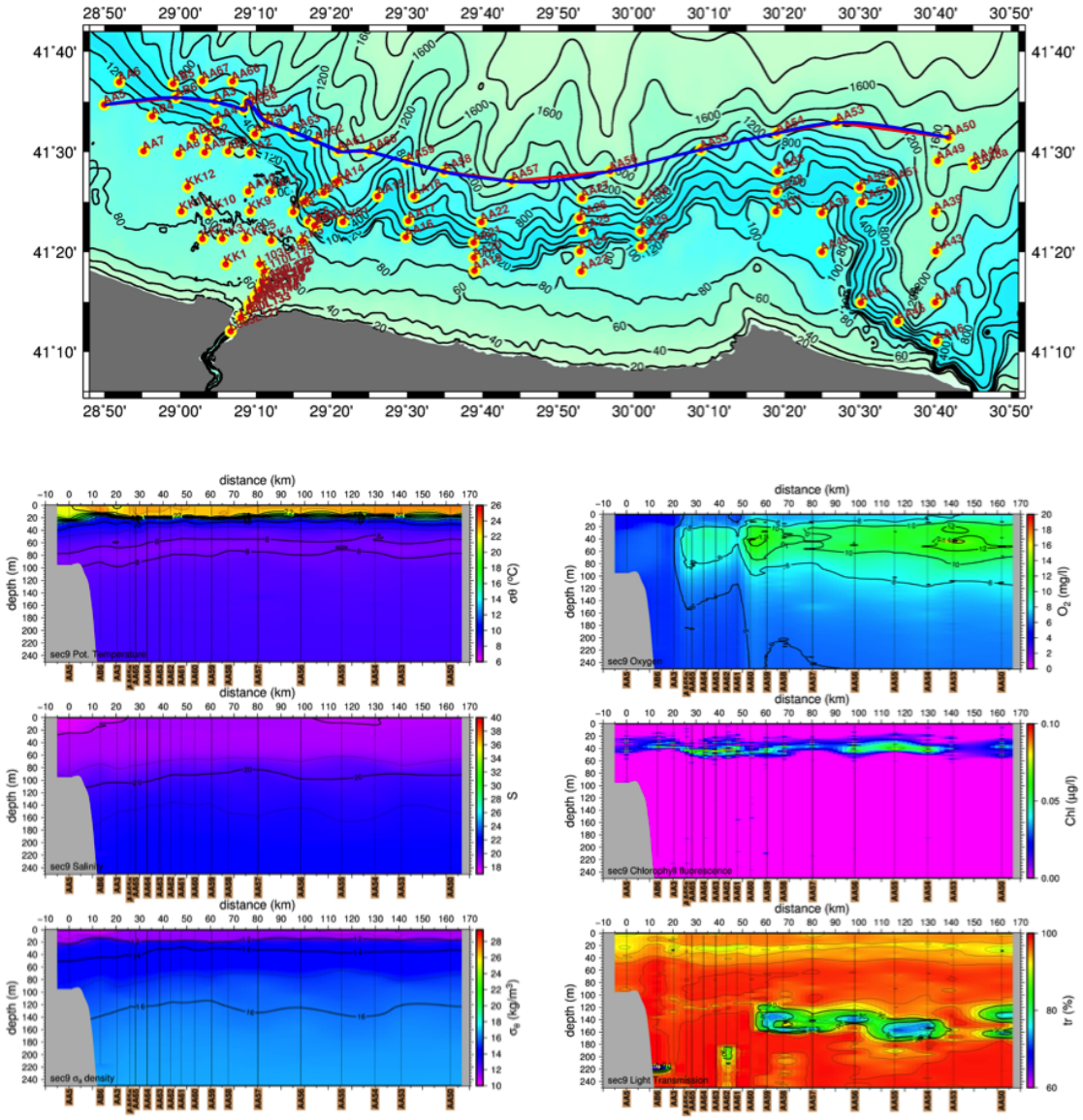


*Fig 38. (a) Station map for the Black Sea continental shelf / slope region and the west-east transect along the shelf and slope, with sections of (b) temperature (°C), salinity and ve $\sigma_\Theta$ density (top to bottom) and (c) dissolved oxygen (mg/l), chllorophyll (µg/l) and light transmission (%) (top to bottom) along the transect.*

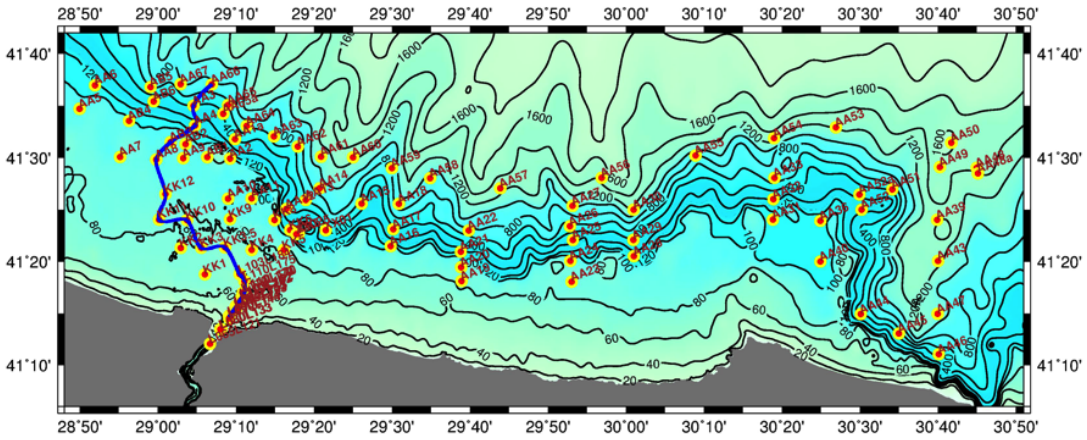
28°50'
29°00'
29°10'
29°20'
29°30'
29°40'
29°50'
30°00'
30°10'
30°20'
30°30'
30°40'
30°50'
41°40'
41°30'
41°20'
41°10'

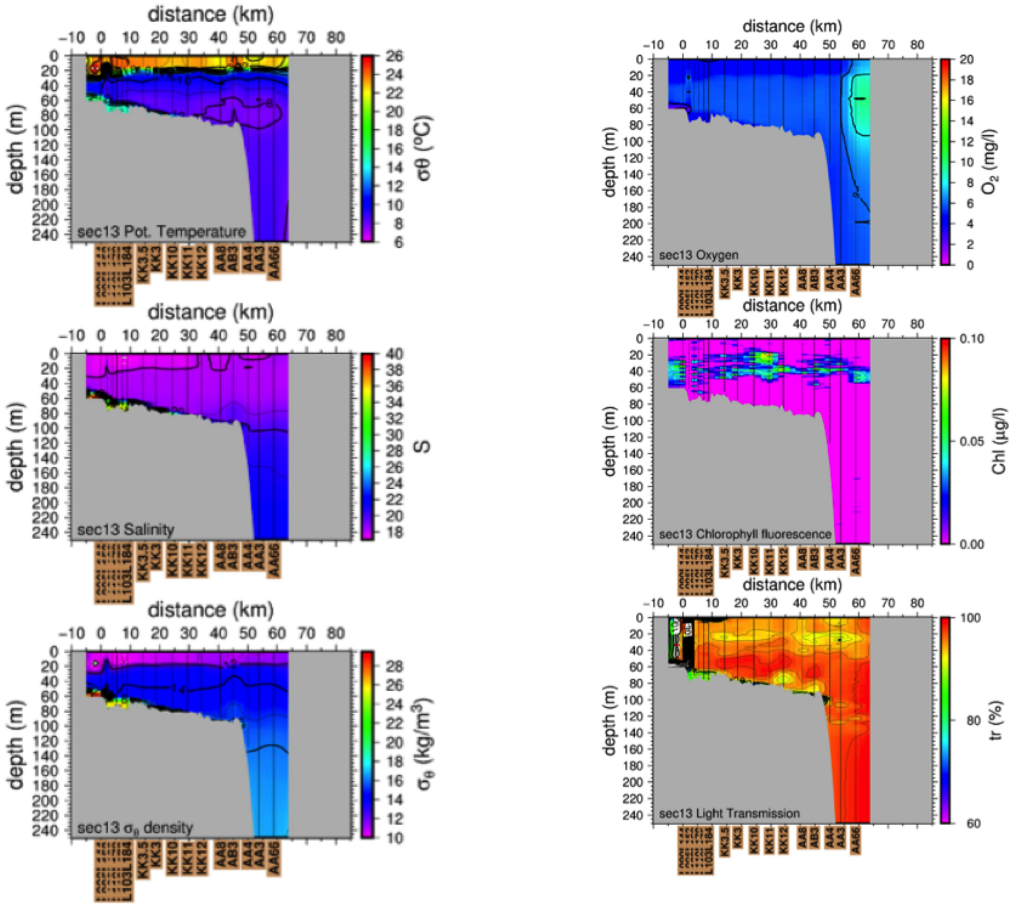


*Fig 43. (a) Station map for the Black Sea continental shelf / slope region and the cross-shelf transect along the canyon across the shelf, with sections of (b) temperature (°C), salinity and ve $\sigma_\Theta$ density (top to bottom) and (c) dissolved oksygen (mg/l), chllorophyll (µg/l) and light transmission (%) (top to bottom) along the transect.*

We review in Fig. 43 the section across the shelf and following the shallow canyon leading up from the Bosphorus to the shelf edge and extending to the deep sea. We observe that the dense water follows the canyon as it flows out from the exit of the Strait, as a very thin layer hardly detected at the bottom. It is not possible, however, to follow the anomalous water past the shelf edge in deep water. This we believe is because the thin layer in the canyon becomes somewhat diluted and dispersed before arriving to the shelf edge, and part of it gets sheaved off the top of the canyon vein and overflows the sides of the canyon to reorganize and flow out from the larger Bosphorus Canyon to the east. The downslope gravity current, carrying the cascading water from the shallow canyon at the shelf edge is also expected to turn towards the east and flow eastwards

along the slope as predicted by modeling of the outflow plume (Özsoy et al., 2001). Whatever details the station network is incapable to capture, we only can speculate. In fact it is almost impossible to capture the narrow and high velocity downslope cascading flows, and we may have missed these details on the slope immediately after the shelf edge. The fact that we do not observe particulate anomalies in deep water at this section, used effectively as a tracer of the intrusions, implies that the cascading sheet of anomalous water veers along the slope without separating from it, and only shows up as a layer of much larger thickness along the western slope of the Bosphorus Canyon slightly to the east. It has already been effectively mixed with ambient waters by entrainment. Thereafter it reaches the depth of its density roughly matching the existing stratification, separates from the slope to spread horizontally and the ensuing intrusion of water is seen as a layer of anomalous properties at depths of 100-200m further east, marked by particulate concentrations. The intrusions are also followed by temperature and salinity anomalies in intermediate waters as examined earlier by Özsoy et al. (1993, 2001).

### 3.1.3 Collective properties and T-S diagrams in the Black Sea region

The collective properties of the CTD profiles obtained in the southwestern Black Sea are described in this section. Later the T-S diagrams are presented by separating clusters of profiles according to the geographical regions described according to the boundaries assigned in Fig. 44.


*Fig 44. The geographic regions used to cluster CTD profiles: Dardanelles Strait, Marmara Sea, Bıshorus Strait and the southwestern Black Sea, sampled by the June 2013 cruise.*

The collective profiles for the southwestern Black Sea are shown in Fig. 45. The spread in the properties is larger in shallower part and decreases with depth, the largest deviation observed in the upper 200 – 300m. The temperature, salinity and density values greatly deviating to become off scale are limited to the upper 100m, indicating those points related to the dense water outflow detected at the bottom on the continental shelf, including those inside the main course and branches of the shallow canyon on the shelf. The cluster of data points showing positive deviation from the normal in temperature (Fig. 45a) especially at depths of 100-300m represent the anomalous intrusions along the continental slope, which are also marked by the cluster of data points with lowered light transmission (Fig. 45d) at the same depths. The fact that the range of anomalies in salinity are smaller than those in temperature, and that the anomalies are mostly limited to the upper 500m are general features that agree with characteristics reported earlier (Özsoy et al. 1993, 2001, Özsoy and Beşiktepe, 1999).

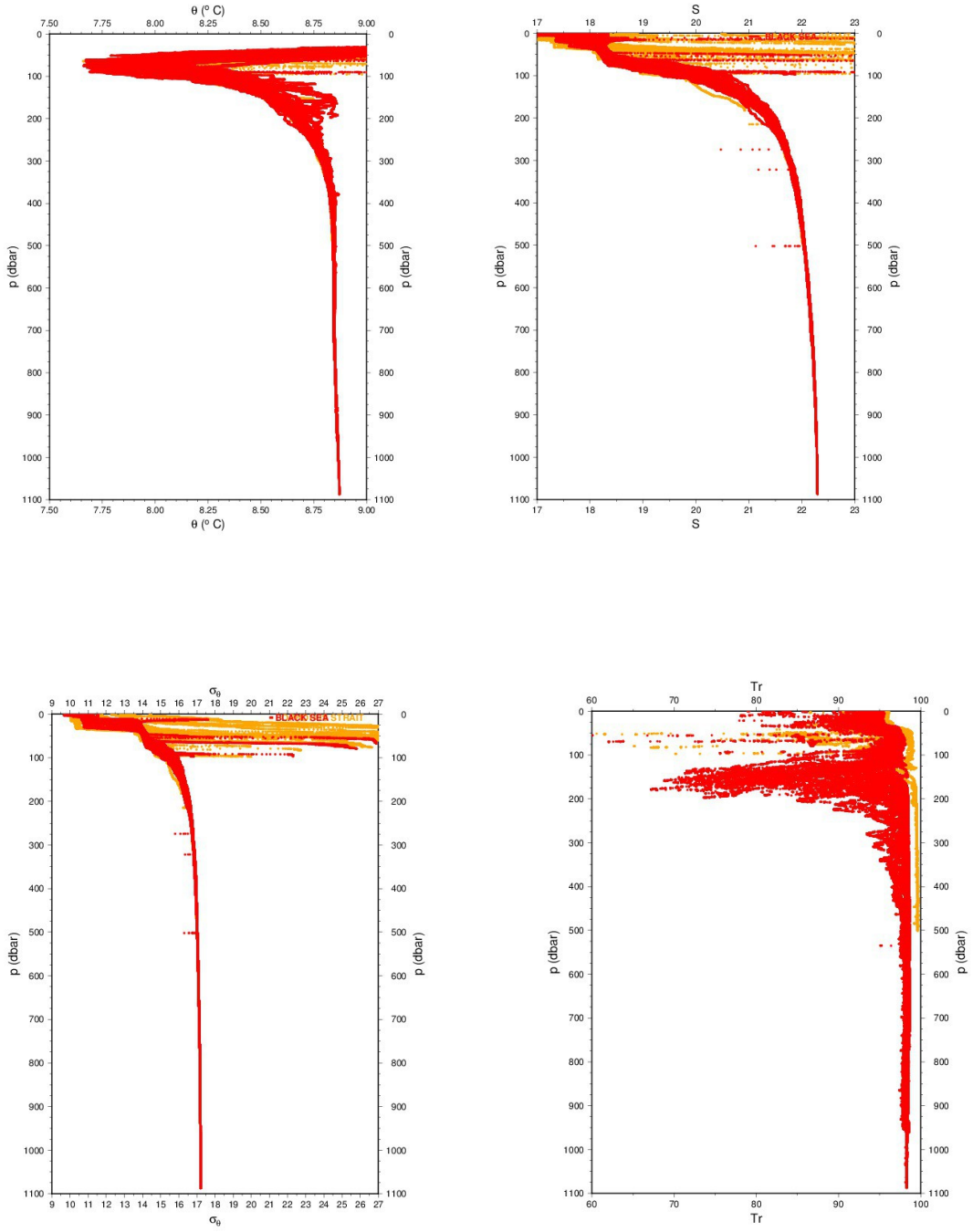


*Fig. 45. Collective profiles of the CTD data obtained in the southwestern Black Sea continental shelf and slope region adjacent to the Bosphorus: (a) temperature temperature (°C), (b) salinity, (c) $\sigma_\Theta$ density, (d) light transmission (%).*

A remarkable difference from the characteristics of intrusions reported earlier (Özsoy et al. 1993, 2001, Özsoy and Beşiktepe, 1999), however, is the sign of the temperature anomalies relative to the normal profiles. The temperature anomalies in Fig. 45a between depths of 100-500m are warmer than the smooth profiles, while those in the 1990's were mostly negative in the same depth range.

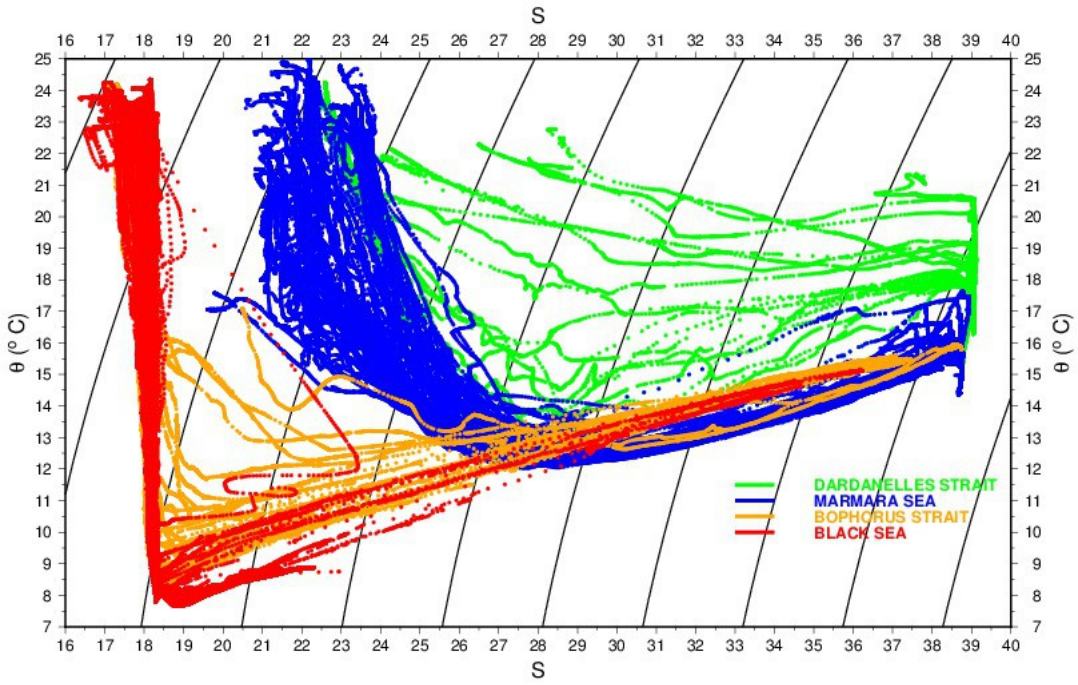


*Fig. 46. Temperature – salinity diagrams of collective CTD data obtained in the June 2013 cruise covering the Dardanelles Strait (green), Marmara Sea (blue), Bosphorus Strait (orange) and southwestern Black Sea continental shelf and slope (red) regions.*

The T-S diagram for the collective data displayed in Fig. 46 differentiates between the evolving characteristics of water masses exchanged across the Turkish Straits System and the neighboring Black Sea. The surface waters on the top left of the diagram evolve from warmer values in the Aegean Sea to colder values in the Black Sea. The deep waters at the far right of the figure are of Mediterranean character, with nearly isothermal state varying slightly between the Aegean and the Marmara Seas. The CIW of the Black Sea is located on the lower left. The points representing the high temperature tail to the right of figure of the Black Sea profiles (red) are the remnants of modified Mediterranean water that is detected on the southwestern Black Sea shelf. The deep water of the Black

Sea is hidden in this figure, represented by the curved line near the temperature range of less than 9°C and salinity of about 22, in the lower left hand side.

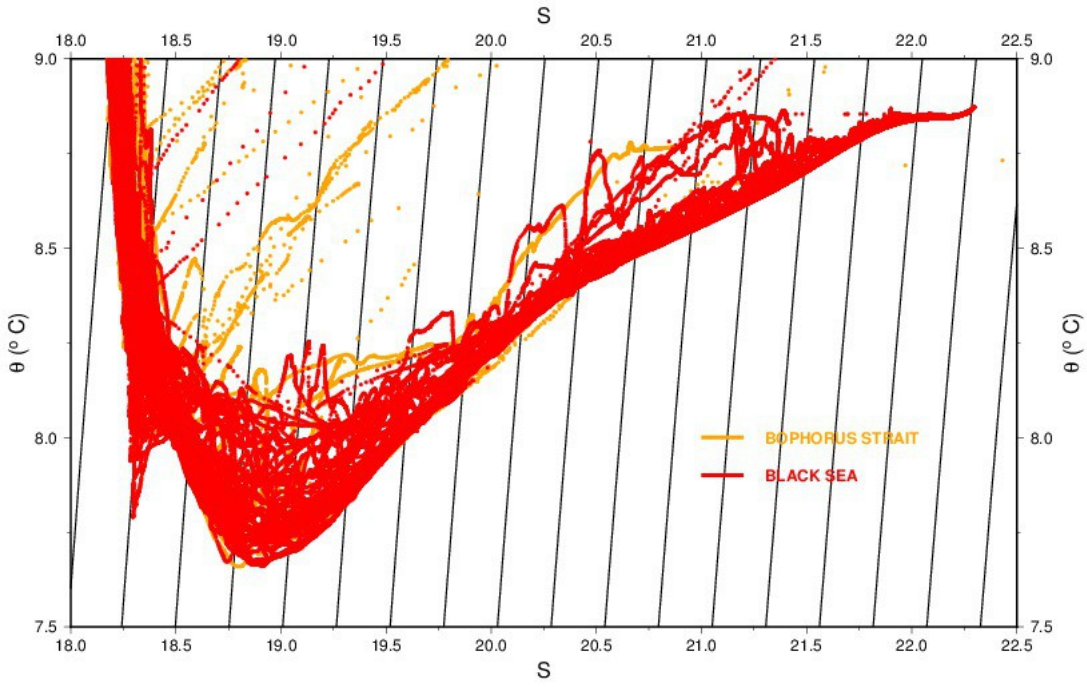


*Figure 47. Temperature – salinity diagram for the southwestern Black Sea region.*

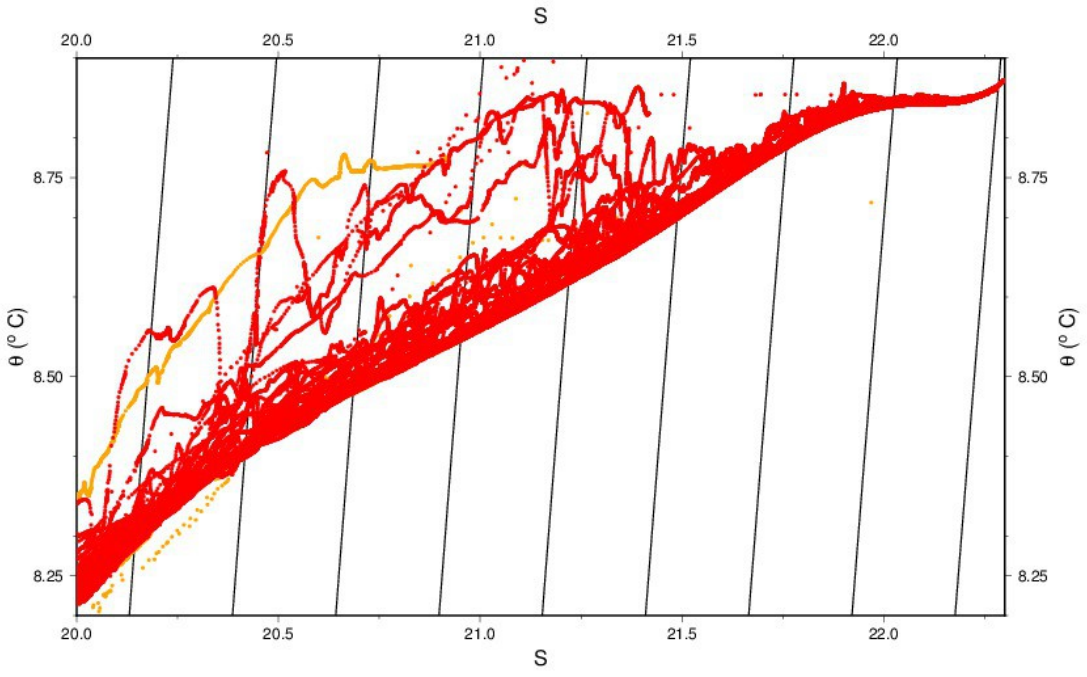


*Figure 48. Temperature – salinity diagram with the deeper part enlarged.*

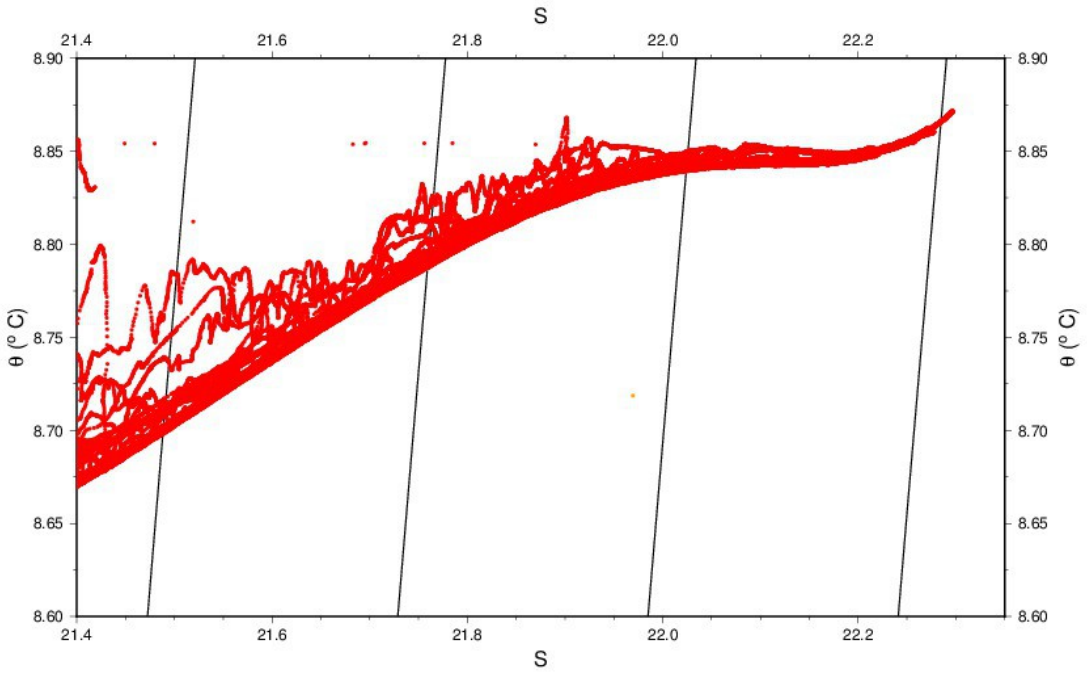


*Figure 49. Temperature – salinity diagram with the deeper part further enlarged.*

The actual T-S diagram for the Black Sea part of the data is shown in Fig. 47. Here the surface waters are to the upper left, the Cold Intermediate Water is to the lower left and the deep water is to the upper right. What is seen as a lot of noisy signals deviating in a positive sense in temperature values from the main body of the curves are due to the numerous layers of intrusions into the Black Sea of the water originally of Mediterranean origin but modified in its course through the TSS and the adjacent Black Sea shelf. the The inclined curves in the T-S diagrams of Fig.s 46-49 are the constant $\sigma_\Theta$ density lines.

Enlarging this in Fig.s 47 and 48 shows the details of the intrusions at the deeper parts, typically between the depths of 100-500m along the continental slope. Once again the anomalies are seen to be positive in temperature values, and roughly aligned with constant density lines. The fact that positive anomalies are observed in recent times as compared to negative anomalies in the 1990's suggests that there are significant climatic changes in the Black Sea as suggested by a number of other authors based on other oceanographic data. The change in the sign of the anomalies could either be related to changes in the external Seas such as the Mediterranean and TSS or changes in the Black Sea, or both, which in fact would of course be related to each other.

### 3.1.4 Chemical oceanography of the southwest Black Sea continental shelf / slope

The Black Sea is under the influence of the cyclonic loop of the rim-current along its shoreline. The southwestern Black Sea continental shelf adjacent to the Bosphorus Strait is therefore under the influence of the Danube river waters arriving from the northwest continental shelf region with the southerly flows along the western coast. The southwest shelf is therefore under the intense pressure of almost eutrophic surface waters rich in organic and inorganic nutrients, transported from the north along the broad continental shelf (Humborg et al., 1997; Konovalov et al., 2005). The inorganic nutrients carried by the river waters are consumed by phytoplankton depending on climatic conditions and turns into organic forms. As a consequence, the concentration of inorganic nutrients in the surface waters is reduced significantly, although with significant variations in space and time (Baştürk et al., 1998; Codispoti et al., 1991; Konovalov, et al., 2001; Tuğrul et al., 1992, 2014). The mixing of the low salinity near-surface waters carried by the cyclonic flow with the saline water outflowing from the Bosporus along the southwest coast produces new water masses with altered physical and biochemical properties. The chemical properties of the saline waters of Mediterranean origin will have been significantly changed in the 6-7 years of residence period in the Sea of Marmara (Polat and Tuğrul, 1995; Polat et al., 1998), with concentrations of nutrients enriched 10-fold and oxygen reduced to sub-oxic levels (<50 μM). The mixing of these waters near the Bosphorus determines the biochemical status of the region. The mixing of the Black Sea Cold Intermediate Water (CIW) with the more salty and warmer Bosphorus outflow water on the continental shelf with subsequent cascading along the continental slope (Özsoy et al., 1993) is known to introduce oxygen and particulate matter (Mn, Fe-oxide) to intermediate depths of the Black Sea (Konovalov et al., 2003; Tuğrul et al., 2014; Yiğiterhan et al., 2011).

When collectively examined, nitrate (defined here as total nitrate + nitrite) concentration in surface waters of the continental shelf mostly vary in the range of 0.05-0.4 μM. In river influenced waters of low salinity (S < 17.5) nitrate was observed to be consumed by photosynthesis, dropping to 0.1 μM. The nitrate concentration increased, reaching 0.25-0.4 μM in coastal waters with salinity values of around 17.5. The reason for this is the higher consumption of other nutrients (phosphorus) leaving nitrate relatively more

abundant. Waters with higher salinity range (S > 17.5) on the continental slope and the open sea again showed a declining trend in nitrate, as the open sea background of nutrients is often smaller, except for the winter period.

The dissolved ammonia ($NH_4$ ion) level in the sea is often low, its main sources being rivers, rainwater and organic nitrogen resulting from decomposition of planktonic organisms. No accumulation ammonia can be expected in the deep waters ventilated to have sufficient oxygen levels, because any released ammonium ions are oxidized to nitrate form. It can be seen from Fig. 1 that the $NH_4$ ion concentration in surface waters is in the range of 0.05-0.4 μM, showing some similarity with the nitrate concentration. $NH_4$ is expected to have higher values in waters having high biological activity. No significant changes due to salinity can be observed; however, a decrease can be observed in open waters (S> 17.5) where nitrate has the same tendency.

Total dissolved inorganic nitrogen (DIN = nitrate + nitrite + $NH_4$ total) is in the 0.65 – 1 μM range in surface waters of the region. Depending on the nitrate increase in salinity of Whereever the continental shelf waters reach salinity values of 17.5, increased values of DIN can be observed in parallel with nitrate. With increasing salinity in the open sea, the DIN concentration has a tendency to decrease.

Ortho-phosphate (o-PO4), which has a very low (<0.05 μM) concentration in low salinity coastal waters, partially tends to increase to higher concentrations (0.01-0.1 μM) towards the open waters of the continental shelf (Fig. 1). The fact that nitrate and phosphate are low in the same waters shows nutrients to be consumed by autotrophic live matter. The nitrate / phosphate ratio (N / P) generally being low in surface waters indicates that both nitrates and phosphates are limiting nutrients in coastal waters.

Reactive silicate transported to the sea through rivers has a very low concentration (<1 μM) in coastal waters, resulting in low silicate / nitrate ratio (Si / N) in the same region (Fig. 2). The low silicate in the river-fed waters of the coastal sea is indicative of the limitation of diatom production by the availability of silicate introduced by rivers. The deep waters of the Black Sea are rich in silicate ions, which are transported to the surface from intermediate depth by physical mixing. Similar mixing events also transport nitrate and phosphate ions to the surface. However, because the intermediate layer silicate concentration is very high (> 50 μM), silica enrichment in the surface waters

becomes very noticable especially during winter. As a result, a significant increase is observed in the silicate Si / N ratio from the continental shelf towards the open sea. The increase in silicate concentration (S> 17.5) at the surface waters of the open sea is therefore an expected result, since phosphate and nitrate are depleted in the same region.

The concentration of oxygen wss found to be at saturation level in the surface waters, varying in the range of 245-270 μM, its solubility being closely related to water temperature and salinity.

It is very important to define the chemical characteristics of water mass transported to the Black Sea by the Bosphorus undercurrent in order to understand regional variations and the intermediate layer features in the southwestern Black Sea. For this purpose, the water column profiles of salinity, temperature, nutrients (nitrate, $NH_4$, phosphate, silicate) and dissolved oxygen at the exit region are shown in Fig. 2. The upper layer in the first 30-40m of at the exit region has low salinity waters of the Black Sea. The lower layer, deeper than 50m has the more saline (S> 30) waters of Marmara Sea, which also has warmer temperature of about 14.5-15°C compared to the Cold Intermediate Water of the Black Sea partially entering into the Bosphorus below the mixed layer. The oxygen concentration, which appears to be at saturation level (250 μM) in the low salinity (S: 17-18.5) Black Sea waters of the upper layer, drop to about 50 μM level in the saline (S: 35-38) waters of the lower layer waters originating from the Marmara Sea.

The nitrate, ammonia, phosphate and silicate concentrations are low in the surface waters of the exit region as they are in the in continental shelf waters of the Black Sea, showing homogeneous values at depths shallower than 30-40m. The nitrate, phosphate and silicate concentrations are enriched whereas oxygen is reduced in the lower layer (Fig. 50). The source of these nutrients is the upper layer photosynthesis products transported to the lower layer and subsequent degradation of organic matter by oxygen-consuming bacteria in the lower layer. The observed extraordinarily high concentrations of $NH_4$ and phosphate ions in the lower layer outflow are results of the domestic wastewater injected into the lower layer without treatment (Özsoy et al., 1995; Beşiktepe et al., 1995). The phosphate concentration is at least 50% higher than the values observed in the past. As a result, salty, oxygen-poor, nutrient-rich waters are transported from the Marmara Sea to the Black Sea via Bosphorus (Polat and Tuğrul, 1995).

According to measurements made in recent years, phosphate and $NH_4$ build-up in the Bosphorus lower layer flow has become very apparent and the amount of nutrients transported to the Black Sea has increased in proportion. The remedy to reduce this load should be the introduction of biological treatment leading to breakdown of organic matter (bacterial decomposition) in the urban wastewater currently discharged to the Bosphporus underflow. Treatment could increase bacterial breakdown of the wastewater to at least 80%, reducing the level of oxygen-consuming and photosynthesis-producing nutrients introduced into the marine environment.

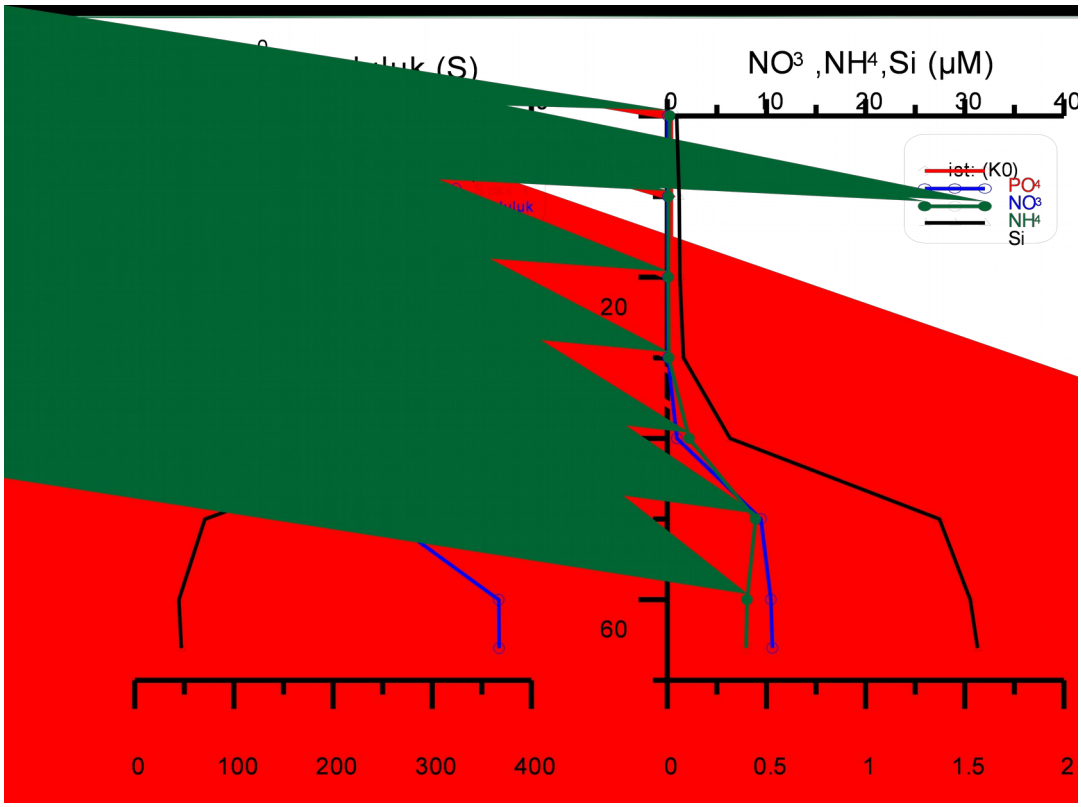


Figure 50. Black Sea Bosphorus output of measured physical and chemical parameters with depth.

The different water masses are monitored with high precision salinity and temperature measurements with a CTD system and the chemical characteristics such as the nutrient and oxygen concentrations in the Bosphorus plume spreading near the shelf bottom and the overlying waters can be monitored (Codispoti et al., 1991; Konovalov et al., 2003; Özsoy et al., 1993; Tuğrul et al., 2014). The salinity at the Cold Intermediate Layer (CIL) located just above the halocline varies in the range 18.0-18.5, renewed only by winter

convection events (Gregg and Yakushev, 2005; Özsoy et al., 1993; Konovalov, et al., 2005). Shelf and open ocean convection events do not penetrate below the halocline levels and therefore the chemical constituents such as nutrients at and below the halocline appear as functions of density alone.

Because the signals in temperature and salinity in deep water are weaker than the shelf area, and according to the hypothesis that if the scalar variables such as nutrient concentration should be a function of the water density alone, they would have to obey one-dimensional vertical diffusion in density coordinates (Gaines et al., 2006), plotting vertical profiles of chemical properties against water density (sigma-t) enables detailed evaluations of their sources and time evolution. By plotting profiles in density coordinates thus allows differentiation between chemical characteristics of different water masses having the same density. For example, phosphate concentration in the anoxic layer (sigma-t: from 16.0-16.3) appeared low near the Bosphorus, but showed a significant increase in the open waters of the Black Sea.

Fig.s 51 and 52 show traces of the Bosphorus plume in the chemical profiles. Fig. 51 shows depth profiles, while Fig. 52 plots them with respect to (sigma-t).

The dissolved oxygen concentration typically decreases till the Black Sea halocline (Codispot et al., 1991; Tugrul et al., 2014). On the continental slope adjacent to the Bosphorus, the oxygen profile indicates intrusions of oxygenated water at depths of up to 160m, which is otherwise accepted to be the anoxic waters below the halocline (Fig. 51), also indicated by interferences in the other chemical properties, such as . in the nitrates, observed at depths below 75 m.

The changes in chemical parameters in the water column in terms of water density (sigma-t) coordinates showed very similar characteristics (Fig.s 52 and 53). The nitrate maximum is observed in the sigma-t range of 15.3-15.5, while the oxygen concentration has fallen below the level of 5 μM at the sigma-t 15.9-16.0 level; in the same depth nitrate (nitrate + nitrite sum) concentration has dropped to 0.1-0.2 μM. Very rapid increase in phosphate concentration below the levels of oxygen containing waters and reaches its maximum value at depth of sigma-t 16.1-16.2. The phosphate maximum is a characteristic of the Black Sea ecosystem and is used as an indicator for monitoring

hydrogen sulphide in the open waters Baştürk et al., 1998; Tuğrul et al., 1992, 2014; Konovalov, et al., 2005).

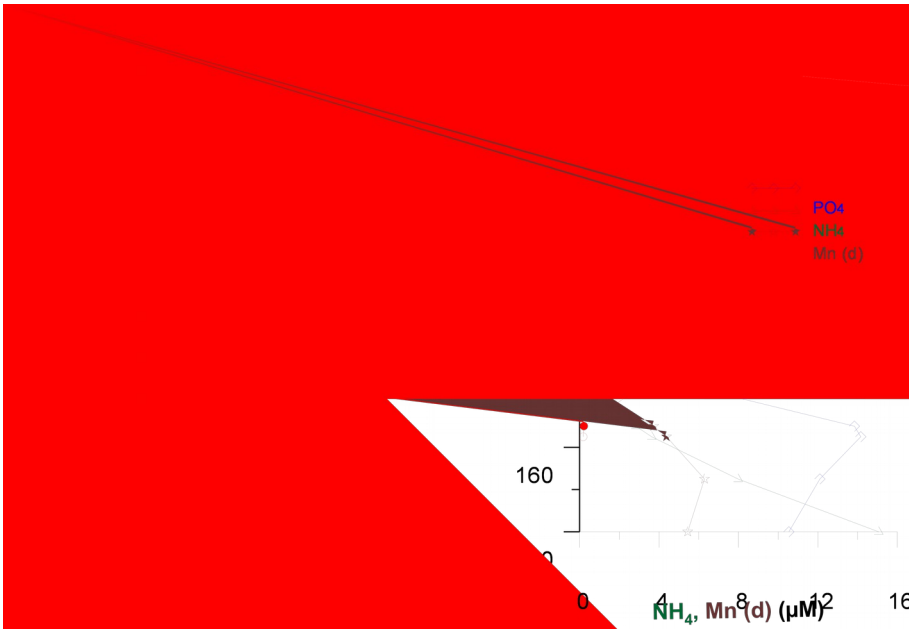


*Figure 51. Profiles of physical and chemical parameters plotted with respect to depth for a station along the southwestern Black Sea continental shelf slope.*

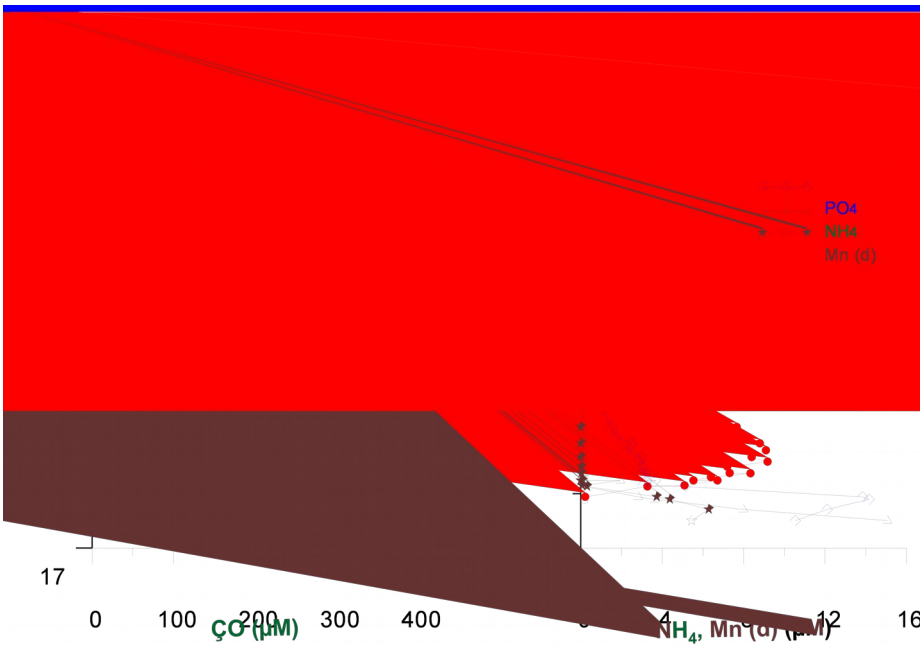


*Figure 52. Profiles of physical and chemical parameters plotted with respect to density for a station along the southwestern Black Sea continental shelf slope.*

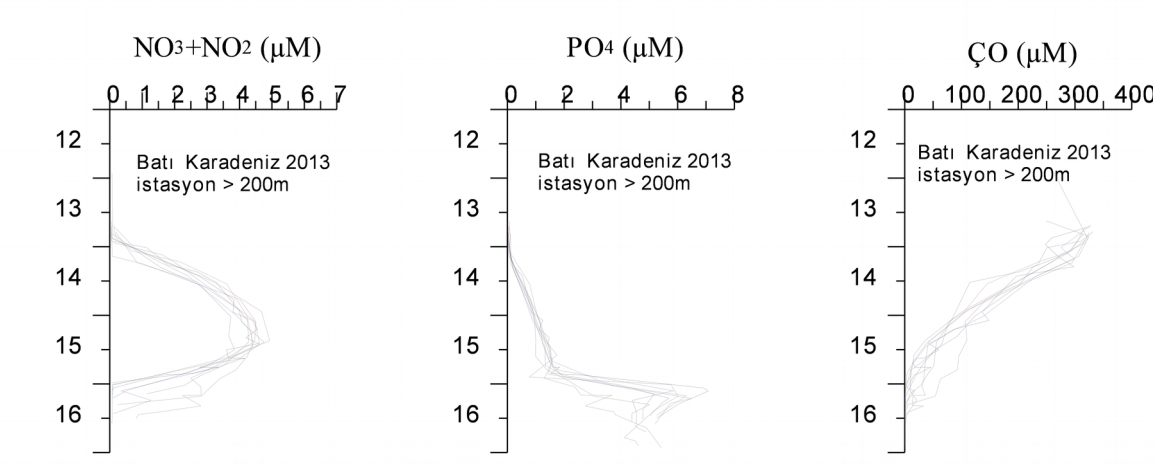


*Figure 53. Collective chemical (nitrates, phosphates, dissolved oxygen) plotted with respect to density along the southwestern Black Sea continental shelf slope.*

Upon mixing with the Black sea waters the warm and salty waters exiting the Black Sea and entering the Black Sea at intermediate depths change their chemical properties, with oxygen depleted and nitrate, ammonia, phosphate and silicate concentrations increased. Fine resolution chemical profiles have been measured earlier by making use of special continuous pumping methods (Codispoti et al. 1991; Tuğrul et. 2014). It also carries the Light transmission measurements concurrently obtained with other physical measurements by the CTD are confirmed by particulate matter samples taken at intermediate depths and filtered through GF / F type filter, showing a significant increase in particulate concentrations. In these samples, particle organic carbon, nitrogen (POC, PON), and particle Mn and Fe are analysed. The results indicated organic carbon and nitrogen contained in particulate matter with measured values close to the POM value in organic rich surface waters. The C / N ratio in POM is in the 6-8.5 range. The particle-containing layer indicates the presence of high biological activity and contains nitrogen comparable to the POM composition of surface waters. The Mn and Fe particle

concentrations at these depths are similar, in the range of 1 to 2 μM. The particle-Mn measured values are lower than those of the dissolved Mn in anoxic water. In the continental slope region the dissolved Mn concentration increased with depth starting from the depth of density of 15.9, increasing where phosphate minimum-maximum has been observed. These changes have been envisaged in earlier publications to be a result of reduced manganese particles (Yakushev et al., 2007, 2009).

Samples were taken from the fine particulate intermediate layers on the continental slope (depths > 200m) near underwater canyons, at staions affected by intermediate depth particulate layers and nutrients, oxygen, hydrogen sulphide, particulate manganese (Mn) and iron (Fe) measurements were made, examples of which are shown in Fig. 54. Fine particulate layers were observed near the continental slope in sub-oxic (<50 μM) waters at depths of 140-200 m. Particle Mn concentration was observed to be higher than Fe. The highest Mn concentration was observed at the oxygen poor intermediate levels where conversion to particle (Mn-Fe oxide) form occurs. Similar results were obtained in research conducted in the western Black Sea (Yemenicioğlu et al., 2006; Yiğiterhan et al., 2011). Because particles of metal oxides are converted to dissolved form in the oxygen-free deep waters, fine particle layers were only observed at depths of 300-350 m. close to the canyons. Dilution and The fine particulate layer disappears in open waters as a result of chemical reactions and dilution.

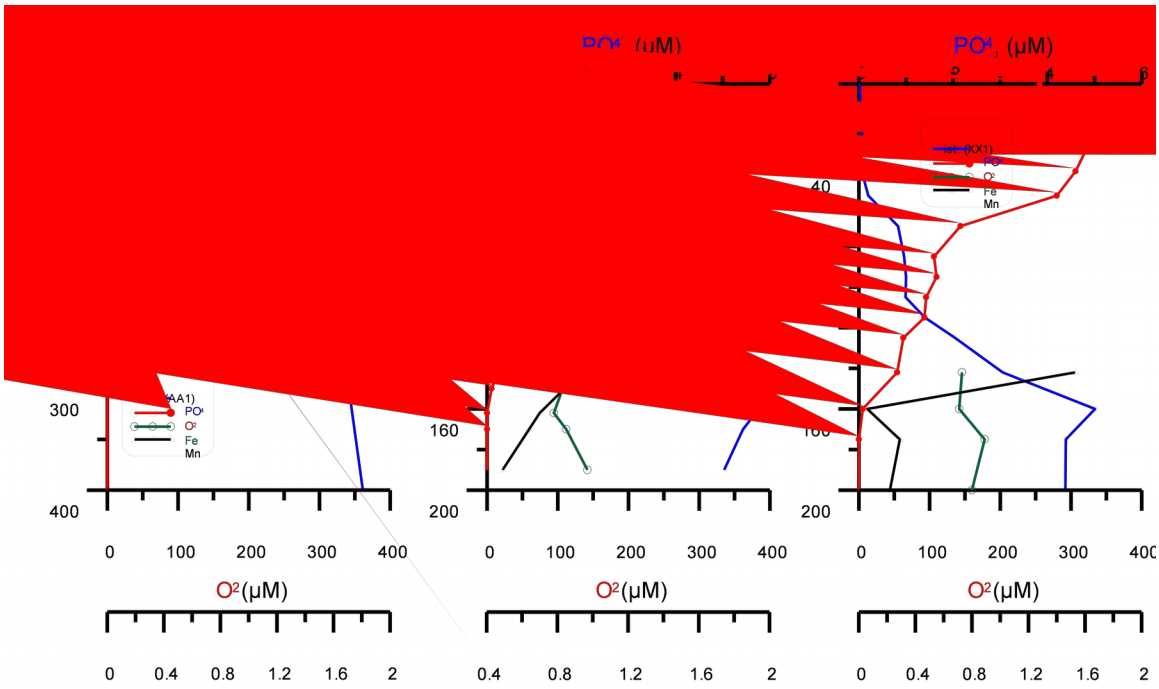


*Figure 54. The slope of the continental shelf (depths> 200m) measured at certain points of the chemical parameters (phosphate, oxygen, particulate Mn, Fe) high and intermediate layer depth changes.*

### 3.2 Model Results

#### 3.2.1 Bosphorus Model - Exchange Flows

In the analyses of the model results, the properties of the strait flow are assigned to layers defined according to the salinity and velocity fields. A two-layer decomposition is defined by allowing the zero-velocity surface to separate the flow into counter-flowing upper and lower layers respectively with volume fluxes of $\mathbf{Q_1}$ and $\mathbf{Q_2}$. Alternatively a three-layer decomposition is defined based on the relatively uniform scalar properties in the top and bottom layers with discharges $\mathbf{Q_T}$ and $\mathbf{Q_B}$ respectively and an interfacial layer of variable properties and discharge $\mathbf{Q_I}$, using salinity, a conservative tracer. The top and bottom layers are defined by delineating surfaces where the salinity differs by 10% respectively from the surface and bottom values at the same horizontal position. The remaining part of the vertical profile is defined as the interfacial layer.

For the first group of runs not shown here (Sözer 2013), the model with realistic geometry is started from a lock-exchange initial condition, releasing two uniform water bodies meeting at the mid-section of the strait, with typical contrasting salinity and temperature constant values in the north, the latter representing seasonal variations of temperature in the Black Sea. To avoid instabilities during start-up, the integration is carried out with a very small baroclinic time step of $\Delta t_i$ = 1.75 s at first, adjusted to 4.0 s after the first day of the run, and using an external time step that is 20 times smaller. In addition to water properties, a constant value of the net barotropic flux is specified at the open boundaries, and varied in the different runs around a value comparable with that observed during the September 1994 measurements of Gregg and Özsoy (2002).

The evolution of the total kinetic energy per unit volume (not shown) in the runs suggests a steady state is reached and volume flux conservation is achieved in less than two days, despite residual oscillations of negligible amplitude (amounting to less than 0.5% of the final). Under the influence of the open boundary conditions, temporal changes in the reservoirs are very slow and their feedbacks to the strait limited; therefore approximate steady state is also achieved for tracer fluxes. The zero velocity line separating the counter-flowing currents is clearly differentiated from the density (salinity) interfacial layer, and positioned higher than this layer in the northern part of the Bosphorus, remaining at about mid-depth over the sill, where the salinity interface is much deeper. Along the strait, the upper layer salinity gradually increases, while the lower layer salinity decreases in the respective flow directions as a result of turbulent mixing and entrainment of fluid parcels from one layer to the other.

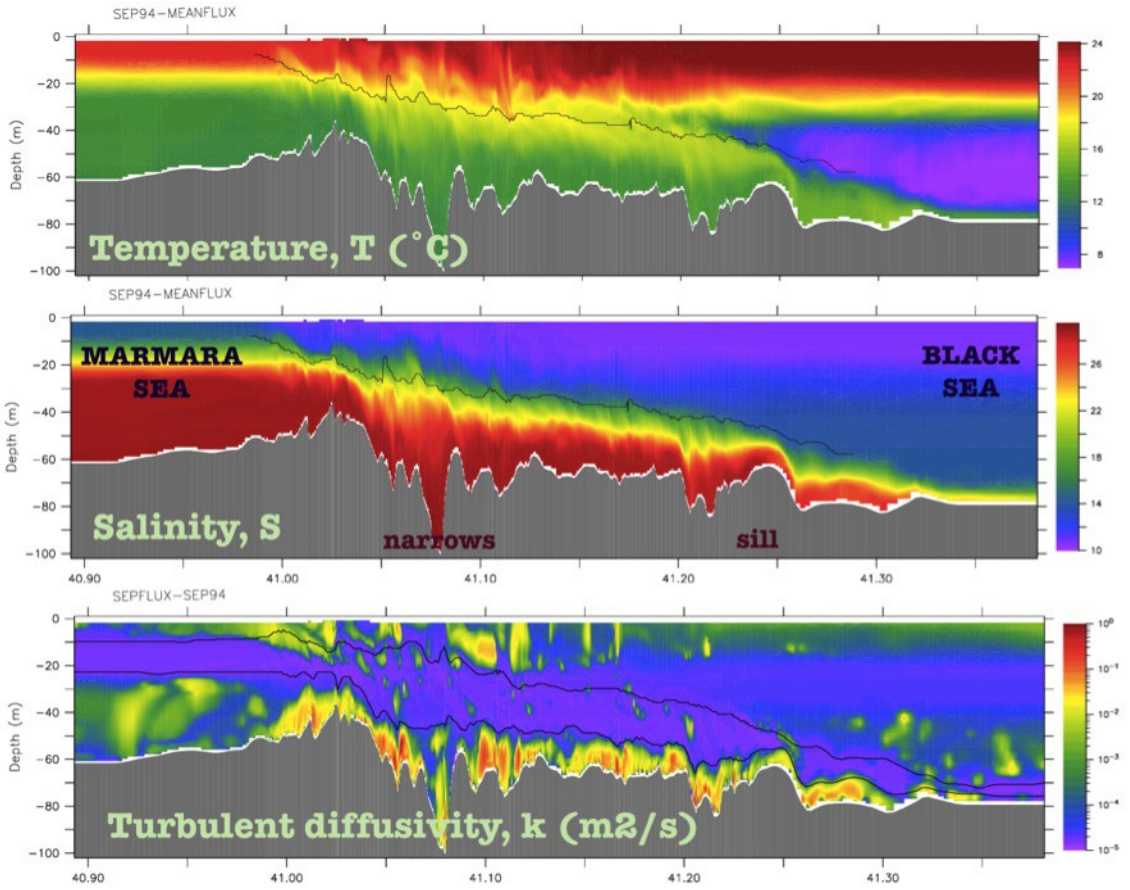


*Figure 55. Along-channel thalweg sections for RUN5 (a) temperature, (b) salinity and (c) turbulent diffusivity.*

Non-uniform, stratified boundary conditions at the two ends of the strait were next introduced by specifying temperature and salinity depth profiles typical of the fall season, consistent with the September 1994 observations of Gregg and Özsoy (2002). Accordingly, constant values **T**=22.5 °C, **S**=23 above 11m and **T**=13°C, **S**=38 below 25m depth, with linear change in between were specified to represent the two-layer stratification on the Marmara side. On the Black Sea side, warm water of **T**=24.1°C in the first 20m depth, with a linear decrease till the Cold Intermediate Water (CIW) layer of **T**=7.0°C starting at 40m depth and extending to the bottom were assumed, and a constant salinity of **S**=17.6 is assumed in the Black Sea. Radiation and nudging boundary conditions were applied, with a nudging coefficient of 0.1 d for outflow and

0.01 d for inflow. Usually several cycles of adjustment oscillations occurred with stratified reservoirs.

The introduction of non-uniform boundary conditions (RUN5, Sözer, 2013) had great impact on model results as a consequence of the CIW contact with the warmer waters of the undercurrent at the interface, changing the density and turbulence properties of the flow. The temperature distribution is significantly (Fig. 55a) without much change in salinity (Fig. 55b), but rather in density (not shown). Large oscillations occurred in properties during the initial adjustment period, with small residual oscillations in temperature until the end of the run, although the model was restarted from the steady state conditions of the earlier run to shorten these adjustments.

The vertical viscosity computed from the turbulence closure scheme is shown in Fig. 55c. Turbulent patches with increased viscosity are found in the upper and lower layers of the flow, with greatly reduced values at the interfacial layer, where the turbulence is suppressed by the density stratification. Due to the suppressing effects of the initial density stratification in the adjacent seas, the penetration of the denser and colder CIW into the interface zone greatly decreases the vertical turbulent viscosity in the upper and lower layers and increases the thickness of the inactive interfacial layer.

Comparisons of the model produced salinity and temperature and the corresponding fields based on observations in September 1994 (Özsoy et al. 2001) are provided in Fig. 56. The temperature fields provide better comparison, while the salinity only has good comparison in the mixing zones south of the contraction and north of the sill. The most prominent difference between the modeled and the observed salinity and to a lesser degree in temperature is in the estimated thickness of the interfacial layer between these two control sections, i.e. in the northern sector of the strait, where the observations suggest relatively sharper gradients at the interface.

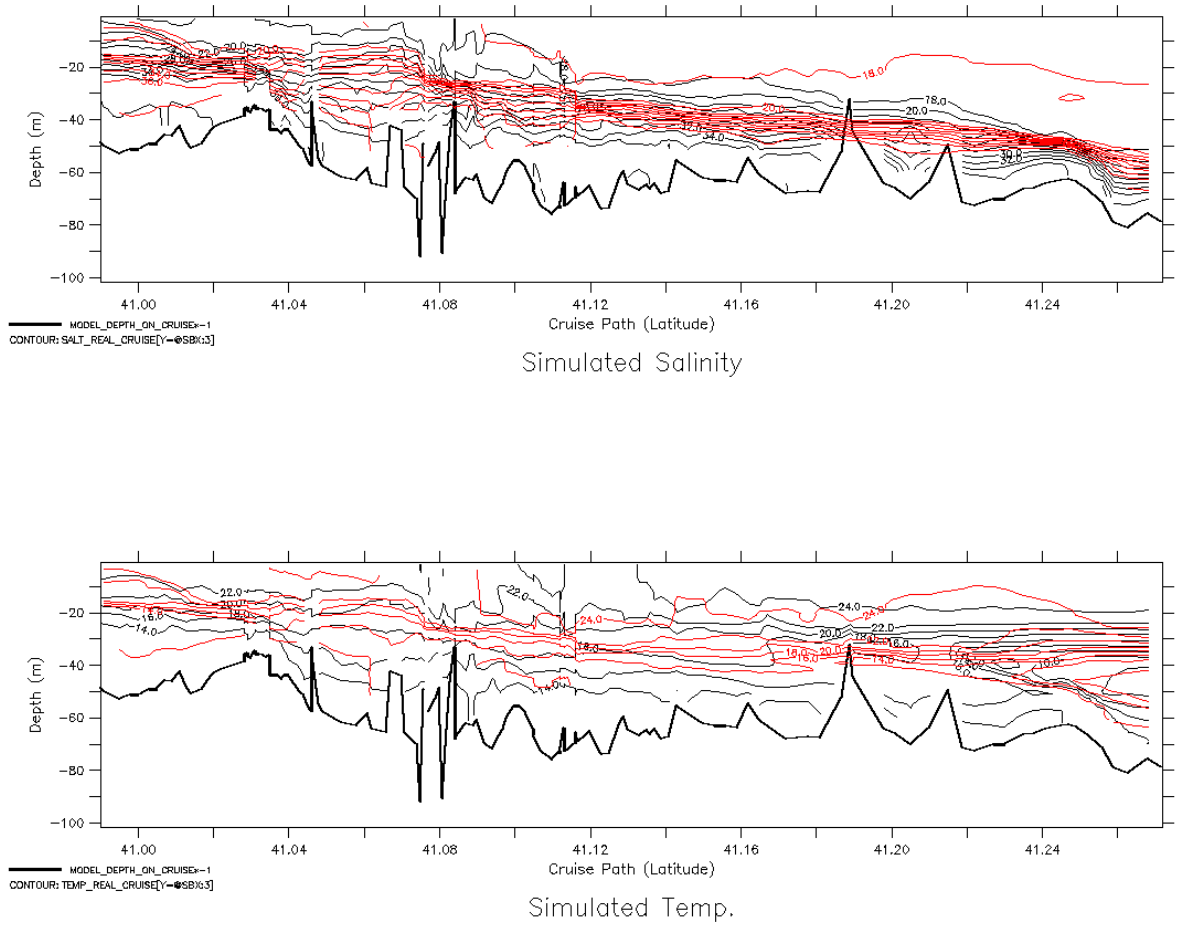


*Figure 56. Model simulated (RUN5, Sözer, 2013) and observed (Özsoy et al, 2001) fields of (a) salinity (b) temperature corresponding to the September 1994 conditions.*

The model solutions qualitatively reproduce many features reported in the earlier observations (e.g. Özsoy et al., 2001; Gregg and Özsoy, 2002), such as the wedge shaped upper and lower layers of rather uniform properties, the thickness and depth of the mixing interfacial layer between them, the apparent hydraulic controls at the contraction and sill, the thin surface layer outflow into the Marmara Sea, the sill overflow and subsequent adjustment on the Black Sea shelf. The overflow over the north sill and the following internal hydraulic jump is successfully demonstrated in all cases. Boundary conditions are able to establish and preserve the intended stratification in the neighboring Seas.

The larger interface thickness in the model could be a result of the interference contribution of the horizontal diffusivity to the vertical mixing, a byproduct of the s-coordinates used by ROMS, which becomes more pronounced when stratified boundary conditions are taken into account. The bottom boundary layer parameterization using a friction term could also limit the level of turbulence in the bottom layer, consequently impacting the interfacial mixing.

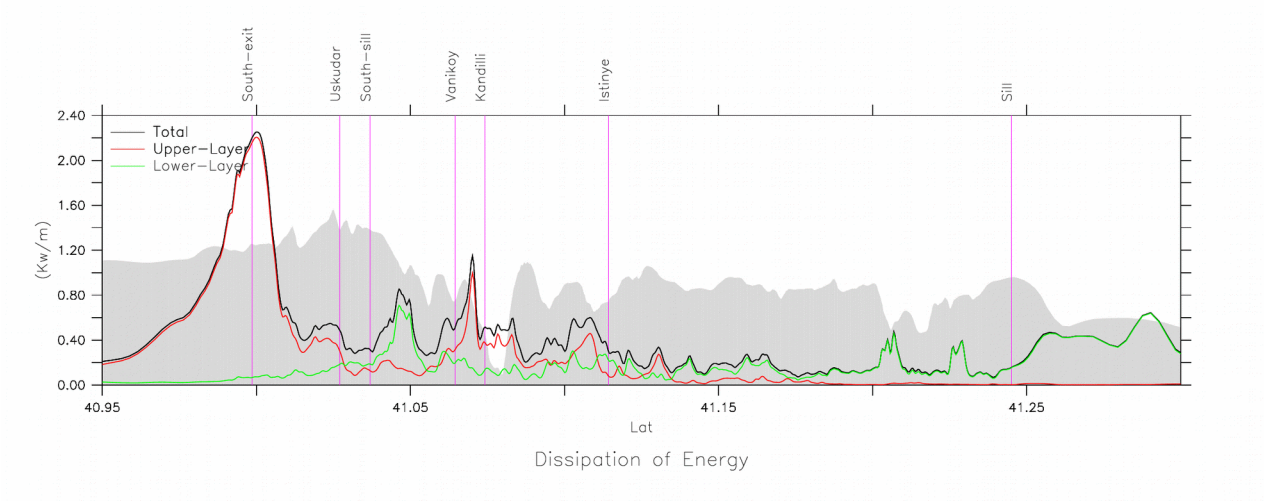


*Figure 56. Variation of the upper, lower layer and total energy dissipation rates along the Bosphorus (bathymetry in the background).*

The mechanical energy dissipation profiles of the strait are given in Fig 57. While the energy loss is minimal and only confined to the lower layer due to frictional effects between the contraction and the northern sill, there are significant peaks past the various hydraulic control regions in either layer. Mechanical energy loss is high at the contraction with a sharp increase past Kandilli point and a greater and wider area of dissipation south of the Marmara exit, almost all of which are contributed by the upper layer. The only exception is the north of the southern sill, where there is an increase in the lower layer overflow past the sill. Then the other area where there is wider scale dissipation in the lower layer is after the northern sill, at the hydraulic jumps.

The horizontal distribution of the upper and lower layer dissipation rates are shown in Fig. 57, confirming large dissipation rates at the various bends and topographic features, at the surface jet issuing into the Marmara Sea, past the northern sill and along the bottom plume on the Black Sea shelf. Total dissipation values of ~10.1Mw and ~7.3Mw

were found for the upper and the lower layers respectively, for the entire model domain.

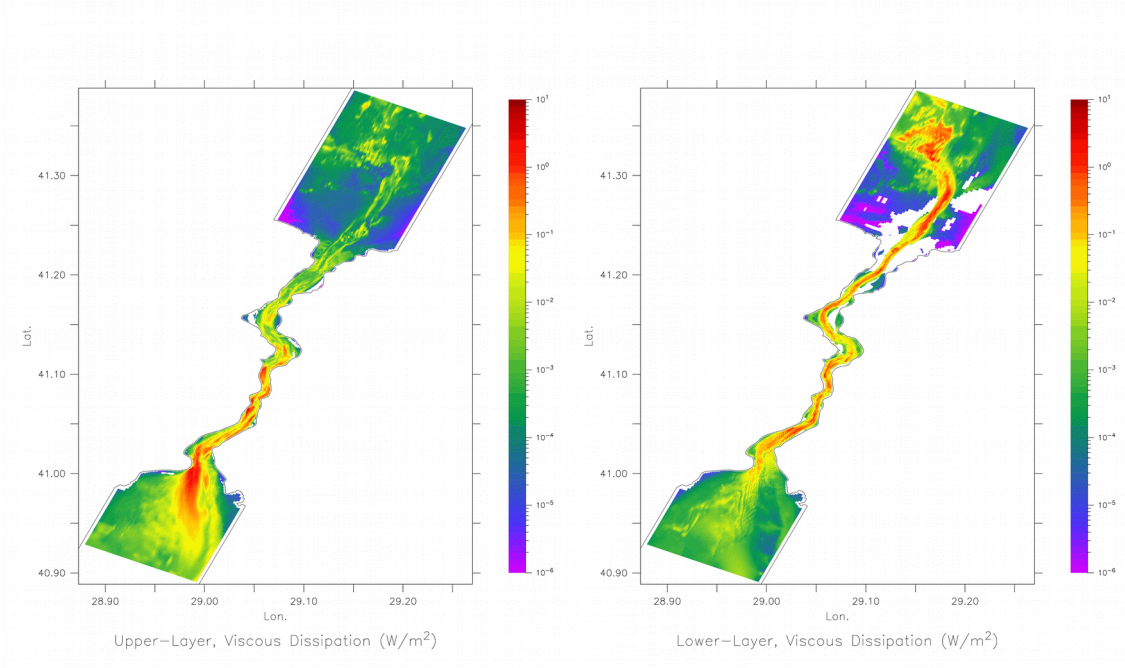


*Figure 57. Horizontal distribution of the mechanical energy dissipation by turbulence in the (a) upper layer and (b) lower layer.*

### 3.2.2 Hydraulic Control

Changes in flow cross-sectional area, width and thickness, demonstrated in the case of RUN1 (Fig. 58), occur in response to the strait bathymetry and coastal geometry. The total cross-sectional area (Fig. 58a) is largest in the northern half of the strait and has a maximum at 41.12-41.16°N, the s-curve of the channel, where a deep cut channel joins wide shallows on either side. The narrowest area occurs at 41.07-41.10°N of the contraction region. Then at about 41.075°N (Kandilli-Bebek section), the narrowest section is co-located with an abrupt turn of the channel and the deepest point of the strait at a depth of 110m.

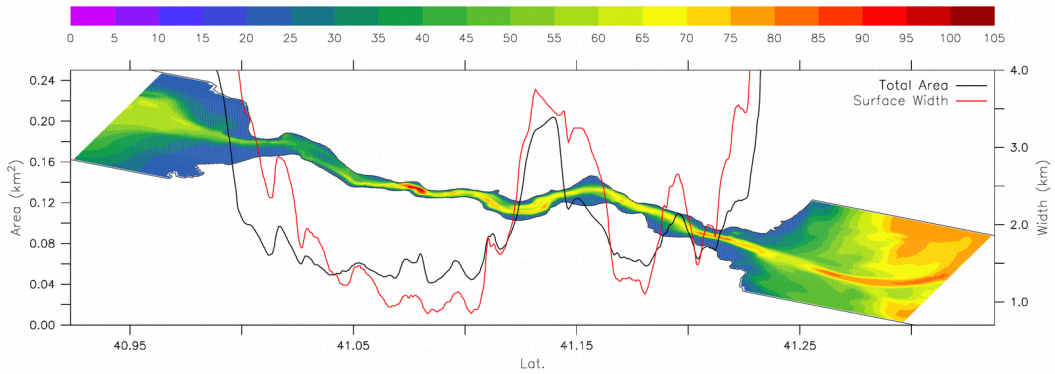


Bathymetry

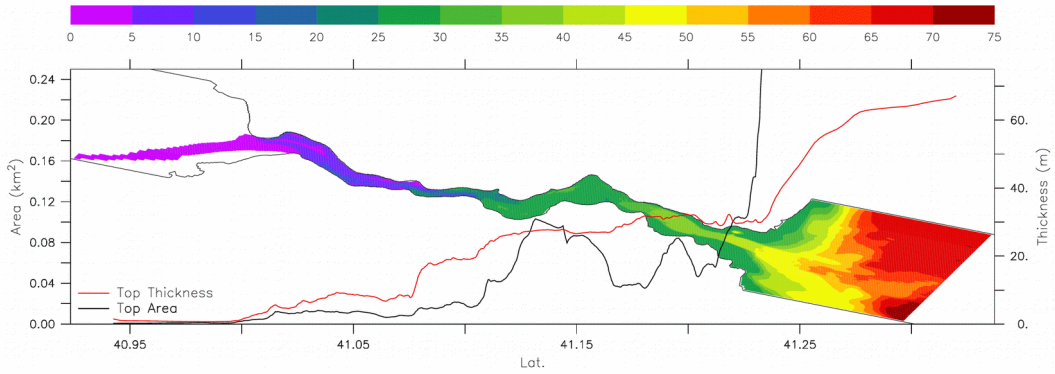


Top–layer Thickness (m)

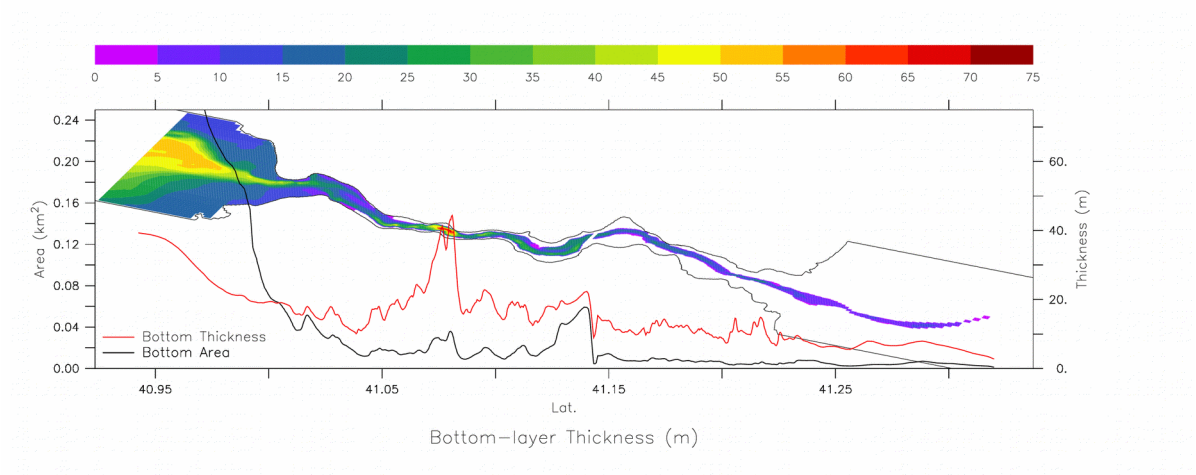


*Figure 58. (a) Variation of the total cross-sectional area and surface width along the strait, with superimposed image of the bathymetry of the Bosphorus, (b) top layer area and thickness as a function of latitude, with superimposed image of the top layer thickness in RUN1, (c) bottom layer area and thickness as a function of latitude, with superimposed image of the bottom layer thickness in RUN1.*

The area and thickness of the top-layer (Fig. 58b) decreases sharply in the contraction region (41.10°N), with a minimum at the promontory of Kandilli (41.075°N), and decreasing further towards the Marmara Sea. The area of the bottom-layer (Fig. 58c) decreases with distance from the southern end, rising in the first lapse of the s-curve in the northern Bosphorus, and decreasing in the second lapse in the deep and narrow channel carrying the flow till after the northern sill.

It is not clear based on measurements if and where hydraulic criticality exists in the Bosphorus. The hydraulic controls often were assumed to exist, but could not be positively demonstrated by the simplified two-layer Froude number calculations except for the northern sill (Gregg and Özsoy, 2002), rather than basing the criteria on the more appropriate stratified Froude number (Pratt, 2008). The Froude number is often calculated from incomplete density and current data respectively obtained from the CTD and ADCP measurements, which often are not simultaneously recorded, or miss velocity data near the surface and the bottom. The two-layer approximation is especially problematic in the Bosphorus because of the existence of a rather thick interfacial layer not fitting the assumptions and a high value of the density ratio $\Delta\rho/\rho$ in the denominator unrealistically reducing the magnitude of the Froude number.

Model results are used to calculate the two-layer composite Froude number for variable flow cross-sections following Pratt (2008), equation (2.8):

$$\mathbf{G^2 = F_{1w}^2 + F_{2w}^2}$$

where $\mathbf{F_{iw}^2 = [w_l^{-1} \int (g' h_i / u_i^2) dx]^{-1}}$ are the squares of the densimetric Froude numbers for the upper and lower layers $\mathbf{i}$=1,2 respectively, expressed as the inverse of an integral across the entire flow area averaged over the width spanned by the interface $\mathbf{w_l}$, such that $\mathbf{u_i}$ is the mean current speed and $\mathbf{h_i}$ the depth at position $\mathbf{x}$ across the section in each layer of the variable depth channel and $\mathbf{g' = g\ \Delta\rho/\rho}$ is the reduced gravity. In order to make the computations on cross-sections that are perpendicular to the main flow direction the data were transferred to a non-orthogonal curvilinear grid that satisfies this criterion at the computed sections, and the computations were made on these sections.

The classical arguments for establishing the existence of hydraulic controls often have been based on simply adding up the simple layer Froude numbers squared $\mathbf{F_i^2 = u_i^2 / g' h_i}$ based on the average velocity and depth of each layer as if they were from a rectangular

section, or alternatively, assigning a nominal thickness approximated by the layer area divided by the width for a variable depth section. In comparison, the Froude number computation of Pratt (2008) not only is a better approximation for variable properties, but also yields higher valued estimates of $\mathbf{G^2}$.

Yet for a topography as complex as in the case of Bosphorus, it is questionable, and hard to demonstrate Froude numbers reaching critical values, since the cross-section often has shallow banks where often lower current speeds are encountered, or deep channels on either side of the strait where the current leans only one side, especially at the various sharp turns.

Both Garrett and Gerdes (2003) and Pratt (2008) pointed out that the Froude number is often underestimated when the flow has shear, implying sluggish parts relative to a faster moving main stream. In those cases the integration of the quadratic term in velocity across the section would produce smaller values of the Froude number, and in the case of a single layer flow it is advised by Garrett and Gerdes (2003) that the Froude numbers squared $\mathbf{F^2}$ be corrected by multiplying with a dimensionless momentum flux factor $\mathbf{M_m=\int P^2(\zeta)d\zeta}$, or alternatively an energy flux factor $\mathbf{M_e=\int P^3(\zeta)d\zeta}$ (Chow, 1959; Henderson, 1966), both having values greater than unity by the Cauchy–Schwartz inequality, since the non-dimensional shape function $\mathbf{P(\zeta)}$ of the velocity profile integrated over the depth variable $\mathbf{\zeta=z/h}$ normalized by the thickness requires that $\mathbf{\int P(\zeta)d\zeta=1.}$

Based on our experience with experimental data and model results, we employed two methods that ultimately could result in more realistic composite Froude numbers providing a better assessment of the existence and localization of hydraulic controls in the Bosphorus Strait. Although the Garrett and Gerdes (2003) formulation strictly applies to single level hydraulics, we extended their suggestion to apply an energy flux correction to the two-layer case where each of the terms in the composite Froude number calculated by the integration method of Pratt (2008) were multiplied by the energy flux factor to yield $\mathbf{G^2 = M_{1e}F_{1w}^2 + M_{2e}F_{2w}^2}$. In this way we keep the critical value to be unity, as compared to Garrett and Gerdes (2003) who reduced the critical value by the same factor. The layer and composite Froude numbers for the uncorrected and corrected terms are displayed in Fig.s 59a,b.

A further significant improvement of the Froude number computation was made by completely excluding the sluggish parts of the flow from the numerical integration carried out across the section. In fact, one can also think of this in the spirit of the correction factors discussed above, but integrating powers of velocity shape functions in the horizontal rather than the vertical coordinates. In the calculation of what we termed as the “active composite Froude number” the velocity vectors that were lower in magnitude compared to the cross-sectional average were excluded from the computation (a further example of how this was done will be given later). The “active $\mathbf{G^2}$”**,** for both energy factor uncorrected and corrected cases are shown by the light blue curve in Fig.s 59a,b.

The along-channel variation of the uncorrected two-layer Froude number estimate plotted in Figure 13a fails to confirm the existence of hydraulic controls anywhere, although local increases are observed at the Marmara exit, the southern sill, south of the contraction and at the northern sill. Between the contraction and the northern sill the Froude number has the smallest values, suggesting that the controlled sections are possibly external to this domain. Indeed the only raised levels, although not reaching the critical value of unity, occur north of the northern sill, and south of the contraction. With the energy corrected plots in Figure 15b, the Froude numbers of each layer and the composite increase significantly, approaching the critical value, but not really reaching it at any location. Yet when the “active composite Froude number” correction selecting only the faster velocities at each section is imposed (light blue in Fig. 59b), then there are few places where we begin to see supercritical flows: these are the south-exit, the headland at Üsküdar, the main contraction and the north sill. The existence of supercritical regions with $\mathbf{G^2 \geq 1}$ at the contraction and northern sill, with only subcritical conditions with $\mathbf{G^2 < 1}$ between them confirms the establishment of the two-layer maximal-exchange regime through the strait, if we are to accept the active composite Froude number concept as appropriate.

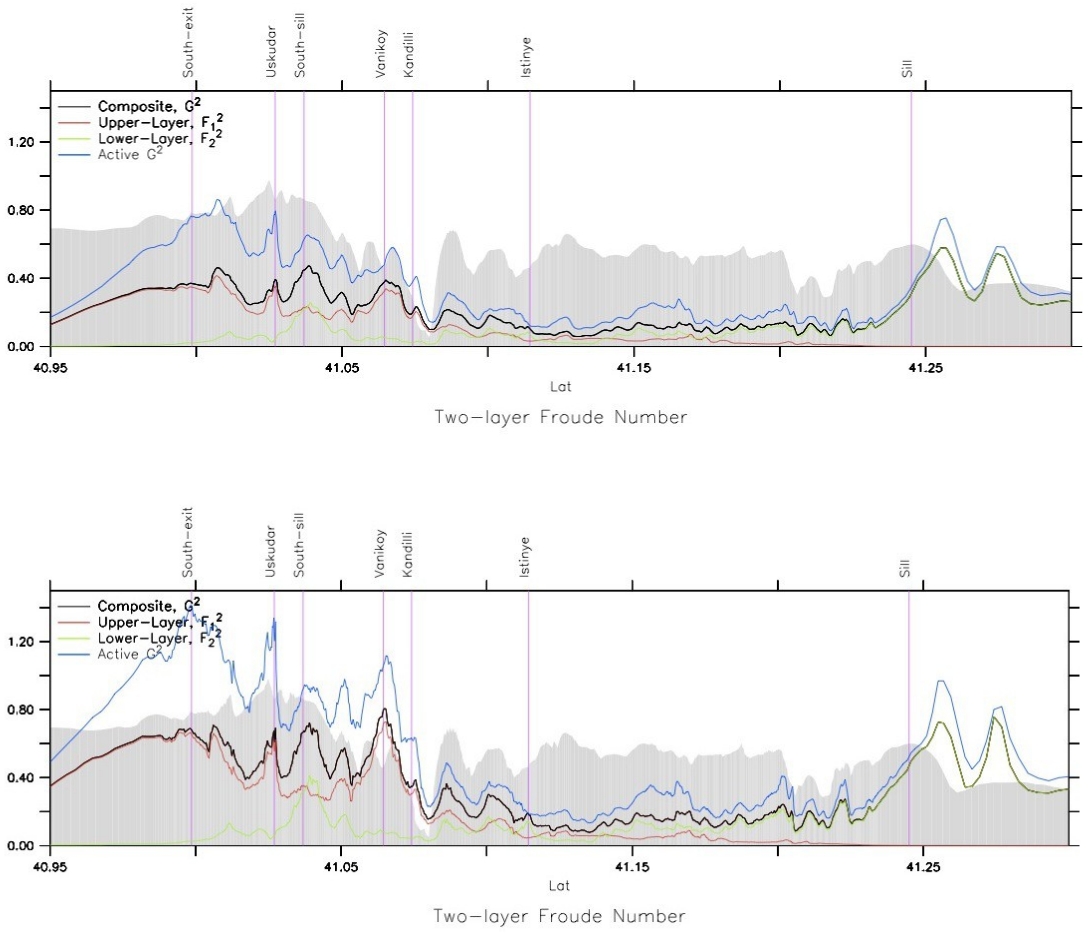


*Figure 59. Two-layer Froude number for the realistic Bosphorus model, showing the total (red), upper layer (green) and lower layer (blue) contributions, based on (a) standard method of computation, (b) with energy correction (bathymetry in the background).*

The lee-side of the northern sill is the only place in the northern sector where the active composite Froude-number, $\mathbf{G^2}$, rises towards a critical value, almost totally contributed by the hydraulically controlled lower layer flowing inside a canyon (Fig. 59b). The controlled flow at the sill is immediately followed by a hydraulic jump, followed by a reformed flow, and later again a second hydraulic jump. We believe the oscillatory trend in $\mathbf{G^2}$ past the sill is sensitively connected to the changes in the flow area of the canyon sloping down to join the Black Sea shelf as illustrated in Fig.s 59b, 60a and also by Özsoy et al. (2001) in their Fig. 9.

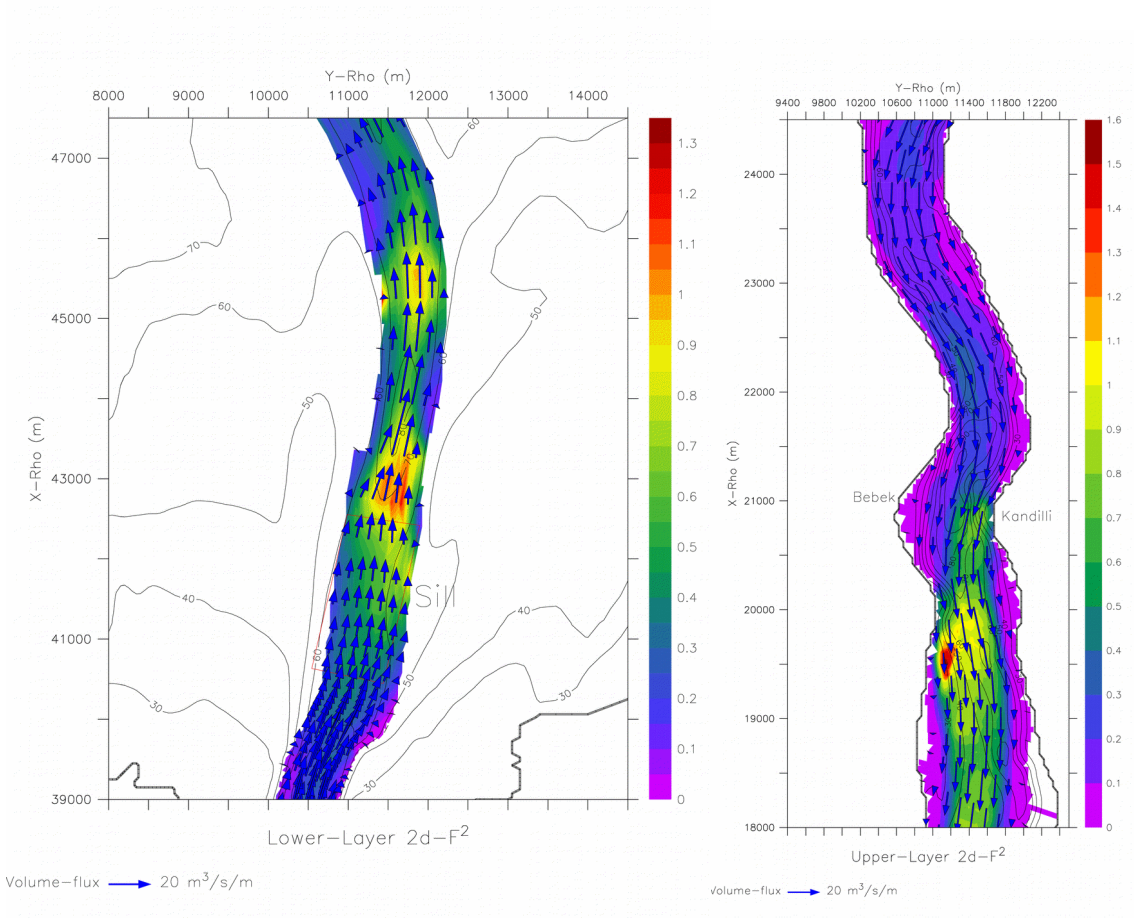


*Figure 60. Two-dimensional displays of Froude numbers calculated with the active current approach for the (a) lower-layer in the northern exit region in the vicinity of the northern sill, (b) upper layer in the main contraction region of the southern Bosphorus.*

Similar cycles of reformation and dissipation are seen (Figs. 59b and 60b) south of the main contraction where the active composite Froude number $\mathbf{G^2}$ once again becomes supercritical. After this hydraulic control at the contraction, there are oscillations where $\mathbf{G^2}$ falls by dissipative mechanisms and again rises by the flow reforming, occasionally coming close but not exceeding the critical value, for example upon meeting the southern sill area. Passing this area then the flow becomes critical once again at Üsküdar, and later at the exit to the Marmara Sea as shown in Fig. 59b. We also note in Fig. 59b that the contribution of the upper layer to the composite Froude number is always much greater than the lower layer in the southern Bosphorus past the contraction. The only exception to this is the southern sill where the lower layer flow

accelerates down its northern slope with an increased contribution to the Froude number, but not sufficient to become supercritical.

Further south, the upper layer flow becomes asymmetrical, first leaning against the Asian shore as a narrow and fast current, becomes supercritical as it hits the protruding headland and its topographic extension into the strait at Üsküdar (Scutari) on the Asian side, before reaching the southern end of the strait. The flow then swings towards the European side against the Cape of Sarayburnu (Seraglio Point) and becomes supercritical once again as it exits from the abrupt opening into the Marmara Sea (Fig. 61a,b). Upper layer average velocity vectors and thickness in Fig. 61a and flux vectors and composite Froude number in Fig. 61b are compared to give an idea on how the active flow elements were selected in the Froude number calculations. Although the upper layer average currents appear to be spread out across the channel, the layer thickness is much smaller on the two sides of the narrow stream arriving from the north, as well as in response to the local topography. Therefore, as shown in Fig. 61b, the flux occurs in a narrow stream where the Froude number is calculated to be critical.

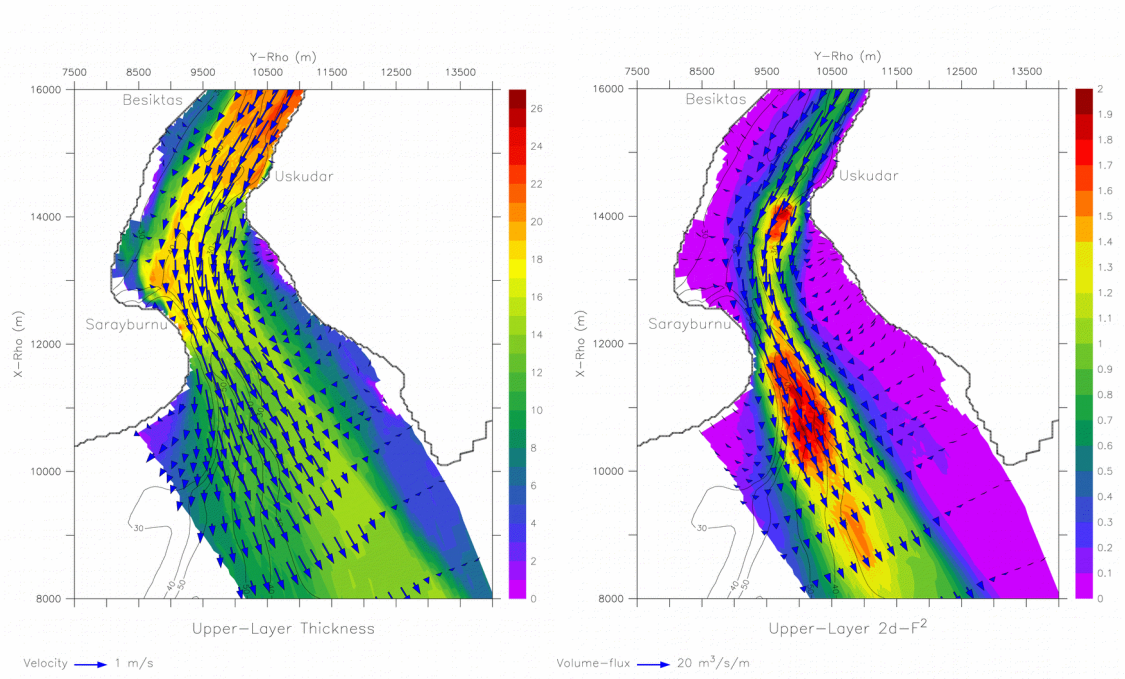


Figure 61. (a) Upper layer depth averaged velocity vectors and layer thickness, (b) upper layer volume flux vectors and active Froude number at the Marmara Sea junction area of the Bosphorus.

**Table 2. Maximum values of the composite densimetric Froude number $G^2$ at regions critical transition regions with anticipated hydraulic control**

| Region | Maximum $G^2$ value | | | Layer | Active/total volume flux (%) | | | Position (km) | |
|---|---|---|---|---|---|---|---|---|---|
| | Standard $G^2$ | With energy flux factor $G^2$ | Active with energy flux factor $G^2$ | | Avg. | Min. | Max. | Start | End |
| South exit | 0.47 | 0.71 | 1.41 | Upper | 80.5 | 76.0 | 87.2 | 8.5 | 12.4 |
| Üsküdar | 0.42 | 0.69 | 1.34 | Upper | 82.9 | 76.3 | 87.0 | 13.5 | 14.4 |
| Contraction | 0.40 | 0.81 | 1.12 | Upper | 78.8 | 76.3 | 83.5 | 19.5 | 19.9 |
| North sill | 0.61 | 0.73 | 0.97 | Lower | 76.9 | 76.9 | 77.0 | 42.7 | 43.0 |

The calculated the composite Froude numbers, and ratios of active fluxes to the total flux are given in Table 1 for the regions where hydraulic control is inferred. The standard method for two-layer hydraulics approximation using the variable sections approach of Pratt (2008) fails to show criticality at the inferred locations. Applying energy flux corrections in account of vertical shear also is not sufficient to raise the Froude numbers above the critical levels. The ratio of the active flux to the total flux is almost always above 75% for these sections, but the effect on the calculation of the calculation of active $\mathbf{G^2}$ is significant. Only by applying the method that selects the active areas as described above, we are able to observe that the northern sill, the main contraction headland at Üsküdar and the southern exit either pass or come vey close to criticality conditions.

### 3.2.3 Response to barotropic forcing

A total of 16 runs has been carried out to test model behavior with respect to changes in the net barotropic flow rate. These simulations are performed by successive initializations of the model starting from the central RUN6, with a barotropic flux of $\mathbf{Q}$ = 9.5 x $10^3$ $m^3/s$, and in each case running at least for about 7 days to reach steady state solutions, despite the residual small oscillations noted earlier. Only some selected

results from these 16 simulations are shown in Fig. 62 for salinity alone for simplicity, including the extreme cases where either the upper or the lower layer is blocked. The top, interfacial and bottom layer volume fluxes $\mathbf{Q_T}$, $\mathbf{Q_I}$, and $\mathbf{Q_B}$ respectively calculated at the mid-strait section and identified by local salinity limits are shown with the heavy arrows in Fig. 62.

In the lower layer blocked solution (Fig. 62a) with a barotropic net flux of $\mathbf{Q} = 33.2 \times 10^3$ $m^3/s$ out of the Black Sea, the zero-velocity line is pushed back into the Bosphorus, as also demonstrated by the measurements. It is noteworthy, however, that the switch to the blocking situation occurs very suddenly as the barotropic forcing is increased, for instance from the unblocked case of $\mathbf{Q} = 28.4 \times 10^3$ $m^3/s$ (Fig. 62b), with only a slightly lower value. As the forcing is decreased to moderate cases with small values of the net flux such as $\mathbf{Q} = 1.92 \times 10^3$ $m^3/s$ (Fig. 62c), there are continuous small changes in the layer fluxes. Note also that the zero velocity isotach, which is depressed below the salinity interfacial layer for the strong barotropic forcing cases (Figs. 62a,b), becomes less aligned and especially higher in the northern part of the strait, for the moderate forcing case (Fig. 62c).

In the cases with reversed net barotropic flux towards the Black Sea, the separation of the zero-velocity isotach from the salinity interface becomes more evident in the northern part of the strait (not shown) and increasingly the background two-layer stratification of the Marmara is advected into the strait, so that a three-layer structure is formed in which the interfacial and bottom layers are co-flowing against the retreating top layer flow, which has been repeatedly noted in earlier measurements, e.g. Latif et al. (1991). As the negative barotropic flux is increased to of $\mathbf{Q} = -19.0 \times 10^3$ $m^3/s$ (Fig. 62d), the co-flowing interfacial and bottom layers, with a larger role of the interfacial layer, are submerged under the zero-velocity contour delineating the top layer in with a small flux. The net effect is that the interfacial layer, which has now become thicker and submerged below the top layer, transports the Marmara Sea surface water to the Black Sea. Only with a further increase of the net flux to $\mathbf{Q} = -28.5 \times 10^3$ $m^3/s$ (Fig. 62e), the upper layer becomes completely blocked, and the stationary wedge of Black Sea water is pushed back into the Bosphorus.

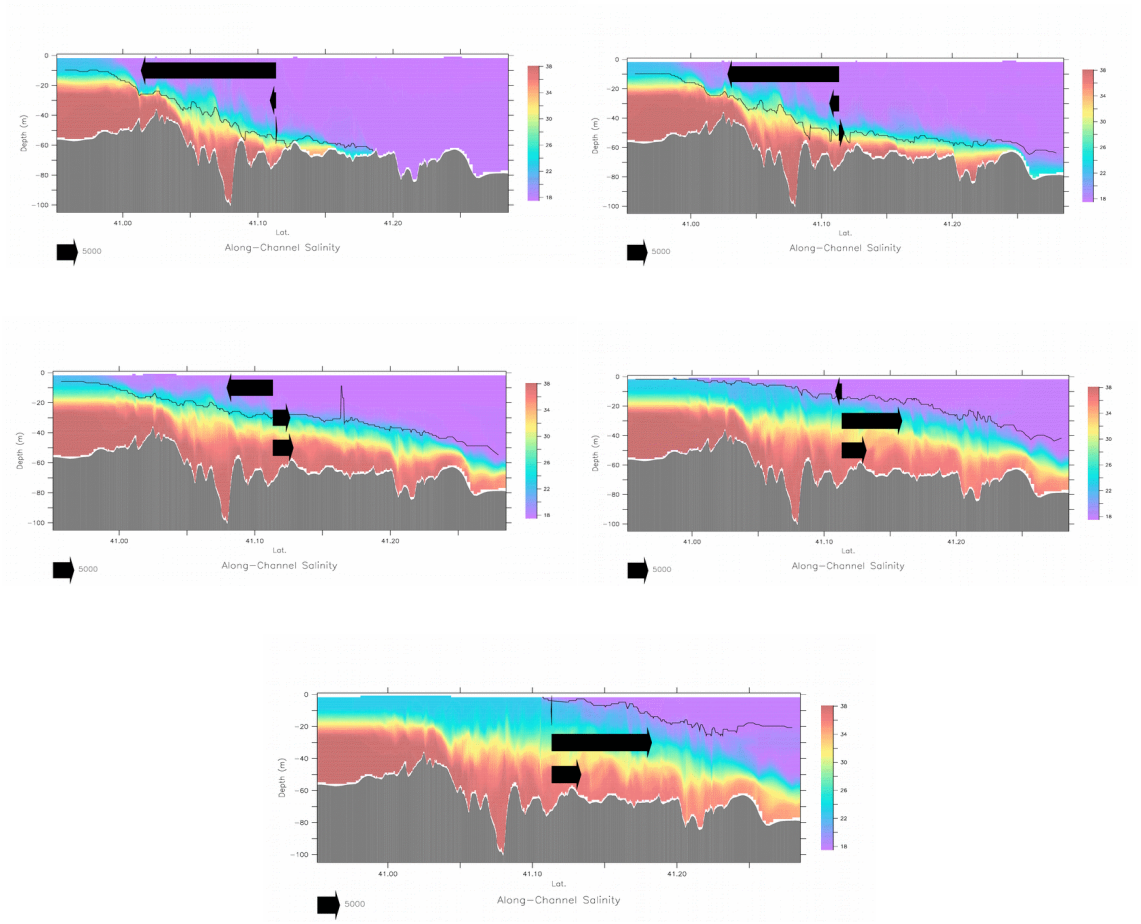


*Figure 62. The salinity distribution, the zero velocity isotach, and arrows showing the relative magnitudes of the top, interfacial and bottom layer fluxes for the net barotropic flux values of (a)* **Q***=33.2x10³ m3/s, (b)* **Q***=28.4x10³ m3/s, (c)* **Q***=1.92x10³ m3/s (towards the Marmara Sea), and (d)* **Q***=-19.0x10³ m3/s, (e)* **Q***=-28.5x10³ m3/s (towards the Black Sea). The layer fluxes are compared to a scale arrow of 5x10³ m3/s at the bottom of each plot.*

What happens with increased northward net fluxes is also of interest: As a consequence of the three-layer flow development with thickened bottom and interfacial layers discussed above, it can be verified that the hydraulic control at the contraction no longer applies, and instead the control may be shifted to the southern sill and the Marmara exit in the southern Bosphorus, and continues to exist at the northern sill. The two-layer $\mathbf{G^2}$ estimates indicate increased values at these locations for the case of $\mathbf{Q}$ = -19.0 x $10^3$ $m^3/s$ (Fig. 63a), where the correction for the active flow areas produces a supercritical

condition near the northern slopes of the southern sill where the lower layer flow past the sill determines the critical transition with an equal share contributed by the upper layer by flow around the sill.

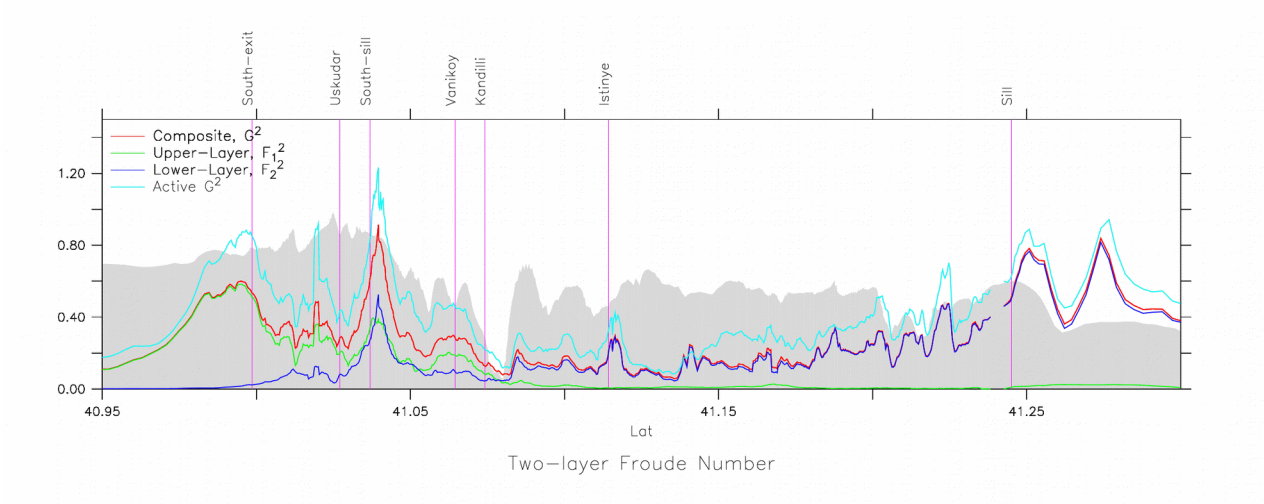


*Figure 63. Estimated upper and lower layer Froude numbers and the composite Froude number* $\boldsymbol{G^2}$*, lupdated with the active approach, using the two-layer approximations for RUN20,* $\boldsymbol{Q}$*=19.0x10*$^3$ *m*$^3$*/s (bathymetry in the background).*

### 3.2.4 Bosphorus sea level difference and exchange fluxes

Historical and modern measurements seem to agree on sea-level differences of 30-60 cm across the entire TSS, and 20-60 cm across the Bosphorus (Marsili, 1681; Möller 1928; Smith, 1942; Gunnerson and Özturgut, 1986; De Filippi et al., 1986; Büyükay, 1989; Alpar and Yüce, 1998; Özsoy et al. 1998; Gregg and Özsoy, 1999; Yüksel et al., 2008). Gregg et al (1999) found rapid, nonlinear changes of sea level near the contraction of the Bosphorus in parallel to the changes in the depth of the density interface. Similar behavior is discovered in our model simulations (Fig. 64), with the largest changes in free-surface height occurring at the Marmara Sea junction and at the contraction region, in consequence of the hydraulic control at these locations. The final elevation difference between the two ends of the strait is about 40 cm in RUN1-RUN4. In RUN5 with stratified boundary conditions amounting to smaller density difference between the two seas, the sea level difference is reduced to about 26 cm, which is

comparable with the values measured by Gregg and Özsoy (2002) during the moderate flow conditions of September 1994.

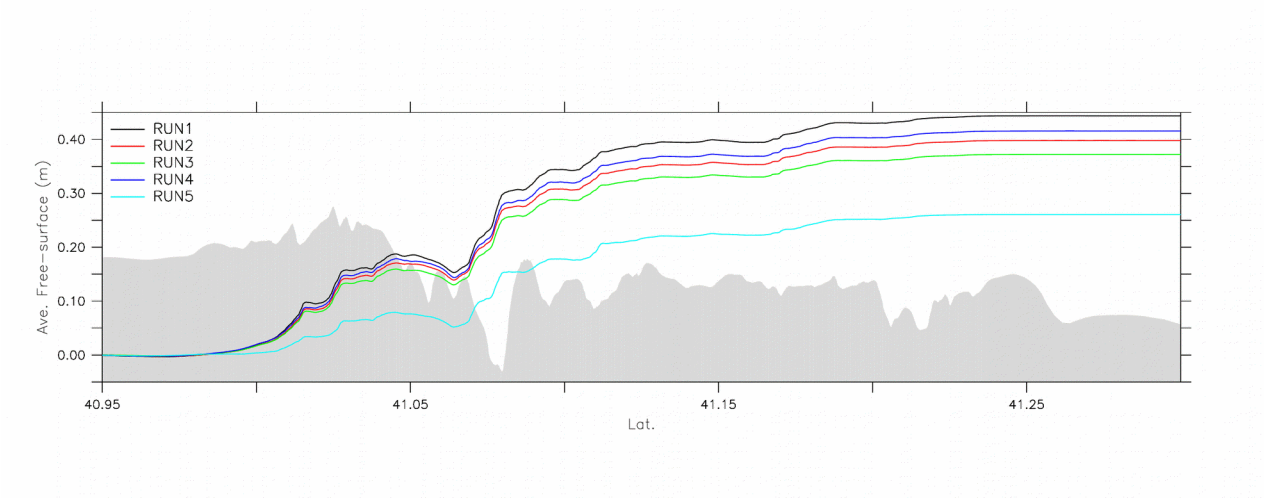


*Figure 64. Sea level changes along the Bosphorus in runs RUN1-RUN5 (bathymetry in the background).*

The relationships between the sea level differential **Δη** across the Bosphorus and the net barotropic flux **Q**, together with the two and three layer fluxes are provided in Fig. 65, based on the model runs summarized in Fig. 62. Blocking of the lower layer occurs for a net flux of **Q** = 33.2x10$^3$ m$^3$/s out of the Black Sea resulting in a sea level difference of **Δη** = 0.49m, while the upper layer blocking is reached when the flow is reversed with **Q** = -28.5x10$^3$ m$^3$/s and when the sea surface is almost levelled out at **Δη** = -0.04 m. The relationship between **Q** and **Δη** is close to a linear one except close to blocking, with average slope 6.6x10$^3$ m$^2$/s. The two-layer fluxes $\mathbf{Q_1}$, and $\mathbf{Q_2}$ are distinguished by the zero velocity isotach, and the three layer fluxes $\mathbf{Q_T}$, $\mathbf{Q_1}$, and $\mathbf{Q_I}$ are distinguished by the salinity limits as described earlier, with $\mathbf{Q = Q_2 - Q_1 = Q_T + Q_I - Q_B}$ by definition. It can be noted that there is a basic misalignment of velocity and salinity based layers in Figs. 62a-e, and the bottom layer not much sensitive to changes in Fig, 65. Especially when the net flow is towards the Black Sea, the interfacial and bottom layers essentially are co-flowing within the three-layer configuration that develops.

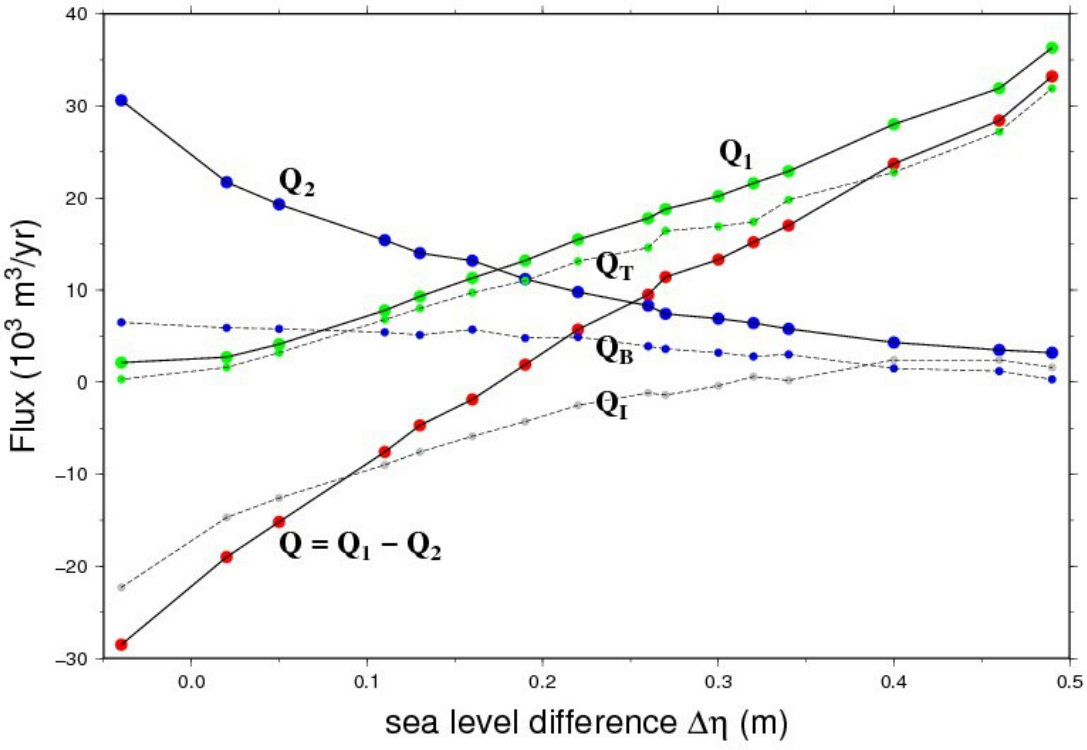


*Figure 65. The variation of the net barotropic flux* **Q** *(red, solid line), and two-layer fluxes in the upper layer,* $\mathbf{Q_1}$ *(green, solid), lower layer,* $\mathbf{Q_2}$ *(blue, solid), thre layer fluxes in the top layer,* $\mathbf{Q_T}$ *(green, dashed), bottom layer,* $\mathbf{Q_B}$ *(blue, dashed) and interfacial layer,* $\mathbf{Q_I}$ *(gray, dashed), with sea level difference* **Δη***, based on the realistic Bosphorus model. (*$\mathbf{Q_T}$*,* $\mathbf{Q_T}$ *and* $\mathbf{Q_I}$ *are positive southward,* $\mathbf{Q_2}$ *and* $\mathbf{Q_B}$ *are positive northward, and* **Δη** *is the sea level difference north-south).*

Continuous current profile measurements were obtained with a bottom mounted cabled ADCP at Baltalimanı in the Bosphorus and sea level, while meteorological variables were monitored at coastal stations at Şile on the Black Sea and Yalova on the Marmara Sea coasts during the years 2008-2102. Although the sensitivity of the ADCP instrument to lower layer currents was affected by a local bottom irregularity, the upper layer currents were better monitored. These data covering a period of four years with were analyzed (Tutsak, 2013), with upper layer currents integrated over the cross-section and sea-level difference low-pass filtered at 30h moving average interval, plotted in Fig. 66 to establish the estimated relationship between upper layer transport and sea-level difference based on measurements and model results. Although the measurements seem to deviate from the realistic Bosphorus model results, there can be several

reasons for this: first of all the Şile and Yalova sea level stations are far away from the two end of the strait, which could result in higher sea-level differences between them; secondly the representativeness of the measurements could have been affected by the various assumptions such as layer cross-section averaging and smoothing used before presenting them in this figure for rather rough comparison.

It is also interesting to note that monthly average sea level differences varied in the range of 15-30 cm for Şile-Yalova stations in relation to the Bosphorus, and 30-40 cm for Yalova-Gökçeada stations in relation to the Dardanelles Straits based on the analysis given by Tutsak (2013).

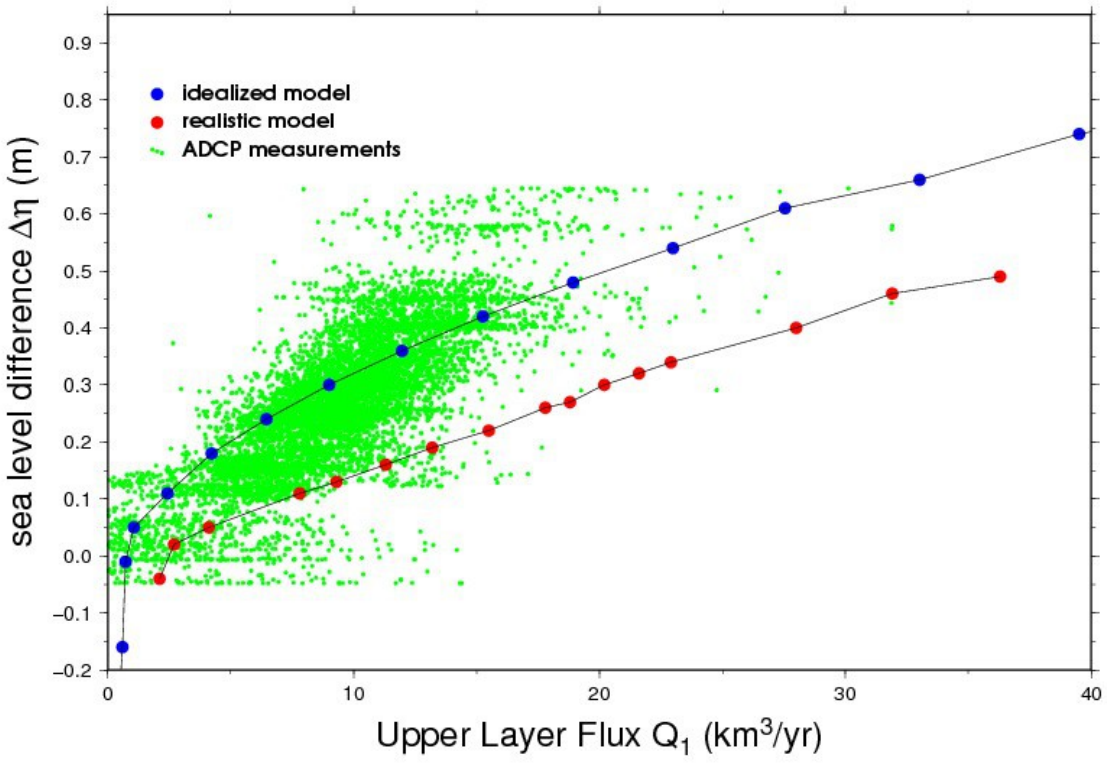


*Figure 66. The relationship between upper layer flux* ***$Q_1$*** *and sea level difference* ***Δη*** *based on idealized (blue) and realistic (red) geometry Bosphorus model results and measurements of ADCP current profiles integrated across the flow area at Baltalimanı versus the sea level difference Şile – Yalova (green) during 2008-2012.*

A review of the climatological estimates of water fluxes trough the TSS is given in Schroeder et al. (2012), based on the earlier box model computations of Ünlüata et al. (1990), Beşiktepe et al. (1993, 1994), and Beşiktepe (2003), making use of the water and salt budgets of the TSS coupled with the Black Sea. The seasonal estimates of the fluxes have been estimated along with nutrient fluxes (Tuğrul et al., 2002). These computations show large entrainment across the halocline, increased fluxes at the Dardanelles relative to the Bosphorus, and an increase of exchange in the spring-early summer season (Tuğrul et al., 2002), which are considerably different from indirect estimates (Stanev and Peneva, 2002; Georgievski and Stanev, 2006). The average fluxes for the rest of the TSS and the Dardanelles Strait are much more variable, but as regards the Bosphorus, the annual average upper and lower layer fluxes respectively estimated as 650 and 325 $km^3/yr$ ($20.5x10^3$ and $10.3x10^3$ $m^3/s$), in agreement with the long-term salt budget of the Black Sea requiring an approximate ratio of $\mathbf{Q_1/Q_2 = S_2/S_1} \approx 2$ (Özsoy and Ünlüata, 1997).

Bosphorus fluxes were also computed from ship mounted ADCP measurements on board the R/V BİLİM (Özsoy et al., 1996, 1998) during the years 1991-1995. Despite data loss near the bottom and immediately below the ship, the measurements yielded average fluxes of $\mathbf{Q_1}$ = 535 $km^3/yr$ ($17x10^3$ $m^3/s$) and $\mathbf{Q_2}$ = 115 $km^3/yr$ ($3.5x10^3$ $m^3/s$), also confirming the expected seasonal trends. The maxima of the instantaneous fluxes were about $\mathbf{Q_1}$ = 1575 $km^3/yr$ (~$50x10^3$ $m^3/s$) and $\mathbf{Q_2}$ = 630 $km^3/yr$ (~$20x10^3$ $m^3/s$), 2-3 times larger than the annual mean fluxes (Beşiktepe, 2003) estimated from the salt budget. The measurements also indicated lower layer blocking for net flux from the Black Sea greater than $\mathbf{Q}$ = 800 $km^3/yr$ (~$25x10^3$ $m^3/s$), and upper layer blocking for net flux in towards the Black Sea exceeding $\mathbf{Q}$ = -580 $km^3/yr$ (~ -19 $x10^3$ $m^3/s$), the latter estimate being consistent with the results of a two-layer model (Oğuz et al., 1990).

Fig. 67 represents a summary of the ideal and realistic model results discussed above, together with a summary of the available flux estimates from ADCP measurements of Özsoy et al. (1996, 1998) and measurements obtained by Merz (Möller, 1928) compiled by Maderich and Konstantinov (2002). The mean fluxes estimated from ADCP measurements are also indicated. The mean values of the upper, lower layer and total fluxes, respectively $\mathbf{Q_{1m}}$, $\mathbf{Q_{2m}}$ and $\mathbf{Q_m}$, are also shown in Fig 67.

The ADCP measurements and Merz estimates are generally in good agreement with model results in Figure 67, while the model-derived fluxes appear higher. We recall the fact that the ADCP measurements are underestimates because of data loss near the surface and the bottom. However, the model results are also not perfect because of the various approximations of bottom friction and and internal turbulence parameterizations. It is also interesting that both the idealized and the realistic models of the Bosphorus give similar results in terms of fluxes.

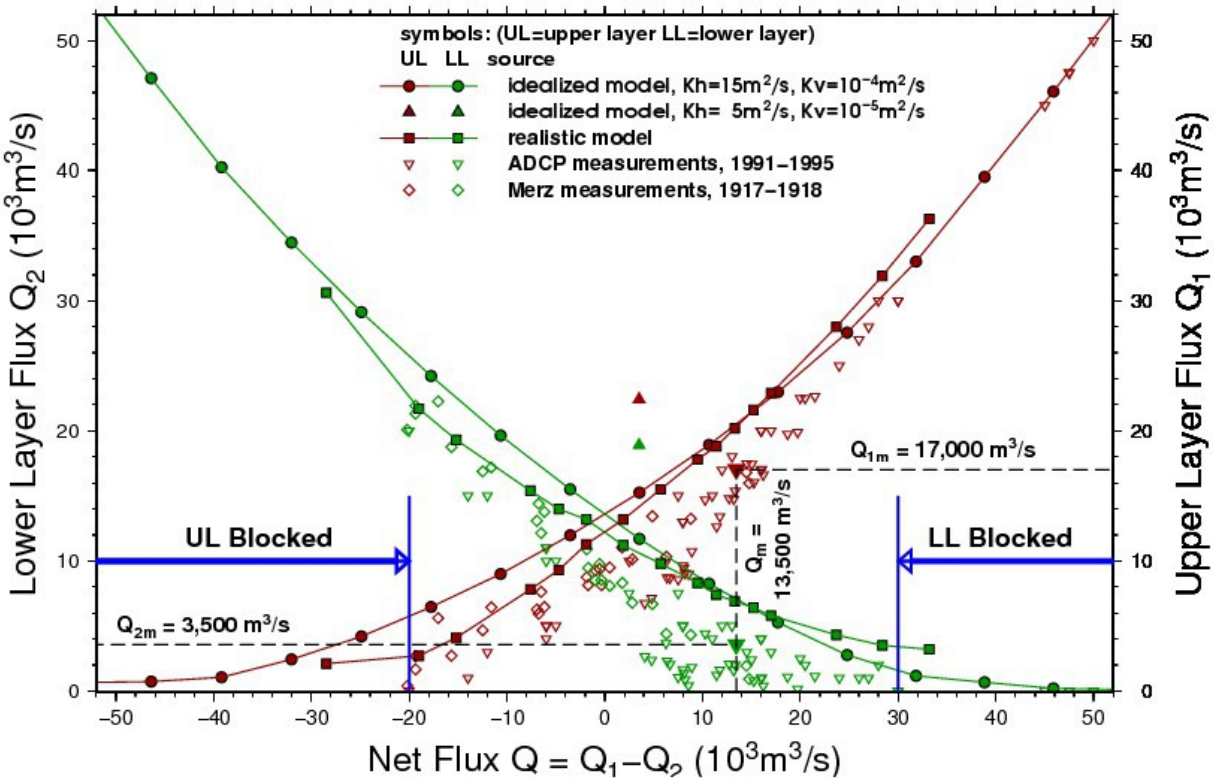


*Figure 67. The volumetric flow rate in the upper layer $Q_1$ (red) and lower layer $Q_2$ (green) of the Bosphorus versus net flow $Q=Q_1-Q_2$. Circles represent the data of Özsoy et al. (1996, 1998) while inverted triangles are data from Merz (Möller, 1928) and respectively. (units conversion factor: $10^3$ $m^3/s$= 31.71 $km^3/yr$).*

The realistic geometry model results presented in Fig. 67 are based on the runs made by Sözer (2013). Based on the example given for the idealistic case run with different horizontal and vertical diffusivities, it can be said in general that the results on exchange

fluxes are sensitive to viscosity and friction effects. The change in the density difference across the strait does not have much influence on the exchange.

It is also noteworthy that the layer fluxes in simulations of RUN1-RUN4 satisfy the approximate relationship $\mathbf{Q_1/Q_2} \approx 1.5 - 2.1$, the lower value being close to the ADCP based estimates of Gregg and Özsoy (2002) and the higher value close to that proposed by Özsoy and Ünlüata (1997) based on long-term budgets. Yet it must be said that these ratios are only valid for moderate flows; varying the net barotropic flux over the full range represented in Fig. 65 results in a higher range of ratios, $\mathbf{Q_1/Q_2} \approx 0.2 - 9$, excluding the completely blocked cases.

The limits for upper and lower layer blocking are suggested based on the series of runs reported and the blocked cases in Fig. 62, and in addition, using the guidance of the available ADCP data of Özsoy et al. (1998).

### 3.2.5 MITgcm Model of the Turkish Straits System

The capability of MITgcm to represent the two-layer exchange dynamics both in the straits and in the Marmara Sea is examined. The non-uniform curvilinear orthogonal grid and the vertical resolution implemented have demonstrated to be sufficient to capture the fine scales within the two Straits and also to well represent mesoscale in the Marmara Sea.

The response of the currents and density structure over the water column to different net flow is also examined through the setup of experiments with varying net barotropic volume flux values of Q = -9600, 0, 5600, 9600, 18000 and 50000 $m^3/s$ respectively. Positive values of Q represent flow from the Black Sea towards the Mediterranean, while negative values represent net flow in the opposite direction.

The capability of MITgcm to represent the two-layer exchange dynamics both in the straits and in the Marmara Sea is examined. The non-uniform curvilinear orthogonal grid and the vertical resolution implemented have demonstrated to be sufficient to capture the fine scales within the two Straits and also to well represent mesoscale in the Marmara Sea. The response of the currents and density structure over the water column

to different net flow is also examined through the setup of experiments with varying net barotropic volume flux values of Q = -9600, 0, 5600, 9600, 18000 and 50000 $m^3/s$ respectively. Positive values of Q represent flow from the Black Sea towards the Mediterranean, while negative values represent net flow in the opposite direction. The free surface variations in the Marmara Sea, corresponding to configurations initialized with vertical profiles representative of the three basins selected from CTD casts in June-July 2013 and variable values of net barotopic flow values are shown in Figure 68.

For the studied flows driven solely by the net flux, an S-shaped current first moving south from the Bosphorus, later turning northwest and finally exiting from the Dardanelles Strait appears to be the basic character of the circulation.

With a negative flux of Q=-9600 $m^3/s$, such that the net flow is towards the Black Sea, the upper layer flow from the Bosphorus into the Marmara Sea is still positive, and sufficient to generate an anticyclonic net circulation in the midst of the Marmara Sea, as shown in Fig. 68.

For zero net flux, the same structure is preserved and as the positive values of the barotropic flux is increased further the size of the central gyre is reduced and the flow becomes increasingly more attached to the northern coast of the Marmara Sea. As the flux is increased to 9600 $m^3/s$, the central anticyclonic circulation cell takes an elongated form.

For the extreme flux values of Q=18000 $m^3/s$ and Q=50000 $m^3/s$, the lower layer flow in the Bosphorus becomes blocked, and qualitative changes occur in the circulation of the Marmara Sea, with a smaller anticyclone near the Bosphorus exit, a jet attached to the northern coast, and a secondary anticyclone further west, and a cyclonic circulation emerging in the south. For these cases, the circulation pattern looks more like the buoyancy driven flow along the coast adjacent to the mouth of a river.

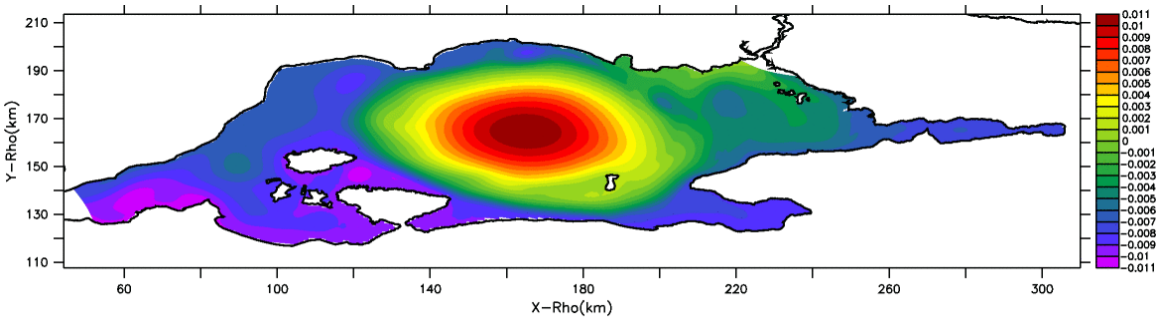


FS, Day=067.00

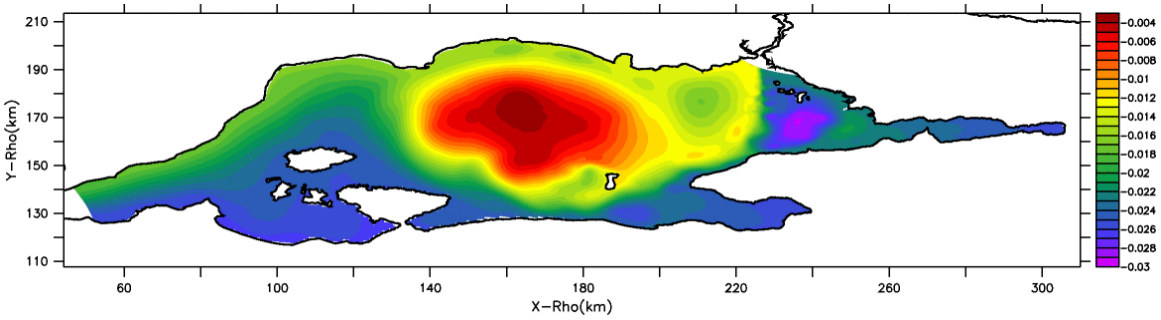


FS, Day=100.00

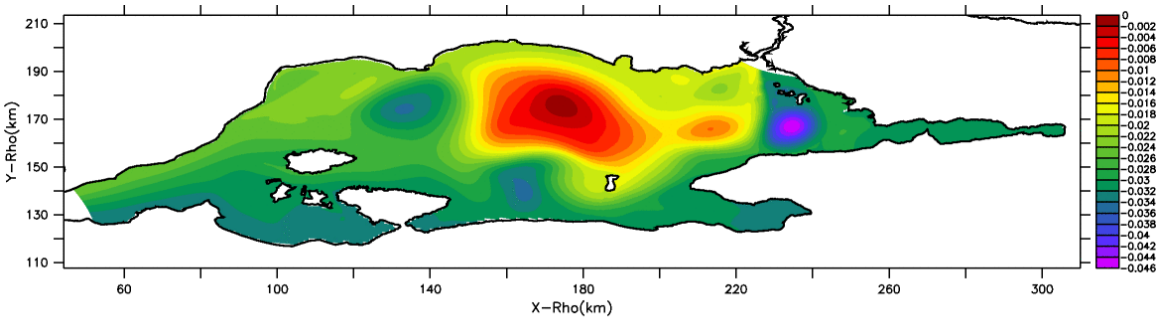


FS, Day=066.00

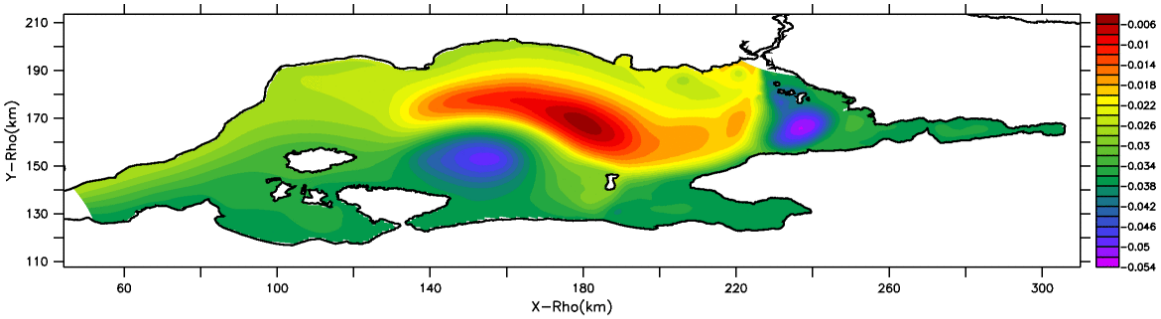


FS, Day=022.00

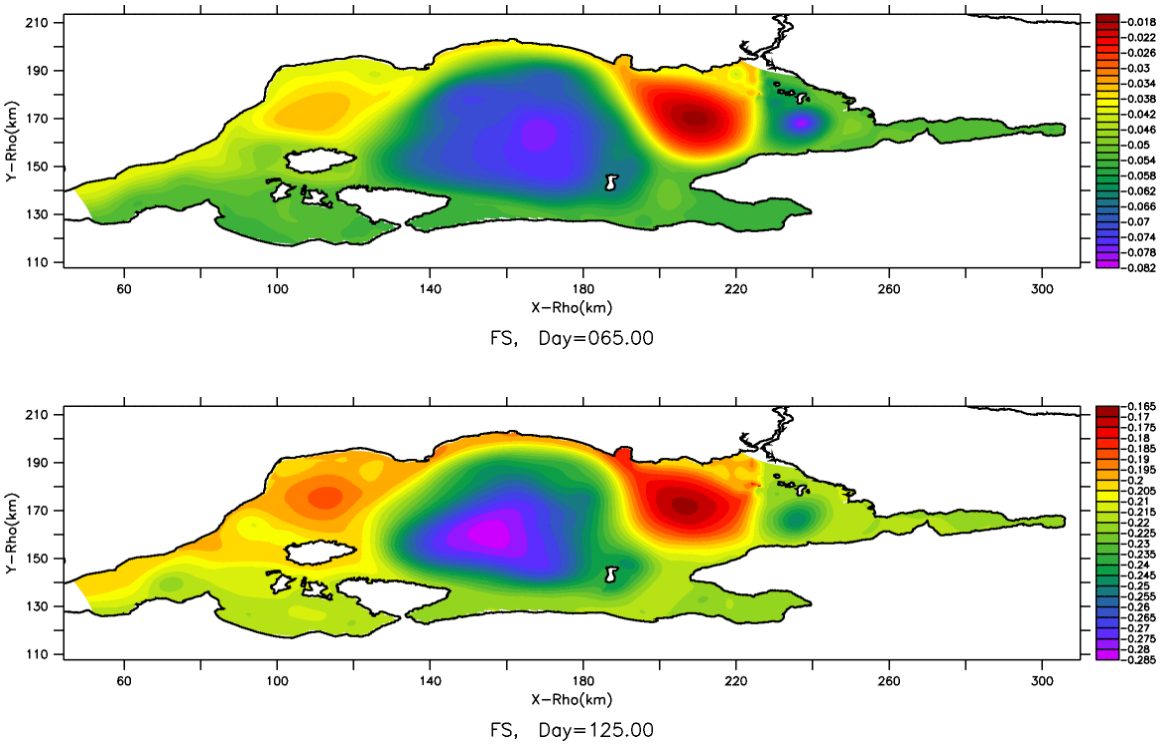


Figure 68. The free surface variations in the Marmara Sea for varying net barotropic volume flux values and total days of run for (a) Q = -9600 (day=67), (b) 0 $m^3/s$ (day 66), (c) 5600 $m^3/s$ (day 100), (d) 9600 $m^3/s$ (day 22), (e) 18000 $m^3/s$ (day 65) and (f) 50000 $m^3/s$ (day125).

The generation of a basic anticyclonic circulation in the Marmara Sea for lower net fluxes, evolving towards a more balanced circulation of cyclonic-anticyclonic eddies appears to be a result of the vorticity balance of the basin. As shown by Spall and Price (1998), and studied by Morrison (2011), the net basin circulation is sensitively determined by the potential vorticity (PV) imports and exports of the basin. From this point of view, the reduction of interface depth (or upper layer thickness) from the Black Sea to the Marmara Sea implies a decrease in fluid vorticity, or anticyclonic circulation assuming the input to have zero vorticity.

The behaviour of the buoyant plume entering the Marmara Sea, initially shooting south and hitting the opposite coast is displayed in all cases in Fig.s 68-70, although the later turning of the flow to the west is typical of buoyant plumes at this scale. Buoyant flows entering the sea are typically attached to the right hand coast (looking out from the exit

in the northern hemisphere, especially for initial vorticity zero below a critical limit (e.g. Nof, 1978, Stern et al. 1982). Often a bulge of the buoyant fluid is formed, as the flow turns right to follow the coast, as often observed at river mouths (e.g. Huq, 2013).

In a two-layer system with variable bottom topography and dynamically active layers, the circulation may develop differently, with topography influencing the lower layer flow, and the resultant interface topography influencing the upper layer flow (Beardsley and Hart, 1978). As the net flux is increased in Fig. 68, the changes in the circulation pattern may be a result of this kind of interactive adjustment of the flow layers to bottom and interface topography.

The qualitative change in the circulation towards a series of anticyclonic and cyclonic eddies following the meander of the currents, when the flux is increased to 18000 $m^3/s$ and 50000 $m^3/s$ is reminiscent of the Alboran Sea, where similar gyres filling the basin develop under high fluxes (Spall and Price, 1998; Riha and Peliz, 2013).

The sea level differences that develop at the two straits, Bosphorus and Dardanelles are given in Table 1, in relation to the net barotropic fluxes and the values obtained from the TSS model are compared with the ROMS model results for the Bosphorus (Sözer, 2013). While the total range of sea level in the Marmara Sea between cyclonic and anticyclonic areas varies between 2-12 cm (Fig. 68), the net sea level differences across straits are much larger, varying between 2-85 cm in the Bosphorus and 1-32 cm in the Dardanelles, while the results for the Bosphorus compare well between the two models. These results would imply sea level differences of about 0-120 cm between the Black Sea and the Aegean Sea, for the range of net transport tested.

Table 1. SEA LEVEL DIFFERENCE AT STRAITS AS A FUNCTION OF NET FLUX

| Net flux Q ($m^3/s$) | Bosphorus (TSS) sea level difference $\Delta\eta$ (cm) | Dardanelles (TSS) sea level difference $\Delta\eta$ (cm) | Bosphorus (ROMS) sea level difference $\Delta\eta$ (cm) |
|---|---|---|---|
| -9600 | 2 | 1.5 | - |
| 0 | 8 | 5 | 14 |
| 5600 | 10 | 7 | 18 |
| 9600 | 14 | 11 | 22 |
| 18000 | 22 | 16 | 30 |
| 50000 | 85 | 32 | - |

The salinity and horizontal current vectors at the surface and at a depth of 36m are shown in Fig.4 for variable barotropic flow cases. The surface features in Fig. 69 reflect similar patterns to the sea level variations in Fig. 68 representing the barotropic circulation of the basin. As the flux is increased, a greater penetration of Mediterranean water from the Dardanelles Strait into the Marmara Sea in the lower layer. The lower layer features at a depth of 36m are shoen in Fig. 70. For lower values of net flux, the penetrating Dardanelles flow along the southern coast forces a reverse circulation at 36 m, which marginally represents upper part of the lower layer flows just below the interface located at about 25m. The lower layer circulation for flux values up to 9600 $m^3/s$ is roughly cyclonic excluding the regions affected by the Bosphorus jet, with easterly flow along the southern coast and westerly flow along the northern coast, i.e. opposite to the central anticyclonic cell in the upper layer.

As the flux is increased to Q=18000 $m^3/s$, the lower layer flow in the Bosphorus gets nearer to being blocked, and with further increase to Q=50000 $m^3/s$ it is completely blocked. A qualitatively different circulation is developed in the Marmara Sea (Fig. 68), while the interface in the Marmara Sea deepens first to about 30m and later to about 35m for these fluxes (see Figs 72-74). The displayed salinity and currents at 36 m in Fig.70 therefore can no longer be qualified as lower layer – they become influenced and move in the same general direction with the upper layer currents.

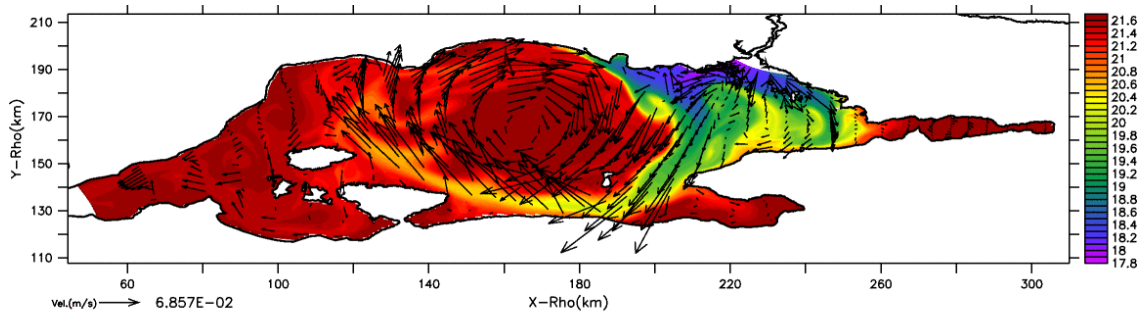


Salt, Z=-0.6m, Day=067.00

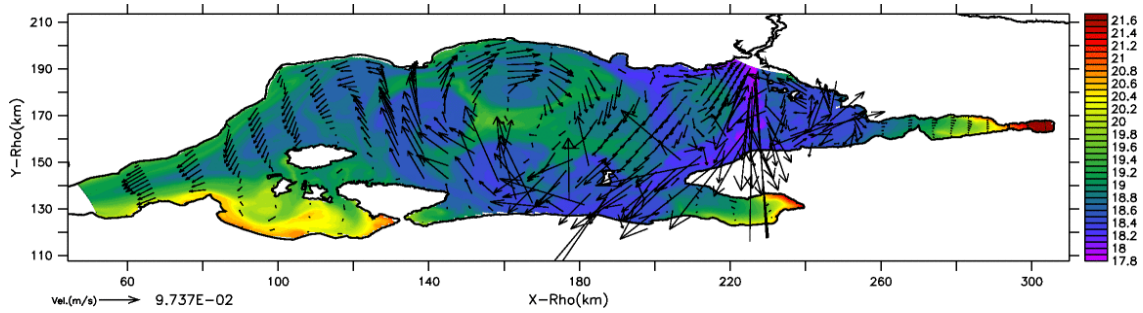


Salt, Z=-0.6m, Day=100.00

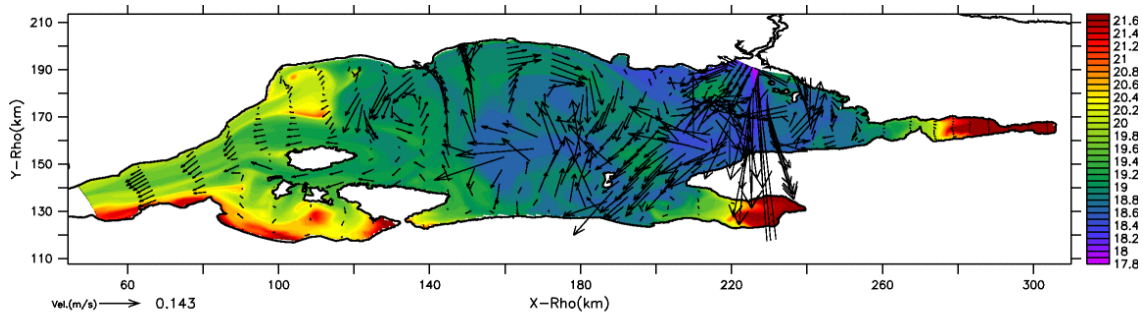


Salt, Z=-0.6m, Day=066.00

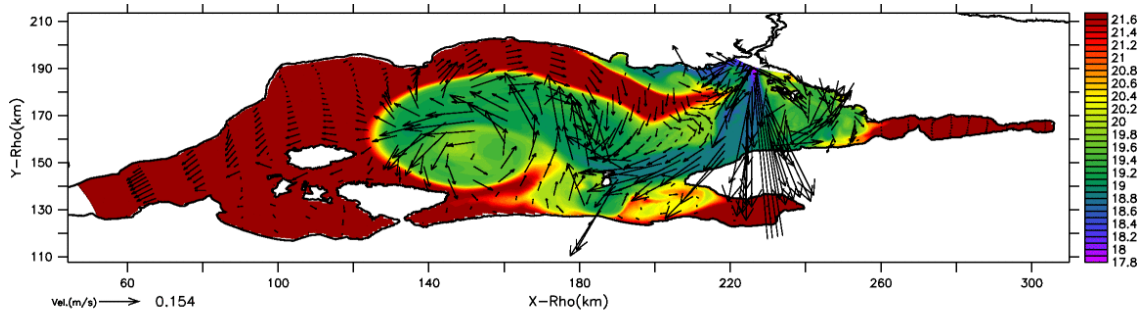


Salt, Z=-0.6m, Day=022.00

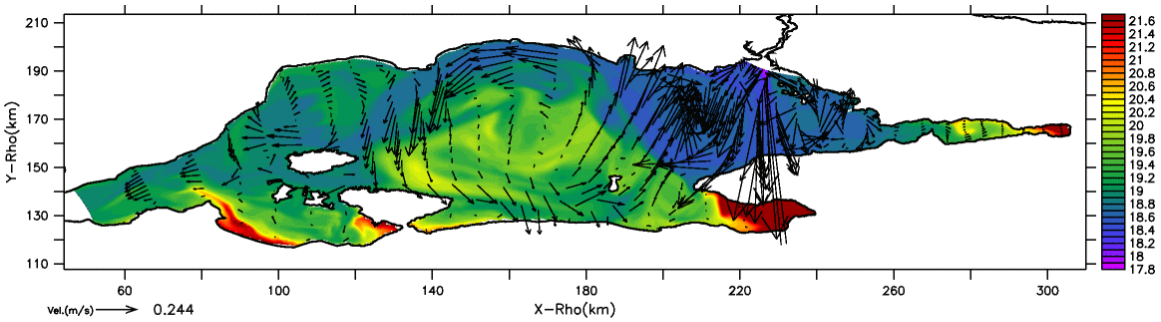


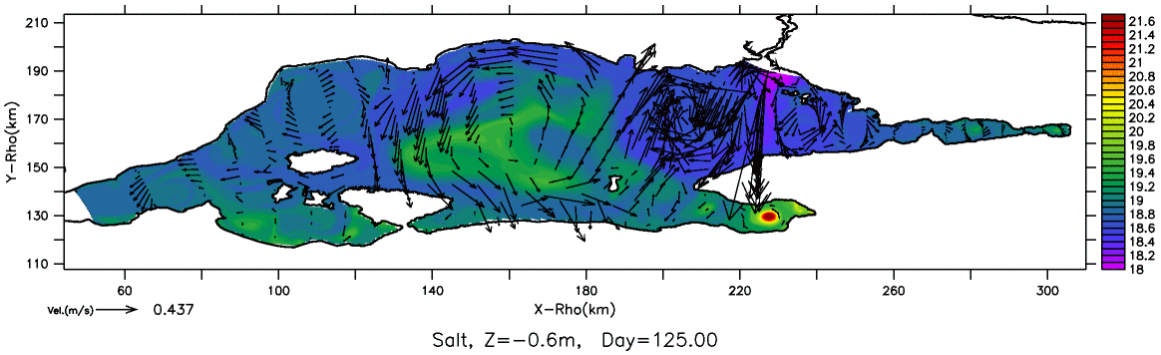


Figure 69. Salinity and current vectors at 0m (surface) in the Marmara Sea for varying net barotropic volume flux values of (a) Q = -9600 (day=67), (b) 0 $m^3/s$ (day 66), (c) 5600 $m^3/s$ (day 100), (d) 9600 $m^3/s$ (day 22), (e) 18000 $m^3/s$ (day 65) and (f) 50000 $m^3/s$ (day125).

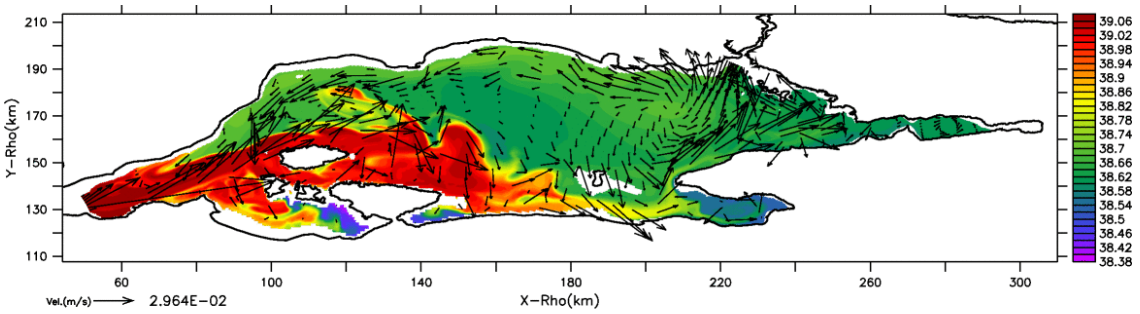


Salt, Z=-36m, Day=067.00

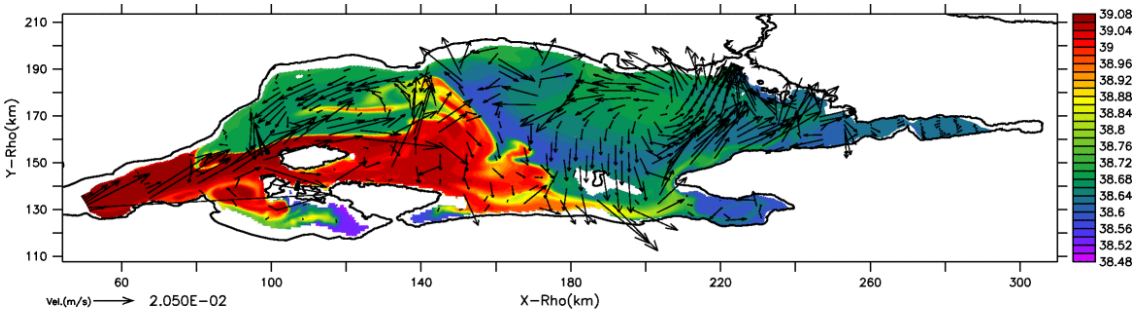


Salt, Z=-36m, Day=100.00

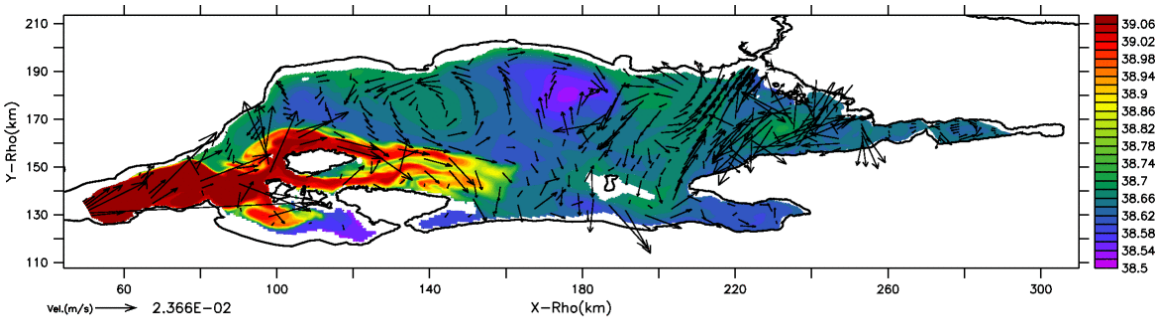


Salt, Z=-36m, Day=066.00

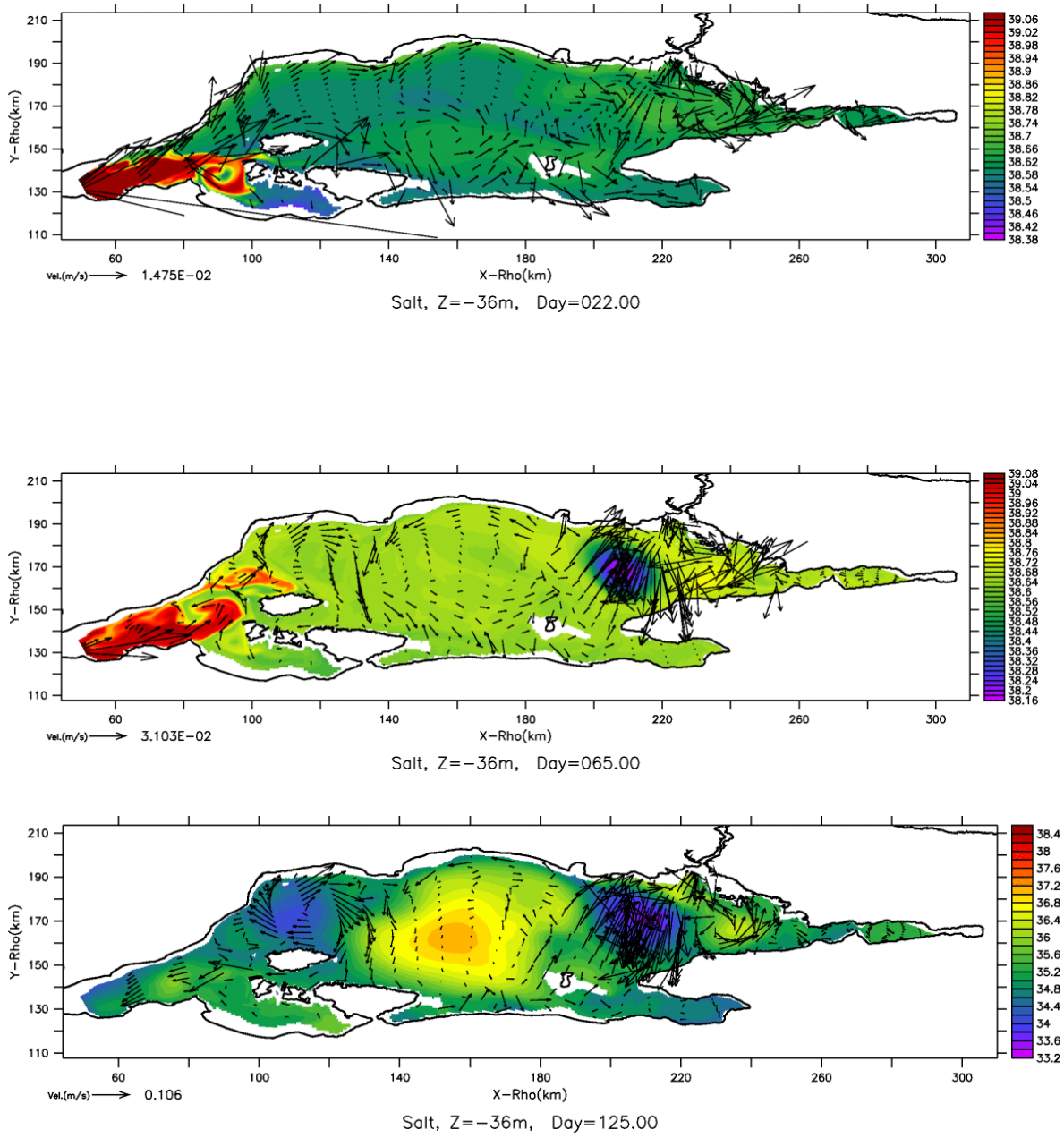


Figure 70. Salinity and current vectors at depth of 36m in the Marmara Sea for varying net barotropic volume flux values of (a) Q = -9600 (day=67), (b) 0 $m^3/s$ (day 66), (c) 5600 $m^3/s$ (day 100), (d) 9600 $m^3/s$ (day 22), (e) 18000 $m^3/s$ (day 65) and (f) 50000 $m^3/s$ (day125).

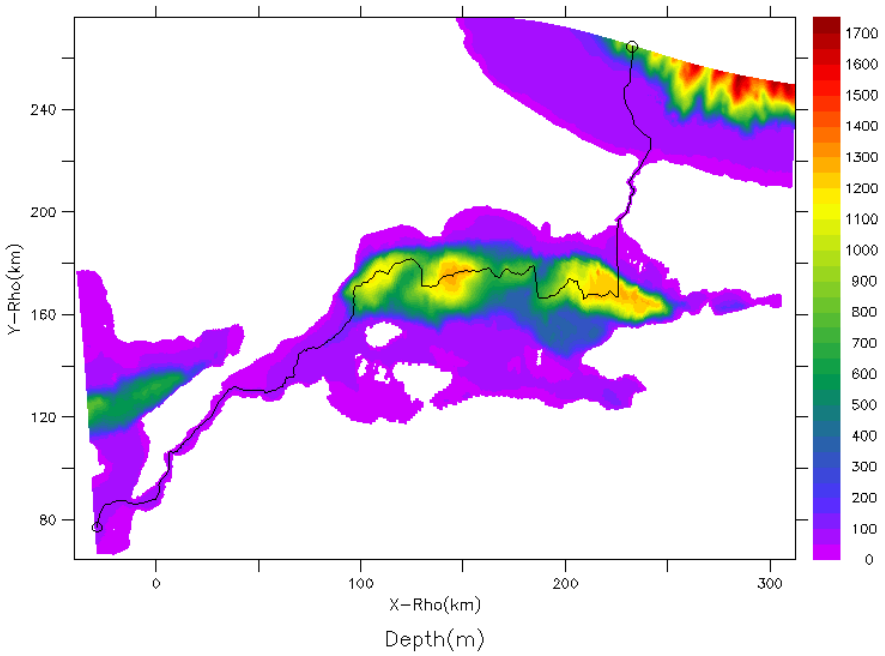


Figure 71. The thalweg line constructed by connecting deepest points along the model topography to display cross sectional properties.

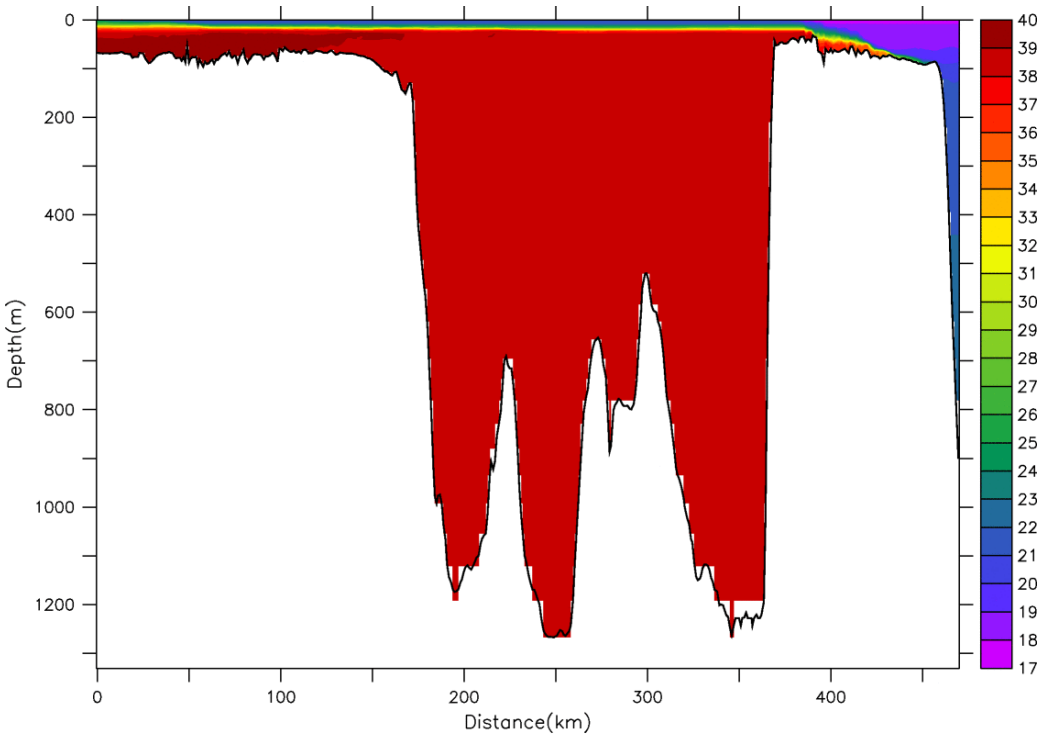


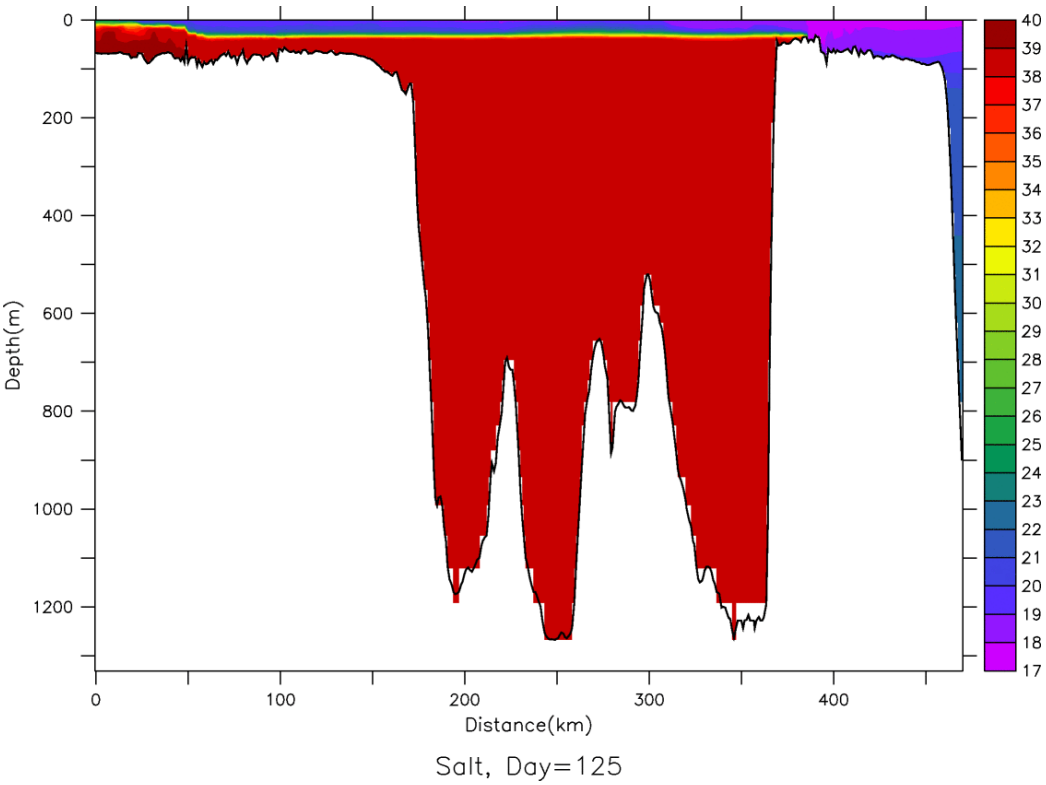


Figure 72. Salinity cross-sections along the thalweg line of Fig.71 in the Marmara Sea for selected net barotropic volume flux values of Q = -9600 and 50000 $m^3/s$.

The salinity cross-sections throughout the TSS are shown in Fig. 72, following the thalweg line of Fig. 71, for selected net barotropic flux values. The upper layer thickness remains around 25 m for fluxes up to 9600 $m^3$/s, and increases to 35 m at the maximum flux value of 50000 $m^3$/s. The upper layer reflects modified Black Sea characteristics while the lower layer reflects Mediterranean characteristics all along the transect, while the most rapid changes in salinity occur in the Bosphorus and Dardanelles straits, by mixing between the two water masses, as also indicated by observational results (Beşiktepe et al., 1993). The interface depth also varies strongly in the two straits, where fast exchange currents subject to hydraulic controls at transition areas (Gregg et al., 1999; Gregg and Özsoy, 1999, 2002; Özsoy et al., 2001, Ilıcak et al., 2009; Sözer, 2013).

Below the sharp pycnocline of the Marmara Sea, properties are rather uniform, except very near the interface where an injection of more saline water from the Dardanelles spreads below the halocline. The spread below the halocline is typical for the summer season of June 2013 for which the model has been initialized. However, the appearance of denser waters at winter time would change this pattern as the dense water sinks to the westernmost depression of the Marmara Sea and spreads along the bottom (Beşiktepe et al., 1993, 1994; Hüsrevoğlu, 1999).

The expanded views of salinity cross-sections for the Bosphorus and Dardanelles are respectively shown in Fig.s 73 and 74.

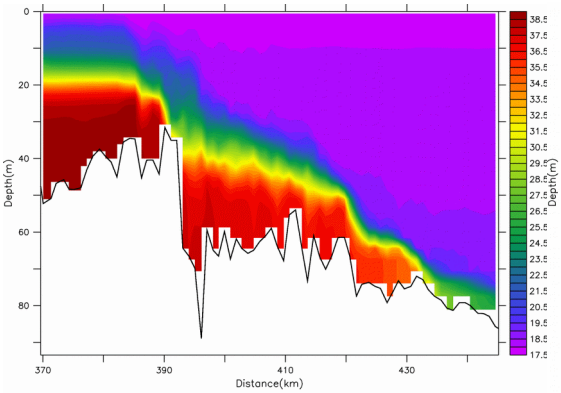


Salt, Day=100

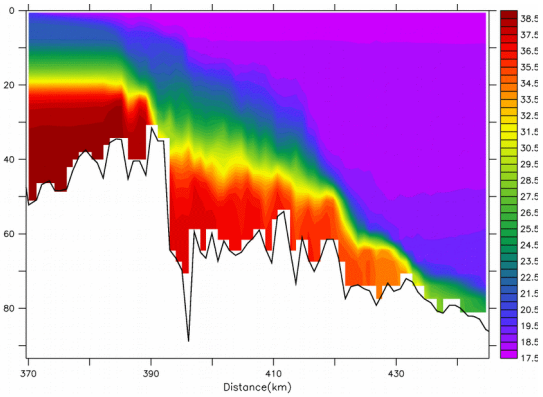


Salt, Day=67

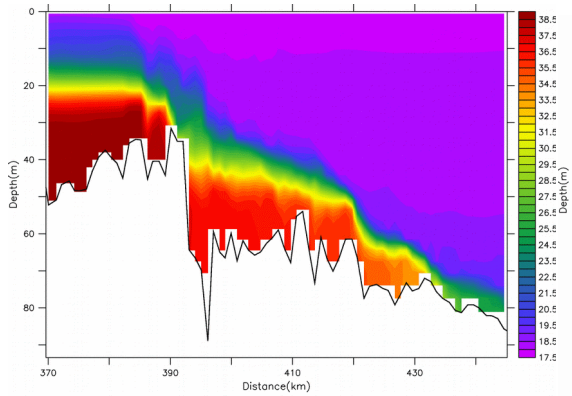


Salt, Day=66

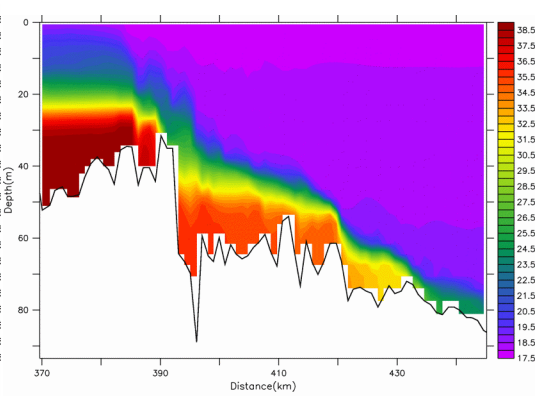


Salt, Day=22

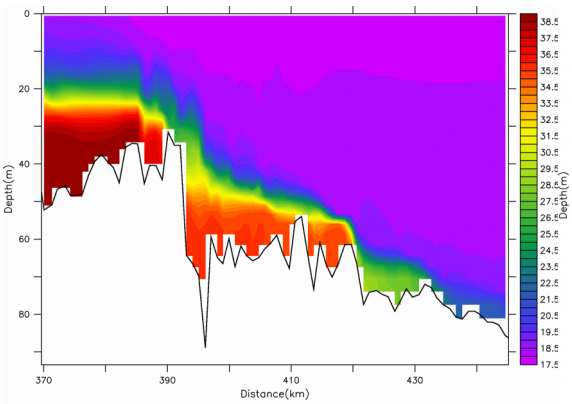


Salt, Day=65

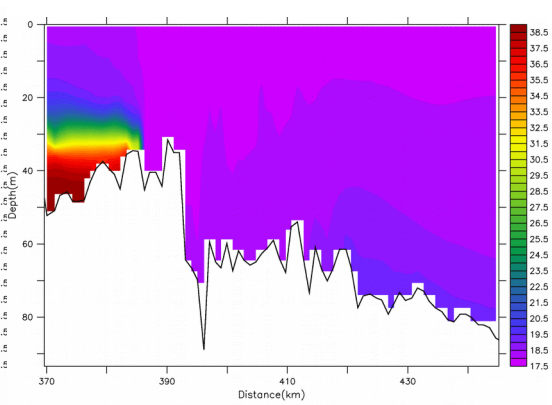


Salt, Day=125

Figure 73. Salinity cross-sections across the Bosphorus along the thalweg in Fig.71, for varying net barotropic volume flux values of Q = -9600, 0, 5600, 9600, 18000 and 50000 $m^3/s$.

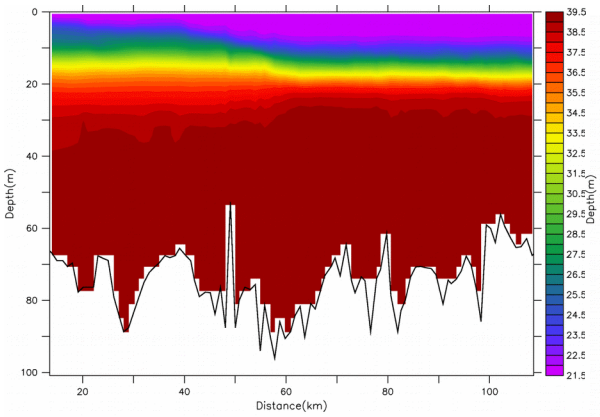


Salt, Day=67

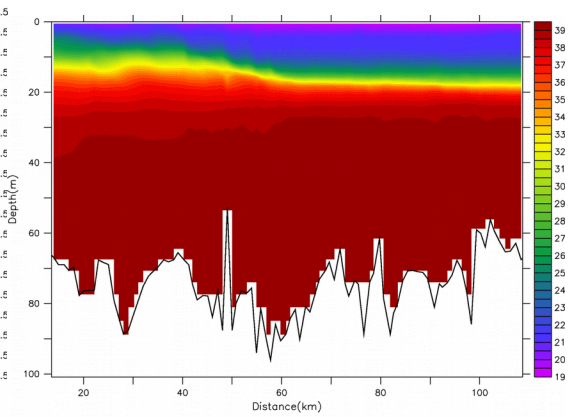


Salt, Day=100

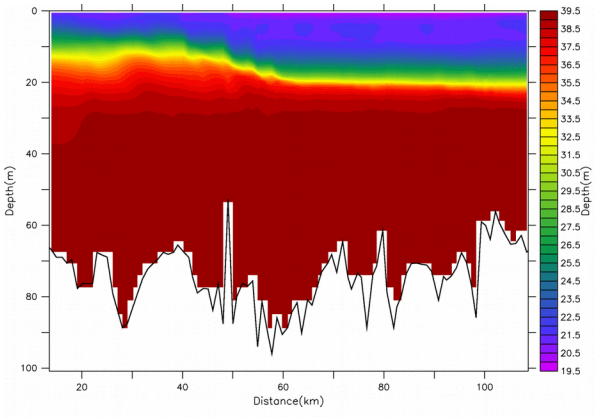


Salt, Day=66

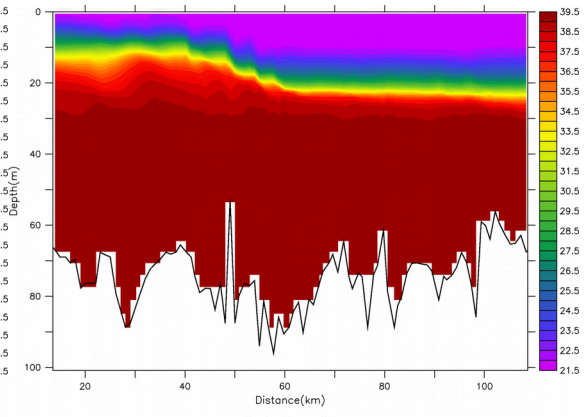


Salt, Day=22

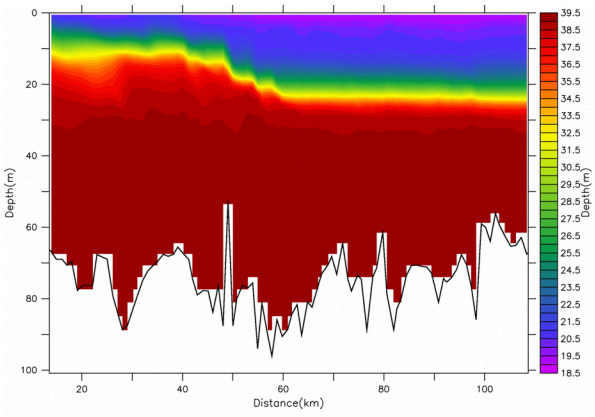


Salt, Day=65

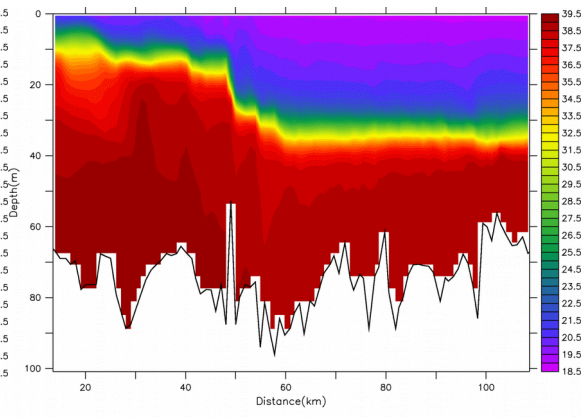


Salt, Day=125

Figure 76. Salinity cross-sections across the Dardanelles along the thalweg in Fig.5, for varying net barotropic volume flux values of Q = -9600, 0, 5600, 9600, 18000 and 50000 $m^3/s$.

The cross sections in Fig.s 75 and 76 confirm the existence of hydraulic transitions at expected hydraulic control sections based on past observations, also better resolved by higher resolution local models of the straits (Gregg et al., 1999; Gregg and Özsoy, 1999, 2002; Özsoy et al., 2001; Ilıcak et al., 2009; Sözer, 2013).

The salinity and current vectors at depths of 0m (surface) and 36m in the Bosphorus for selected values of net barotropic volume flux are shown in Fig.s 77 and 78.

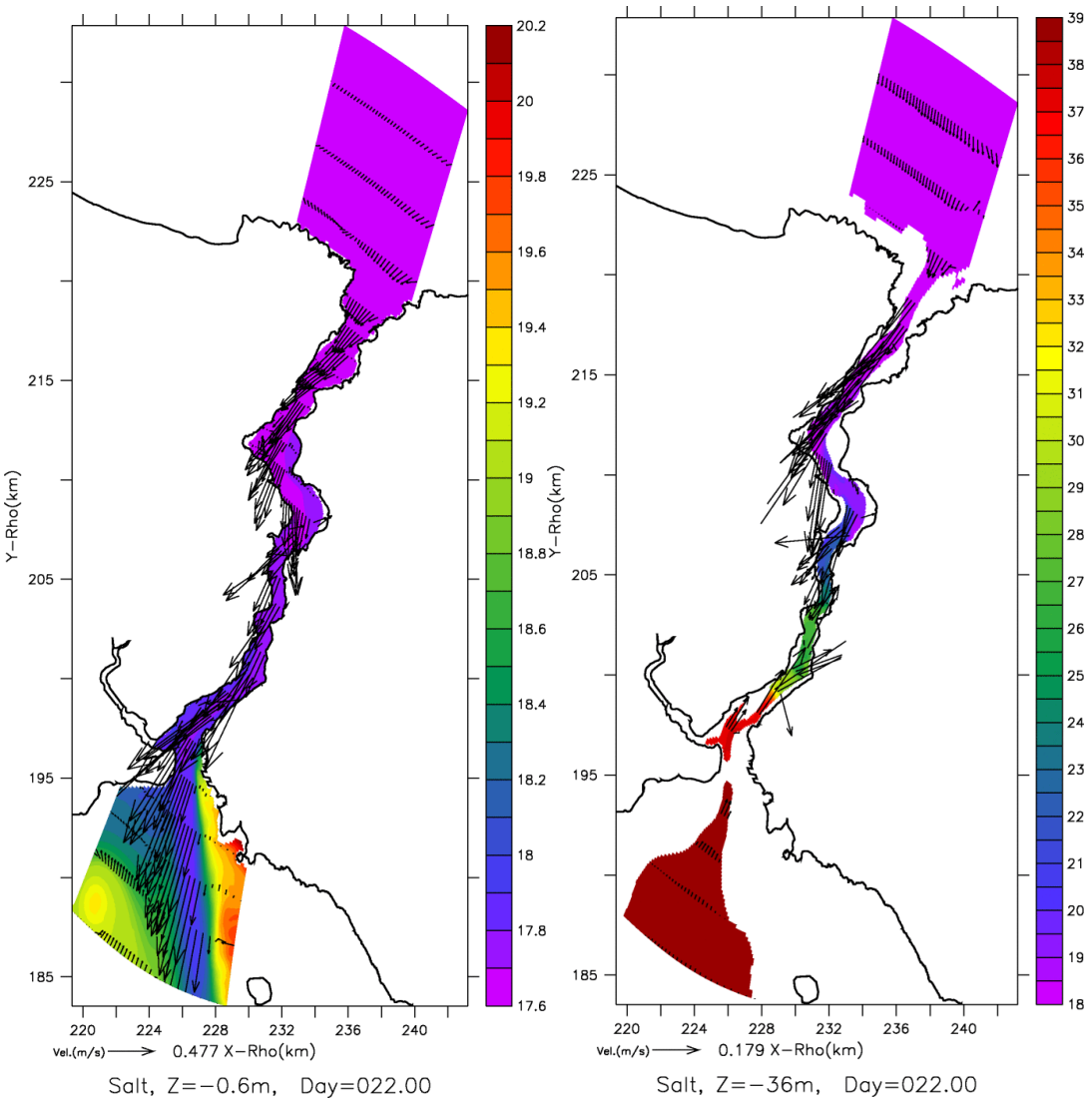

Figure 77. Salinity and current vectors at depths of 0m (surface) and 36m in the Bosphorus for net barotropic volume flux of Q = 9600 $m^3$/s.

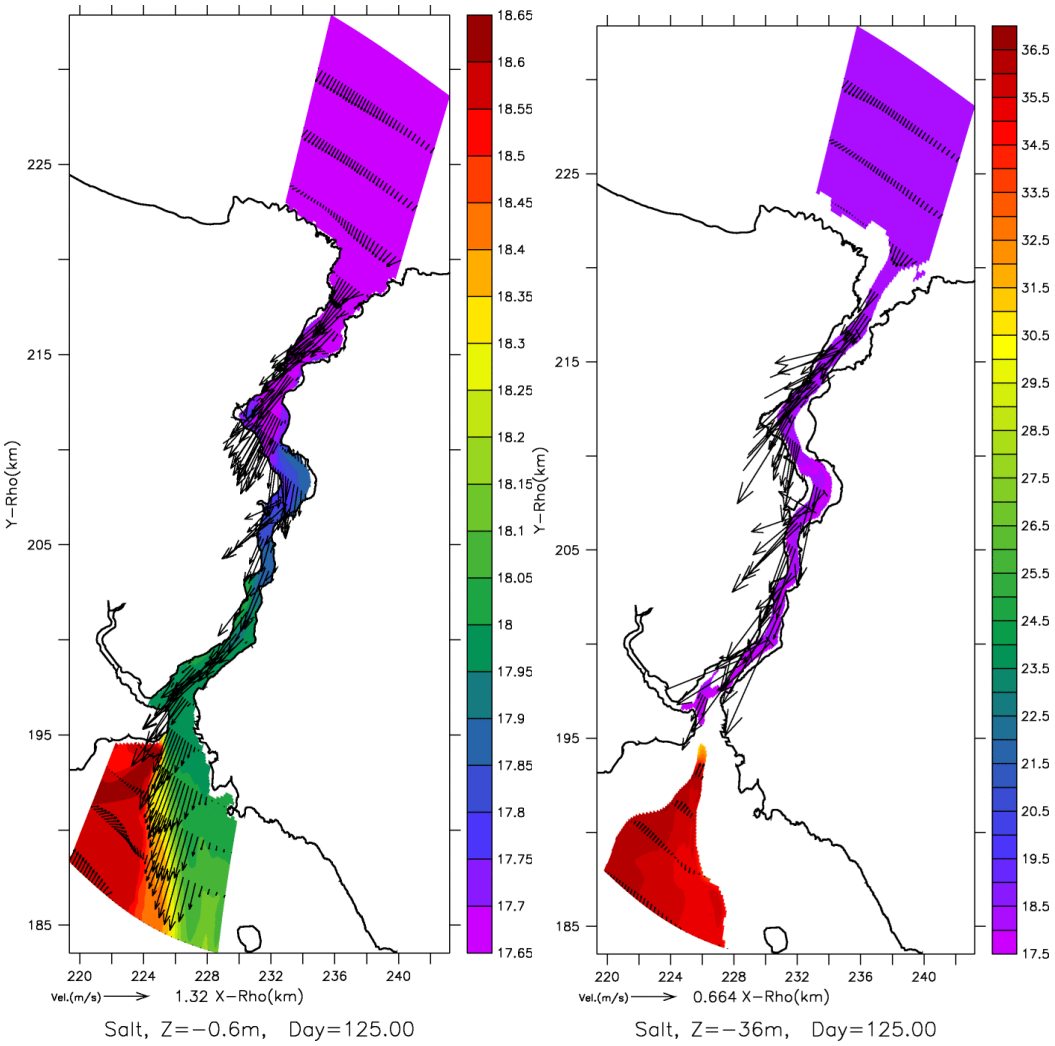


Figure 78. Salinity and current vectors at depths of 0m (surface) and 36m in the Bosphorus for net barotropic volume flux of Q = 50000 $m^3/s$.

Similarly the salinity and current vectors at depths of 0m (surface) and 36m in the Dardanelles for selected values of net barotropic volume flux are shown in Fig.s 89 and 80.

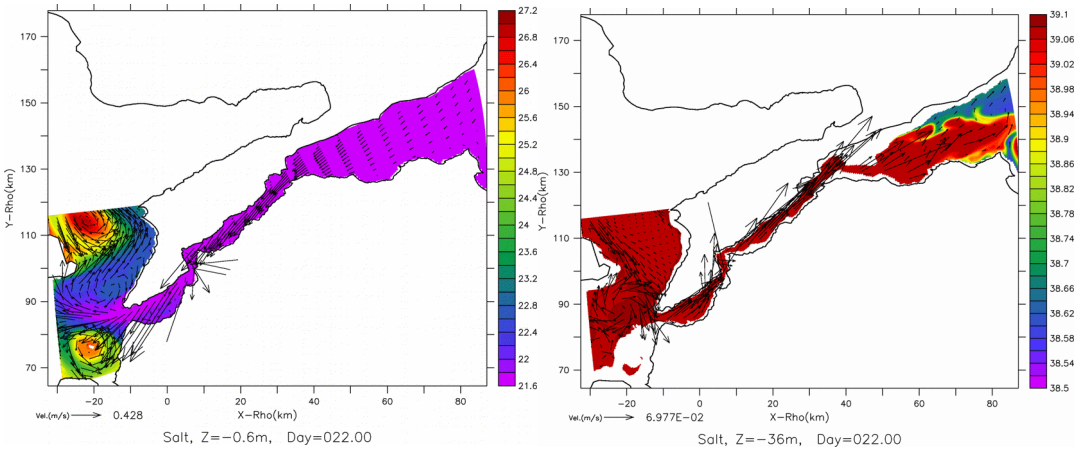


Figure 79. Salinity and current vectors at depths of 0m (surface) and 36m in the Dardanelles for net barotropic volume flux of Q = 9600 $m^3/s$.

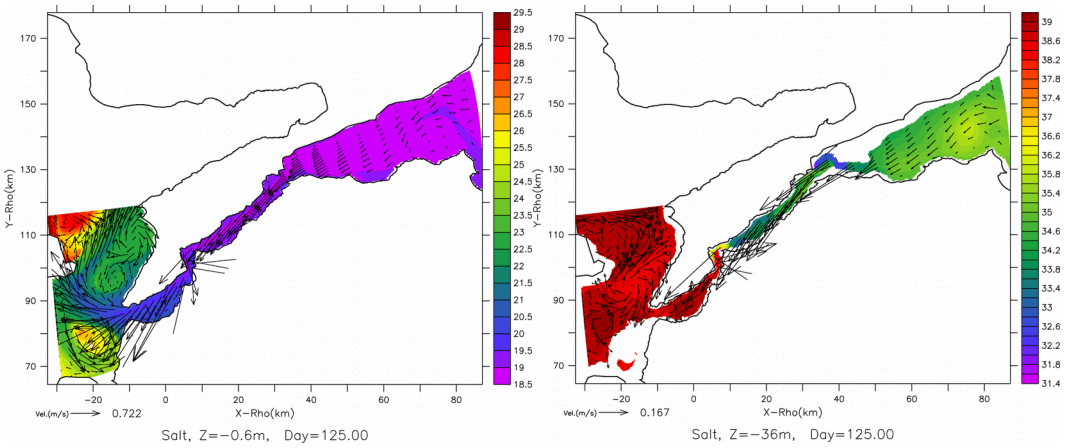


Figure 80. Salinity and current vectors at depths of 0m (surface) and 36m in the Dardanelles for net barotropic volume flux of Q = 50000 $m^3/s$.

The TSS model (MITgcm) results are compared with results from the Bosphorus model (ROMS) obtained by sözer (2013) in Fig. 81. Although the two models sre different in many ways, including the underlying physics and parameterizations, the much higher resolution of the Bosphorus model and the much greater areal coverage of the TSS model, this model-model comparison is excellent, showing that most of the essential

features, such as the hydraulic controls at the topographical barriers, contraction and sill of the Bosphorus, the interface thickness, and the mixing properties are equally well represented in the TSS model, producing comparable results..

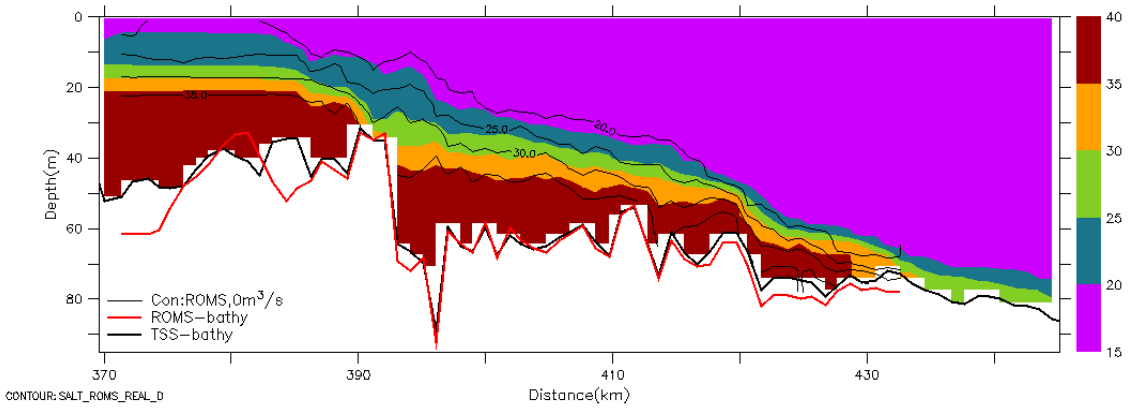


TSS Salt, Day=104, 0m$^3$/s

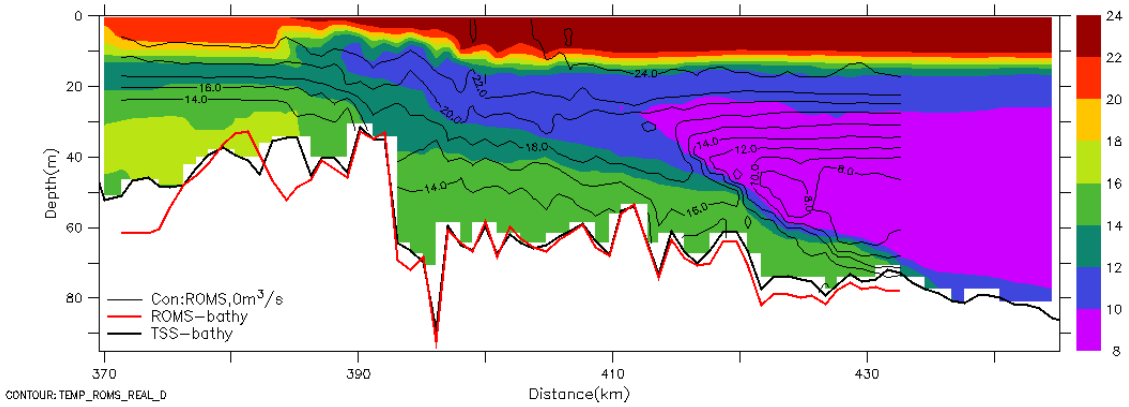


TSS Temp, Day=104, 0m$^3$/s

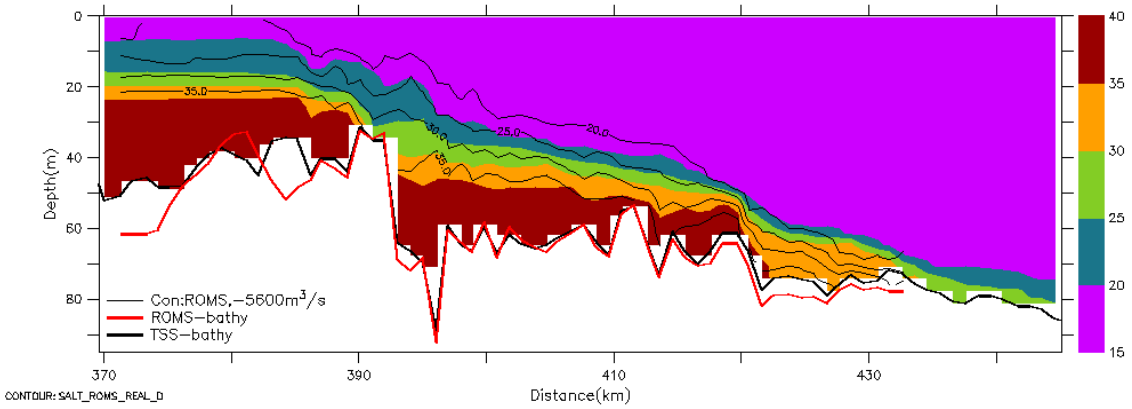


TSS Salt, Day=66, −5600m$^3$/s

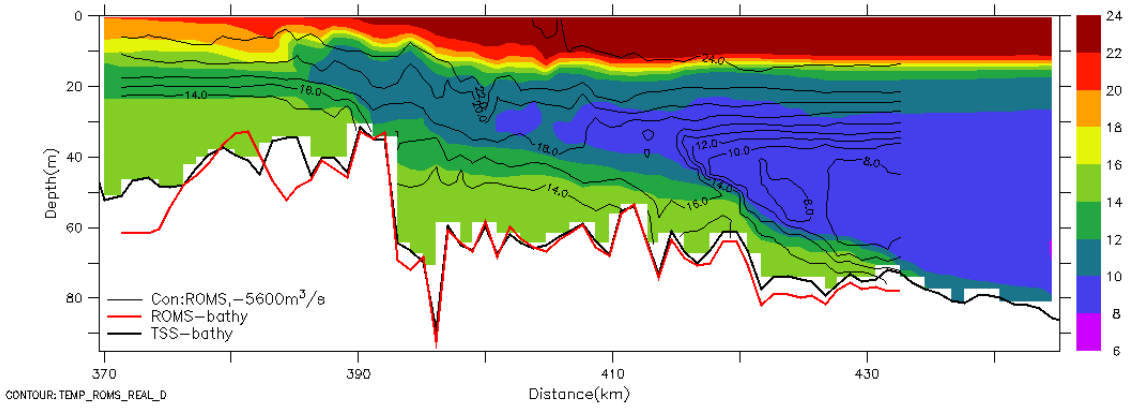


TSS Temp, Day=66, −5600m$^3$/s

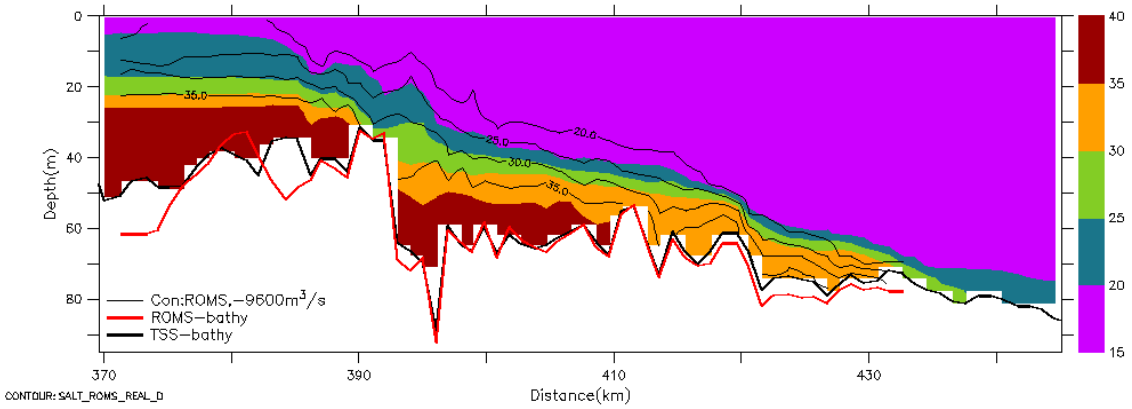


TSS Salt, Day=22, −9600m$^3$/s

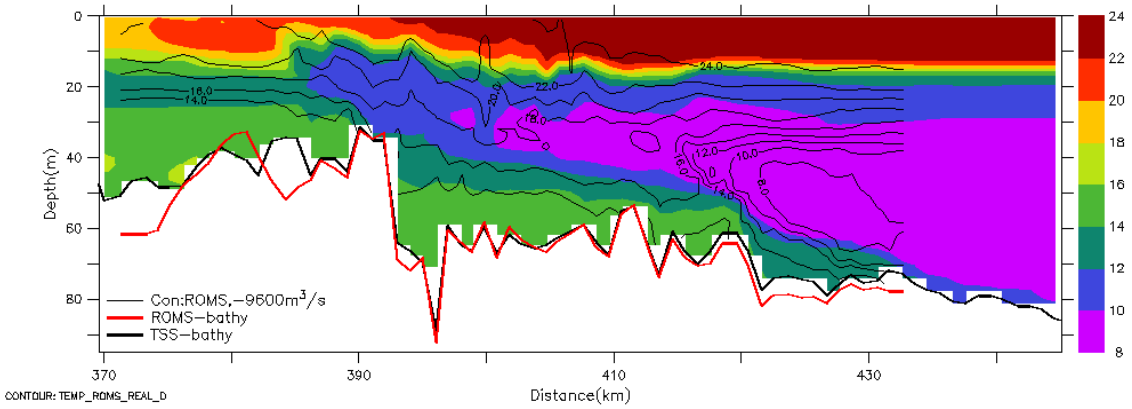


TSS Temp, Day=22, −9600m$^3$/s

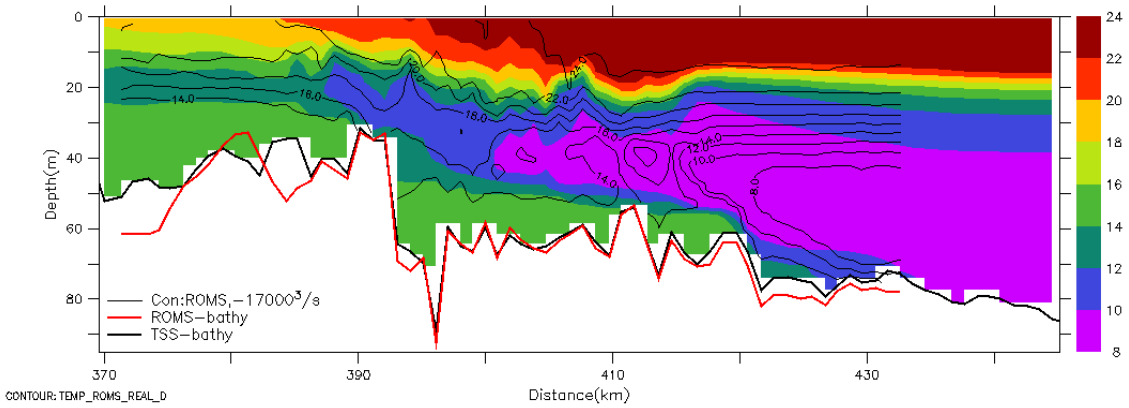


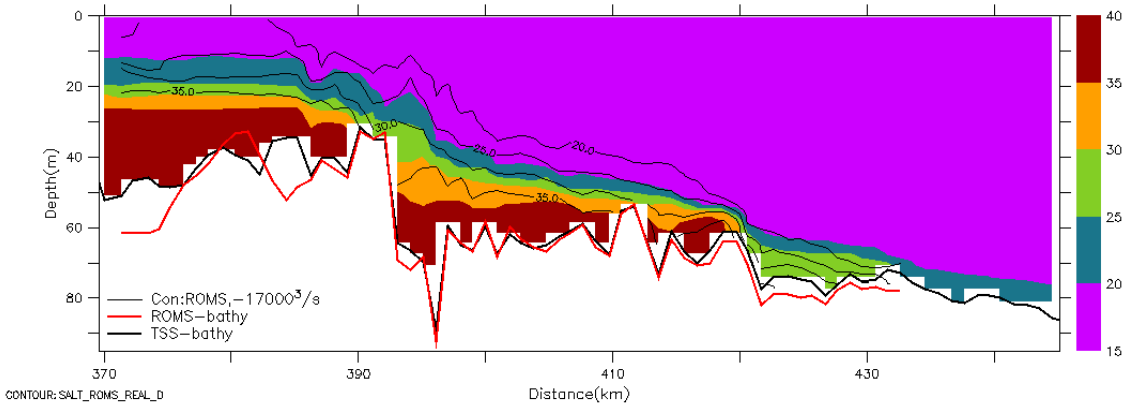


Figure 81. Comparison of the salinity and temperature along the Bosphorus produced by the TSS (MITgcm, colours) and Bosphorus (ROMS, contours) models for net barotropic flux values of Q= 0, 5600, 9600 and 18000 $m^3/s$.

Because the TSS has distinct regions of varied geometrical properties with a wide range of dynamical processes active in these regions, the physical response is different in each region. The evolution of kinetic energy is shown in Fig. 82 for different regions. It is observed that the approach to a steady state is very fast in the two straits, while the wider areas of the three adjacent basins respond much slower.

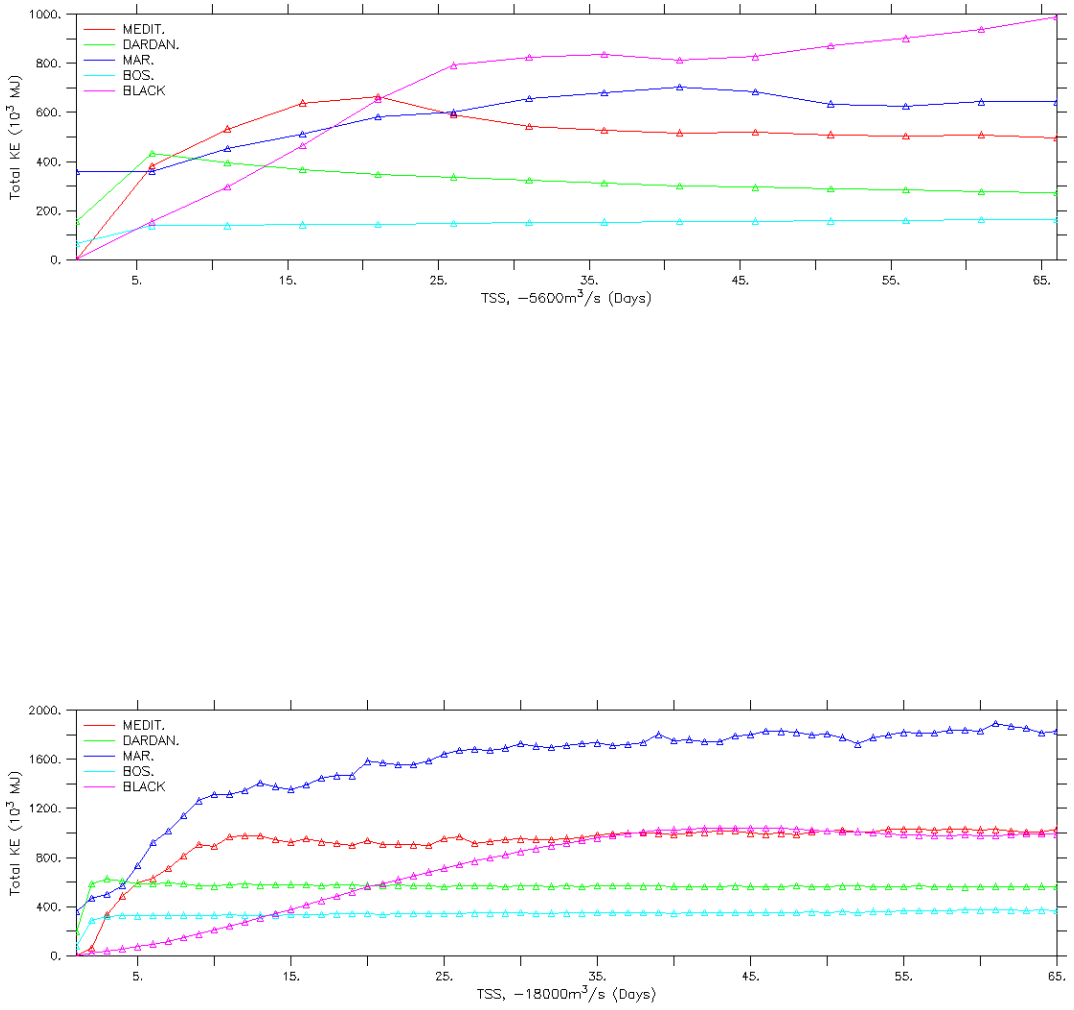


Figure 82. Evolution of kinetic energy for different regions of the TSS for selected values of net transport, Q=5600 and 18000 m$^3$/s.

The comparison between model results and observations are shown in Fig.s 83-89, comparing the June 2013 cruise data at CTD stations with the model.

In Fig. 83 the CTD stations are shown superposed on a grid used for interpolation. The salinity and temperature at 10m depth, interpolated from station data and based on TSS model results are compared in Fig.s 84 and 85.

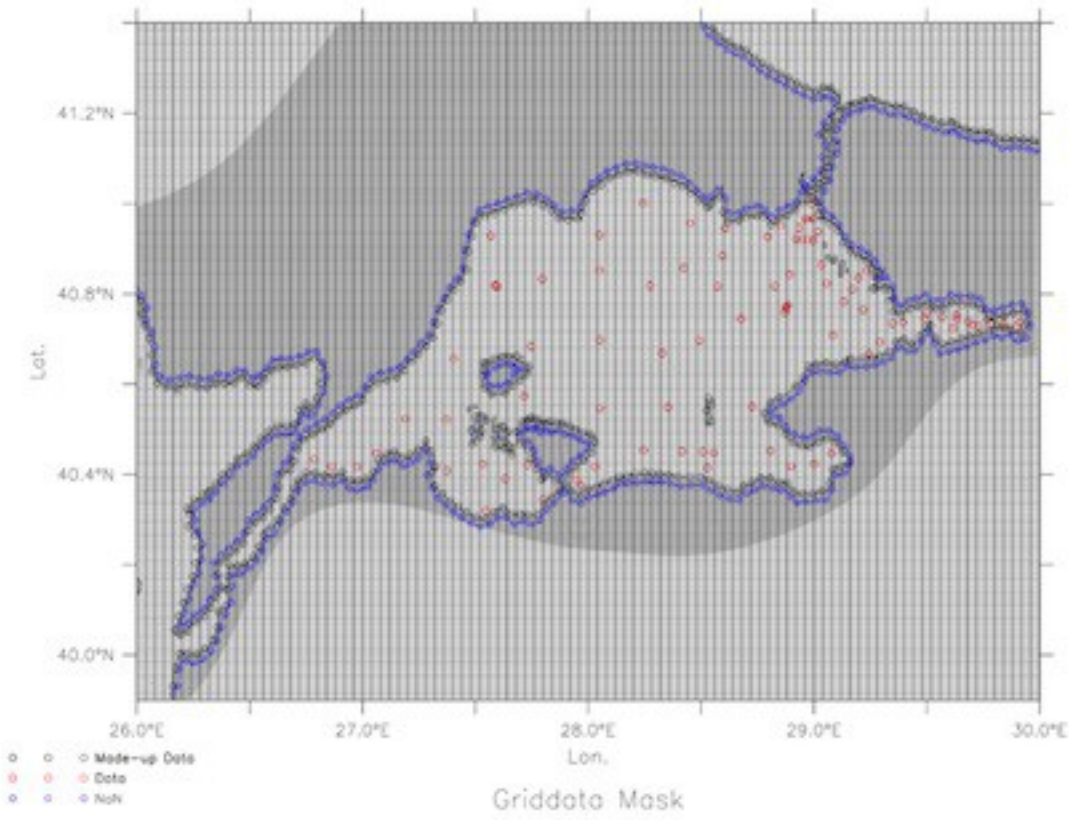


Figure 83. The June 2013 CTD stations of the R/V BİLİM, and the interpolation grid, with superposed TSS model grid area.

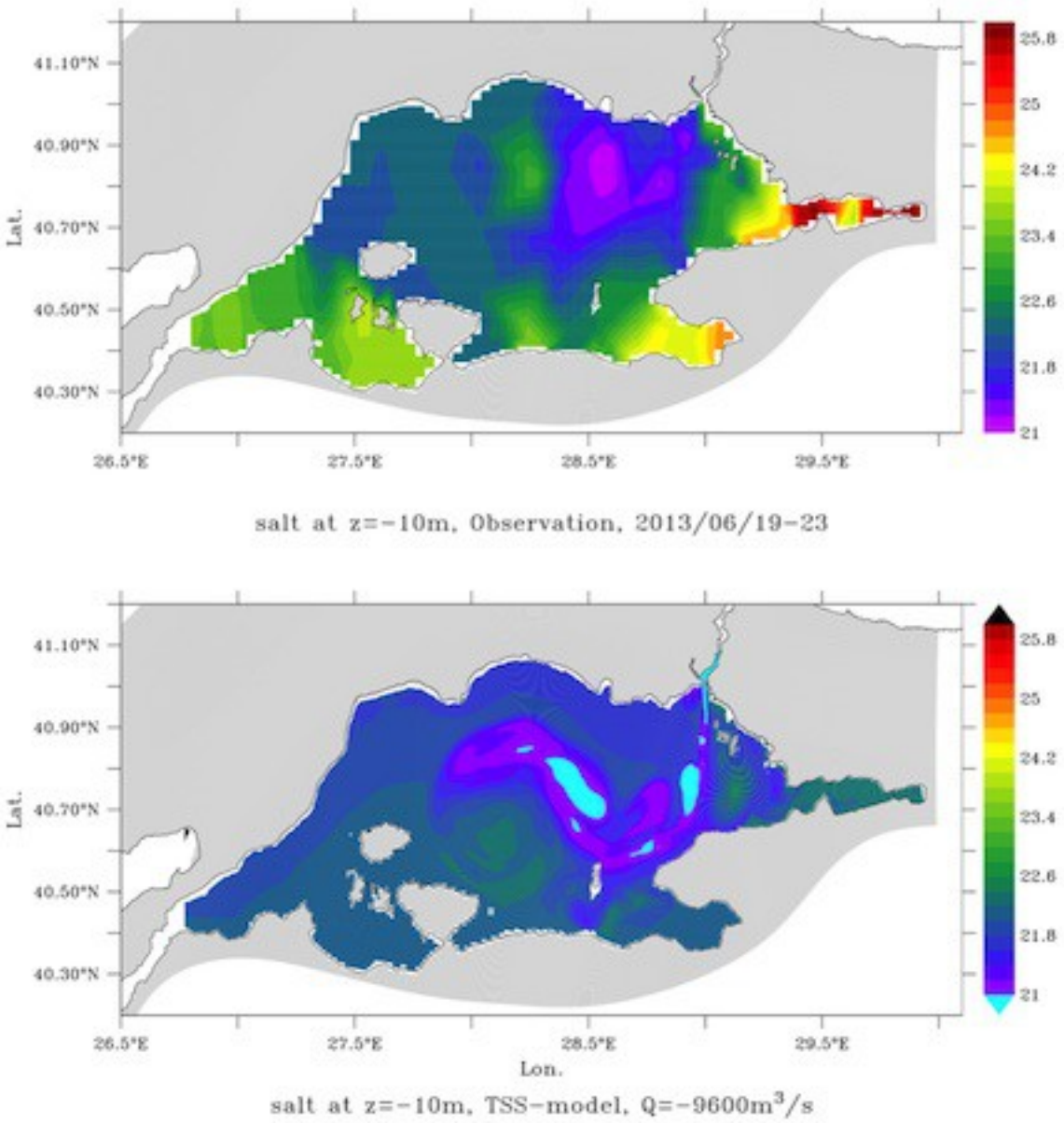


Figure 84. Salinity at 10 m depth, based on interpolation of June 2013 observations (top) and TSS model results (bottom) for net flux of Q=9600 $m^3/s$.

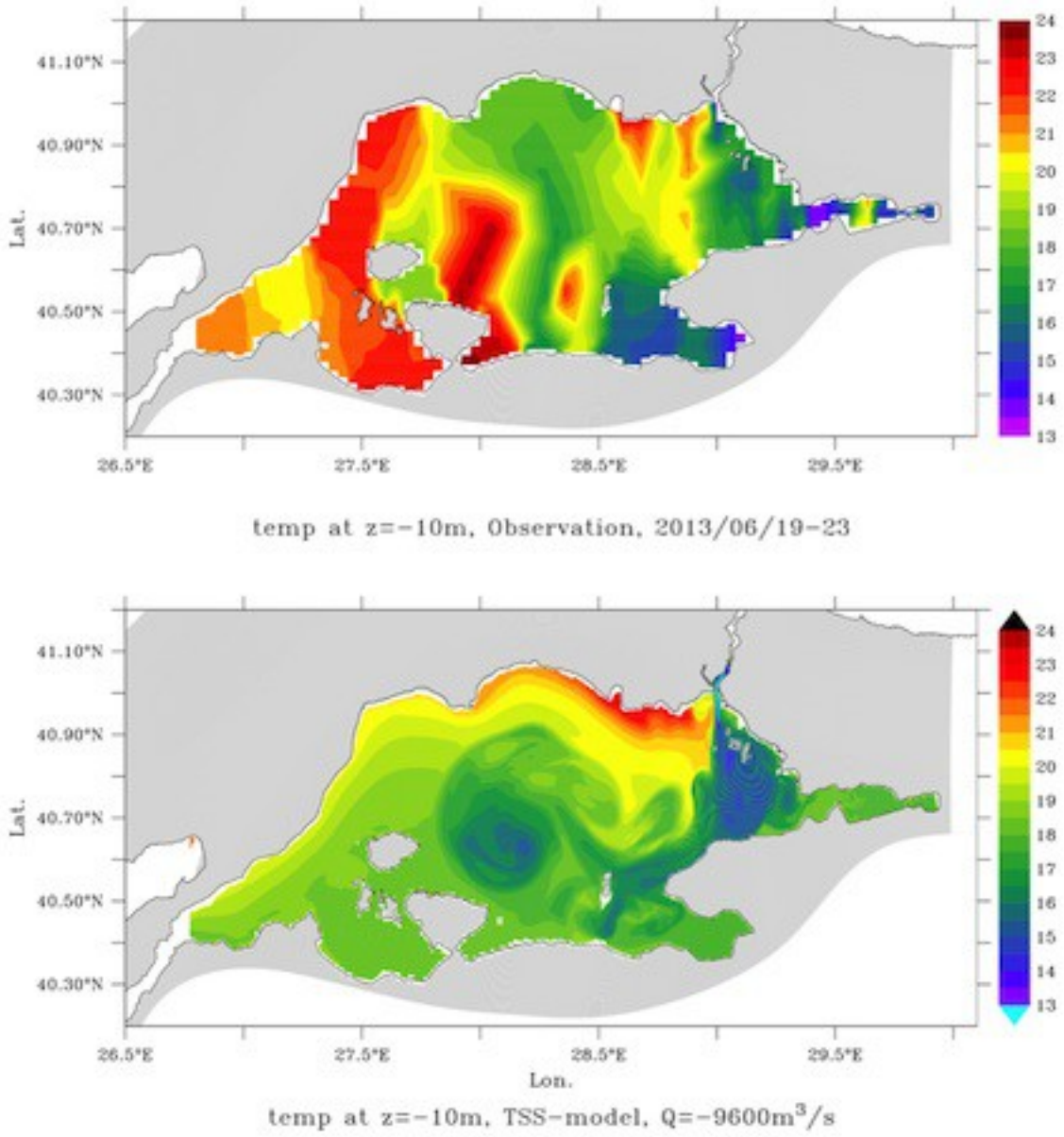


Figure 85. Temperature at 10 m depth, based on interpolation of June 2013 observations (top) and TSS model results (bottom) for net flux of Q=9600 $m^3/2$.

Fig. 86 displays the locations of two sections, one across the TSS and the other along the Bosphorus extending to the Black Sea shelf area used for comparisons of June 2013 observations with TSS model results.

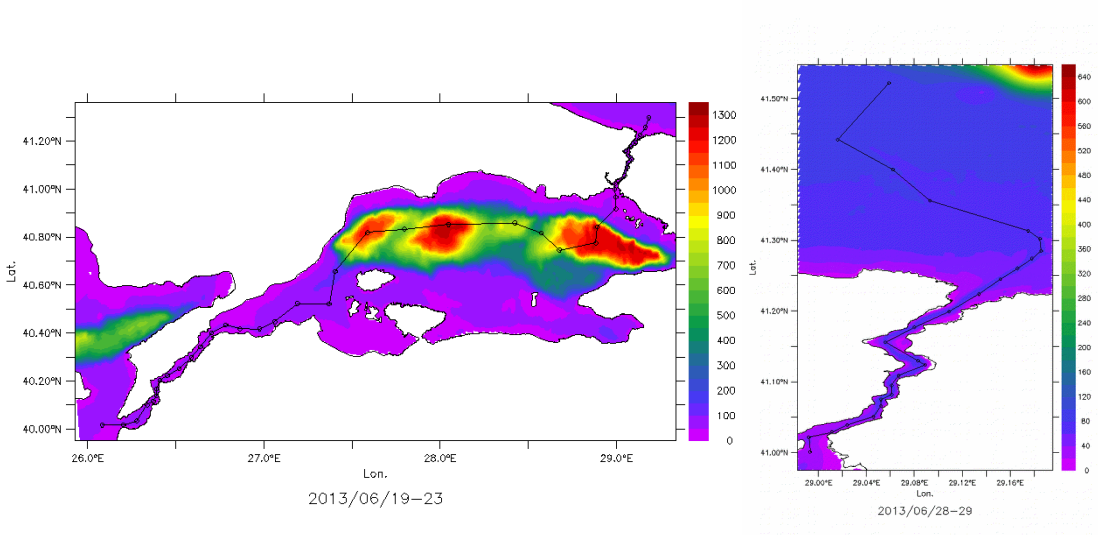


Figure 86. Section 1 following CTD stations in the TSS and Section 2 along the Bosphorus extending into the Black Sea shelf.

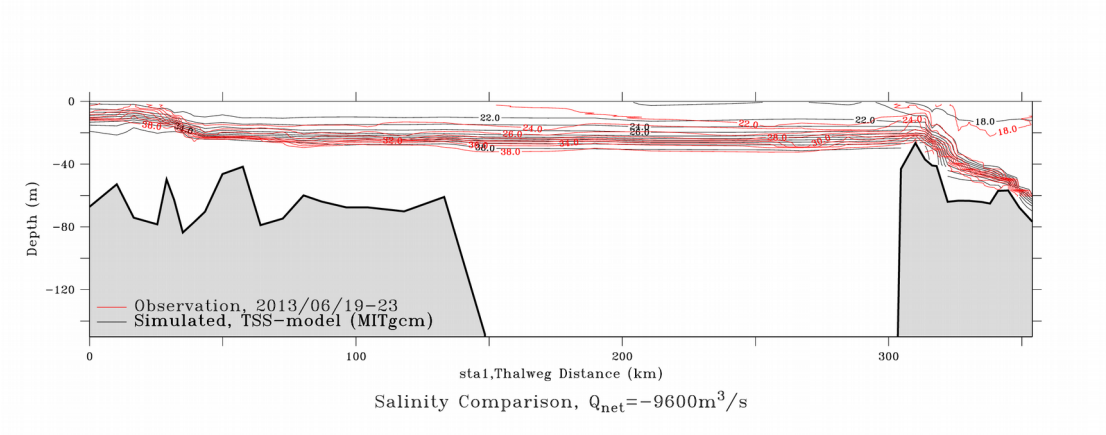

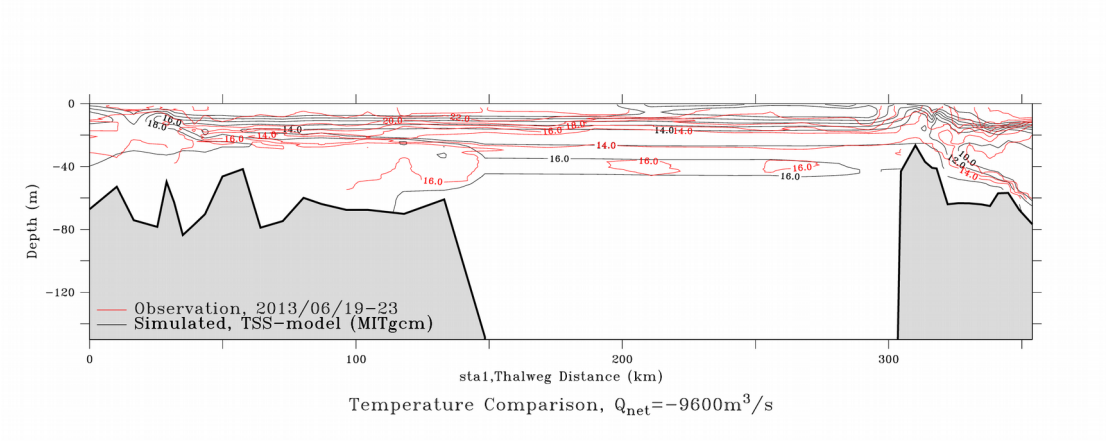


Figure 87. Comparison of salinity (top) and temperature (bottom) interpolated from CTD data (red contours) and obtained from the TSS model (black contours) along Section 1.

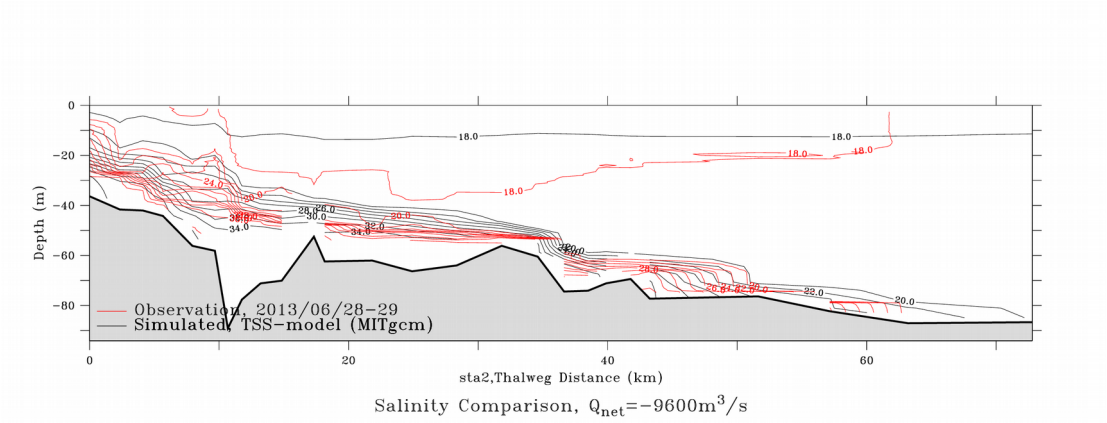


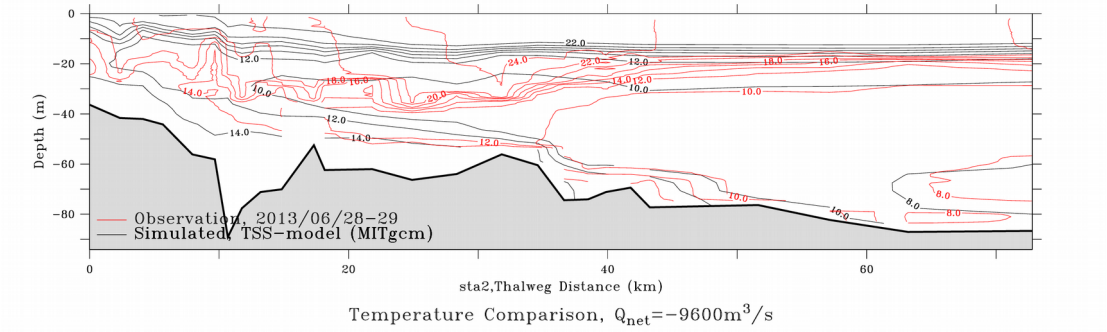

Figure 88. Comparison of salinity (top) and temperature (bottom) interpolated from CTD data (red contours) and obtained from the TSS model (black contours) along Section 2 covering the Bosphorus Strait and the adjacent Black Sea shelf.

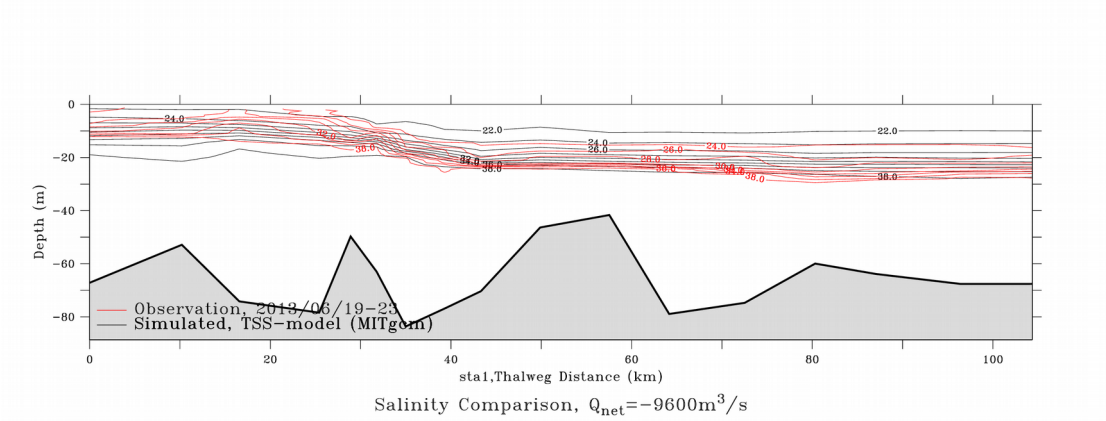


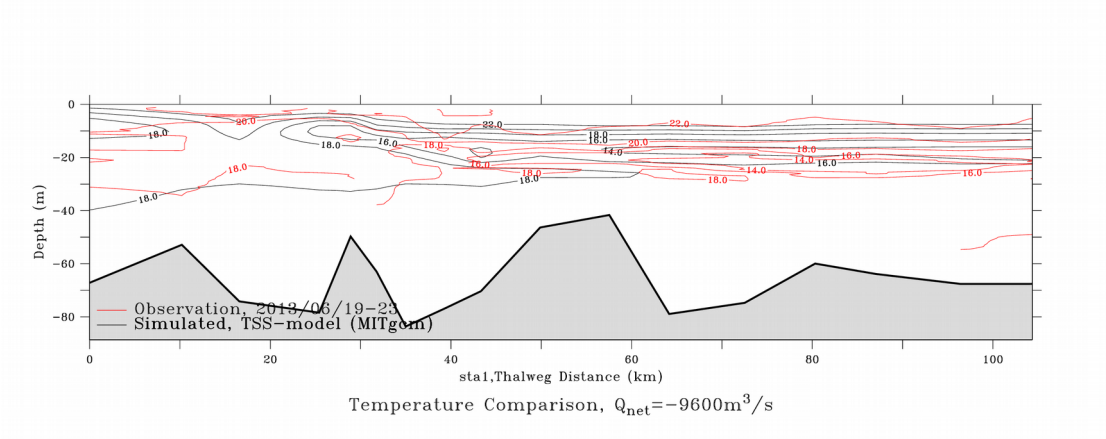


Figure 89. Comparison of salinity (top) and temperature (bottom) interpolated from CTD data (red contours) and obtained from the TSS model (black contours) along part of Section 1 covering the Dardanelles Strait.

Finally a comparison is made of the upper-layer ($Q_1$) and lower-layer ($Q_2$) volume fluxes through the Boshorus, based on observational data and the results from the Bosphorus

model (ROMS) of Sözer (2013) and the TSS (MITgcm) models. Although the Bosphorus model is more specific to the Strait and has better resolution, the TSS model results perform even better in comparison with observations.

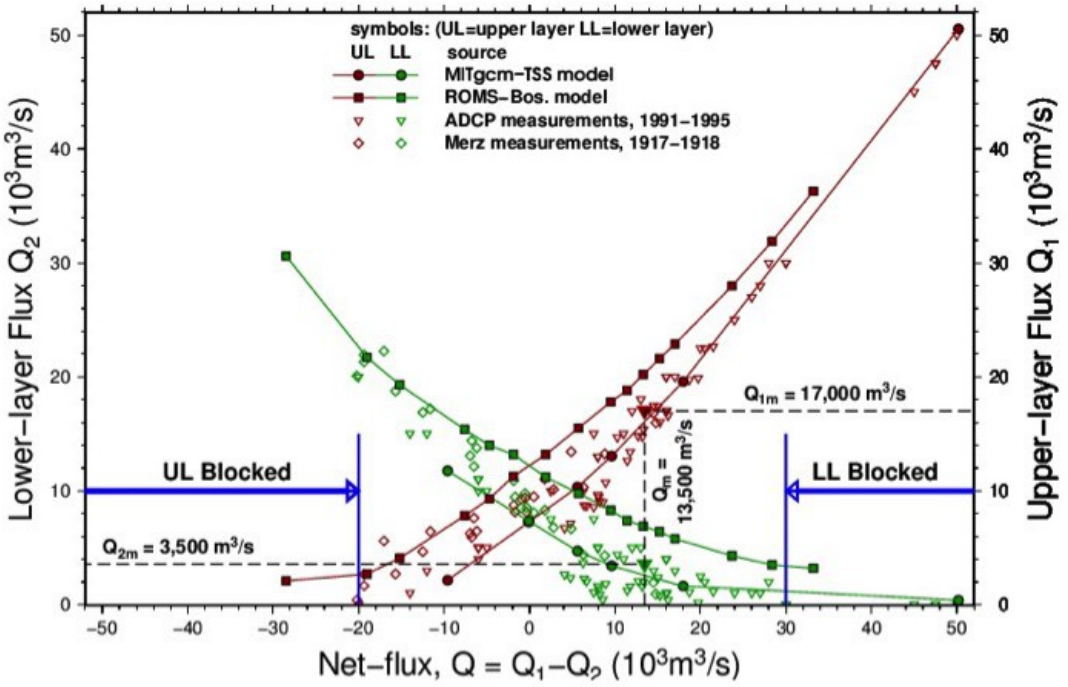


Figure 90. Upper-layer ($Q_1$) and lower-layer ($Q_2$) volume fluxes through the Boshorus as a function of the and net flux ($Q=Q_1-Q_2$), based on observational data and compared with the results from the Bosphorus model (ROMS) of Sözer (2013) and the TSS (MITgcm) models.

**References**


Alpar, B. and H. Yüce (1998). Sea-Level Variations and their Interactions between the Black Sea and the Aegean Sea. Estuarine, *Coastal and Shelf Science*, **46,** 609-619.

Andersen, J. J. and E. C. Carmack (1984). Observations of Chemical and Physical Fine-structure in a Strong Pycnocline, Sea of Marmara. *Deep-Sea Res.*, **21**, 877-886.

Baştürk, Ö., Tuğrul, S., Konovalov, S., Salihoğlu, İ., 1998. Effects of circulation on the spatial distributions of principle chemical properties and unexpected short- and long-term changes in the Black Sea. In: Ivanov, L.I. and Oğuz T. (eds.) Ecosystem modeling as a management tool for the Black Sea. NATO Science Series, Vol. 47, Kluwer Academic publishers, Netherlands, pp. 39-54.

Beardsley, R. C. and J. Hart (1978). A Simple Theoretical Model for the Flow of an Estuary on to a Continental Shelf, J. Geophys. Res., 83:873-883.

Beşiktepe, Ş., Özsoy, E. and Ü. Ünlüata (1993). Filling of the Marmara Sea by the Dardanelles Lower Layer Inflow, *Deep-Sea Res.*, **40**, 1815-1838,

Beşiktepe, Ş., Sur, H. İ., Özsoy, E., Latif, M. A., Oğuz, T. and Ü. Ünlüata (1994), The Circulation and Hydrography of the Marmara Sea, *Prog. Oceanogr.*, **34**, 285-334.

Beşiktepe, Ş., Özsoy, E., and M. A. Latif (1995). Sewage Outfall Plume in the Two-Layer Channel: An Example of Istanbul Outfall, Wat. Sci. Tech., 32(2), 69-75.

Beşiktepe, Ş., E. Özsoy, M. A. Latif ve T. Oğuz (2000). Marmara Denizi'nin hidrografisi ve Dolaşımı, (Hydrography and circulation of the Marmara Sea), Marmara Sea 2000 Symposium, İstanbul, Nov. 11-12, 2000, 14 pp. (in Turkish).

Beşiktepe, Ş. T. (2003). Density Currents in the Two-Layer Flow: An example of Dardanelles Outflow, *Oceanologica Acta*, **26**, p.243-253.

Book, J. W., E. Jarosz, J. Chiggiato, and S¸. Beşiktepe (2014), The oceanic response of the Turkish Straits System to an extreme drop in atmospheric pressure, *J. Geophys. Res.* Oceans, 119, 3629–3644, doi:10.1002/ 2013JC009480.

Bursa, P. (2010). *Antikçağ'da Anadolu'da Balık ve Balıkçılık*, (Fish and Fishing in Anatolia in the Antiquity), Türk Eskiçağ Bilimleri Enstitüsü Yayınları, **28**, 60pp. (in Turkish).

Büyükay, M. (1989). The surface and internal oscillations in the Bosphorus, related to meteorological forces, M.Sc. Thesis, Institute of Marine Sciences, Middle East Technical University, 169p.

Chiggiato, J., Jarosz, E., Book, J. W., Dykes, J., Torrisi, L., Poulain, P.-M., Gerin, R., Horstmann, J. and Ş. Beşiktepe, (2011). Dynamics of the circulation in the Sea of Marmara: numerical modeling experiments and observations from the Turkish straits system experiment, Ocean Dynamics, 62 (1), 139-159.

CIESM, 2010. *Climate forcing and its impacts on the Black Sea marine biota*. No. 39 in CIESM Workshop Monographs [F. Briand, Ed.], 152 pages, Monaco.

Cociasu, A., Lazar, L., Vasiliu, D. (2008) "New tendency in nutrients evolution from Romanian coastal waters", *Recherches Marine*, 38, pp: 7-24.

Codispoti, L.A., Friederich, G.E., Murray, J.W., Samatamota, C.M., 1991. Chemical variability in the Black Sea: implications of data obtained with a continuous vertical profiling system that penetrated the oxic/anoxic interface. Deep-Sea Res., 38(Suppl.2), 691-710.

Çetin, N. (1999). Analysis of the exchange flow through the Bosphorus Strait. M.Sc. Thesis, Institute of Marine Sciences, METU, Erdemli, Mersin, 109 pp.

De Filippi, G. L., Iovenitti, L. and A. Akyarlı (1986). Current analysis in the Marmara-Bosphorus Junction. 1st AIOM (Assoclazione di Ingegneria Offshore e Marina) Congress, Venice, June 1986, 5-25.

Deacon, M. (1982). *Modern Concepts of Oceanography*, Hutchinson Ross, 385 pp., 1982.

Defant, A. (1961). *Physical Oceanography*, Pergamon Press, London, 1961. Vol. 1, pp. xvi + 729; Vol. 2, pp. viii + 598.

Delfanti, R., Özsoy, E.; Kaberi, H., Schirone, A., Salvi, S., Conte, F., Tsabaris C. and C. Papucci (2013). Evolution and fluxes of 137Cs in the Black Sea / Turkish Straits System / North Aegean Sea, (this volume).

Demyshev, S. G., Knysh, V. V. and G. K. Korotaev (2003). Numerical modeling of the seasonal variability of hydrophysical fields in the Black Sea, *Morsk. Gidrofiz. Zh*., **3**, 12–26.

Demyshev S. G. and S. V. Dovgaya (2007). Numerical Experiment Aimed At Modeling the Hydrophysical Fields in the Sea Of Marmara with regard for Bosporus and Dardanelles, *Physical Oceanography,* **17** (3), 141-153.

Demyshev, S. G., S. V. Dovgaya and V. A. Ivanov (2012). Numerical modeling of the influence of exchange through the Bosporus and Dardanelles Straits on the hydrophysical fields of the Marmara Sea, *Izvestiya, Atmospheric and Oceanic Physics*, **48**(4 ), 418-426.

Di Iorio, D. and H. Yüce (1999). Observatİons of Mediterranean flow İnto the Black Sea, J. Geophys. Res., 104, 3091-3108.

Ducet, N., Le Traon, P. Y. and P. Gauzelin (1999). Response of the Black Sea mean level to atmospheric pressure and wind forcing, *J. Mar. Sys.*, **22**, 311 – 327.

Farmer, D. M. and L. Armi (1986). Maximal two-layer exchange over a sill and through the combination of a sill and contraction with barotropic flow, *J. Fluid Mech*., **164**, 53-76.

Gaines, A. F., Copeland, G. M., Çoban-Yıldız, Y., Özsoy, E., Davie, A. M. And S. K. Konovalov (2006). The Contrasting Oceanography Of The Rhodes Gyre And The Central Black Sea, Turkish J. Eng. Env. Sci., 30, 69 – 81.

Georgievski, G., and E. V. Stanev (2006). Paleoevolution of Euroasian watersheds: Water transport through the Bosporus Straits as an indicator of the Late Glacial-Holocene transition, *Climate Dynamics*, **26** (6), 631-644.

Gill, A. E., *Atmosphere-Ocean Dynamics*, Academic Press, 662 pp., 1982

Gökaşan, E., Tur, H., Ecevitoğlu, B., Görüm, T., Türker, A., Tok, B., Çağlak, F., Birkan, H. and M. Şimşek (2005). Evidence and implications of massive erosion along the Strait of İstanbul (Bosphorus), *Geo-Mar. Lett*., **25**, 324–342.

Gökaşan, E., M. Ergin, M. Özyalvaç, H. İ. Sur, H. Tur, T. Görüm, T. Ustaömer, F. G. Batuk, H. Alp, H. Birkan, A. Türker, E. Gezgin, M. Özturan (2007). Factors controlling the morphological evolution of the Çanakkale Strait (Dardanelles, Turkey), *Geo-Mar. Lett.*, 28, 107-129.

Grasshoff, K., Erhardt, M., Kremling, K., 1983. Methods of Sea Water Analysis, 2nd ed., Verlag Chemie GmbH, 419 sayfa.

Gregg, M. C., Özsoy E. and M. A. Latif (1999). Quasi-Steady Exchange Flow in the Bosphorus, *Geophys. Res. Lett.*, **26**, 83-86.

Gregg, M. C. and E. Özsoy (1999). Mixing on the Black Sea Shelf North of the Bosphorus, *Geophys. Res. Lett.*, **26**, 1869-1872.

Gregg, M. C. and E. Özsoy (2002). Flow, Water Mass Changes and Hydraulics in the Bosphorus, *J. Geophys. Res*., **107** (C3), 10.1029/2000JC000485.

Gregg, M. C. and Yakushev, E., 2005. Surface ventilation of the Black Sea's cold intermediate layer in the middle of the western gyre. Geophys. Rec. Lett., 32, L03064.

Gungerich, R., (ed.) (1958). Dionysius of Byzantium: Dionysia Byzantio Anaplus Bospori: a cum scholiis, Berlin, Weidmannos.

Gunnerson, C. G., & Özturgut, E. (1974). The Bosphorus. In: E. T. Degens, & D. A. Ross (Eds), *The Black Sea – Geology, Chemistry and Biology* (American Association of Petroleum Geologists, Tulsa, p. 103).

Gündüz, M. and E. Özsoy (2004). Effects of the North Sea Caspian Pattern on Surface Fluxes of Euro-Asian-Mediterranean Seas, *Geophys. Res. Letters*, L21701, doi: 10.1029/2005GL024315.

Gündüz, M. and E. Özsoy (2014). Inter-annual variability of upper layer blocking of the Dardanelles Strait and its connection with the fish catch in the Aegean sea (1979-2013), MedCLIVAR 2014 Conference “Understanding Climate Evolution and Effects on Environ-

ment and Societies in the Old World region", Ankara, June 2014.

Güler, I., Yüksel, Y., Yalçıner, A. C., Çevik, E. and C. Ingerslev (2006). Measurement and Evaluation of the Hydrodynamics and Secondary Currents in and near a Strait Connecting Large Water Bodies - A Field Study, *Journal of Ocean Engineering*, **33**, 1718-1748.

Gyllii, Petri (1561). *De Bosporo Thracio Libri III*, Lyon 1561 (2nd printing, Leiden 1632).

Haidvogel, D. B., H. G. Arango, K. Hedstrom, A. Beckmann, P. Malanotte-Rizzoli, and A. F. Shchepetkin (2000), Model evaluation experiments in the North Atlantic Basin: Simulations in nonlinear terrain-following coordinates, *Dyn. Atmos. Oceans*, **32**, 239-281.

Hay, B. J. and S. Honjo (1989). Particle Deposition in the Present and Holocene Black Sea, *Oceanography*, **2**(1), 26-31.

Hedström, K. S., 1997. Draft User's Manual for an S-Coordinate Primitive Equation Ocean Circulation Model (SCRUM) Version 3.0, Institute of Marine and Coastal Sciences, Rutgers University, Rutgers University.

Humborg, C., Ittekot, V., Cociasu, A., v. Bodungen, B., 1997. Effect of Danube River dam on Black Sea biogeochemistry and ecosystem structure. Nature, 386, 385-388.

Hundsdorfer, W., B. Koren, M. Vanloon, and J. Verwer (1995), A positive finite-difference advection scheme, J. Computational Physics, 117 (1), 35–46.

Huq, P. (2013). Buoyant Outflows to the Coastal Ocean, Handbook of Environmental Fluid Dynamics, Volume One, edited by H. J. S. Fernando. CRC Press / Taylor & Francis Group, LLC, 1:207-215.

Hüsrevoğlu, Y. S. (1999). Modelling of the Dardanelles Strait lower-layer flow into the Marmara Sea, M.Sc. Thesis, Institute of Marine Sciences, METU, Erdemli, Mersin.

Ilıcak, M., Özgökmen, T. M., Özsoy, E. and Fischer, P. F. (2009). Non-hydrostatic Modeling of Exchange Flows Across Complex Geometries, *Ocean Modeling*, **29**, 159–175.

IMS-METU (1999). A Study of the Turkish Straits System Currents at Various Space – Time Scales, unpublished report, Institute of Marine Sciences, METU, Erdemli, Mersin, December 1999.

Jarosz, E., W. J. Teague, J. W. Book, and Ş. Beşiktepe (2011a). On flow variability in the Bosphorus Strait, *J. Geophys. Res.,* **116**, C08038, doi:10.1029/2010JC006861.

Jarosz, E., W. J. Teague, J. W. Book, and Ş. Beşiktepe (2011b). Observed volume fluxes in the Bosphorus Strait, *Geophys. Res. Lett.,* **38,** L21608, doi:10.1029/ 2011GL049557.

Jarosz, E., W. J. Teague, J. W. Book, and Ş. T. Beşiktepe (2012), Observations on the characteristics of the exchange flow in the Dardanelles Strait, *J. Geophys. Res.*, **117**, C11012, doi:10.1029/2012JC008348.

Kahraman, C. (2007). *The winter of 1929, An Urban Legend*, Türkiye İş Bankası Kültür Yayınları, İstanbul, 186 pp. (in Turkish).

Kanarska, Y. and V. Maderich (2008). Modelling of seasonal exchange flows through the Dardanelles Strait, Estuarine, *Coastal and Shelf Science*, **79**, 449–458.

Konovalov, S.K. and Murray, J.W. 2001. Variations in the chemistry of the Black Sea on a time scale of decades (1960-1995). J. Mar. Syst. 31, 217-243.

Konovalov, S.K., Luther, G.W., Friedrich, G.E., Nuzzio, D.B., Tebo, B.M., Murray, J.W., Oğuz, T., Glazer, B., Trouwborst, R.E., Clement, B., Murray, K.J., Romanov, A.S., 2003. Lateral injection of oxygen with the Bosphorus plume-fingers of oxidizing potential in the Black Sea. Limnol. and Oceanogr. 48(6), 2369-2376.

Konovalov, S., Murray, J.W., Luther, G.W.III, 2005. Basic Processes of Black Sea Biogeochemistry. Oceanography, 18, 25-35.

Korfmann, M. and J. Neumann (1985). Subsurface countercurrent in the Bosporus already known to 6th century A. D. Byzantine fishermen, *Ocean Dynamics*, 189-190.

Latif, M. A., Özsoy, E., Oğuz, T. and Ünlüata, Ü. (1991). Observations of the Mediterranean inflow into the Black Sea, *Deep-Sea Res.*, **38** (Suppl. 2), 711–723.

Lagaria, A., S. Psarra, A. Gogou, S. Tuğrul, U. Christaki (2013). Particulate and dissolved primary production along a pronounced hydrographic and trophic gradient (Turkish Straits System – NE Aegean Sea), *J. Mar. Sys.*, **119–120**, 1-10.

Lee, B-S., Bullister, J. L., Murray, J. W. and R. E. Sonnerup (2002). Anthropogenic chlorofluorocarbons in the Black Sea and the Sea of Marmara*, Deep Sea Res.*, **49**, 895–913.

Leith, C. (1968). Parameterization of vertical mixing in numerical models of tropical oceans, Physics of Fluids, 10, 1409–1416.

Lionello, P., Malanotte-Rizzoli, P. and R. Boscolo (eds.) (2006). *Mediterranean Climate Variability*, Elsevier Science, 438 pp.

Ludwig, W., Dumont, E., Meybeck, M. Heussner, S. (2009). River discharges of water and nutrients to the Mediterranean and Black Sea: Major drivers for ecosystem changes during past and future decades?, *Progress in Oceanography*, **80**, 199–217.

Maderich, V. S. (1998). Modelling of Mediterranean system-changes under climate variations and human impact, *Environmental Modelling and Software*, **13**, 405–412.

Maderich, V. and S. Konstantinov (2002). Seasonal Dynamics of the System Sea-Strait: Black Sea–Bosphorus Case Study, Estuarine, *Coastal and Shelf Science*, **55**, 183–196.

Makarov, S. O. (1885). On the Water Exchange between the Black and Mediterranean Seas, Prilozh. to Zapiski Akad. Nauk, **2** (6), 1–147.

Marsili, L. F. (1681). *Osservazioni Intorno al Bosforo Tracio overo Canale di Constantinopoli,* Rappresentate in Lettera alla Sacra Real Maestá Cristina Regina di Svezia da Luigi Ferdinando Marsigli. Nicoló Angelo Tinassi, Roma.

Merz, A. and L. Möller (1928). *Hydrographische Untersuchungen in Bosporus und Dardanellen*, Alfred Merz. Bearb. von Lotte Möller, Berlin : E. S. Mittler & Sohn, 1 Atlas of 16 charts, 3 figures, 8 tables of sizes 47 x 39 cm and text 133p.

Morrison, A. (2011). Upstream Basin Circulation of Rotating, Hydraulically Controlled Flows, 2011 Summer Program in Geophysical Fluid Dynamics, WHOI, 429 pp.

Möller, L. (1928). *Alfred Merz' hydrographische Untersuchungen im Bosphorus und Dardanellen*. Veröffentlichungen des Instituts für Meereskunde an der Universität Berlin, **18** (Neue Folge A), 284.

Nielsen, J. N. (1912). Hydrography of the Mediterranean and adjacent waters. In: J. Schmidt (Ed.) Report of the Danish oceanographic expedition 1908–1910 to the Mediterranean and adjacent waters. (Vol. **1**, pp. 72–191). Copenhagen: Andr. Fred Høst & Søn.

Nof, D. (1978). On Geostrophic Adjustment in Sea Straits and Wide Estuaries: Theory and Laboratory Experiments. Part II – Two-Layer System, J. Phys. Ocean. 8, 861-872.

Oğuz, T. and H. İ. Sur (1989). A two-layer model of water exchange through the Dardanelles Strait, *Oceanology Acta*, **12**, 23-31.

Oğuz, T., Özsoy, E., Latif, M. A., Sur, H. İ. and Ünlüata Ü. (1990). Modelling of Hydraulically Controlled Exchange Flow in the Bosphorus Strait, *Journal of Physical Oceanography*, **20**, 945-965.

Oğuz, T. (2003). Climatic Warming Impacting Pelagic Fish Stocks in the Black Sea Due To An Ecological Regime Shift During Mid-1990s, *Globec International Newsletter*, **9** (2), 3-5.

Oğuz, T. (2005). Hydraulic adjustment of the Bosphorus exchange flow, *Geophys. Res. Letters*, **32**, L06604, doi:10.1029/2005GL022353.

Östlund, H.G., Dyrssen, D. (1986). Renewal rates of the Black Sea deep water. In: Dyrssen, D., Walin, G. (Eds.), The Chemical and Physical Oceanography of the Black Sea. Reports of the Chemistry of the Sea XXXIII. University of Göteborg, Göteborg, Sweden.

Özsoy, E., Ünlüata, Ü. and Z. Top, (1993). The Mediterranean Water Evolution, Material Transport by Double Diffusive Intrusions, and Interior Mixing in the Black Sea, *Prog. Oceanogr.*, **31**, 275-320.

Özsoy, E. and Ş. Beşiktepe, (1995). Sources of Double Diffusive Convection and Impacts on Mixing in the Black Sea, pp. 261-274, in: Brandt, A. and H. J. S. Fernando

(editors), *Double-Diffusive Convection*, Geophysical Monograph **94**, American Geophysical Union, 334 pp.

Özsoy, E., M. A. Latif, S. Tuğrul, and Ü. Ünlüata (1995). Exchanges with the Mediterranean, Fluxes and Boundary Mixing Processes in the Black Sea, In: F. Briand, (editor), *Mediterranean Tributary Seas*, Bulletin de l'Institut Oceéanographique, Monaco, Special Number 15, CIESM Science Series No. 1, Monaco p. 1-25.

Özsoy, E., Latif, M. A., Beşiktepe, Ş. and A. F. Gaines (1995). Fluorescent Dye Measurements of the Mixing and Transport of Wastewater Discharge in the Bosphorus, Wat. Sci. Tech., 32(2), 61-68.

Özsoy, E., M. A. Latif, H. İ. Sur and Y. Goryachkin (1996). A Review of the Exchange Flow Regimes and Mixing in the Bosphorus Strait, in: F. Briand, (editor), *Mediterranean Tributary Seas*, Bulletin de l'Institut Oceéanographique, Monaco, Special Number 17, CIESM Science Series No. 2, Monaco.

Özsoy, E. and Ü. Ünlüata (1997). Oceanography of the Black Sea: A Review of Some Recent Results, *Earth Sci. Rev.*, **42** (4), 231-272.

Özsoy, E. and Ü. Ünlüata (1998). The Black Sea, in: A. R. Robinson and K. Brink (editors), *The Sea: The Global Coastal Ocean: Regional Studies and Syntheses*, 11, John Wiley and Sons, New York, pp. 889-914.

Özsoy, E., Latif, M. A., Beşiktepe, S., Çetin, N., Gregg, N. Belokopytov, V., Goryachkin, Y. and V. Diaconu (1998). The Bosphorus Strait: Exchange Fluxes, Currents and Sea-Level Changes, in: L. Ivanov and T. Oğuz (editors), *Ecosystem Modeling as a Management Tool for the Black Sea*, NATO Science Series 2: Environmental Security **47**, Kluwer Academic Publishers, Dordrecht, vol. 1, 367 pp + vol. 2, 385 pp.

Özsoy, E. (1999). Sensitivity to Global Change in Temperate Euro-Asian Seas (the Mediterranean, Black Sea and Caspian Sea): A Review, *The Eastern Mediterranean as a Laboratory Basin for the Assessment of Contrasting Ecosystems*, editors: P. Malanotte-Rizzoli and V. N. Eremeev, NATO Science Series 2, Environmental Security, **51**, Kluwer Academic Publishers, Dordrecht, s. 281-300.

Özsoy, E., Di Iorio, D., Gregg, M. and J. Backhaus (2001). Mixing in the Bosphorus Strait and the Black Sea Continental Shelf: Observations and a Model of the Dense Water Outflow, *J. Mar. Sys.*, **31**, 99-135.

Özsoy, E., Rank D. and İ. Salihoğlu, (2002). Pycnocline and Deep Vertical Mixing in the Black Sea: Stable Isotope and Transient Tracer Measurements, *Est., Coastal and Shelf Sci.*, **54**, 621-629.

Özsoy, E., Latif, M. A. and Ş. Beşiktepe (2002). The Current System of the Bosphorus Strait Based on Recent Measurements, The 2nd Meeting on the Physical Oceanography of Sea Straits, Villefranche, 15th-19th April 2002, 177-180.

Özsoy, E., Sözer, A., Gündüz, M., Yücel, İ., Yağcı, B., Mert, İ., Yıldız, H., Simav, M. and M. Elge (2009). Meteorology and Oceanography Network of Excellence (MOMA) – Observation and Model Forecast Systems, 3rd National Defense Applications Modelling and Simulation Conference, Ankara, 17-18 June 2009, 27 pp.

Öztürk B. (ed.) (2010), Proceedings of the Symposium 'The Marmara Sea 2010', TÜDAV, İstanbul.

Pacanowski, R., and S. Philander (1981), Parameterization of vertical mixing in numerical-models of tropical oceans, J. Phys. Oceanogr., 11 (11), 1443–1451.

Pektaş, H. (1953). Surface currents in the Bosphorus and the Sea of Marmara, Publication of the Hydrobiology Research Institute, Faculty of Science, University of Istanbul, Hydrobiology Series, A, **1** (4), 154-169 (in Turkish).

Peneva, E., E. Stanev, V. Belokopytov, and P.-Y. Le Traon (2001). Water Transport in the Bosphorus Straits Estimated from Hydro-meteorological and Altimeter Data: Seasonal to Decadal Variability. *J. Mar. Sys.*, **31**, 21-33.

Pinardi, N. (2009). Misurare il mare. Luigi Ferdinando Marsili nell'Egeo e nel Bosforo 1679-1680, Bononia University Press (collana Grandi opere), 83pp.

Polat, Ç. and S. Tuğrul (1995) Nutrient and Organic Carbon Exchanges between the Black and Marmara Seas through the Bosphorus Strait, *Cont. Shelf Res.* **15** (9), 1115-1132.

Polat, Ç., Tuğrul, S., Çoban, Y., Baştürk, Ö. and İ. Salihoğlu (1998). Elemental Composition of Seston and Nutrient Dynamics in the Sea of Marmara, *Hydrobiologia*, **363**, 157-167.

Pratt, L. J. (2008). Critical conditions and composite Froude numbers for layered flow with transverse variations in velocity*, J. Fluid Mech.*, **605**, 281291, doi:10.1017/S002211200800150X.

Preller, R. H. (1986). A Numerical Model Study of the Alboran Sea Gyre, Prog. Oceanogr., 16(3):113-146.

Rank, D., Özsoy, E. and İ. Salihoğlu (1998). Oxygen $^{18}O$, Deuterium and Tritium in the Black Sea and the Sea of Marmara, *J. Env. Rad.*, **43**, 231-245.

Riha and Peliz (2013). A 2-Layer Primitive Equation Model of an Idealized Strait of Gibraltar Connected to an Eastern Basin, Ocean Dynamics, 6, 615-631.

Runnels, C. and M. Özdoğan (2001). The Paleolithic of the Bosphorus Region, NW Turkey, Journal of Field Archeology, 28 (1/2), 69-92.

Ryan, W. B. F., Pitman III, W. C., Major, C. O., Shimkus, K., Maskalenko, V., Jones, G. A., Dimitrov, P., Görür, N., Sakınç, M., and Yüce, H. (1997). An Abrupt Drowning of the Black Sea Shelf, Mar. Geol., **138**, 119-126.

Sannino, G., Sözer, A. and E. Özsoy (2014). Recent advancements on modelling the exchange flow dynamics through the Turkish Strait System, MedCLIVAR 2014 Conference "Understanding Climate Evolution and Effects on Environment and Societies in the Old World region", Ankara, June 2014.

Sannino, G., Sözer, A. and E. Özsoy (2014). MOTUS: A High-Resolution Modelling Study of the Turkish Straits System Utilizing HPC, PRACE project report, 40p.

Shchepetkin, A. F., and J. C. McWilliams (2005), The regional oceanic modeling system (ROMS): A split-explicit, free-surface, topography- following-coordinate oceanic model, *Ocean Modeling*, 9, 347 – 404.

Schroeder, K., Garcìa-Lafuente, J., Josey, S. A., Artale, V., Nardelli, B. B., Carrillo, A., Gačić, M, Gasparini, G. P., Herrmann, M., Lionello, P., Ludwig, W., Millot, C., Özsoy, E.,

Pisacane, G., Sánchez-Garrido, J. C., Sannino, G., Santoleri, R., Somot, S., Struglia, M., Stanev, E., Taupier-Letage, I., Tsimplis, M. N., Vargas-Yáñez, M., Zervakis, V., G. Zodiatis (2012). Chapter 3: *Circulation of the Mediterranean Sea and its Variability,* In: Lionello, P. (ed.), *The Climate of the Mediterranean Region - From the past to the future,* Elsevier, 592 p.

SHOD (2009). *Turkish Straits Oceanography Atlas*, Turkish Navy Navigation, Hydrography and Oceanography Office (in Turkish).

Shpindler, I. B. (1896). Materials on the Hydrology of the Sea of Marmara," *Zapiski Imper. Russ. Geogr. Obshch*., **33** (2), 1–70.

Smith, W. E. (1942). Some Observations on Water-levels and Other Phenomena Along the Bosphorus, *Transactions of the American Geophysical Union*, **27** (1), 61-68.

Soffientino, B., and M. Pilson (2005). The Bosporus Strait: A Special Place in the History of Oceanography. *Oceanography*, **18** (2), 17-23.

Sözer, A. and E. Özsoy (2002). A Three-Dimensional model of Bosphorus Strait Dynamics, The 2nd Meeting on the Physical Oceanography of Sea Straits, Villefranche, 15th-19th April 2002, 207-210.

Sözer, A. and E. Özsoy (2002). A Three-Dimensional model of Bosphorus Strait Dynamics, The 2nd Meeting on the Physical Oceanography of Sea Straits, Villefranche, 15th-19th April 2002, 207-210.

Sözer, A. (2013). Numerical Modeling of the Bosphorus Exchange Flow Dynamics, Institute of Marine Sciences, Middle East Technical University, Erdemli, Mersin, Turkey (unpublished Ph.D. thesis).

Sözer, A., Sannino, G. and E. Özsoy (2015). Bosphorus Strait Exchange Flow Dynamics Focused on Numerical Ocean Models Intercomparison, Journal of the Mediterranean and Black Sea Environment.

Spall, M. and J. F. Price (1998). Mesoscale Variabilty in Denmark Strait: The PV Outflow Hypothesis, J. Phys. Ocean. 28:1598-1623.

Stanev, E. V., J. A. Simeonov, and E. L. Peneva (2001). Ventilation of Black Sea Pycnocline by the Mediterranean plume. *J. Mar. Sys.*, **31**, 77-97.

Stanev, E. V., and E. L. Peneva (2002). Regional sea level response to global climatic change: Black Sea examples, *Global and Planetary Change*, **32**, 33-47.

Stashchuk, N. and K. Hutter (2001). Modelling of water exchange through the Strait of the Dardanelles, *Continental Shelf Research*, **21**, 1361–1382.

Stashchuk, N. and K. Hutter (2003). Modelling Gravity Current Flowing from the Bosphorus to the Black Sea, *Geophys. Astrophys. Fluid Dynamics*, **97**, No. 1, pp. 1–24

Stern, M., Whitehead, J. and B. Hua (1982). The Intrusion of a Density Current along the Coast of a Rotating Fluid, J. Fluid Mech., 123:237–265.

Tekin, O. (2010). *Eskiçağ'da İstanbul'da Balık ve Balıkçılık*, (Fish and Fishing in İstanbul in the Old Age), *Arkeoloji ve Sanat Yayınları*, 72pp. (in Turkish).

Tolmazin, D., (1985). Changing Coastal Oceanography of the Black Sea, II. Mediterranean Effluent, *Prog. Oceanogr.*, **15**, 277-316.

Tuğrul, S., Baştürk, Ö., Saydam, C., Yılmaz, A. (1992). Changes in the hydrochemistry of the Black Sea inferred from water density profiles. Nature, 359, 137-139.

Tuğrul, S., Beşiktepe, Ş. B., Salihoğlu, İ. (2002) "Nutrient exchange fluxes between the Aegean and Black Seas through the Marmara Sea". Medit. Marine Sciences, **3,** 33-42

Tuğrul, S. and Ş. Beşiktepe (2007). Nutrient exhange fluxes between the Black Sea and Mediterranean through the Turkish Strait System (Marmara Sea, Bosphorus and Dardanelles), CIESM Congress, İstanbul.

Tuğrul, S., Murray, J:W., Gernot, F., Salihoğlu, I. (2014). Spatial and temporal variability in the chemical properties of the Black Sea, J. Mar. Systems, 135, 29-43.

Turney, C. S. M. and H. Brown (2007). Catastrophic early Holocene sea level rise, human migration and the Neolithic transition in Europe, *Quaternary Science Reviews*, **26**, 2036–2041.

Tutsak, E. (2013). Analyses of marine and Atmospheric Observations along the Turkish Coast, Institute of Marine Sciences, Middle East Technical University, Erdemli, Mersin, Turkey, Masters thesis, 125 pp.

Ünlüata, Ü., Oğuz, T., Latif, M. A., and E. Özsoy, (1990). On the Physical Oceanography of the Turkish Straits, in: *The Physical Oceanography of Sea Straits*, L. J. Pratt (editor), NATO/ASI Series, Kluwer, Dordrecht, 25-60.

Yanko-Hombach, V., Gilbert, A. S., Panin, N. and P. M. Dolukhanov (2006). *The Black Sea Flood Question*, Springer, 999pp.

Yakushev, E. V., Pollehne, F., Jost. G., Kuznetsov, I., Schneider, B., Umlauf, L., 2007. Analysis of the water column oxic/anoxic interface in the Black and Baltic Seas with a numerical model, Mar. Chem., 107, 388-410.

Yakushev, E. V., Pakhomova, S., Sørenson K., Skei, J., 2009. Importance of the different manganese species in the formation of water column redox zones: Observations and modeling. Mar. Chem., 117, 59-70.

Yavuz, V., Akçar, N., C. and C. Schluechter (2003). The Frozen In Bosphorus And Its Paleoclimatic Implications - A Summary of the Historical Data, the Geological Society of America, XVI INQUA Congress, Reno, Nevada

Yemenicioglu, S., Erdoğan, S.,Tuğrul, S., 2006. Distributions of dissolved forms of iron and manganese in the Black Sea. Deep-Sea Res. Part II: Tropical Studies in Oceanography 53 (17-19), 1842-1855.

Yiğiterhan, O., Murray, J.W., Tuğrul, S., 2011. Trace metal composition of suspended particulate matter in the water column of the Black Sea. Mar. Chem., 126, 207-228.

Yüce, H., (1993). Water level variations in the Sea of Marmara. *Oceanologica Acta*, **16**, 4, 335-340.

Yüksel, Y., Ayat, B., Öztürk, M. N., Aydoğan, B., Güler, I., Çevik, E. O. and A. C. Yalçıner (2008). Responses of the Stratified Flows to their Driving Conditions - A Field Study, *Ocean Engineering*, **35** (13), 1304-1321.

Appendix 1

**Table 1.**
**R/V BİLİM stations in the Turkish Straişts and Southern Black Sea – June - July 2013**

| Record | Station name | Lat (deg) | (min) | Lon (deg) | (min) | Date | Time (EET) | Cast Depth (m) | Total Depth (m) |
|---|---|---|---|---|---|---|---|---|---|
| TK098100 | I060J750 | 39 | 57.0795N | 26 | 06.0417E | 06/18/13 | 03:58 | 20 | 24 |
| TK098101 | I050K015 | 40 | 00.9649N | 26 | 05.0373E | 06/18/13 | 04:40 | 63.5 | 67 |
| TK098102 | I157K039 | 40 | 03.9197N | 26 | 15.6939E | 06/18/13 | 08:58 | 60 | 63 |
| TK098103 | I123K014 | 40 | 01.0874N | 26 | 12.3440E | 06/18/13 | 09:55 | 50 | 52 |
| TK098104 | I172K025 | 40 | 02,0466N | 26 | 16.7585E | 06/18/13 | 10:36 | 71 | 74.9 |
| TK098105 | I202K060 | 40 | 06.0010N | 26 | 20,2756E | 06/18/13 | 11:24 | 75 | 78.3 |
| TK098106 | I221K074 | 40 | 07.0366N | 26 | 22.3708E | 06/18/13 | 11:53 | 27.5 | 31.3 |
| TK098107 | I232K083 | 40 | 08.3375N | 26 | 23.4398E | 06/18/13 | 12:18 | 50 | 76.3 |
| TK098108 | I233K101 | 40 | 10.0663N | 26 | 23.5113E | 06/18/13 | 12:43 | 65 | 85.3 |
| TK098109 | I245K123 | 40 | 12.2176N | 26 | 24.6484E | 06/18/13 | 13:17 | 50 | 67.7 |
| TK098110 | I271K132 | 40 | 13.3636N | 26 | 27.1348E | 06/18/13 | 13:43 | 78 | 87.3 |
| TK098111 | I305K155 | 40 | 15.0806N | 26 | 31.2492E | 06/18/13 | 14:46 | 43 | 47 |
| TK098112 | I343K181 | 40 | 17.8175N | 26 | 35.3143E | 06/18/13 | 15:26 | 35 | 38 |
| TK098113 | I383K204 | 40 | 20.5314N | 26 | 38.4860E | 06/18/13 | 16:01 | 76 | 79 |
| TK098114 | I424K244 | 40 | 24.0304N | 26 | 42.1566E | 06/18/13 | 16:47 | 75 | 78 |
| TK098115 | I470K260 | 40 | 25.9833N | 26 | 47.1459E | 06/18/13 | 18:06 | 96 | 99.8 |
| TK098116 | I514K253 | 40 | 25.0793N | 26 | 51.8658E | 06/18/13 | 18:42 | 46 | 49.6 |
| TK098117 | I583K251 | 40 | 25.0039N | 26 | 58.5807E | 06/18/13 | 19:26 | 55 | 61 |
| TK098118 | J034K265 | 40 | 26.8232N | 27 | 03.6922E | 06/18/13 | 20.03 | 60 | 60.5 |
| TK098119 | J113K312 | 40 | 31.3852N | 27 | 11.4833E | 06/18/13 | 21:01 | 60 | 67.1 |
| TK098120 | J242K392 | 40 | 39.4019N | 27 | 24.2849E | 06/18/13 | 22:43 | 150 | 157.4 |
| TK098121 | J222K312 | 40 | 31.3364N | 27 | 22.2581E | 06/19/13 | 00:19 | 55 | 60.8 |
| TK098122 | J222K244 | 40 | 24.5061N | 27 | 22.4664E | 06/19/13 | 01:17 | 31 | 34 |
| TK098128 | J430K342 | 40 | 34.3817N | 27 | 42.9379E | 06/19/13 | 08:12 | 62 | 66.3 |
| TK098129 | J445K411 | 40 | 41.0599N | 27 | 44.8402E | 06/19/13 | 09:15 | 150 | 307.6 |
| TK098130 | J360K490 | 40 | 49.0435N | 27 | 35.8680E | 06/19/13 | 10:43 | 100 | 1122 |
| TK098131 | J360K490 | 40 | 49.1012N | 27 | 35.3340E | 06/19/13 | 11:17 | 50 | 1124 |
| TK098132 | J360K490 | 40 | 49.1505N | 27 | 35.3040E | 06/19/13 | 12:01 | 1050 | 1124 |
| TK098133 | J342K554 | 40 | 55.7478N | 27 | 34.1337E | 06/19/13 | 13:26 | 50 | 62 |
| TK098134 | J475K500 | 40 | 49.9882N | 27 | 47.8397E | 06/19/13 | 15:49 | 525 | 578.3 |
| TK098135 | K030K510 | 40 | 51.1488N | 28 | 02.9116E | 06/19/13 | 17:56 | 1080 | 1243 |
| TK098136 | K030K555 | 40 | 55.7769N | 28 | 03.0139E | 06/19/13 | 19:47 | 500 | 528 |
| TK098137 | K143L000 | 41 | 00.0428N | 28 | 14.6328E | 06/19/13 | 21:26 | 55 | 62 |
| TK098138 | K265L573 | 40 | 57.4160N | 28 | 27.1167E | 06/20/13 | 04:20 | 65 | 68 |
| TK098139 | K253K513 | 40 | 51.4523N | 28 | 25.4242E | 06/20/13 | 05:33 | 725 | 772.7 |
| TK098140 | K343K490 | 40 | 49.0156N | 28 | 34.4599E | 06/20/13 | 07:36 | 500 | 544.25 |
| TK098141 | EK1 | 40 | 53.0786N | 28 | 35.7176E | 06/20/13 | 08:33 | 250 | 301.65 |
| TK098142 | K362K565 | 40 | 56.7041N | 28 | 36.3759E | 06/20/13 | 09:17 | 54 | 57.13 |
| TK098143 | K475K553 | 40 | 55.5873N | 28 | 47.6740E | 06/20/13 | 11:08 | 80 | 87 |
| TK098145 | K552K551 | 40 | 55.2695N | 28 | 55.3913E | 06/20/13 | 12:20 | 75 | 85 |
| TK098155 | EK-5 | 40 | 46.9518N | 29 | 07.9785E | 06/20/13 | 17:41 | 650 | 780 |
| TK098156 | EK-6 | 40 | 48.6214N | 29 | 10.1751E | 06/20/13 | 18:35 | 100 | 109.8 |
| TK098175 | EK-15 | 40 | 41.6339N | 29 | 17.4541E | 06/21/13 | 13:09 | 460 | 550 |
| TK098177 | EK-16 | 40 | 42.5436N | 29 | 05.0209E | 06/21/13 | 14:57 | 740 | 1220 |
| TK098178 | K460K402 | 40 | 40.2381N | 28 | 46.0816E | 06/21/13 | 17:06 | 300 | 327 |
| TK098179 | K435K331 | 40 | 33.0152N | 28 | 43.6446E | 06/21/13 | 18:15 | 90 | 100 |
| TK098188 | K253K321 | 40 | 32.9581N | 28 | 21.1649E | 06/22/13 | 08:00 | 50 | 53.9 |
| TK098193 | K031K330 | 40 | 32.7430N | 28 | 03.0667E | 06/22/13 | 13:09 | 40 | 46.3 |
| TK098194 | K030K420 | 40 | 41.8575N | 28 | 03.1458E | 06/22/13 | 14:41 | 280 | 322 |
| TK098195 | K130K371 | 40 | 40.1155N | 28 | 19.7061E | 06/22/13 | 16:30 | 120 | 128 |
| TK098196 | K163K491 | 40 | 49.1499N | 28 | 16.4615E | 06/22/13 | 17:41 | 600 | 648 |

| | | | | | | | | | |
|---|---|---|---|---|---|---|---|---|---|
| TK098197 | EK-18 | 40 | 41.8446N | 28 | 29.5987E | 06/22/13 | 19:51 | 212 | 399 |
| TK098198 | EK-19 | 40 | 44.7205N | 28 | 40.6486E | 06/22/13 | 21:27 | 150 | 780 |
| TK098201 | 45-C | 40 | 46.0858N | 28 | 52.5167E | 06/23/13 | 06:51 | 1180 | 1218.6 |
| TK098203 | EK-20 | 40 | 49.0177N | 28 | 49.5369E | 06/23/13 | 08:52 | 300 | 1182.3 |
| TK098204 | K533K504 | 40 | 50.6091N | 28 | 53.5326E | 06/23/13 | 09:30 | 500 | 1167.7 |
| TK098205 | EK-21 | 40 | 57.9208N | 28 | 58.5457E | 06/23/13 | 10:57 | 45 | 50 |
| TK098206 | K593L000 | 40 | 59.9239N | 28 | 59.5110E | 06/23/13 | 11:37 | 55 | 59 |
| TK098207 | K593L012 | 41 | 01.3546N | 28 | 59.5731E | 06/23/13 | 11:57 | 35 | 42 |
| TK098208 | L004L015 | 41 | 01.8048N | 29 | 00.6655E | 06/23/13 | 12:12 | 34 | 39 |
| TK098209 | L025L032 | 41 | 03.3147N | 29 | 02.8840E | 06/23/13 | 12:50 | 65 | 70 |
| TK098210 | EK-22 | 41 | 05.4009N | 29 | 03.7931E | 06/23/13 | 13:20 | 55 | 60 |
| TK098211 | L051L072 | 41 | 07.3733N | 29 | 05.0307E | 06/23/13 | 13:45 | 58 | 65 |
| TK098212 | L032L093 | 41 | 09.5669N | 29 | 03.3495E | 06/23/13 | 14:14 | 63 | 70 |
| TK098213 | L044L104 | 41 | 10.6716N | 29 | 04.9895E | 06/23/13 | 14:34 | 65 | 70.8 |
| TK098214 | L065L121 | 41 | 11.8306N | 29 | 06.5696E | 06/23/13 | 14:52 | 63 | 70 |
| TK098215 | L080L133 | 41 | 13.5206N | 29 | 08.0712E | 06/23/13 | 15:15 | 67 | 75 |
| TK098216 | L095L153 | 41 | 15.3595N | 29 | 09.8570E | 06/23/13 | 15:39 | 60 | 64 |
| TK098217 | L110L175 | 41 | 17.8010N | 29 | 11.0211E | 06/23/13 | 16:28 | 73 | 78 |
| TK098218 | EK-23 | 41 | 20.6089N | 29 | 10.6765E | 06/23/13 | 16:58 | 71 | 77 |
| TK098300 | K593L000 | 41 | 00.0504N | 28 | 59.5806E | 06/28/13 | 05:48 | 35 | 42 |
| TK098301 | K593L012 | 41 | 01.3262N | 28 | 59.5189E | 06/28/13 | 06:10 | 36 | 42 |
| TK098302 | L004L015 | 41 | 01.7150N | 29 | 00.6441E | 06/28/13 | 06:10 | 36 | 42 |
| TK098303 | L014L023 | 41 | 02.3418N | 29 | 01.4509E | 06/28/13 | 07:13 | 41 | 45 |
| TK098304 | L025L032 | 41 | 03.0498N | 29 | 02.7795E | 06/28/13 | 07:34 | 51 | 55 |
| TK098305 | L030L041 | 41 | 03.9418N | 29 | 03.1138E | 06/28/13 | 07:54 | 55 | 61 |
| TK098306 | L031L043 | 41 | 04.5295N | 29 | 03.1320E | 06/28/13 | 08:07 | 95 | 104 |
| TK098307 | L034L050 | 41 | 04.8916N | 29 | 03.6672E | 06/28/13 | 08:22 | 62 | 71.7 |
| TK098308 | L034L054 | 41 | 05.6800N | 29 | 03.6459E | 06/28/13 | 08:42 | 61 | 68 |
| TK098309 | L040L063 | 41 | 06.5529N | 29 | 04.0311E | 06/28/13 | 08:56 | 48 | 52 |
| TK098310 | L051L072 | 41 | 07.4554N | 29 | 05.3112E | 06/28/13 | 09:14 | 35 | 37.7 |
| TK098311 | L051L072D | 41 | 07.7982N | 29 | 04.9804E | 06/28/13 | 09:25 | 65 | 71.3 |
| TK098312 | L032L093 | 41 | 09.3721N | 29 | 03.3602E | 06/28/13 | 09:53 | 54 | 65.1 |
| TK098313 | L044L104 | 41 | 10.6163N | 29 | 04.8174E | 06/28/13 | 10:19 | 66 | 69.4 |
| TK098314 | L065L121 | 41 | 11.9168N | 29 | 06.5304E | 06/28/13 | 10:43 | 65 | 66.8 |
| TK098315 | L080L133 | 41 | 13.4659N | 29 | 08.0121E | 06/28/13 | 11:07 | 62 | 71.9 |
| TK098316 | L090L144 | 41 | 14.6896N | 29 | 09.1135E | 06/28/13 | 21:52 | 55 | 62.2 |
| TK098317 | L095L153 | 41 | 15.5720N | 29 | 09.9569E | 06/28/13 | 22:12 | 75 | 81 |
| TK098318 | L103L162 | 41 | 16.4138N | 29 | 10.6505E | 06/28/13 | 22:26 | 70 | 75 |
| TK098319 | L110L170 | 41 | 17.0935N | 29 | 11.1573E | 06/28/13 | 22:46 | 65 | 70 |
| TK098320 | L110L175 | 41 | 18.1030N | 29 | 11.0901E | 06/28/13 | 23:09 | 75 | 81 |
| TK098321 | L103L184 | 41 | 18.7868N | 29 | 10.4743E | 06/28/13 | 23:29 | 75 | 80 |
| TK098322 | KK1 | 41 | 18.7694N | 29 | 06.0153E | 06/29/13 | 00:04 | 70 | 75 |
| TK098323 | KK2 | 41 | 21.3181N | 29 | 02.9292E | 06/29/13 | 00:48 | 75 | 81 |
| TK098324 | KK3 | 41 | 21.3312N | 29 | 05.5502E | 06/29/13 | 01:14 | 75 | 79 |
| TK098325 | KK3.5 | 41 | 21.3609N | 29 | 08.5959E | 06/29/13 | 01:41 | 65 | 69.5 |
| TK098326 | KK4 | 41 | 21.1282N | 29 | 12.0092E | 06/29/13 | 02:09 | 75 | 81 |
| TK098327 | KK5 | 41 | 21.1196N | 29 | 16.1408E | 06/29/13 | 02:42 | 82 | 86 |
| TK098328 | KK6 | 41 | 23.0408N | 29 | 16.9572E | 06/29/13 | 03:07 | 110 | 125 |
| TK098329 | KK5.5 | 41 | 22.6823N | 29 | 18.0625E | 06/29/13 | 03:38 | 180 | 210 |
| TK098330 | KK8 | 41 | 24.0070N | 29 | 14.9446E | 06/29/13 | 06:56 | 92 | 100 |
| TK098331 | KK9 | 41 | 24.0938N | 29 | 09.2358E | 06/29/13 | 07:43 | 78 | 86.9 |
| TK098332 | KK10 | 41 | 23.9955N | 29 | 03.7190E | 06/29/13 | 08:23 | 82.5 | 86.9 |
| TK098333 | KK11 | 41 | 24.0473N | 29 | 00.1307E | 06/29/13 | 08:55 | 81.5 | 85.1 |
| TK098334 | KK12 | 41 | 26.5058N | 29 | 00.9631E | 06/29/13 | 09:29 | 83 | 88 |
| TK098335 | AB1 | 41 | 30.0602N | 29 | 06.3175E | 06/29/13 | 10:31 | 93 | 98 |
| TK098336 | AB2 | 41 | 31.3119N | 29 | 03.5390E | 06/29/13 | 11:02 | 97 | 102 |
| TK098337 | AB3 | 41 | 31.5047N | 29 | 01.6187E | 06/29/13 | 11:58 | 95 | 100 |
| TK098338 | AB4 | 41 | 33.5495N | 28 | 56.2886E | 06/29/13 | 12:48 | 96 | 101 |
| TK098339 | AB5 | 41 | 36.8000N | 28 | 59.0455E | 06/29/13 | 17:49 | 497 | 570 |

| | | | | | | | | | |
|---|---|---|---|---|---|---|---|---|---|
| TK098340 | AB6 | 41 | 35.4228N | 28 | 59.4487E | 06/29/13 | 19:54 | 210 | 200 |
| TK098341 | L065L121 | 41 | 12.0514N | 29 | 06.6731E | 07/02/13 | 20:38 | 65 | 75 |
| TK098342 | L080L133 | 41 | 13.4739N | 29 | 08.0937E | 07/02/13 | 21:01 | 65 | 70 |
| TK098343 | L090L144 | 41 | 14.7644N | 29 | 09.1289E | 07/02/13 | 21:19 | 58 | 62 |
| TK098344 | L095L153 | 41 | 15.6951N | 29 | 10.0030E | 07/02/13 | 21:37 | 78 | 82 |
| TK098345 | L103L162 | 41 | 16.5207N | 29 | 10.7034E | 07/02/13 | 21:54 | 74 | 78 |
| TK098346 | L110L170 | 41 | 17.1469N | 29 | 11.1340E | 07/02/13 | 22:08 | 71 | 75 |
| TK098347 | AA9 | 41 | 29.9582N | 29 | 03.2352E | 07/02/13 | 23:58 | 94 | 98 |
| TK098348 | AA8 | 41 | 29.8233N | 28 | 59.7780E | 07/03/13 | 00:29 | 87 | 91 |
| TK098349 | AA7 | 41 | 30.0760N | 28 | 55.1489E | 07/03/13 | 01:05 | 85 | 90 |
| TK098350 | AA6 | 41 | 36.9678N | 28 | 51.9305E | 07/03/13 | 02:06 | 105 | 110 |
| TK098351 | AA5 | 41 | 34.7096N | 28 | 49.9468E | 07/03/13 | 02:41 | 91 | 96 |
| TK098352 | AA4 | 41 | 33.1001N | 29 | 04.7459E | 07/03/13 | 04:13 | 125 | 140 |
| TK098353 | AA3 | 41 | 35.0046N | 29 | 04.5594E | 07/03/13 | 04:41 | 325 | 330 |
| TK098354 | AA2 | 41 | 29.9235N | 29 | 09.2456E | 07/03/13 | 05:42 | 96 | 103 |
| TK098355 | AA1 | 41 | 31.7952N | 29 | 09.8800E | 07/03/13 | 06:07 | 440 | 445 |
| TK098356 | AA1 | 41 | 31.7952N | 29 | 09.8800E | 07/03/13 | 06:58 | 300 | 445 |
| TK098357 | AA10 | 41 | 26.0556N | 29 | 08.9902E | 07/03/13 | 10:30 | 92 | 97 |
| TK098358 | AA11 | 41 | 26.0873N | 29 | 12.0051E | 07/03/13 | 11:00 | 95 | 103 |
| TK098359 | AA12 | 41 | 25.0754N | 29 | 16.4637E | 07/03/13 | 11:35 | 195 | 205 |
| TK098360 | AA13 | 41 | 25.9319N | 29 | 18.9529E | 07/03/13 | 12:05 | 560 | 574 |
| TK098361 | AA14 | 41 | 27.0644N | 29 | 20.7310E | 07/03/13 | 12:47 | 900 | 940 |
| TK098362 | AA15 | 41 | 25.5772N | 29 | 26.0991E | 07/03/13 | 14:00 | 520 | 540 |
| TK098363 | AA18 | 41 | 25.5658N | 29 | 30.8907E | 07/03/13 | 14:57 | 850 | 896 |
| TK098364 | AA17 | 41 | 23.1169N | 29 | 30.1675E | 07/03/13 | 16:05 | 140 | 147 |
| TK098365 | AA16 | 41 | 21.4856N | 29 | 29.8330E | 07/03/13 | 16:43 | 90 | 97 |
| TK098366 | AA19 | 41 | 18.1189N | 29 | 38.9266E | 07/03/13 | 17:46 | 80 | 86 |
| TK098367 | AA20 | 41 | 19.4443N | 29 | 38.8758E | 07/03/13 | 18:17 | 84 | 90 |
| TK098368 | AA21 | 41 | 20.9487N | 29 | 38.8272E | 07/03/13 | 18:39 | 127 | 140 |
| TK098369 | AA22 | 41 | 22.9990N | 29 | 39.8436E | 07/03/13 | 19:04 | 630 | 780 |
| TK098370 | AA27 | 41 | 25.3731N | 29 | 53.1471E | 07/03/13 | 20:48 | 1025 | 1092 |
| TK098371 | AA26 | 41 | 23.4130N | 29 | 52.8173E | 07/03/13 | 21:52 | 655 | 754 |
| TK098372 | AA25 | 41 | 22.0727N | 29 | 53.1931E | 07/03/13 | 22:39 | 420 | 453 |
| TK098373 | AA24 | 41 | 20.0624N | 29 | 52.8807E | 07/03/13 | 23:35 | 85 | 92 |
| TK098374 | AA23 | 41 | 18.0495N | 29 | 53.0395E | 07/04/13 | 00:06 | 81 | 85 |
| TK098375 | AA28 | 41 | 20.5257N | 30 | 01.0098E | 07/04/13 | 01:01 | 89 | 95 |
| TK098376 | AA29 | 41 | 22.0928N | 30 | 00.9457E | 07/04/13 | 01:21 | 261 | 269 |
| TK098377 | AA30 | 41 | 25.0036N | 30 | 00.9828E | 07/04/13 | 02:09 | 1075 | 1150 |
| TK098378 | AA33 | 41 | 28.0683N | 30 | 19.0388E | 07/04/13 | 04:25 | 740 | 760 |
| TK098379 | AA32 | 41 | 26.0119N | 30 | 18.8941E | 07/04/13 | 05:16 | 127 | 136 |
| TK098380 | AA31 | 41 | 24.0433N | 30 | 18.8439E | 07/04/13 | 05:50 | 100 | 109 |
| TK098381 | AA36 | 41 | 23.9285N | 30 | 24.9315E | 07/04/13 | 06:27 | 110 | 120 |
| TK098382 | AA40 | 41 | 20.0046N | 30 | 24.9286E | 07/04/13 | 07:01 | 100 | 109 |
| TK098383 | AA44 | 41 | 14.9335N | 30 | 30.1148E | 07/04/13 | 08:01 | 501 | 523 |
| TK098384 | AA45 | 41 | 13.0481N | 30 | 34.9962E | 07/04/13 | 08:56 | 220 | 240 |
| TK098385 | AA46 | 41 | 11.0430N | 30 | 40.1084E | 07/04/13 | 09:42 | 450 | 480 |
| TK098386 | AA47 | 41 | 14.9492N | 30 | 39.9646E | 07/04/13 | 10:32 | 950 | 1021 |
| TK098387 | AA43 | 41 | 20.0597N | 30 | 40.0160E | 07/04/13 | 11:52 | 950 | 1224 |
| TK098388 | AA39 | 41 | 24.0169N | 30 | 39.8918E | 07/04/13 | 13:07 | 950 | 1517 |
| TK098389 | AA48 | 41 | 29.0283N | 30 | 44.9705E | 07/04/13 | 14:41 | 120 | 1350 |
| TK098390 | AA48 | 41 | 28.4990N | 30 | 45.1282E | 07/04/13 | 15:26 | 950 | 1346 |
| TK098391 | AA50 | 41 | 31.4469N | 30 | 41.7128E | 07/04/13 | 16:47 | 950 | 1628 |
| TK098392 | AA49 | 41 | 29.1059N | 30 | 40.2524E | 07/04/13 | 18:25 | 950 | 1701 |
| TK098393 | AA51 | 41 | 26.9497N | 30 | 34.1442E | 07/04/13 | 19:44 | 530 | 563 |
| TK098394 | AA52 | 41 | 24.9999N | 30 | 30.2103E | 07/04/13 | 20:34 | 112 | 120 |
| TK098395 | AA52a | 41 | 26.4596N | 30 | 29.9342E | 07/04/13 | 20:54 | 250 | 340 |
| TK098396 | AA53 | 41 | 32.9262N | 30 | 26.9205E | 07/04/13 | 22:13 | 500 | 1509 |
| TK098397 | AA54 | 41 | 31.8812N | 30 | 18.9891E | 07/04/13 | 23:22 | 500 | 1330 |
| TK098398 | AA55 | 41 | 30.2181N | 30 | 08.9191E | 07/05/13 | 00:40 | 500 | 1098 |

| | | | | | | | | | |
|---|---|---|---|---|---|---|---|---|---|
| TK098399 | AA56 | 41 | 28.0765N | 29 | 56.8904E | 07/05/13 | 02:11 | 500 | 1460 |
| TK098400 | AA57 | 41 | 27.0600N | 29 | 43.8985E | 07/05/13 | 03:42 | 500 | 1417 |
| TK098401 | AA58 | 41 | 28.0328N | 29 | 34.8960E | 07/05/13 | 04:56 | 950 | 1043 |
| TK098402 | AA59 | 41 | 29.0022N | 29 | 29.9973E | 07/05/13 | 06:03 | 500 | 900 |
| TK098403 | AA60 | 41 | 30.0391N | 29 | 25.0094E | 07/05/13 | 06:54 | 500 | 1282 |
| TK098404 | XX02 | 41 | 22.6355N | 29 | 17.7404E | 07/05/13 | 12:25 | 120 | 150 |
| TK098405 | XX01 | 41 | 23.0140N | 29 | 21.5104E | 07/05/13 | 13:08 | 300 | 415 |
| TK098406 | AA61 | 41 | 30.1013N | 29 | 20.9022E | 07/05/13 | 14:24 | 950 | 1043 |
| TK098407 | AA62 | 41 | 31.0821N | 29 | 17.9320E | 07/05/13 | 15:27 | 500 | 718 |
| TK098408 | AA63 | 41 | 32.0603N | 29 | 14.8678E | 07/05/13 | 16:09 | 500 | 714 |
| TK098409 | AA64 | 41 | 33.0606N | 29 | 11.3703E | 07/05/13 | 16:55 | 500 | 660 |
| TK098410 | AA65 | 41 | 35.0754N | 29 | 08.9847E | 07/05/13 | 17:44 | 500 | 611 |
| TK098411 | AA65 | 41 | 34.2287N | 29 | 08.3627E | 07/05/13 | 18:42 | 400 | 611 |
| TK098412 | AA66 | 41 | 37.0509N | 29 | 06.9039E | 07/05/13 | 19:32 | 501 | 688 |
| TK098413 | AA67 | 41 | 37.0825N | 29 | 02.8983E | 07/05/13 | 20:17 | 500 | 718 |
| TK098414 | L110L170 | 41 | 16.9785N | 29 | 10.8789E | 07/05/13 | 22:58 | 72 | 76 |
| TK098415 | L110L162 | 41 | 16.2451N | 29 | 10.6057E | 07/05/13 | 23:11 | 71 | 75 |
| TK098416 | L095L153 | 41 | 15.3959N | 29 | 09.9737E | 07/05/13 | 23:27 | 62 | 65 |
| TK098417 | L090L144 | 41 | 14.5156N | 29 | 09.1191E | 07/05/13 | 23:49 | 56 | 60 |
| TK098418 | L080L133 | 41 | 13.4659N | 29 | 08.0121E | 07/06/13 | 00:10 | 70 | 60 |

Appendix 2

Papers, conference proceedings and presentations

| # | Product | Authors | Title | Location | Date |
|---|---|---|---|---|---|
| 1 | Working visit | E. Özsoy | Inter-basin Coupling of the Black Sea and Mediterranean Sea through the Turkish Straits System and Ensuing Mixing Processes | LeedsUniversity | 28 May 2013 |
| 2 | PhD thesis | A. Sözer | Three-dimensional modelling of exchange flows in the Bosphorus Strait | ODTÜ DBE, Erdemli | Sep 2013 |
| 3 | Conference proceeding | G. Sannino, A. Sözer, E. Özsoy | Modelling the Turkish Straits System: a grand challenge for Mediterranean and Black Seas climate studies | 40th CIESM Congress, Marseille | 28 Oct 2013 |
| 4 | Conference proceeding | A. Sözer, E. Özsoy | Modelling the Bosphorus Strait Hydrodynamics: Hydraulically Controlled Turbulent Exchange Flows, | 17. Ulusal Sıvı Hal Sempozyumu, İstanbul | 13 - 14 Dec 2013 |
| 5 | Panel presentation | E. Özsoy | Kanal İstanbul Çevresel Yıkım Tehdidi Karşısında Türk Boğazlar Sistemi'nin Denizbilim ve İklimbilimde, Ekoloji ve Sosyal Tarihteki Yeri ve Etkileri | Hukuki, Kentsel ve Ekolojik Yönleriyle "Kanal İstanbul" Paneli, İstanbul Bilgi Üniversitesi, İstanbul | 28 Jan 2014 |
| 6 | Conference proceeding | G. Sannino, A. Sözer, E. Özsoy | Recent advancements on modelling the exchange flow dynamics through the Turkish Strait System | EGU General Assembly 2014, Vienna | 30 Apr 2014 |
| 7 | Conference proceeding | A. Sözer, G. Sannino, E. Özsoy | Bosphorus Strait Exchange Flow Dynamics Focused on Numerical Ocean Models Intercomparison | EGU General Assembly 2014, Vienna | 30 Apr 2014 |
| 8 | Conference proceeding | M. Gündüz, E. Özsoy | Inter-annual variability of upper layer blocking of the Dardanelles Strait and its connection with the fish catch in the Aegean sea (1979-2013) | MedCLIVAR 2014 Conference "Understanding Climate Evolution and Effects on Environment and Societies in the Old World region" | 22-25 Jun 2014 |
| 9 | Conference proceeding | G. Sannino, A. Sözer, E. Özsoy | Recent advancements on modelling the exchange flow dynamics through the Turkish Strait System | MedCLIVAR 2014 Conference "Understanding Climate Evolution and Effects on Environment and Societies in the Old World region" | 22-25 Jun 2014 |
| 10 | Article in magazine | E. Özsoy | Bir Çılgın Proje: Kanal İstanbul | ODTÜ'lü dergisi | Jun 2014 |
| 11 | Summer school lecture | E. Özsoy | Can Mega-Cities achieve Blue Growth?The Case of Istanbul, a world heritage, from Scientific, Natural and Cultural perspectives | OGS Summer School "Sustainable Blue Growth in South East Europe", Trieste | 14-18 Jul 2014 |

| | | | | | |
|---|---|---|---|---|---|
| 12 | Journal paper | R. Delfanti, E. Özsoy, H. Kaberi, A. Schirone, S. Salvi, F. Conte, C. Tsabaris, C. Papucci | Evolution and fluxes of $^{137}Cs$ in the Black Sea/Turkish Straits System/North Aegean Sea | Journal of Marine Systems | Jul 2014 |
| 13 | Journal paper | S. Tuğrul, J. W. Murray, G. E. Friederich, İ. Salihoğlu | Spatial And Temporal Varıabilty In The Hydro-Chemical Properties Of The Black Sea Upper Layer | Journal of Marine Systems | Jul 2014 |
| 14 | Journal paper | S, Kioroglou , E. Tragou, V. Zervakis, Georgopoulos, B. Herut, I. Gertman, V. Kovacevic, E. Özsoy, E. Tutsak | Vertical diffusion processes in the Eastern Mediterranean — Black Sea System | Journal of Marine Systems | Jul 2014 |
| 15 | Journal paper | S. Zervoudaki, E.D. Christou, G. Assimakopoulou, H. Örek, A. C. Gucu, A. Giannakourou, P. Pitta, T. Terbiyik, N. Yücel, T. Moutsopoulos, K. Pagou, S. Psarra, E. Özsoy, E. Papathanassiou | Copepod communities, production and grazing in the Turkish Straits System and the adjacent northern Aegean Sea during spring | Journal of Marine Systems | Jul 2014 |
| 16 | Symmpozium presentation | E. Özsoy, A. Sözer, Ö. Gürses, M. Gündüz, G. Sannino | Nonlinear Hydrodynamics of Sea Straits - Bosphorus and Dardanelles Examples | Turkish Nonlinear Science Working Group, XIV. International Symposium on “Disorder Systems: Theory and Its Applications”, Mordoğan, İzmir | 21-25 Aug 2014 |
| 17 | Technical report | G. Sannino, A. Sözer, E. Özsoy | MOTUS: A High-Resolution Modelling Study of the Turkish Straits System Utilizing HPC | PRACE project report | Oct 2014 |
| 18 | Workshop presenttation + technical report | E. Özsoy | Turkish Straits System Exchange Fluxes between the Black and Mediterranean Seas | Workshop on “The Mediterranean Sea mass and heat budget: Understanding its forcing, uncertainties and time evolution”, Palma de Mallorca | 9-10 Oct 2014 |
| 19 | Workshop poster | Ö. Gürses, N. Pinardi, E. Özsoy, P. Oddo, R. Timmermann | Modeling of the Turkish Straits System Using FEOM | Workshop on “The Mediterranean Sea mass and heat budget: Understanding its forcing, uncertainties and time evolution”, Palma de Mallorca | 9-10 Oct 2014 |
| 20 | Workshop poster | G. Sannino, A. Sözer, E. Özsoy | Recent Advancements on Modelling the Exchange Flow Dynamics through the Turkish Straits System | Workshop on “The Mediterranean Sea mass and heat budget: Understanding its forcing, uncertainties and time evolution”, Palma de Mallorca | 9-10 Oct 2014 |
| 21 | Workshop | A. Sözer, G. | Bosphorus Strait Exchange | Workshop on “The | 9-10 Oct 2014 |

| | | | | | |
|---|---|---|---|---|---|
| | poster | Sannino, E. Özsoy | Flow Dynamics Focused on Numerical Ocean Models Comparison | Mediterranean Sea mass and heat budget: Understanding its forcing, uncertainties and time evolution", Palma de Mallorca | |
| 22 | Symposium presentation | E. Özsoy, A. Sözer, Ö. Gürses, E. Tutsak, M. Gündüz*, G. Sannino | The Leading Role of the Turkish Straits System in Ocean Science and the Environmental Degradation Imposed on Unique Natural-Cultural Heritage by Canal İstanbul | İstanbul'un Jeolojisi Sempozyumu 4, Kadir Has Üniversitesi Cibali Kampüsü – İstanbul | 26-28 Dec 2014 |
| 23 | Conference proceeding + journal paper | G. Sannino, A. Sözer, E. Özsoy | Recent advancements on modelling the exchange flow dynamics through the Turkish Strait System | Journal of the Mediterranean and Black Sea Environment | Mar 2015 |
| 24 | Conference Proceeding | E. Özsoy, G. Sannino, Adil Sözer, Ö. Gürses | A Review of the Turkish Straits System: Challenges for Modeling, Inter-Basin Coupling and the Envi-ronment | European Geosciences Union (EGU) General Assembly 2015, Viyana, Avusturya | 12-17 Apr 2015 |
| 25 | Conference proceeding | E. Özsoy, Ö. Gürses, E. Tutsak | Turkish Straits System and Southern Black Sea: Exchange. Mixing and Shelf / Canyon Interactions | European Geosciences Union (EGU) General Assembly 2015, Viyana, Avusturya | 12-17 Apr2015 |
| 26 | Conference proceeding | Ö. Gürses, A. Aydoğdu, N. Pinardi, E. Özsoy | Modeling the Turkish Straits System: Circulation and Mixing based on Inter-Basin Coupling | 47th Liege Collquium "Marine Environmental Monitoring, Modelling and Prediction" University of Liège, Liège, Belçika | 4-8 May 2015 |
| 27 | Journal paper | Ö. Gürses, A. Aydoğdu, N. Pinardi, E. Özsoy | Variable Resolution Modeling of the Turkish Straits System | Journal of Marine Systems | Oct 2015 (submitted) |
| 28 | Journal paper | G. Sannino, A. Sözer, E. Özsoy | High Resolution Modelimg of the Turkish Straits System | Journal of Marine Systems | Oct 2015 (submitted) |

# TÜBİTAK
# PROJE ÖZET BİLGİ FORMU

| | |
|---|---|
| Proje Yürütücüsü: | Prof. Dr. EMİN ÖZSOY |
| Proje No: | 111Y308 |
| Proje Başlığı: | Yüksek Enerji Çevre Dinamiği: Türk Boğazlar Sistemi'nde Süreçler - TURBO |
| Proje Türü: | Uluslararası |
| Proje Süresi: | 36 |
| Araştırmacılar: | SÜLEYMAN TUĞRUL |
| Danışmanlar: | |
| Projenin Yürütüldüğü Kuruluş ve Adresi: | ORTA DOĞU TEKNİK Ü. DENİZ BİLİMLERİ ENSTİTÜSÜ |
| Projenin Başlangıç ve Bitiş Tarihleri: | 15/08/2012 - 15/08/2015 |
| Onaylanan Bütçe: | 417518.0 |
| Harcanan Bütçe: | 201395.21 |
| Öz: | The Turkish Straits System (TSS) controls the exchange between the Black Sea and the Mediterranean Sea. A sound understanding of the circulation and transport mechanisms of this complex system depends on a series of experimental investigations and modelling development that have been carried out. investigations highlighted the fine-scale details of the exchange and the intrusions and mixing of water masses between adjacent basins. High resolution modeling of the TSS is undertaken to assess its transport and mixing properties. |
| Anahtar Kelimeler: | Water and material exchange, transport, mixing, Dardanelles Straits, Marmara Sea, Black Sea. |
| Fikri Ürün Bildirim Formu Sunuldu Mu?: | Hayır |